

# ***In vivo* Lumbar Spine Biomechanics: Vertebral Kinematics, Intervertebral Disc Deformation, and Disc Loads**

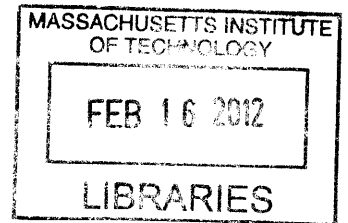
By  
Shaobai Wang

B.S., Mechanical Engineering, University of Michigan, 2006  
S.M., Mechanical Engineering, Massachusetts Institute of Technology, 2008

Submitted to the Department of Mechanical Engineering  
in partial fulfillment of the requirements for the degree of

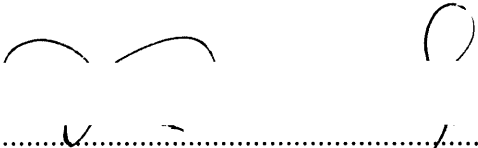
Doctor of Philosophy in Mechanical Engineering  
at the  
MASSACHUSETTS INSTITUTE OF TECHNOLOGY


February 2012

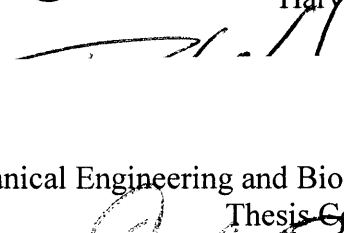



**ARCHIVES**

© 2012 MASSACHUSETTS INSTITUTE OF TECHNOLOGY

Signature of Author.....  
  
.....  
Department of Mechanical Engineering  
January 20, 2012

Certified by.....  
  
.....  
Guoan Li  
Professor of Orthopaedic Surgery/Bioengineering  
Harvard Medical School  
Thesis Supervisor

Certified by.....  
  
.....  
Peter So  
Professor of Mechanical Engineering and Biological Engineering  
Thesis Committee Chairman

Accepted by.....  
  
.....  
David E. Hardt  
Professor of Mechanical Engineering  
Chairman, Department Committee on Graduate Students



# ***In vivo* Lumbar Spine Biomechanics: Vertebral Kinematics, Intervertebral Disc Deformation, and Disc Loads**

By

Shaobai Wang

Submitted to the Department of Mechanical Engineering on January 20, 2012 in partial fulfillment of the requirements for the degree of Doctor of Philosophy in Mechanical Engineering

## **Abstract**

Knowledge of lumbar spine biomechanics in living human subjects is fundamental for understanding mechanisms of spinal injury and pathology, for improvement of corresponding clinical treatments, and for design of spinal prosthesis. However, due to the complicated spine anatomy and loading conditions as well as high risks in these direct measurements, it has been a challenge to determine the *in vivo* biomechanics of the lumbar spine. To address this problem, the overall objective of this thesis was to develop and implement a dual fluoroscopic imaging system to non-invasively study human lumbar spine biomechanics. In line with this objective, the first goal was to quantify the ability of the dual fluoroscopic imaging system to determine vertebral kinematics. The second goal was to implement this technique to investigate spinal motion in both healthy subjects and patients with pathology. The third goal was to explore the feasibility of using kinematic data obtained from this system as boundary conditions in finite element analysis to calculate the physiological loads on the intervertebral disc.

The system was shown to be accurate and repeatable in determining the vertebral kinematics in all degrees of freedom. For the first time, six degree-of-

freedom motion of different structures of the spine, such as the vertebral body, intervertebral disc, facet joint and spinous process were measured *in vivo* in both healthy subjects and subjects with pathology during functional activities. In general, the group of subjects with pathology showed a significantly abnormal kinematic response during various physiological functional activities. Preliminary studies have shown the applicability and high accuracy of finite element modeling to calculate disc loads using *in vivo* vertebral kinematics as displacement boundary conditions.

Thesis Supervisor: Guoan Li, Ph.D.  
Professor of Orthopaedic Surgery/Bioengineering  
Harvard Medical School

Committee Chair: Peter So, Ph.D.  
Professor of Mechanical Engineering and Biological Engineering  
Massachusetts Institute of Technology

Committee Member: Alan Grodzinsky, Sc.D.  
Professor of Electrical, Mechanical, and Biological Engineering  
Massachusetts Institute of Technology

## Acknowledgments

As a Chinese tradition and truly from my heart, first and foremost I thank my Mom Du, Chen and Dad Wang, Hui Lian for their love and support. They are very proud of me at this time. But no matter I was successful or not, their love and support will not change. That's the thing I have learned after the highs and lows during my studying aboard for seven years. I wish them healthy and happy.

I must thank Dr. Guoan Li to be a great advisor both in academic and in life. With him, the journey of pursuing Ph.D. is not only to achieve academic success, but more importantly, to become a man with proper skills, strong mind and prepared heart for the upcoming challenges. I also would like to thank my thesis committee members, Professor Peter So and Professor Alan Grodzinsky for all their input to this work. I have learned a lot from their knowledge and great personalities. I would like to extend special thanks to Dr. Kirkham Wood, whom I regard as my clinical advisor, for his help, care and encouragement.

I would like to thank the lab mates/friends from the Bioengineering Laboratory (in no specific order): Jeffrey Bingham, George Hanson, Angela Moynihan, Louis Defrate, Ramprasad Pappanagari, Ali Hosseini, Daniel Massimini, Lu Wan, Michal Kozanek, Peter Passias, Kartik Varadarajan, Hemanth Gadikota, Sam Van de Velde, Dr. Xia, Dr. Miao, Dr. Wu, Dr. Chen, Dr. Nha, Dr Seon, Dr. Sim, Dr. Taka one and two, Zongmiao Wan, Thomas Zumbrunn, Won Man Park, Tsung-Yuan Tsai and Jing-Sheng Li. All of you made the lab a very comfortable place to work. And I also enjoy the time with you after work. I wish all of you successful.

I would also like to thank my lots of friends in the United States and in

China, including: Xiaoting Jia, Guohao Ding, Yanan Wang, Haijie Chen, Wener Lv, Shangchao Lin, Jinrong Lin, Binghuai Lin, Fujing Cao, Xiaoping Zhang, Marcus Chao and Dr. Chang. All of you have made my world more interesting.

To conclude, thank you all, listed or not listed here, for the help which made me successfully finished my Ph.D. work and enjoyed my time during Ph.D.

# Table of Contents

<b>ABSTRACT.....</b>	<b>3</b>
<b>ACKNOWLEDGMENTS .....</b>	<b>5</b>
<b>TABLE OF CONTENTS.....</b>	<b>7</b>
<b>LIST OF FIGURES .....</b>	<b>15</b>
<b>LIST OF TABLES.....</b>	<b>21</b>
<b>LIST OF ABBREVIATIONS .....</b>	<b>25</b>
<b>CHAPTER 1 INTRODUCTION .....</b>	<b>27</b>
1.1 THE ANATOMY OF HUMAN LUMBAR SPINE .....	27
1.2 DEFINITION OF BASIC AND CLINICAL TERMINOLOGIES .....	35
1.3 LUMBAR SPINE BIOMECHANICS .....	39
1.3.1 <i>Diseases and abnormal biomechanics</i> .....	40
1.3.2 <i>Surgeries and altered biomechanics</i> .....	43
1.4 OBJECTIVE AND APPROACH.....	46
1.5 ORGANIZATION OF THE THESIS.....	47
1.6 REFERENCES .....	49
<b>CHAPTER 2 STUDY <i>IN VIVO</i> LUMBAR SPINE BIOMECHANICS: SYSTEM SETUP AND VALIDATION.....</b>	<b>53</b>
2.1 SYSTEM SETUP AND TECHNICAL DETAILS .....	53
2.1.1 <i>MRI</i> .....	54

2.1.2	<i>CT</i> .....	56
2.1.3	<i>MRI and CT comparison</i> .....	57
2.1.4	<i>Dual orthogonal fluoroscopic</i> .....	59
2.1.5	<i>Matching</i> .....	60
2.1.6	<i>Data analysis</i> .....	62
2.1.7	<i>Summary</i> .....	63
2.2	VALIDATION.....	64
2.2.1	<i>Ovine vertebrae validation</i> .....	65
2.2.2	<i>Human cadaveric lumbar spine validation</i> .....	70
2.2.3	<i>In vivo validation</i> .....	73
2.2.4	<i>Summary</i> .....	75
2.3	DISCUSSION AND CONCLUSION .....	76
2.4	REFERENCES .....	78

**CHAPTER 3    SEGMENTAL VERTEBRAL MOTION OF NORMAL  
HEALTHY SUBJECTS *IN VIVO*..... 81**

3.1	INTRODUCTION.....	81
3.2	MATERIAL AND METHODS .....	82
3.3	RESULTS .....	88
3.3.1	<i>Primary rotations</i> .....	88
3.3.2	<i>Coupled translations and rotations</i> .....	89
3.4	DISCUSSION.....	91
3.5	REFERENCES .....	97

**CHAPTER 4    OVERALL GEOMETRIC DEFORMATION OF LUMBAR  
DISCS UNDER *IN VIVO* WEIGHT-BEARING STANDING .....99**

4.1	INTRODUCTION:.....	99
-----	--------------------	----



4.2	MATERIAL AND METHODS .....	100
4.3	RESULTS: .....	103
4.3.1	<i>Disc deformation patterns</i> .....	103
4.3.2	<i>Quantitative measurements at representative locations</i> .....	105
4.4	DISCUSSION: .....	107
4.5	APPENDIX: .....	112
4.6	REFERENCES .....	116
<b>CHAPTER 5</b>	<b>RANGE OF MOTION AND ORIENTATION OF THE</b>	
	<b>LUMBAR FACET JOINTS <i>IN VIVO</i></b> .....	<b>119</b>
5.1	INTRODUCTION .....	119
5.2	MATERIAL AND METHODS .....	120
5.2.1	<i>Lumbar facet joint motion</i> .....	120
5.2.2	<i>Facet orientation</i> .....	121
5.2.3	<i>Statistical analysis</i> .....	122
5.3	RESULTS .....	124
5.3.1	<i>Facet motion FROM supine position to standing</i> .....	124
5.3.2	<i>Facet motion during flexion to extension of the trunk</i> .....	127
5.3.3	<i>Facet motion during side to side bending of the trunk</i> .....	127
5.3.4	<i>Facet motion during left to right torsion of the trunk</i> .....	128
5.3.5	<i>Facet orientation</i> .....	128
5.4	DISCUSSION .....	130
5.5	REFERENCES .....	134
<b>CHAPTER 6</b>	<b><i>IN VIVO</i> RANGE OF MOTION OF THE SPINOUS PROCESS</b>	
	<b>137</b>	
6.1	INTRODUCTION: .....	137

6.2	MATERIALS AND METHODS:.....	138
6.3	RESULTS:.....	141
6.4	DISCUSSION: .....	143
6.5	APPENDIX: .....	147
6.6	REFERENCES .....	151

**CHAPTER 7    *IN VIVO* MOTION CHARACTERISTICS OF LUMBAR VERTEBRAE IN THE SAGITTAL AND TRANSVERSE PLANES..... 153**

7.1	INTRODUCTION.....	153
7.2	MATERIALS AND METHODS .....	154
7.2.1	<i>Coordinate system of the vertebral body:</i> .....	154
7.2.2	<i>Coordinate system of the spinal canal:</i> .....	156
7.2.3	<i>Coordinate system of the spinous process:</i> .....	156
7.2.4	<i>Data analysis:</i> .....	156
7.3	RESULT.....	157
7.4	DISCUSSION.....	160
7.5	REFERENCES .....	164

**CHAPTER 8    SEGMENTAL LUMBAR MOTION IN PATIENTS WITH DISCOGENIC LOW BACK PAIN DURING FUNCTIONAL WEIGHT-BEARING ACTIVITIES ..... 167**

8.1	INTRODUCTION:.....	167
8.2	MATERIALS AND METHODS:.....	168
8.2.1	<i>Patient Recruitment:</i> .....	168
8.2.2	<i>Combined imaging technique:</i> .....	170
8.2.3	<i>Data analysis:</i> .....	172
8.3	RESULTS:.....	173

8.3.1	<i>Primary rotations In Patients with Degenerative Disc Disease:</i> .....	173
8.3.2	<i>Coupled translations and rotations</i> .....	175
8.3.3	<i>Comparison with Normal Subjects:</i> .....	175
8.4	DISCUSSION: .....	178
8.5	REFERENCES: .....	182

**CHAPTER 9 LUMBAR DISC DEFORMATION IN PATIENTS WITH DEGENERATIVE DISC DISEASE AT THE CEPHALIC ADJACENT LEVELS**

**187**

9.1	INTRODUCTION:.....	187
9.2	MATERIAL AND METHODS: .....	189
9.2.1	<i>Subject recruitment:</i> .....	189
9.2.2	<i>Calculation of IVD deformation:</i> .....	191
9.3	RESULTS:.....	192
9.3.1	<i>Deformation patterns:</i> .....	192
9.3.2	<i>Maximum tensile and shear deformations:</i> .....	195
9.3.3	<i>Difference between L3-4 and L2-3 discs:</i> .....	196
9.4	DISCUSSION: .....	197
9.5	REFERENCES .....	202

**CHAPTER 10 LUMBAR FACET JOINT MOTION IN PATIENTS WITH DEGENERATIVE DISC DISEASE.....207**

10.1	INTRODUCTION:.....	207
10.2	MATERIALS AND METHODS .....	209
10.3	RESULTS .....	212
10.3.1	<i>Ranges of motion of facet joints in Patients with DDD</i> .....	212
10.3.2	<i>Comparison with healthy subjects</i> .....	215

10.4	DISCUSSION.....	217
10.5	REFERENCES .....	221

**CHAPTER 11 PREDICT FORCES AND MOMENTS ON THE LUMBAR INTERVERTEBRAL DISC – A VALIDATION STUDY .....223**

11.1	INTRODUCTION.....	223
11.2	MATERIAL AND METHODS .....	226
11.2.1	<i>Specimen preparation.....</i>	226
11.2.2	<i>In vitro testing protocol.....</i>	227
11.2.3	<i>Determination of the kinematics of the disc endplates.....</i>	229
11.2.4	<i>Finite element models of the IVDs.....</i>	231
11.3	RESULTS.....	234
11.3.1	<i>Accuracy in each tested DOF.....</i>	234
11.3.2	<i>Accuracy in the other 5 DOF.....</i>	235
11.4	DISCUSSION.....	239
11.5	REFERENCES .....	243

**CHAPTER 12 IN VIVO DISC LOADS – A PRELIMINARY INVESTIGATION .....249**

12.1	INTRODUCTION.....	249
12.2	MATERIAL AND METHODS .....	250
12.3	RESULTS.....	254
12.3.1	<i>Overall disc deformation and loads.....</i>	254
12.3.2	<i>Intradiscal Pressure .....</i>	255
12.3.3	<i>Stress and strain in the AF fibers.....</i>	256
12.3.4	<i>Stress and strain in the AF bulk .....</i>	257
12.4	DISCUSSION.....	259

12.5	REFERENCES .....	265
<b>CHAPTER 13</b>	<b>CONCLUSIONS.....</b>	<b>267</b>
13.1	PROLOGUE .....	267
13.2	SUMMARY .....	268
13.3	FUTURE WORK.....	270



# List of Figures

Fig 1-1. Human evolution.....	28
Fig 1-2. Lateral and posterior view of the spine .....	29
Fig 1-3. Superior view of a lumbar vertebra. Courtesy to Schnuerer. ....	30
Fig 1-4. Posterior view of a lumbar vertebral motion segment .....	31
Fig 1-5. Lateral view of a lumbar vertebral motion segment .....	31
Fig 1-6. Endplate and disc .....	33
Fig 1-7. Disc anatomy .....	33
Fig 1-8. Three anatomical planes.....	35
Fig 1-9. Three anatomical planes in the lumbar spine .....	36
Fig 1-10. Definition of terminologies in the sagittal view .....	38
Fig 1-11. Pfirrmann grading (I-V from left to right) of disc degeneration .....	41
Fig 1-12. Example of a herniated disc on MRI and in a sketch.....	42
Fig 1-13. Normal motion segments (left) and segments with spondylolisthesis (right) .....	43
Fig 1-14. Idea of spinal fusion and anterior and posterior fusion on X-ray. ....	44
Fig 1-15. Example of an artificial disc .....	45
Fig 2-1. Mid-sagittal MRI slice of the lumbar spine using the custom protocol .....	55
Fig 2-2. a) Digitization of vertebral contours. b) 3D vertebral mesh models .....	55
Fig 2-3. a) Automatic segmentation on CT. b) 3D model constructed from the digitized data. c) Individual vertebra mesh model after manual editing. ....	56
Fig 2-4. a) Iterative closest point algorithm registers the ovine MRI model with CT model. b) Comparison suggests satisfying geometric agreement with subtle differences. ....	58
Fig 2-5. DFIS setup .....	58
Fig 2-6. A patterned plexi-plate used to restore the distortion. ....	60
Fig 2-7. a) Virtual computer environment of DFIS with 3D MRI vertebral models. b) Matching 3D model to 2D features on fluoroscopic images. ....	61

Fig 2-8. Coordinate system used to describe 6DOF vertebrae kinematics. ....	63
Fig 2-9. Local coordinate system to determine 6DOF kinematics of the ovine lumbar spine.....	65
Fig 2-10. Experiment setup of MTS machine and DFIS .....	66
Fig 2-11. Imaging matching during manual flexion-extension of the lumbar spine.....	67
Fig 2-12. Implantation of metal beads in human cadaveric spine for RSA validation .....	71
Fig 2-13. Image matching of the human cadaveric spine implanted with beads .....	72
Fig 2-14. a) Experiment setup of testing living subjects in DFIS b) Reproduction of the <i>in vivo</i> vertebrae position from matching .....	74
Fig 2-15. Vertebral models and local coordinates used to determine 6DOF kinematics. L/R: left/right, ML: medial-lateral, AP: anterior-posterior, PD: proximal-distal.....	74
Fig 3-1. a) Vertebral segmentation on MRI. b) 3D reconstructed vertebrae models from MRI and local coordinate system.....	84
Fig 3-2. a) DFIS setup. b) Reproduction of <i>in vivo</i> position of L2-L5. ....	85
Fig 3-3. <i>In vivo</i> positions of the lumbar spine under various functional activities .....	86
Fig 3-4. Range of primary rotations during: a) flexion-extension. b) left-right lateral bending. and c) left- right twisting. ....	88
Fig 4-1. a) Coordinate systems to characterize the kinematics of the disc endplates. b) Definition of local disc heights. c) Calculation of overall tensile and shear deformation .....	101
Fig 4-2. Representative locations: A-Anterior, P-Posterior, L-Left, R-Right, C-Center.....	103
Fig 4-3. a) Overall tensile deformation. b) Overall shear deformation. Averaged from 8 subjects and mapped on “standard discs” at different vertebral levels. ....	104
Fig 4-4. Tensile deformation at the 9 representative locations on disc surfaces. A-Anterior, P-Posterior, L- Left, R-Right, C-Center. Error bars shows the standard deviation from 8 subjects. *: L2-3 different from L3-4, #: L2-3 different from L4-5, &: L3-4 different from L4-5, $p < 0.05$ . ....	106
Fig 4-5. Shear deformation at the 9 representative locations on disc surfaces. A-Anterior, P-Posterior, L- Left, R-Right, C-Center. Error bars shows the standard deviation from 8 subjects. *: L2-3 different from L3-4, #: L2-3 different from L4-5, &: L3-4 different from L4-5, $p < 0.05$ . ....	106



Fig 4-6. Tensile deformation of a) a typical case and; b) an extreme case .....	114
Fig 4-7. Shear deformation of a) a typical case and; b) an extreme case.....	115
Fig 5-1. Anatomical coordinate system to measure facet motion .....	122
Fig 5-2. Measurement of transverse facet angle: the angle between the line of the facet width projected onto the transverse plane and the anterior-posterior axis of the vertebra. ....	123
Fig 5-3. Measurement of longitudinal facet angle: the angle between the line of the facet length projected onto the sagittal plane and the cranian-caudal axis of the vertebra. ....	123
Fig 5-4. Ranges of facet joint rotations in 6DOF. The bars represent statistical significance upon within- level comparison while the symbols (*,+,x) represent statistical significance upon between-level comparison. $p<0.05$ .....	125
Fig 5-5. Ranges of facet joint translations in 6DOF. The bars represent statistical significance upon within- level comparison while the symbols (*,+,x) represent statistical significance upon between-level comparison. $p<0.05$ .....	126
Fig 6-1. a) shortest distance was measured between adjacent processes; b) Local coordinate systems were established at the tip of the process to measure rotational angle and displacement in the transverse plane .....	140
Fig 6-2. Shortest distance between processes at various postures and different levels (* $p<0.05$ ).....	141
Fig 6-3. Distance change between processes during flexion and extension .....	142
Fig 6-4. ISP distance at approximated ISPD positions (between a and b). Shortest ISP distances were also shown for reference.....	147
Fig 6-5. Distance between processes measured at approximated ISPD locations at various postures and different levels (* $p<0.05$ ).....	149
Fig 6-6. Distance change between processes during flexion and extension at different levels, measured at approximated ISPD locations.....	150
Fig 7-1. Coordinate systems at the volumetric center of the vertebral body (B), the center of spinal canal (C), and the tip of spinous process (P) based on anatomic features. ....	155
Fig 7-2. Mid-sagittal and transverse planes were determined for calculating ROMs and CORs .....	155

Fig 7-3. Schematic of COR's location calculated from points of zero displacement points: a) in the sagittal plane; and b) in the transverse plane .....	157
Fig 8-1. a) T2 MR image of LBP patient showing DDD at L4-5 and L5-S1. b) Digitized contours of vertebrae in the sagittal plane. c) 3D anatomic vertebral models from MRI.....	171
Fig 8-2. a) DFIS experiment setup. b) Reproduction of the <i>in vivo</i> vertebrae positions. ....	171
Fig 8-3. Local coordinate systems to calculate the 6DOF kinematics of the cephalad vertebra with respect to the caudad vertebra. $\alpha$ (flexion-extension), $\beta$ (left-right bending), and $\gamma$ (left-right twisting). ....	172
Fig 8-4. Primary rotation (and SD) of patients with DDD and normal subjects at different levels during physiological activities. The numbers on the x axis indicate the vertebral level; for example, "23" indicates L2-L3, *: statistically significant difference within DDD group, #: statistically significant difference of DDD group compared to normal. ....	177
Fig 9-1: a): 3D vertebrae models were constructed from sagittal MR images. b): reproduction of <i>in vivo</i> vertebrae positions by matching 3D model projections to 2D osseous contours .....	190
Fig 9-2. a): Local heights and disc transverse plane were determined. b): Calculation of the tensile and shear deformations, with respect to local heights in standing as references.....	191
Fig 9-3. Typical disc tensile deformation of a): patient with DDD and b): healthy subject. Typical disc shear deformation of c): patient with DDD and d): healthy subject.....	193
Fig 10-1. Anatomical coordinate system to measure kinematics of the facet joints. ....	211
Fig 10-2. Ranges of facet joint translations of patients with DDD along three principal axes under : a) torsion, b) bending, and c) flexion of the torso. The symbols (*, +, x) represent statistical significance upon between-level comparison ( $p < 0.05$ ). ....	213
Fig 10-3. Ranges of facet joint rotations of patients with DDD around three principal axes under: a) torsion, b) bending, and c) flexion of the torso. There was no statistical difference between levels. ....	214
Fig 11-1. Experiment design.....	226
Fig 11-2. Experiment setup a) Installation of the lumbar MSU on the 6DOF robotic system. b) Capturing fluoroscopic images of the MSU using DFIS.....	228

Fig 11-3. Reproduction of the positions of the vertebrae using an established image matching protocol.	230
Fig 11-4. Determination of the coordinate system for the IVD center and the principal directions. a)	
Recording the relative position of the coordinate system and several titanium beads using a digitizer.	
b) Registering the coordinate system with the FEA model by matching the titanium beads.	230
Fig 11-5. FE modeling of IVD and kinematic inputs to calculated disc loads.	232
Fig 11-6. Comparison of the force-displacement curves between FEA and experiment measurements under various loading cases for IVD#1.	236
Fig 11-7. Comparison of the force-displacement curves between FEA and experiment measurements under various loading cases for IVD#2.	237
Fig 11-8. Comparison of the force-displacement curves between FEA and experiment measurements under various loading cases for IVD#3.	238
Fig 12-1. Weight lifting flexion-extension activity using 15lb dumbbells. The kinematics of lumbar spine were obtained from image matching.	251
Fig 12-2. Shape of the three discs during flexion-extension.	253
Fig 12-3. Overall disc deformation and loads at the center of the disc during flexion-extension. x axis from 1 to 5: from flexion to extension, respectively.	255
Fig 12-4. Intradiscal pressure during flexion-extension. x axis from 1 to 5: from flexion to extension, respectively.	256
Fig 12-5. An example showing maximum fiber stress found at the posterolateral corner of the disc during upright weight-bearing.	257
Fig 12-6. Maximum AF bulk strain in a subject with narrowed disc space at posterior.	258
Fig 12-7. Despite some similarity in strain patterns, our study showed larger AF bulk strains than an <i>in vitro</i> MRI study from literature.	263



# List of Tables

Table 2-1: Accuracy of the image matching method in terms of vertebrae motion distance and speed .....	68
Table 2-2: 6DOF repeatability of reproducing the relative vertebral positions. x: left-right (medial lateral), y:anterior-posterior, z: proximal-distal, $\alpha$ : flexion-extension, $\beta$ : left-right bending, $\gamma$ : left-right rotation .....	70
Table 2-3. Average 6DOF accuracy in reproduce positions and orientations of lumbar vertebrae with respect to RSA as gold standard. x: left-right (medial lateral), y:anterior-posterior, z: proximal-distal, $\alpha$ : flexion-extension, $\beta$ : left-right bending, $\gamma$ : left-right rotation .....	72
Table 2-4: 6DOF repeatability of the relative positions of L2 with respect to L3 from 5 times of matching at various body positions. x: left-right, y:anterior-posterior, z: proximal-distal, $\alpha$ : flexion-extension, $\beta$ : left-right bending, $\gamma$ : left-right rotation .....	75
Table 3-1: 6DOF ROM of lumbar vertebrae at different levels during various functional activities. Primary rotations were <i>italicized</i> . Coupled ranges of translations were labeled as LR (left-right), AP (anterior-posterior) and PD (proximal-distal). Ranges of rotations were labeled as FE (flexion-extension), Bend (left-right bending) and Twist (left-right twisting). $p<0.05$ , *: statistically different compare to other levels. # statistically different compare to other DOFs. ....	90
Table 5-1: Transverse Orientation of Lumbar Facets in Degrees° .....	129
Table 5-2: Longitudinal Orientation of Lumbar Facets in Degrees° .....	129
Table 6-1: Shortest distance between processes (* $p<0.05$ when compared with MRI; # $p<0.05$ when compared with Flexion) .....	142
Table 6-2: ISP rotation and displacement in the transverse plane .....	143
Table 6-3: Distance between processes measured between approximated ISPD location at various postures and different levels (* $p<0.05$ compare with MRI; # $p<0.05$ compare with Flexion) .....	148
Table 7-1: Anatomic measurement (average $\pm$ SD) of distances: from the center of vertebral body to that of the canal (B-C), from the center of the canal to the tip of the spinous process (C-P), and from the anterior to posterior edge of the vertebral body (B) .....	157

Table 7-2: ROM (average $\pm$ SD) measured at different anatomical locations on the lumbar vertebral segments. Centers of vertebral body (B), centers of the canal (C), tips of the spinous process (P) .	158
Table 7-3: Average slope of the linear fitting lines and calculated COR locations. (+) indicating a distance anterior to the anterior edge of the vertebral body and (-) indicating a distance posterior to that. ....	159
Table 8-1: Disc degeneration graded using Pfirrmann grading for both normal and DDD subjects at the studied levels. Data reported as average $\pm$ SD. ....	170
Table 8-2: 6DOF translational and rotational ROMs in DDD group during various body positions. Shaded cells represent the primary rotations. Data are average $\pm$ SD. ....	174
Table 9-1: Numbers of subjects fall into each disc degeneration grade of Pfirrmann's classification. The grading was performed by both a radiologist and a spine surgeon. ....	189
Table 9-2: Area (average $\pm$ SD) of the discs under minimal deformation (<5%) during end ranges of torso motion. *: $p < 0.05$ between DDD and normal subjects. ....	194
Table 9-3: Tensile and shear deformations (average $\pm$ SD) at the center of the discs in the patients with DDD and in the normal subjects during end ranges of motion of the torso. *: significant differences between DDD and normal subjects, $p < 0.05$ . ....	194
Table 9-4: Maximum tensile (tension and compression) and shear deformation (average $\pm$ SD) of the discs in the patients with DDD and in the normal subjects during end ranges of motion of the torso. *: $p < 0.05$ between DDD and normal subjects, ....	196
Table 10-1: Weishaupt's classification of lumbar facet joint in normal subjects and in Patients with DDD. The values were presented as mean (standard deviation). ....	209
Table 10-2: Comparison of rotation ranges between normal and DDD groups. Primary axes of rotation were shaded. Values were mean (standard deviation) in degrees. Red Font: * $P < 0.05$ , ML: medial-lateral, AP: anterior-posterior, and CC: cranial-caudal. ....	216
Table 11-1: Material properties used in FE models. ....	233
Table 11-2: Errors in estimation of the forces and moments at the end steps of various loading cases. ....	233
Table 11-3. Errors in estimation of the overall area under the force-displacement curves of various loading cases. ....	235

Table 12-1: Material properties used in FE disc models.....	253
Table 12-2: Maximum fiber strain calculated during dynamic flexion-extension, *, compared with existing literature: Heuer [5], Schmidt [6], Tencer [7], Stokes [8] and ultimate failure strain [9]. .....	257
Table 12-3: Maximum average AF bulk strain calculated during dynamic flexion-extension. *, compare with existing <i>in vivo</i> study in Chapter 9 [10]. .....	258
Table 12-4: Maximum average AF bulk strain calculated during dynamic flexion-extension. *, compare with existing <i>in vivo</i> study in Chapter 9 [10]. **, compare with <i>in vitro</i> studies [11, 12]. .....	260





# List of Abbreviations

2 Dimensional (2D)

3 Dimensional (3D)

3 Tesla (3T)

Adjacent Segment Degeneration (ASD)

Annulus Fibrosus (AF)

Body Weight (BW)

Computer Tomography (CT)

Degenerative Disc Disease (DDD)

Digital Imaging and Communications in Medicine (DICOM)

Dual Orthogonal Fluoroscopic Imaging System (DFIS)

Finite Element (FE)

Finite Element Analysis (FEA)

Finite Element Models (FEM)

Functional Spinal Units (FSU)

Institutional Review Board (IRB)

Intervertebral disc (IVD)

Iterative Closest Point (ICP)

Low Back Pain (LBP)

Magnetic Resonance (MR)

Magnetic Resonance Imaging (MRI)

Material Testing System (MTS)

Motion Segment Unit (MSU)

Nucleus Pulposus (NP)

RadioStereometric Analysis (RSA)

Range Of Motion (ROM)

Six Degree-Of-Freedom (6DOF)

Standard Deviation (SD)

Total Disc Replacement (TDR)

# Chapter 1

## Introduction

The human lumbar spine is a masterpiece of nature and has been remodeled through millions of years of evolution (**Fig 1-1**). There are at least twelve distinct hypotheses as to how and why bipedalism evolved in humans, and also some debate as to when [1]. But there is a common agreement that bipedalism is only achieved in humans that the lumbar spine is aligned in the way it is today, i.e. the back is completely upright in humans. The complex structure and function of the lumbar spine provides adequate supports, weight bearing and providing stability, allowing us to stand, walk, run and perform all kinds of daily activities. These features have distinguished mankind from the rest of mammals since he began walking on Earth, hundreds of thousands of years ago. The knowledge of structure and function of the lumbar spine is fundamental towards *in vivo* biomechanical studies.

### 1.1 The Anatomy of Human Lumbar Spine

Knowledge of anatomy is the first step towards better understanding of lumbar spine biomechanics. The lumbar spine is responsible for protecting the spinal cord and nerve roots, providing flexibility of motion, and providing structural support and balance for an upright posture. It allows motion in six degree-of-freedom (6DOF), such as flexion-extension (forward-backward bending), side bending and twisting (torsion). Most often these motions are combined during daily functional activities. For example, bending over to pick up

money from the floor is a combination of flexion, side bending and rotation. The lumbar spine bears the weight of the superior part of the body, including head, neck, shoulders and thorax. It attempts to keep the body's weight balanced, which reduces the amount of work required by the spinal muscles and can eliminate muscle fatigue and back pain.

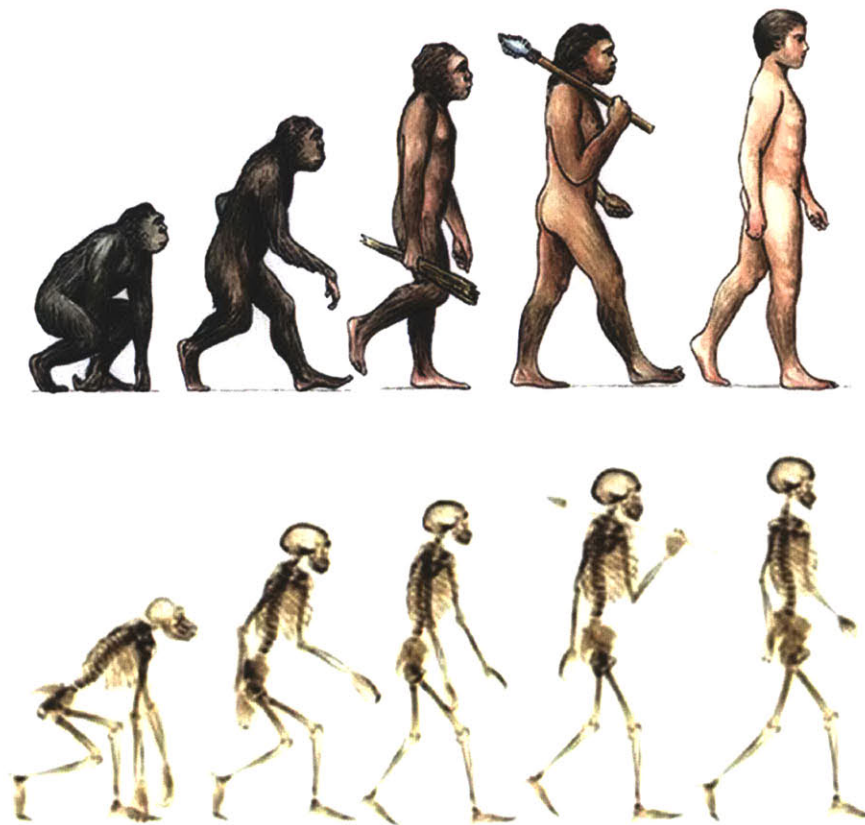


Fig 1-1. Human evolution

The lumbar spine is made up of five vertebrae, L1 to L5 (**Fig 1-2**). They are aligned straight in the coronal plane (see definition in section 1.2) in a normal spine. When viewed in the sagittal plane, the normal adult lumbar spine has a lordotic curve, i.e. a curvature in the sagittal plane with posterior concavity (concavity towards the back). Normal lumbar lordosis is 30° to 50°.

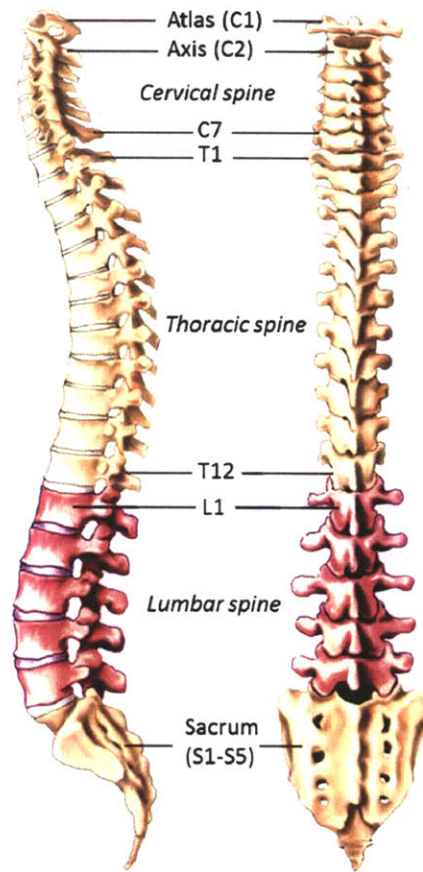


Fig 1-2. Lateral and posterior view of the spine

Each vertebra consists of several common structures that have specific features and functions (**Fig 1-3, 1-4, 1-5**. Courtesy to Schnuerer). The vertebral body is a thin ring of dense cortical bone encompassing trabecular, cancellous bone. It is shaped like an hourglass from the sagittal and coronal views, thinner in the center and thicker at the ends. It is kidney-shaped when viewed from the top,

being wider in the medial-lateral dimension than in the anterior-posterior dimension. The special structure and shape allows it to bear about 80% of the weight passing through the vertebra [2]. The superior and inferior end of each vertebral body has an endplate composed of two layers: a cartilaginous external layer and a bony internal layer (Fig 1-6). When using intervertebral fusion devices, it is important to leave as much of the bony endplate intact as possible. This will prevent subsidence of the device into the soft cancellous bone. The pedicles are two short, oval-shaped processes that extend posteriorly from the lateral margin of the dorsal surface of the vertebral body. They are made of thick cortical bone and as a result are often used as fixation points for bone screws. The laminae are two flattened plates of bone extending medially from the pedicles to form the posterior wall of the spinal canal, through which the spinal cord passes.

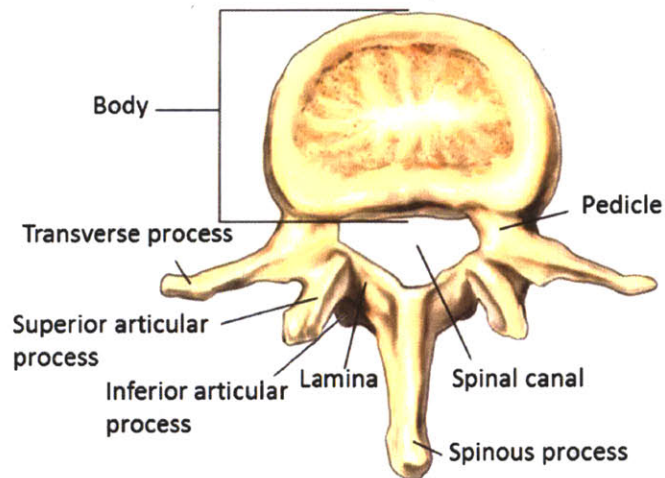


Fig 1-3. Superior view of a lumbar vertebra. Courtesy to Schnuerer.

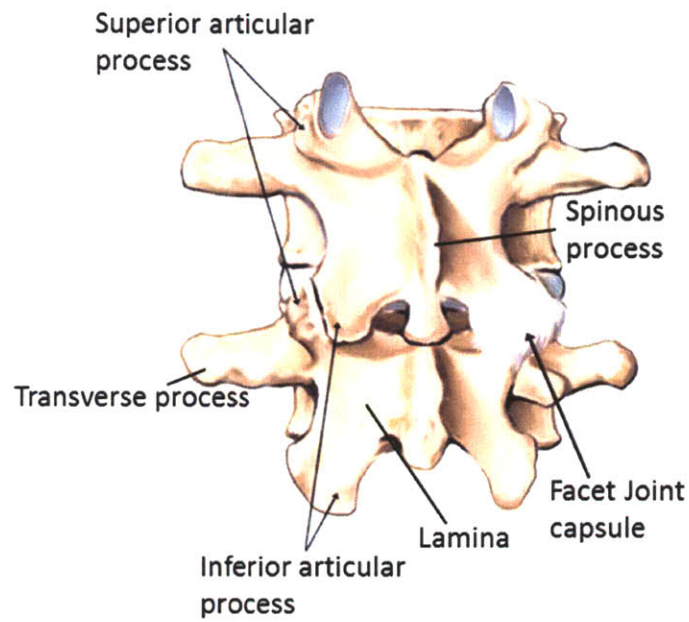


Fig 1-4. Posterior view of a lumbar vertebral motion segment

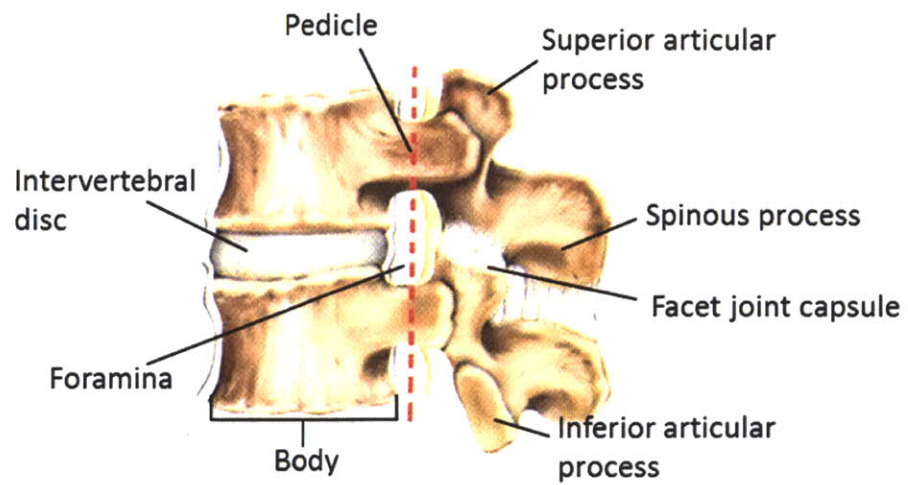


Fig 1-5. Lateral view of a lumbar vertebral motion segment

Connecting to the laminae, there are three kinds of processes that are important structures for insertion points for ligaments and tendons (**Fig 1-3, 1-4, 1-5**). There are two superior and two inferior articular processes extending from each vertebra. The superior processes join with the inferior processes of the vertebrae above to form the zygapophyseal joints, or commonly called the facet joints. They are synovial joints work in conjunction with the intervertebral disc to allow for motion between the adjacent vertebrae. The facet joints and the lateral margin of the corresponding vertebral bodies and disc enclosed the intervertebral foramina, through which the spinal nerve roots leave the spinal cord and exit to the body. The facet joints are important in stabilizing the spine. Degenerative or pathological changes at the facet joints can cause abnormal facet movements, which may results spinal pathology such as instability, spondylolisthesis and stenosis. There are two transverse processes, one on each side of the junction of the lamina and pedicle extending laterally and serving as connecting points for ligaments and tendons. A single spinous process extends posteriorly from the junction of the two laminae. Like the other processes, the spinous process serves as an attachment point for tendons and ligaments and acts as a lever to effect motion of the vertebra. Recently, minimal invasive surgical techniques have been developed with the use of interspinous process devices for the treatments of stenosis by enlarging the distance between two adjacent spinous processes.

Intervertebral discs (IVDs) are located between the two vertebral body endplates (**Fig 1-6, 1-7**. Courtesy to Schnuerer). They make up one fourth of the total length of the lumbar spinal column. The discs are composed of the annulus fibrosus and the nucleus pulposus. The annulus fibrosus makes up the outer part of the disc. It consists of a fibrous collagen matrix embedded within an aqueous gel of proteoglycans, water and other proteins [3]. It arranged in concentric layers



called lamellae (Fig 1-7). Within each lamella, the fibers are oriented obliquely about  $30^\circ$  to the horizontal and reversed in each adjacent layer. This fiber structure has great strength towards bending and torsion. The nucleus pulposus is the gelatinous internal substance of the disc. It occupies about 30-50% of the total disc volume [2]. It maintains disc pressure and acts to resist compression in axial loading forces.

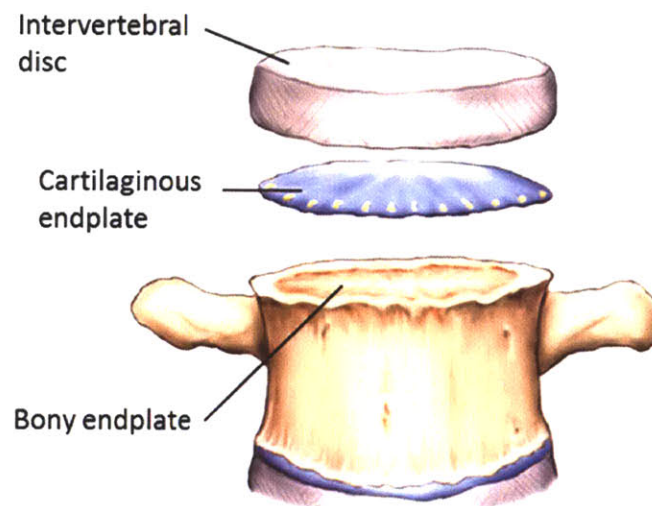


Fig 1-6. Endplate and disc

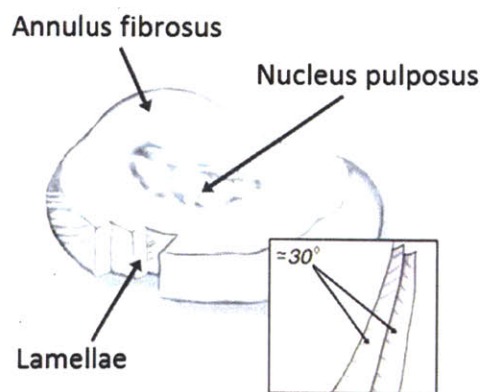


Fig 1-7. Disc anatomy

IVDs form the most important and unique articulating system in the lumbar spine, allowing for multi-planar motion of motion segments. A motion segment is the basic functional unit of the spinal column and is composed of two adjacent vertebrae, the IVD between them, the connecting facet joints and the ligamentous structures attached to the vertebrae (**Fig 1-4, 1-5**). Each disc permits slight flexion, extension, lateral flexion, rotation and some circumduction. Movement at a single motion segment is limited, but there is considerable movement throughout the lumbar spine from multiple motion segments. Besides allowing for motion, the discs act as shock absorbers to prevent injury. However, IVDs are the largest avascular (without blood supply) structures in the human body [4]. When damage of the discs happens, spontaneously repair or regeneration is not possible. A vast amount of spinal injuries and diseases are thus closely related to problems in the discs.

Sometimes, the immediate level inferior to L5, S1, is also involved in lumbar spine biomechanics studies due to the high incidence of spinal pathology at between L5 and S1 levels (**Fig 1-2**). S1 is part of the sacrum which is made up of five vertebrae that have fused to form a single bone. Thus the bony shape of S1 is different from the lumbar segments such as wedge-shaped vertebral body and fused processes. In addition, the superior endplate of S1 is angled from 30° to 60° in the horizontal plane. A great deal of shear stress is placed on the disc between L5 and S1 due to this large tilt angle.

## 1.2 Definition of basic and clinical terminologies

For a better understanding of anatomical positions and to describe lumbar spine biomechanics, in this thesis there are some words that commonly used by surgeons in the literature. These terminologies are sometimes different from daily language and scientific definitions.

Spine surgeons often refer to specific body planes to simplify three dimensional (3D) problems into two dimensional (2D) planes. There are three principal planes that divide the spine into vertical or horizontal parts. (Fig 1-8, 1-9)

Sagittal Plane (or frontal plane): divides the spine into left and right parts

Coronal Plane (or median plane): divides the spine into front and back parts

Axial Plane (or transverse plane): divides the spine into upper and lower parts

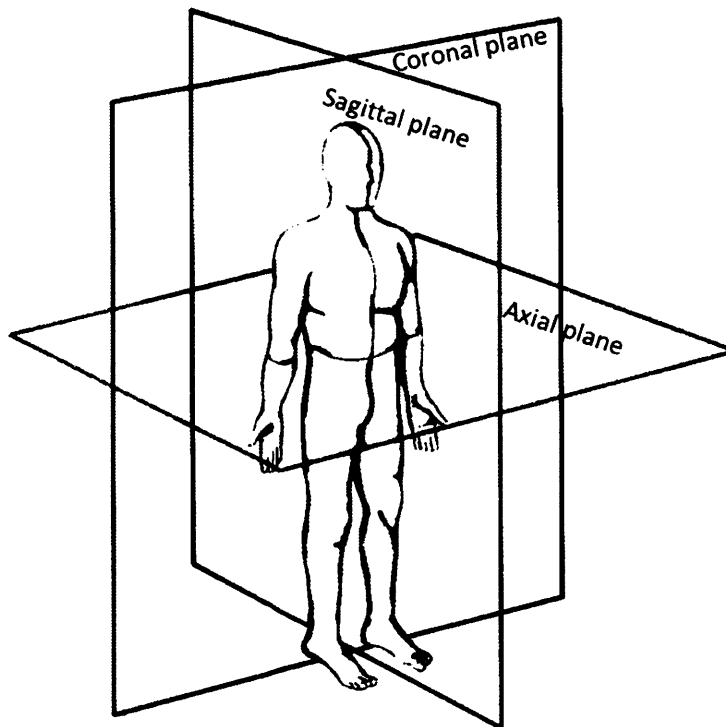


Fig 1-8. Three anatomical planes

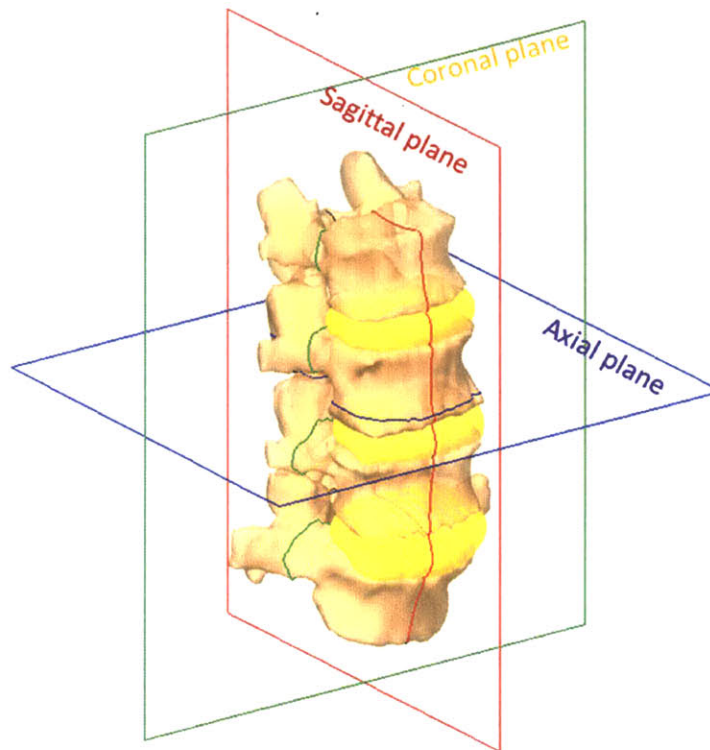


Fig 1-9. Three anatomical planes in the lumbar spine

The definition of anatomical planes is extremely important and useful for medical imaging of the lumbar spine. In lumbar spine checkup and research, magnetic resonance imaging (MRI) is usually performed with images in the sagittal plane. The mid-sagittal plane image is extensively used to evaluate the degeneration of the disc. Computed tomography (CT) is another imaging option that usually was performed with images in the axial plane, due to the physical setup that the x-ray source of the machine usually spins around a subject in the axial plane. Clinical x-ray images of the lumbar spine are usually taken as a pair in both the sagittal and coronal planes. They are commonly called lateral and AP (anterior-posterior) view images.

There are also six degree-of-freedom (6DOF), three translational and three rotational, to fully describe the location and/or motion of the lumbar spine in 3D.

In addition, in each DOF location/motion can be either positive or negative with respect to a reference. Thus, altogether twelve terms are needed to fully describe the location/motion. (Fig 1-10)

Translational DOFs:

Anterior: towards the front or in the front

Posterior: towards the back or in the back

Medial: closer to or towards the midline

Lateral: Away from the midline

Cranial (or cephalad, proximal): close to or towards head, means “up”

Caudal (or caudad, distal): close to or towards foot, means “down”

Superior: the upper part of a structure or above a specific location

Inferior: the lower part of a structure or below a specific location

The above terms can also be used as prefixes and combined, such as anterolateral, posteromedial, etc.

Rotational DOFs:

Flexion: forward bending

Extension: backward bending

Left/Right lateral bending: Left/Right side bending

Left/Right torsion: Left/Right twisting (or rotation)

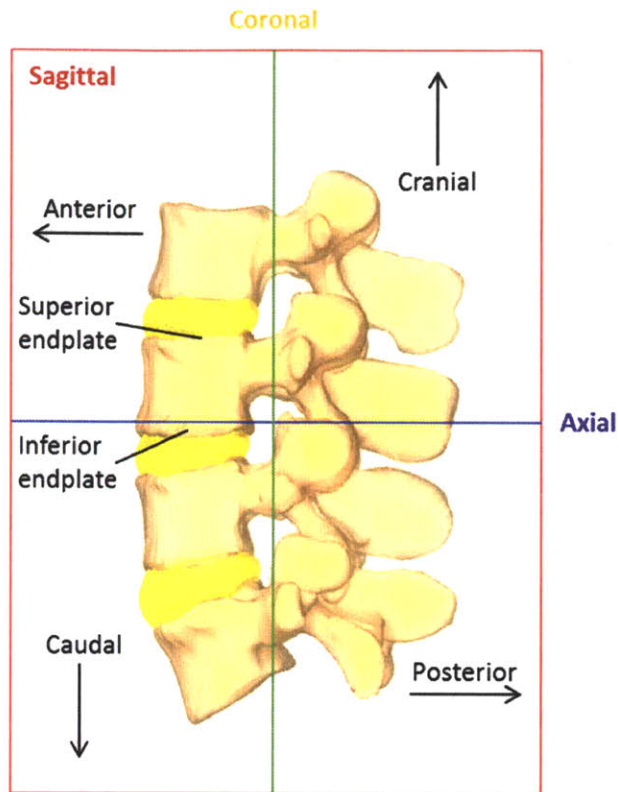


Fig 1-10. Definition of terminologies in the sagittal view

Motion of the body and the lumbar spine can both be described using the above listed 6DOF. However, body motion and spinal motion are usually different and should not be confused. When the body performed certain rotational activity in certain DOF, there is always complex combined motion in the lumbar spine. To clearly describe such combined motion in the lumbar spine, the corresponding rotational DOF is defined as primary (or principal) DOF and the rest 5 DOFs are defined as coupled motion. For example, during flexion/extension of the body, flexion/extension of the lumbar spine is the primary motion and the coupled motion is responsible for the translations, bending and twisting of the spine.

Some additional clinical terms used in this thesis include:

Hypermobility: describes the joint motion larger than is normal

Hypomobility: describes the joint motion smaller than is normal

Kyphosis, adj. kyphotic: A spinal curvature in the sagittal plane with anterior concavity

Lordosis, adj. lordotic: A spinal curvature in the sagittal plane with posterior concavity

Discogenic: Relating to a disorder originating in or from an intervertebral disc

### **1.3 Lumbar spine biomechanics**

The human lumbar spine is essentially a mechanical structure that operates via a system of levers, pivots activators and restrains. This biomechanical roles of the lumbar spine mainly consist of three parts: to allow a certain range of motion in 6DOF for the need of daily activities; to provide stability and maintain balance in both the sagittal and coronal planes for upright posture; and to sustain the majority of the weight of the trunk and upper extremities during motion.

The motion segment is the functional unit of the spine and is in essence how the spine works (Fig 1-4, 1-5). It is the smallest part of the spine that exhibits the same biomechanical behavior as the entire spinal column. The motion segment consists of two adjacent vertebrae, the IVD, the facet joints and capsules and the connecting ligamentous tissues. Corresponding to the three biomechanical roles, studies of lumbar spine biomechanics had focused essentially on determination of the ranges of motion (ROMs) of different motion segments, extending to the kinematic behavior of different components of the motion segments, i.e. mainly the IVDs and the facet joints. Stability and instability has

been studied and clinical instability criteria had been set based on the ROM of the vertebral bodies between flexion and extension (typically within 4mm for translation and 10° for rotation in the sagittal plane). Loads on the motion segment had been mainly studied through computational methods such as finite element analysis (FEA).

However, due to the complex structures, complex physiological loading conditions and limitation in techniques, knowledge of the *in vivo* biomechanics of the lumbar spine is still limited. For example, up to date, there is still no clear quantitative knowledge of the ROM of various segments of the lumbar spine, of the deformation of the discs, of the contact of the facet joints, of how the loads transfer through and shared by various structures of the lumbar spine, and much more during daily activities in living human subjects.

### **1.3.1 Diseases and abnormal biomechanics**

The knowledge of the biomechanics of the human lumbar spine in living subjects (i.e. *in vivo*) is important for understanding the etiology of spinal disease and necessary for the improvement of surgical treatments of spinal diseases which may alter the vertebral motion patterns. The lumbar spine is strong and complex, yet delicate and fragile. Like any joint, the articulations may face large and varying loads with physiological movement and ultimately may degenerate and fail. Common lumbar spine related pathologies and diseases include low back pain (LBP), degenerative disc diseases (DDD), herniated disc, instability, scoliosis, spondylolisthesis, and etc. All of which may involve abnormal vertebral biomechanics as a critical factor for causing and/or development of the disorders. However, again due to the complex anatomy and limited technology, there is currently limited published study that has investigated the biomechanics of the lumbar spine under physiologic functional activities.



LBP is an overwhelming problem in the United States and in the rest of the world. It has been reported that at least 80% of all adults will experience LBP at some point in their lifetime [5, 6]. The annual total cost exceeding \$100 billion in the United States alone [7, 8]. LBP is thought to be multi-factorial in etiology [9, 10], and DDD in the lumbar spine is the leading cause of pain. Degeneration of the disc is part of the normal aging process, is a long term process involving all the components of the motion segments. There are several grading systems to evaluate the degree of degeneration [11-14]. Based on MRI, Pfirrmann scale is one of the most commonly used clinical grading system [14] (Fig 1-11. Courtesy to Pfirrmann). The Pfirrmann grading describes the morphology of the disc as seen on axial T2-weighted MRIs. Grade I represents a homogenous bright white disc with clear distinction of annulus and nucleus. Grade V then represents inhomogeneous black disc with lost distinction of annulus and nucleus. Even though various biological and biomechanical reasons have been proposed to be related to DDD, no quantitative data has been reported to describe the mechanisms of this degeneration. Altered vertebral biomechanics has been assumed to be a critical factor leading to this development. Due to the narrowed intervertebral space as the discs are affected by the “wear and tear” of aging, motion patterns and mechanical loading of the motion segment were changed and may adversely affect the disease.



Fig 1-11. Pfirrmann grading (I-V from left to right) of disc degeneration

Herniated disc, commonly called a “ruptured disc”, is one of the most frequently surgically treated pathologies of the spine (**Fig 1-12**). It is estimated that there are over 300,000 lumbar cases performed in the United States annually [4]. Herniation is essentially the formation of a protrusion, and most frequently occurs at the posterior lateral margins of the disc. The structural changes are not the same as those seen with DDD. DDD is part of the normal aging process, which is a long term process involving all the components of the motion segments. Herniation is thought to be the culmination of a series of acute traumatic events to the disc, such as lifting heavy weight. It is of great interest to study biomechanics of the disc such as deformation and loads, especially at the posterior lateral part to understand the mechanism of herniation and help prevent the pathology.

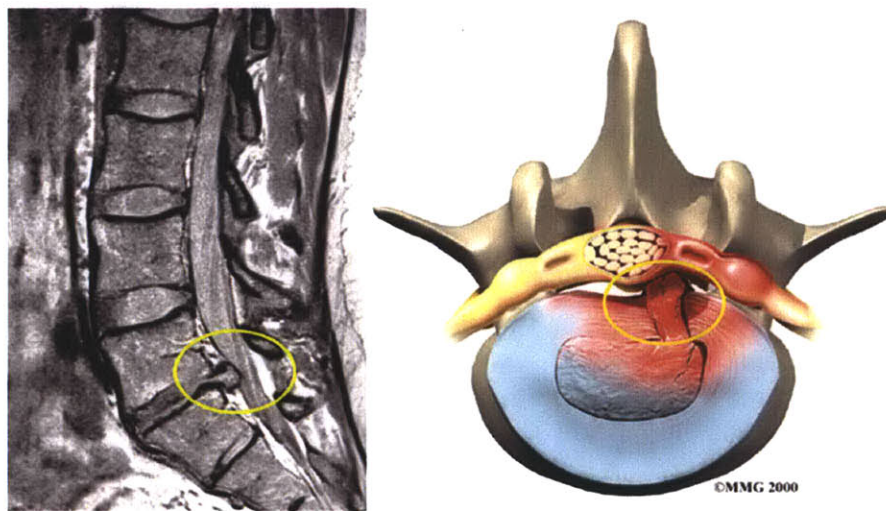


Fig 1-12. Example of a herniated disc on MRI and in a sketch

Instability of the spine may be caused by a myriad of disorders, including degenerative changes or deformities like spondylolisthesis. Gradual degeneration of the disc may permit excessive movement of the segment, resulting in pain from trapped neurologic elements. Spondylolisthesis is a defect in the lamina allows the vertebral body to slip forward (**Fig 1-13**). This may result in an abnormal

amount of motion of the affected segment and thus pain. There is much confusion and debate among spine surgeons as to when the spine is considered to be unstable. Under physiologic loads, the normal spine is able to provide two important stabilizing features. First, the normal spine limits the amount of displacement of the vertebral structures so that injury or irritation does not occur to neurologic tissues. Second, the spine maintains its structural integrity, preventing the development of significant deformity and/or debilitating pain. Therefore, the spine is generally considered unstable if displacement of its structures results in actual or potential neurologic injury, or if pain or deformity results from its incapacity to carry physiologic loads. In either case, the knowledge of biomechanics such as physiological motion or loads is fundamental to evaluate stability.

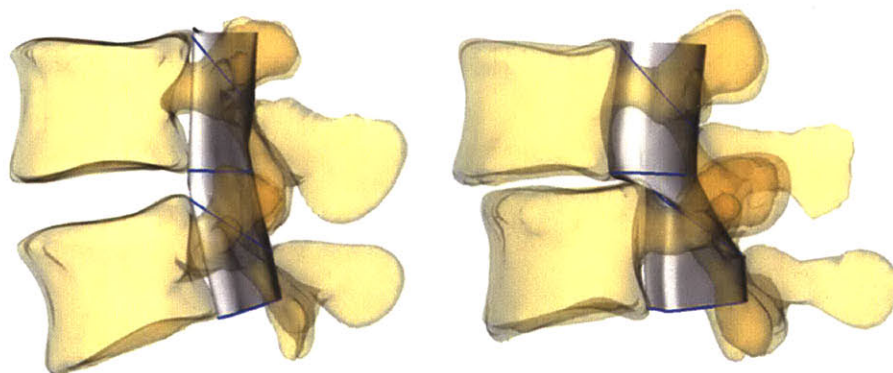


Fig 1-13. Normal motion segments (left) and segments with spondylolisthesis (right)

### **1.3.2 Surgeries and altered biomechanics**

Lumbar fusion surgery or arthrodesis remains the "gold standard" for treating LBP patients who are not helped by nonsurgical methods (**Fig 1-14**). It is called a "spine fusion" because the surgery involves placing small morsels of bone either in the front of the spine (in the disc space) and/or along the posterior of the

spine so that the bone grows together and fuses that section of the spine. The fusion is designed to eliminate motion in that fused segment of the spine, thereby decreasing or eliminating the back pain created by the motion. Although many people with low back pain find relief with lumbar fusion, the results of the surgery vary. There are many reasons for the failure to improve after fusion surgery, but some believe it may be due to the fact that fusion prevents normal motion in the spine. In addition, it has been reported that in patients with DDD, the IVDs adjacent to the diseased levels have a greater tendency to degenerate [15-17], especially after surgical fusion treatment of the diseased segments [18-21]. In a literature review by Park et al., [22] the incidence of lumbar adjacent segment degeneration (ASD) after arthrodesis has been reported to range from 5.2% to 100%, whereas the incidence of symptomatic ASD range from 5.2% to 18.5%. Numerous studies have suggested that altered biomechanics, such as abnormal loading and/or motion patterns [22-24], are the causative factors of ASD.

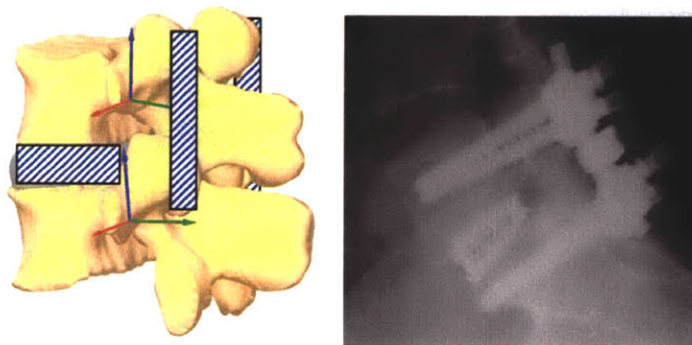


Fig 1-14. Idea of spinal fusion and anterior and posterior fusion on X-ray.

Nonfusion devices such as total disc replacement (TDR) or arthroplasty has emerged as an alternative treatment option for low back pain (**Fig 1-15**). Similar to hip or knee joint replacements, a disc replacement substitutes a mechanical device for an IVD in the spine. The device is meant to restore motion to the spine by replacing the worn, degenerated disc. Artificial discs are designed to maintain

intervertebral space, provide an acceptable, if not normal, range of spine motion. TDR has been suggested to normalize spinal mobility and biomechanics and thereby reduce the incidence of adjacent spinal deterioration. Although the early results of total disc replacement are satisfactory, the basic premise that motion preservation will diminish ASD is yet to be proven [25, 26]. A recent review by Harrop et al. [27] noted that the incidence of ASD is approximately 9% after arthroplasty, whereas the incidence of symptomatic ASD is approximately 1%.

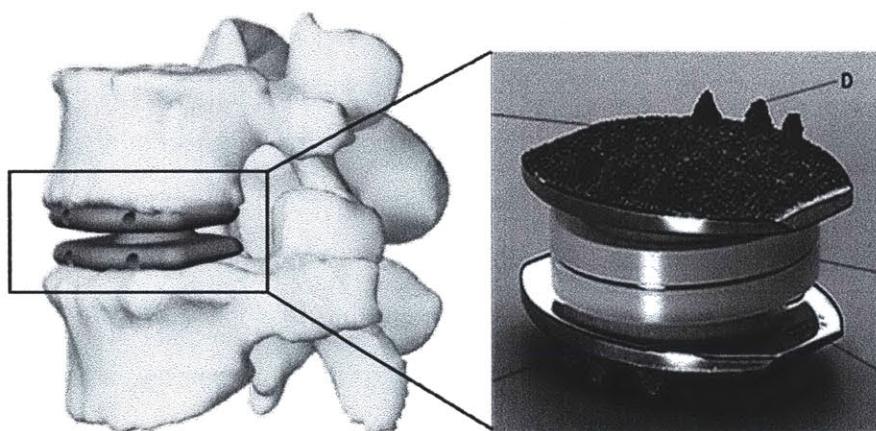


Fig 1-15. Example of an artificial disc

Abnormal biomechanical changes at the adjacent segments after surgical treatments of the DDD have been reported in both arthrodesis and arthroplasty patients, in terms of mobility [28-32], change in disc height [28, 33-35], loading on the facet joints [36-40], intradiscal pressure [41-44], disc bulging [45], and stress-strain [26, 46, 47]. All of these have suggested surgical treatments can have an adverse effect on ASD. Therefore, a quantitative knowledge of the biomechanics at the adjacent segments under physiologic weight-bearing conditions is instrumental to delineate the biomechanical factors associated with ASD.

## 1.4 Objective and Approach

The above background information has revealed that the knowledge of lumbar spine biomechanics in living human subjects is fundamental for understanding mechanisms of spinal injury and pathology, for improvement of corresponding clinical treatments, and for design of spinal prosthesis. However, due to the complicated spinal anatomy and loading conditions as well as high risks in direct measurements, it has been a challenge to determine the *in vivo* biomechanics of the lumbar spine. To address this problem, the overall objective of this thesis was to develop and implement a dual fluoroscopic imaging system (DFIS) to non-invasively study human lumbar spine biomechanics. The newly developed technique involves various medical imaging techniques, such as MRI, CT and digital fluoroscopic imaging. The fundamental principle behind the technique is utilizing 3D to 2D imaging matching to quantify the *in vivo* lumbar spine biomechanics. 3D MRI/CT models of the lumbar spine segments are constructed and matched to the features of the spine acquired on 2D fluoroscopic images in the two perpendicular views during different physiologic functional activities to study lumbar spine biomechanics. Details of the system will be presented in **Chapter 2** of this thesis.

To complete the overall objective, three goals were set and completed longitudinally. The first goal was to quantify the ability of the DFIS to determine vertebral kinematics. Accuracy of the technique to determine 6DOF translation and rotation of the lumbar spine were studied using material testing system (MTS) and radiostereometric analysis (RSA) as gold standards. Repeatability was tested both *in vitro* and *in vivo*. The second goal was to implement this technique to investigate spinal motion in both healthy subjects and pathological patients. As a first time, 6DOF motion of different structures of the spine, such as vertebral body,

intervertebral disc, facet joint and spinous process were measured *in vivo* in both healthy subjects and patients with lumbar pathologies during functional activities. The third goal was to explore the feasibility of using kinematic data obtained from this system as boundary conditions in FEA to calculate the physiological loads on the IVDs. Preliminary studies have shown the applicability and high accuracy of finite element modeling to calculate disc loads using *in vivo* vertebral kinematics as displacement boundary conditions.

## 1.5 Organization of the Thesis

This thesis is organized into 13 chapters. **Chapter 2** describes our DFIS system setup to study *in vivo* lumbar spine biomechanics and discusses the accuracy and repeatability of the technique. **Chapter 3 to 7** focus on the kinematics of various structures of the normal healthy lumbar spine. **Chapter 3** investigates the ROM of lumbar vertebrae segments of different levels in normal healthy subjects. **Chapter 4** investigates the deformation of the IVDs. **Chapter 5** investigates the motion of the facet joints. **Chapter 6** investigates the motion of the spinous processes. **Chapter 7** summarizes the motion characteristics of the normal healthy lumbar spine and investigates centers of rotation. Correspondingly, **Chapter 8 to 10** studied the ROM, disc deformation, motion of the facet joints, and the spinous processes in patients with lumbar spine disorders and compared with those of the normal subjects. Further, **Chapter 11** discusses utilizing a robotic testing protocol to validate the approach that used kinematic boundary conditions as inputs in FEA to calculate disc loads. **Chapter 12** extends the *in vivo* kinematic responses of the lumbar spine obtained from the DFIS to calculated disc loads in FEA. **Chapter 13** presents summary of the findings of this thesis and implications for future studies.

This work is based on the following publications:

**Wang S, Passias P, Li G, Li G, Wood K.** “Measurement of vertebral kinematics using noninvasive image matching method-validation and application.” *Spine (Phila Pa 1976)*. 2008 May 15;33(11):E355-61.

**Li G, Wang S, Passias P, Xia Q, Li G, Wood K.** “Segmental *in vivo* vertebral motion during functional human lumbar spine activities.” *Eur Spine J*. 2009 Jul;18(7):1013-21. Epub 2009 Mar 20.

**Xia Q, Wang S, Kozanek M, Passias P, Wood K, Li G.** “*In vivo* motion characteristics of lumbar vertebrae in sagittal and transverse planes.” *J Biomech*. 2010 Jul 20;43(10):1905-9. Epub 2010 Apr 9.

**Kozanek M, Wang S, Passias PG, Xia Q, Li G, Bono CM, Wood KB, Li G.** “Range of motion and orientation of the lumbar facet joints *in vivo*.” *Spine (Phila Pa 1976)*. 2009 Sep 1;34(19):E689-96.

**Xia Q, Wang S, Passias PG, Kozanek M, Li G, Grottkau BE, Wood KB, Li G.** “*In vivo* range of motion of the lumbar spinous processes.” *Eur Spine J*. 2009 Sep;18(9):1355-62. Epub 2009 Jun 19.

**Wang S, Xia Q, Passias P, Wood K, Li G.** “Measurement of geometric deformation of lumbar intervertebral discs under *in vivo* weight-bearing condition.” *J Biomech*. 2009 Apr 16;42(6):705-11. Epub 2009 Mar 6.

**Passias PG, Wang S, Kozanek M, Xia Q, Li W, Grottkau B, Wood KB, Li G.** “Segmental lumbar rotation in patients with discogenic low back pain during functional weight-bearing activities.” *J Bone Joint Surg Am*. 2011 Jan 5;93(1):29-37.



Li W, Wang S, Xia Q, Passias P, Kozanek M, Wood K, Li G. “Lumbar facet joint motion in patients with degenerative disc disease at affected and adjacent levels: an *in vivo* biomechanical study.” *Spine (Phila Pa 1976)*. 2011 May 1;36(10):E629-37.

Wang S, Xia Q, Passias P, Li W, Wood K, Li G. “How does lumbar degenerative disc disease affect the disc deformation at the cephalic levels *in vivo*?” *Spine (Phila Pa 1976)*. 2011 Apr 20;36(9):E574-81.

Wang S, Park WM, Gadikota, HR, Miao J, Kim YH, Wood KB, Li G. “A combined numerical and experimental technique for estimation of the forces and moments in the lumbar intervertebral disc.” *Comput Methods Biomech Biomed Engin.*[In Press]

## 1.6 References

1. Lovejoy, C.O., *Evolution of human walking*. Sci Am, 1988. **259**(5): p. 118-25.
2. White, A.A. and M.M. Panjabi, *Clinical biomechanics of the spine*. 2nd ed. 1990, Philadelphia: Lippincott. xxiii, 722 p.
3. Iatridis, J.C., et al., *Degeneration affects the anisotropic and nonlinear behaviors of human annulus fibrosus in compression*. J Biomech, 1998. **31**(6): p. 535-44.
4. Schnuerer, A.P., J. Gallego, and M.S. Danek, *Basic anatomy and pathology of the spine*. 2003: Medtronic Sofamor Danek.
5. Jandric, S. and B. Antic,[*Low back pain and degenerative disc disease*]. Med Pregl, 2006. **59**(9-10): p. 456-61.
6. Kosharsky, B. and D. Rozen,[*Discogenic low back pain. Minimally invasive interventional therapies*]. Anesthesiol Intensivmed Notfallmed Schmerzther, 2007. **42**(4): p. 262-7.
7. Katz, J.N., *Lumbar disc disorders and low-back pain: socioeconomic factors and consequences*. J Bone Joint Surg Am, 2006. **88** Suppl 2: p.

- 21-4.
8. Eubanks, J.D., et al., *Prevalence of lumbar facet arthrosis and its relationship to age, sex, and race: an anatomic study of cadaveric specimens*. Spine, 2007. **32**(19): p. 2058-62.
  9. Smedley, J., et al., *Natural history of low back pain. A longitudinal study in nurses*. Spine, 1998. **23**(22): p. 2422-6.
  10. Heliovaara, M., et al., *Descriptive epidemiology and public health aspects of low back pain*. Ann Med, 1989. **21**(5): p. 327-33.
  11. Modic, M., *Degenerative disc disease: genotyping, MR imaging and phenotyping*. Skeletal Radiol, 2007. **36**: p. 91-93.
  12. Kuisma P, K.J., Haapea M, Lammentausta E, Niinimaki J, *Modic changes in vertebral endplates: a comparison of MR imaging and multislice CT*. Skeletal Radiol, 2009. **38**: p. 141-147.
  13. Kjaer P, K.L., Bendix T, Sorensen J, Leboeuf-Yde C, *Modic changes and their associations with clinical findings*. Eur Spine J, 2006. **15**: p. 1312-1319.
  14. Pfirrmann C, M.A., Zanetti M, Hodler J, Boos N, *Magnetic resonance classification of lumbar intervertebral disc degeneration*. Spine, 2001. **26**: p. 1873-1878.
  15. Elfering, A., et al., *Risk factors for lumbar disc degeneration: a 5-year prospective MRI study in asymptomatic individuals*. Spine (Phila Pa 1976), 2002. **27**(2): p. 125-34.
  16. Waris, E., et al., *Disc degeneration in low back pain: a 17-year follow-up study using magnetic resonance imaging*. Spine (Phila Pa 1976), 2007. **32**(6): p. 681-4.
  17. Ghiselli, G., et al., *Adjacent segment degeneration in the lumbar spine*. J Bone Joint Surg Am, 2004. **86-A**(7): p. 1497-503.
  18. Lee, C.K., *Accelerated degeneration of the segment adjacent to a lumbar fusion*. Spine (Phila Pa 1976), 1988. **13**(3): p. 375-7.
  19. Goel, V.K., J.N. Weinstein, and editors, *Biomechanics of the Spine - Clinical and Surgical Perspective*. 1990, Boca Raton, FL: CRC press.
  20. Kumar, M.N., F. Jacquot, and H. Hall, *Long-term follow-up of functional outcomes and radiographic changes at adjacent levels following lumbar spine fusion for degenerative disc disease*. Eur Spine J, 2001. **10**(4): p. 309-13.
  21. Phillips, F.M., J. Reuben, and F.T. Wetzel, *Intervertebral disc degeneration adjacent to a lumbar fusion. An experimental rabbit model*. J Bone Joint Surg Br, 2002. **84**(2): p. 289-94.
  22. Park, P., et al., *Adjacent segment disease after lumbar or lumbosacral fusion: review of the literature*. Spine (Phila Pa 1976), 2004. **29**(17): p.

- 1938-44.
23. Adams, M.A., et al., *Mechanical initiation of intervertebral disc degeneration*. Spine (Phila Pa 1976), 2000. **25**(13): p. 1625-36.
  24. Stokes, I.A. and J.C. Iatridis, *Mechanical conditions that accelerate intervertebral disc degeneration: overload versus immobilization*. Spine (Phila Pa 1976), 2004. **29**(23): p. 2724-32.
  25. Anderson, P.A. and J.P. Rouleau, *Intervertebral disc arthroplasty*. Spine (Phila Pa 1976), 2004. **29**(23): p. 2779-86.
  26. Chen, S.H., et al., *Biomechanical comparison between lumbar disc arthroplasty and fusion*. Med Eng Phys, 2009. **31**(2): p. 244-53.
  27. Harrop, J.S., et al., *Lumbar adjacent segment degeneration and disease after arthrodesis and total disc arthroplasty*. Spine (Phila Pa 1976), 2008. **33**(15): p. 1701-7.
  28. Frymoyer, J.W., et al., *A comparison of radiographic findings in fusion and nonfusion patients ten or more years following lumbar disc surgery*. Spine (Phila Pa 1976), 1979. **4**(5): p. 435-40.
  29. Stokes, I.A., et al., *1980 Volvo award in clinical sciences. Assessment of patients with low-back pain by biplanar radiographic measurement of intervertebral motion*. Spine (Phila Pa 1976), 1981. **6**(3): p. 233-40.
  30. Axelsson, P., R. Johnsson, and B. Stromqvist, *The spondylolytic vertebra and its adjacent segment. Mobility measured before and after posterolateral fusion*. Spine (Phila Pa 1976), 1997. **22**(4): p. 414-7.
  31. Panjabi, M., et al., *Hybrid testing of lumbar CHARITE discs versus fusions*. Spine (Phila Pa 1976), 2007. **32**(9): p. 959-66; discussion 967.
  32. Auerbach, J.D., et al., *Segmental contribution toward total lumbar range of motion in disc replacement and fusions: a comparison of operative and adjacent levels*. Spine (Phila Pa 1976), 2009. **34**(23): p. 2510-7.
  33. Guigui, P., et al., *[Long-term influence of associated arthrodesis on adjacent segments in the treatment of lumbar stenosis: a series of 127 cases with 9-year follow-up]*. Rev Chir Orthop Reparatrice Appar Mot, 2000. **86**(6): p. 546-57.
  34. Schulte, T.L., et al., *Disc height reduction in adjacent segments and clinical outcome 10 years after lumbar 360 degrees fusion*. Eur Spine J, 2007. **16**(12): p. 2152-8.
  35. Ekman, P., et al., *A prospective randomised study on the long-term effect of lumbar fusion on adjacent disc degeneration*. Eur Spine J, 2009. **18**(8): p. 1175-86.
  36. Lee, C.K. and N.A. Langrana, *Lumbosacral spinal fusion. A biomechanical study*. Spine (Phila Pa 1976), 1984. **9**(6): p. 574-81.
  37. Bastian, L., et al., *Evaluation of the mobility of adjacent segments after*

- posterior thoracolumbar fixation: a biomechanical study.* Eur Spine J, 2001. **10**(4): p. 295-300.
38. Denoziere, G. and D.N. Ku, *Biomechanical comparison between fusion of two vertebrae and implantation of an artificial intervertebral disc.* J Biomech, 2006. **39**(4): p. 766-75.
  39. Rohlmann, A., et al., *Comparison of the effects of bilateral posterior dynamic and rigid fixation devices on the loads in the lumbar spine: a finite element analysis.* Eur Spine J, 2007. **16**(8): p. 1223-31.
  40. Park, C.K., K.S. Ryu, and W.H. Jee, *Degenerative changes of discs and facet joints in lumbar total disc replacement using ProDisc II: minimum two-year follow-up.* Spine (Phila Pa 1976), 2008. **33**(16): p. 1755-61.
  41. Chow, D.H., et al., *Effects of short anterior lumbar interbody fusion on biomechanics of neighboring unfused segments.* Spine (Phila Pa 1976), 1996. **21**(5): p. 549-55.
  42. Chen, C.S., C.K. Cheng, and C.L. Liu, *A biomechanical comparison of posterolateral fusion and posterior fusion in the lumbar spine.* J Spinal Disord Tech, 2002. **15**(1): p. 53-63.
  43. Weinhoffer, S.L., et al., *Intradiscal pressure measurements above an instrumented fusion. A cadaveric study.* Spine (Phila Pa 1976), 1995. **20**(5): p. 526-31.
  44. Cunningham, B.W., et al., *The effect of spinal destabilization and instrumentation on lumbar intradiscal pressure: an in vitro biomechanical analysis.* Spine (Phila Pa 1976), 1997. **22**(22): p. 2655-63.
  45. Kim, Y.E., et al., *Effect of disc degeneration at one level on the adjacent level in axial mode.* Spine (Phila Pa 1976), 1991. **16**(3): p. 331-5.
  46. Chiang, M.F., et al., *Biomechanical comparison of instrumented posterior lumbar interbody fusion with one or two cages by finite element analysis.* Spine (Phila Pa 1976), 2006. **31**(19): p. E682-9.
  47. Kumar, N., et al., *Analysis of stress distribution in lumbar interbody fusion.* Spine (Phila Pa 1976), 2005. **30**(15): p. 1731-5.

# Chapter 2

## Study *in vivo* lumbar spine biomechanics: system setup and validation

### 2.1 System setup and technical details

With the technological advancements in medical imaging such as magnetic resonance imaging (MRI) and computed tomography (CT), highly accurate 3D anatomical models of the lumbar spine with sub-millimeter precision can be recreated. On the other hand, fluoroscopes, which is essentially low dose digital x-ray machines, is capable of recording real time quasi-static and dynamic 2D perspective image of the lumbar spine during functional activities while subjects are not restricted in prone or supine position as in MRI or CT. Taking advantage of the advanced imaging techniques, 3D to 2D imaging matching was the core concept behind the newly developed combined MRI/CT and dual orthogonal fluoroscopic imaging system (DFIS) technique [1]. In summary, highly accurate 3D models are obtained through MRI and CT. Two fluoroscopes are positioned in a perpendicular setup so that pairs of 2D lumbar spine images can be taken simultaneously during various functional activities. Compare to conventional single plane x-ray or fluoroscopic imaging, the dual orthogonal setup can account for both in-plane and out-of-plane accuracy. After obtained the images, a virtual dual fluoroscopes setup were recreated in a computer environment, where 6DOF

positions and orientations of the 3D lumbar spine models can be quantitatively determined from matching the 3D models to the excessive 2D features in fluoroscopic images. When model and features are matched, the kinematics of the lumbar spine at the corresponding positions is determined.

The system setup and technical details of MRI, CT, fluoroscopy and matching process were included in this Chapter.

### **2.1.1 MRI**

MRI can be used to create anatomic 3D model of lumbar spine. Patients are asked to lie supine in a 3 Tesla (3T) MRI machine (MAGNETOM Trio, Siemens, Germany). Using a spine surface coil and a T2 weighted fat suppressed 3D SPGR sequence [2], parallel sagittal images with a thickness of 1.5 mm without gap, and with a resolution of 512 x 512 pixels were obtained. A field of view of 220×220 mm is able to capture the whole lumbar vertebral segment from level L1 to S1. (**Fig 2-1**)

The MR images of the lumbar spine were then imported into a solid modeling software Rhinoceros® (Robert McNeel & Associates, Seattle, WA) to construct a 3D anatomical model of the segments using a protocol established in our laboratory [3]. The contours of the vertebrae bodies were digitized manually based on image intensity using B-Spline curves (**Fig 2-2a**). The contour lines were then output into Rhinoceros to construct a 3D anatomical mesh model of the segments. An example of the digitization and mesh is shown in (**Fig 2-2b**).



Fig 2-1. Mid-sagittal MRI slice of the lumbar spine using the custom protocol

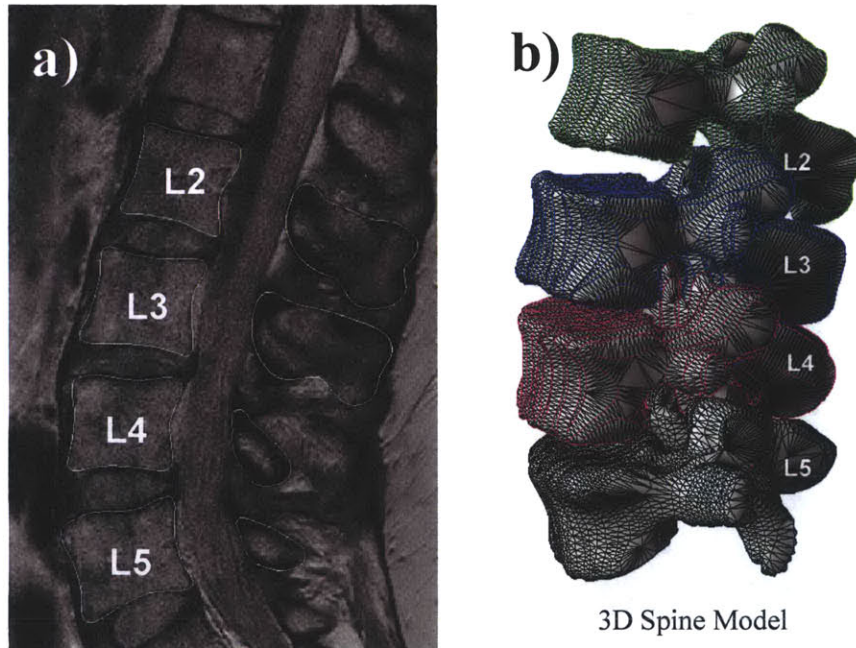


Fig 2-2. a) Digitization of vertebral contours. b) 3D vertebral mesh models

### 2.1.2 CT

The spine model can also be obtained from CT scanner (LightSpeed Pro16, GE, Waukesha, WI) using high-resolution axial plane images in the supine position. Images were obtained with a thickness of 0.625 mm and a gap of 0.625 mm, and with a resolution of 512 x 512 pixels. The CT images of the spinal segment were then imported into Matlab® (the MathWorks, Natick, MA). Based on the gradient of image intensity caused by bony structures, automated Canny edge detection algorithm implemented in Matlab has been utilized to automatically segment the vertebral bodies [4]. The edges created are further reduced by applying a threshold and examining connectivity (**Fig 2-3a**).

Due to the complex geometry of lumbar vertebral anatomical structures and the inherent lack of an edge in biological images, the outlines from the automatic edge detection are manually reviewed. Manual editing is especially necessary at the facet joints at between inferior facets of the proximal segments and superior facets of the distal segments as there are decrease in intensity gradient. After this semi-automatic edge outline procedure, 3D anatomical mesh models of the vertebrae were created from the digitized data (**Fig 2-3b,c**).



Fig 2-3. a) Automatic segmentation on CT. b) 3D model constructed from the digitized data. c) Individual vertebra mesh model after manual editing.



### **2.1.3 MRI and CT comparison**

MRI and CT have their own merits and drawbacks in general and in specific for the imaging matching technique to study lumbar spine biomechanics. CT images may facilitate automatic segmentation with better image quality to identify bony structures. In contrast, segmentation for MR models currently still relies on human eyes and manual labor and is time consuming. However, the better image intensity on bony structures in CT scans was achieved at the cost of high radiation dosage. This may present an ethical concern for the safety of the individuals being tested. Furthermore, MRI provides with greater visualization of the ligamentous and soft tissues surrounding the lumbar vertebra as well as their relation to relevant neurologic structures in this area, which may facilitate the evaluation of subject specific health/degeneration condition of the lumbar spine. Therefore, although more time consuming in modeling, MRI is preferred in most cases in the studies in the following Chapters unless the subject is a patient and CT is part of the clinical routine checkup.

Since CT models have been widely used by researchers to study spine kinematics [5-14] and CT model is generated from automatic segmentation based on Canny edge detection, we employed it as a comparison with MR models. The constructed CT and MR image-based spine models were then mapped together using a customized code implemented in the Matlab based on the iterative closest point (ICP) method [15]. About 4000 points were picked from both vertebral body models. The determination of the optimal shape matching of the two models was characterized by a convergence criterion that using changes in directional derivative of the matching process [15]. The average difference between the two mesh models was calculated to be  $0.07 \pm 1.1$  mm when mapping MR model to CT model. **(Fig 2-4)** The results showed good agreement between MR and CT

models, thus both MR and CT models can be used interchangeably in the image matching process.

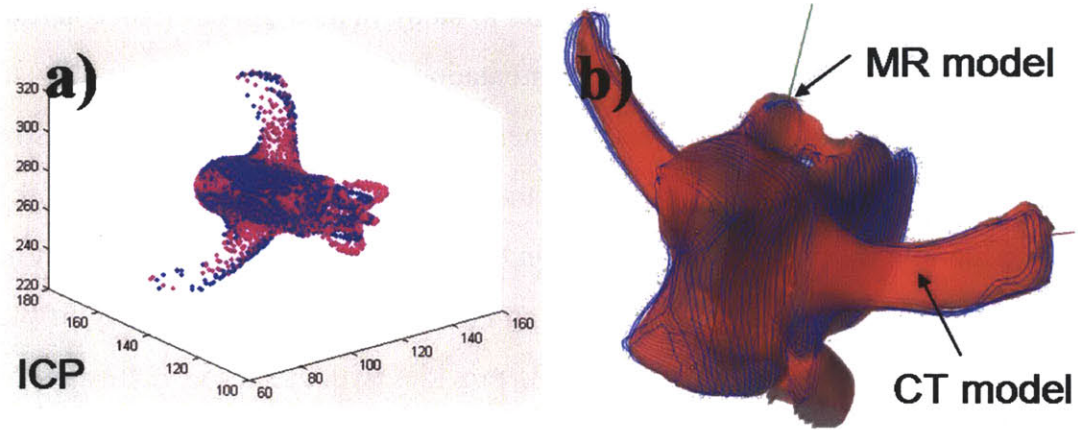


Fig 2-4. a) Iterative closest point algorithm registers the ovine MRI model with CT model. b) Comparison suggests satisfying geometric agreement with subtle differences.

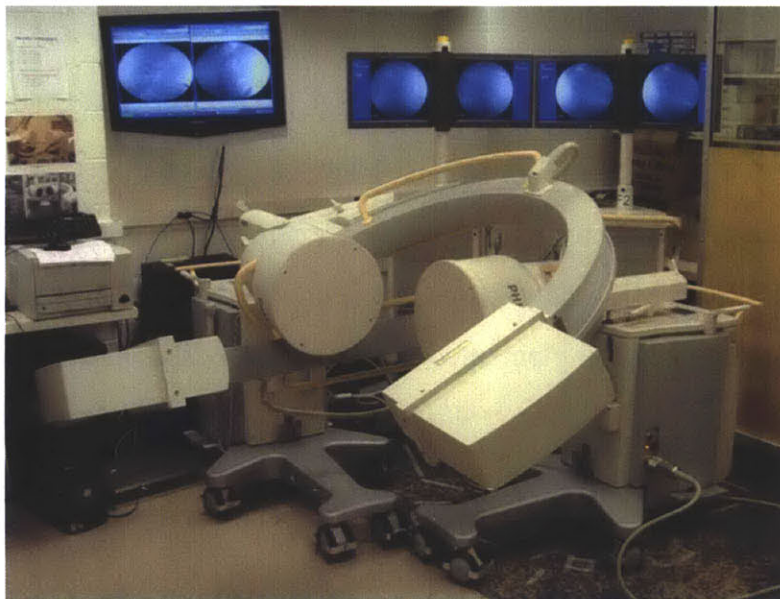


Fig 2-5. DFIS setup

#### **2.1.4 Dual orthogonal fluoroscopic**

The DFIS consists of two fluoroscopes (BV Pulsera, Philips, Netherlands) positioned perpendicular to each other. A subject is free to move within the common imaging zone of the two fluoroscopes (up to  $30 \times 30 \times 30 \text{ cm}^3$ ). The system is capable to capture real time images of the spine segments simultaneously. A demonstration of the DFIS is shown in **Fig 2-5**.

The fluoroscopes use pulsed snapshots to capture images. In quasi-static mode, a pair of images is taken when the lumbar spine of the subject is at the desired posture. In dynamic mode, the fluoroscopes have a maximum frame rate of 125Hz. 30, 15, or 8 snapshot images per second can be selected that are evenly distributed among the 125 Hz frame rate, which can efficiently reduce the radiation exposure under a high frame rate. The fluoroscope has a clearance of approximately 1 m between the X-ray source and the receiver, allowing the subject to be imaged by the fluoroscopes in real time as he or she actively performs different maneuvers. With a 1K x 1K resolution of both fluoroscopes, the total imaging volume can reach up to  $30 \times 30 \times 30 \text{ cm}^3$ .

The fluoroscopic images commonly suffer from small amounts of distortion caused by the slightly curved surface of the image intensifier and environmental perturbations of the x-ray. In order to remove "swirl" caused by electro-magnetic disturbance and "fish-eye" from the curved image surface, a known plexi-glass plate grid with a pattern of holes in concentric circles is imaged and the subsequent image is mapped to the known geometry (**Fig 2-6**). A global surface mapping using a polynomial fitting technique adapted from Gronenschild is used to correct the image distortion [16].

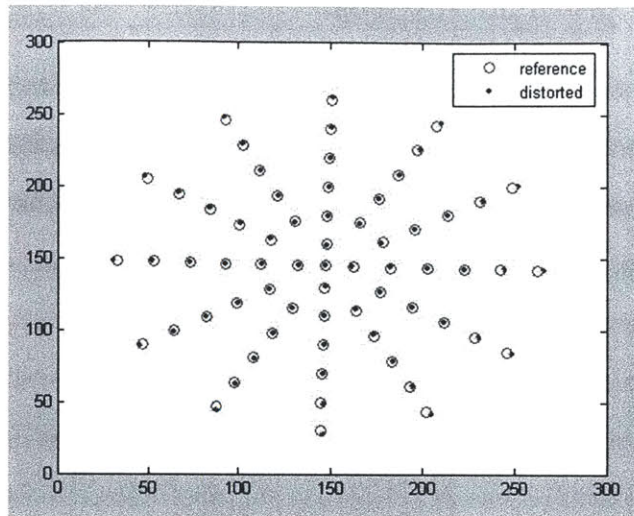


Fig 2-6. A patterned plexi-plate used to restore the distortion.

### **2.1.5 Matching**

The geometry of the dual fluoroscopes from these tests was reproduced virtually in Rhinoceros. Pairs of fluoroscopic images were placed at the two virtual intensifiers. The CT/MR models of the vertebrae were introduced into the virtual system and viewed from the perspective views of the virtual sources. The 3D models were then independently translated and rotated in 6DOF until their projections matched the osseous outlines of the fluoroscopic images from the two orthogonal views (**Fig 2-7**) [1].

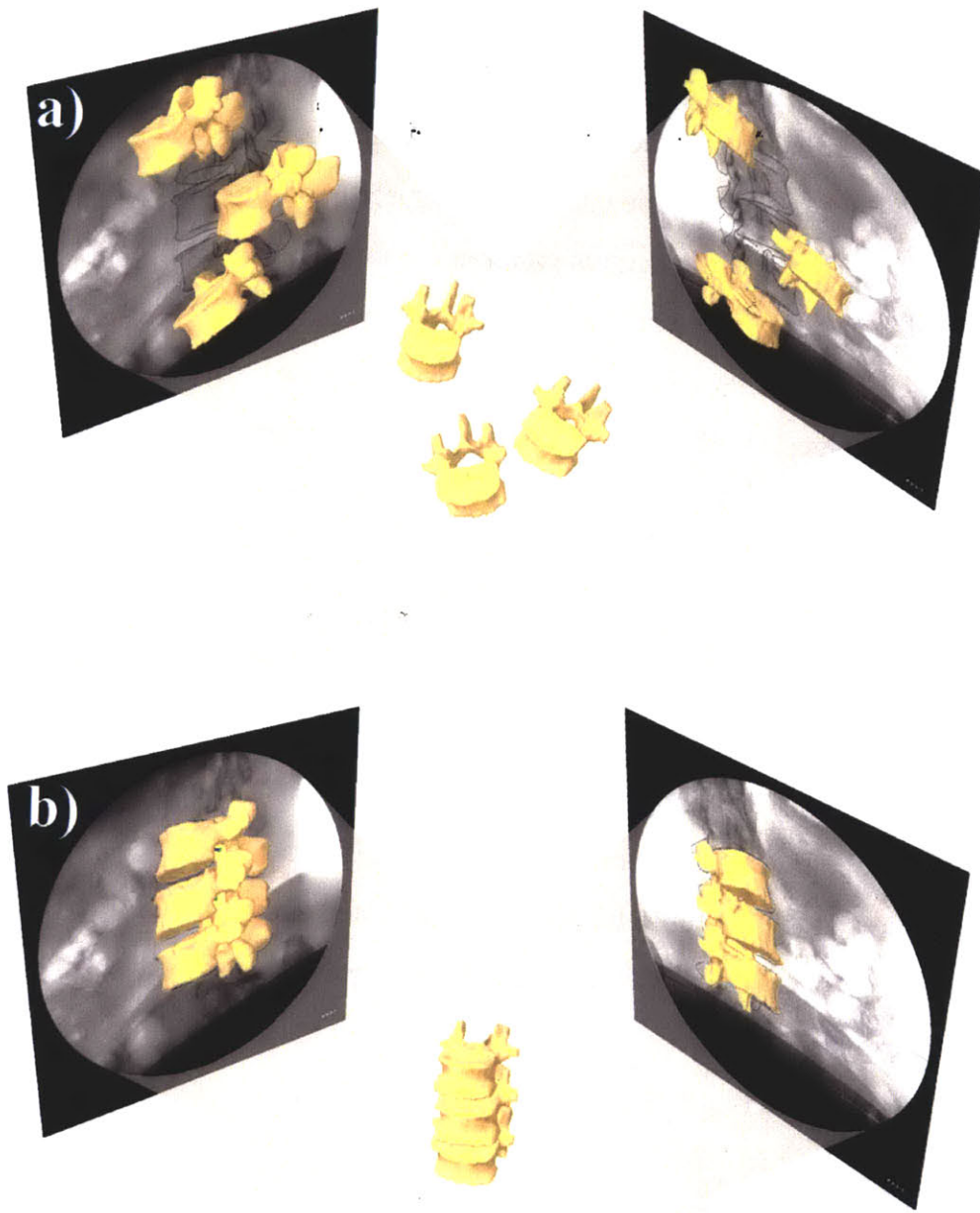


Fig 2-7. a) Virtual computer environment of DFIS with 3D MRI vertebral models. b) Matching 3D model to 2D features on fluoroscopic images.

The *in vivo* positions of the vertebrae at various physiologic functional weight-bearing positions can be reproduced in the Rhinoceros using the 3D models of the vertebrae and the orthogonal fluoroscopic images [1]. The pair of fluoroscopic images of the spine captured at a specific posture were imported into the modeling software and placed in calibrated orthogonal planes, reproducing the actual positions of the image intensifiers of the fluoroscopes. Two virtual cameras were created inside the virtual space to reproduce the positions of the x-ray sources with respect to the image intensifiers. Therefore, the geometry of the DFIS can be recreated in the solid modeling software Rhinoceros. The MR or CT image-based 3D vertebral models will then be introduced into the virtual fluoroscopic system and viewed from the perspective views of the two virtual cameras (**Fig 2-7a**). The 3D models of the vertebrae could be independently translated and rotated in 6DOF until their outlines match the osseous outlines captured on the two orthogonal fluoroscopic images. This process can be executed using an existing protocol established in our laboratory [17]. The software allowed the model to be manually translated and rotated in increments of 0.01 mm and 0.01. Using this technique, the vertebral positions during *in vivo* weight-bearing activities are reproduced, representing the 6DOF kinematics at each *in vivo* posture (**Fig 2-7b**).

#### **2.1.6 Data analysis**

After reproducing the *in vivo* vertebral positions using the 3D anatomic vertebral models, the relative motions of the vertebrae can be analyzed using right hand Cartesian coordinate systems constructed at different anatomic land marks of the vertebrae. For example, to study the ROM of the vertebral body, the geometric center of the vertebra body is chosen as the origin of the coordinate system (**Fig 2-8**). The x-axis is in coronal plane and pointed to the left direction;

the y-axis is in the sagittal plane and pointed to the posterior direction; and the z-axis is perpendicular to the x-y plane and pointed proximally. The relative motions of the proximal vertebra with respect to the distal vertebra can thus be calculated at different vertebral levels. Three translations using x, y and z are defined as the motions of the proximal vertebral coordinate system origin in the distal coordinate system: anterior-posterior, left-right and proximal-distal translations. Three rotations using  $\alpha$ ,  $\beta$  and  $\gamma$  are defined as the orientations of the proximal vertebral coordinate system in the distal vertebral coordinate system using Euler angles (in x-y-z sequence): flexion-extension, left-right side bending and left-right twisting (**Fig 2-8**).

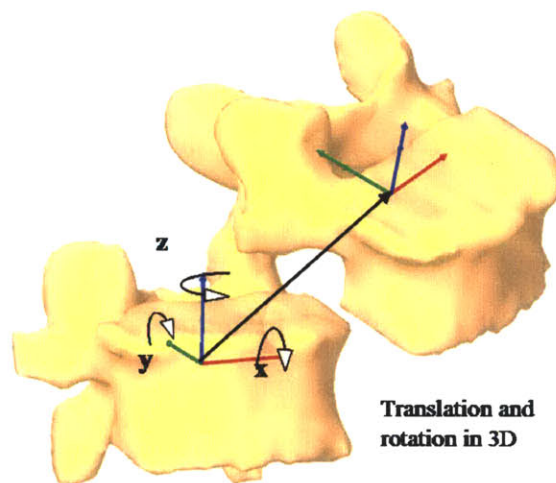


Fig 2-8. Coordinate system used to describe 6DOF vertebrae kinematics.

### 2.1.7 Summary

To understand the biomechanical factors that affect spinal pathology, it is critical to accurately determine the spinal structural functions under *in vivo* physiologic functional activities. While many approaches have been taken to study spine kinematics, quantitative understanding of the human spine

biomechanics under *in vivo* physiologic functional activities is elusive. Limitations of current technology and the complex anatomy of the spine have made *in vivo* data limited. A newly developed, non-invasive imaging technique was proposed to quantitatively investigate the intrinsic biomechanics of human spine under physiologic functional activities. The system setup and technique details were discussed in this section. The accuracy of this technique will be validated in the following section.

## 2.2 Validation

In the previous section the idea for employing a non-invasive image matching technique has been illustrated. The accuracy and repeatability however, requires careful validation before this method can be efficiently applied in spine biomechanics study. The overall goal is to investigate the feasibility for clinical application of the novel technique. The validation of this technique was conducted in three phases [1]. The first step used an ovine spine specimen to validate the accuracy of the technique of determining the spine positions in space, compared with the results from a material testing system (MTS) machine as gold standard. Both CT and MR based image models were constructed for the ovine vertebrae in this validation. The second phase used a human cadaveric lumbar spine implanted with titanium bead. Kinematics of the cadaveric vertebrae during manual motion was compared with those from beads based radio stereometric analysis (RSA) as gold standard [18]. The third phase was the application of this method to a living human subject in order to determine if the repeatability of the method was maintained under *in vivo* conditions. Only MR model has been used to minimize the radiation dosage to the subject.



### 2.2.1 Ovine vertebrae validation

#### Experiment setup

An ovine lumbar spine specimen, with all the surrounding soft tissues intact was selected and L2 and L3 vertebrae were focused for this study. The ovine spine is proved to share similar anatomic features as human spine [19]. The spine was CT and MR scanned according to the protocol in the previous section. The contours of L2 and L3 were digitized from both CT and MR images to reconstruct 3D mesh models. The constructed CT and MR image-based models were then mapped together using a customized code implemented in the Matlab based on the ICP method. A local coordinate system was created for each spine vertebral segment model (**Fig 2-9**). In this study, 6DOF was expressed using the x, y and z axes for left-right, anterior-posterior and proximal-distal translations and using  $\alpha$ ,  $\beta$  and  $\gamma$  in Euler angle x-y-z sequence for flexion-extension, left-right bending and left-right rotation of the vertebrae. For the purpose of comparison, the same coordinate system was used by both CT and MRI models.

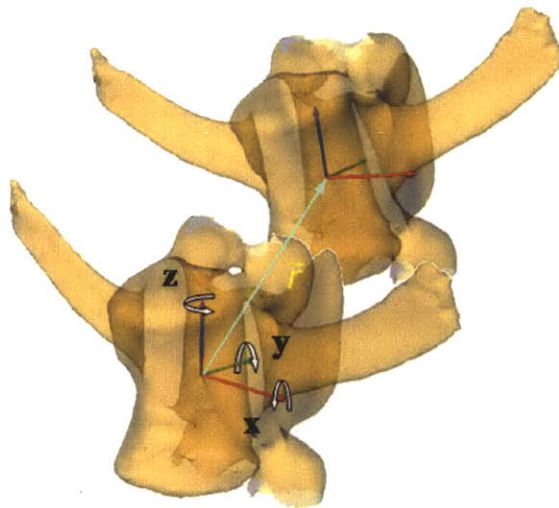


Fig 2-9. Local coordinate system to determine 6DOF kinematics of the ovine lumbar spine.

The specimen was imaged during two tests using DFIS to validate the accuracy and repeatability. First, a gold standard for precisely obtain spine positions was chosen by using an MTS machine (MTS QTest 5, Minneapolis, MN). The MTS machine has an accuracy of 0.001 mm in translation. The specimen was bounded to the MTS machine which moves vertically upward at 1000 mm/min while dynamic images were taken by the DFIS (Fig 2-10). This test was aimed to validate the accuracy of the image system in determination of spine translation and speed. In the other test, the specimen was manually flexed to simulate dynamic physiologic flexion-extension motion (Fig 2-11). Dynamic orthogonal images were taken simultaneously from the posteromedial and posterolateral directions aimed at the target spinal segment.

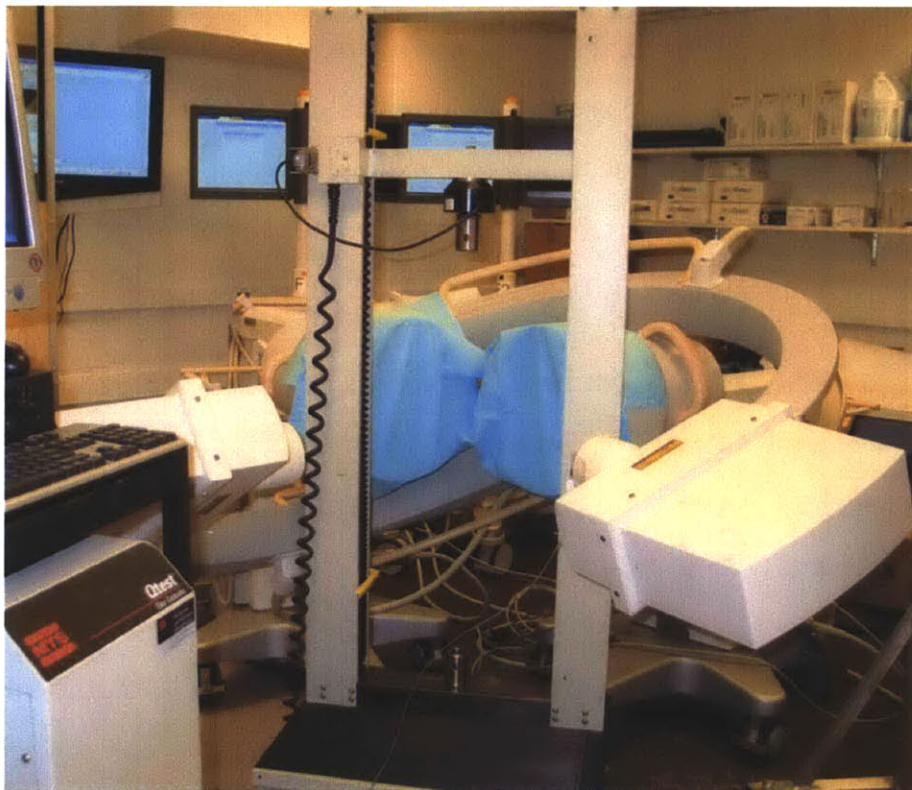


Fig 2-10. Experiment setup of MTS machine and DFIS

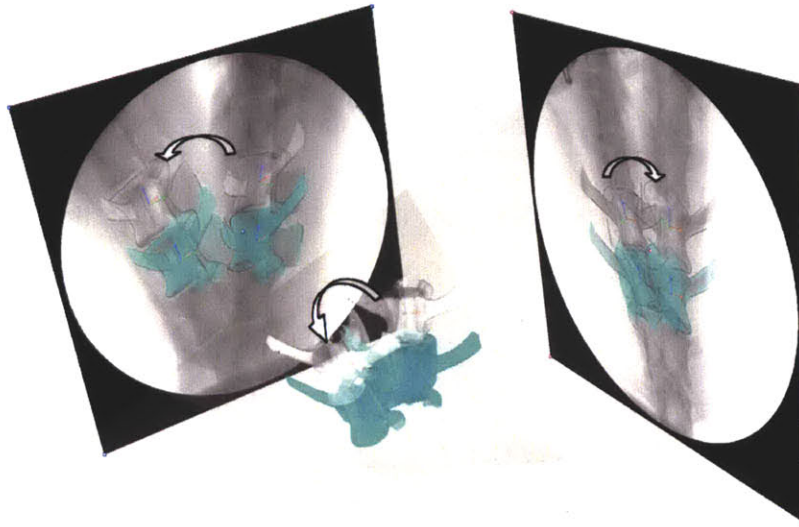


Fig 2-11. Imaging matching during manual flexion-extension of the lumbar spine.

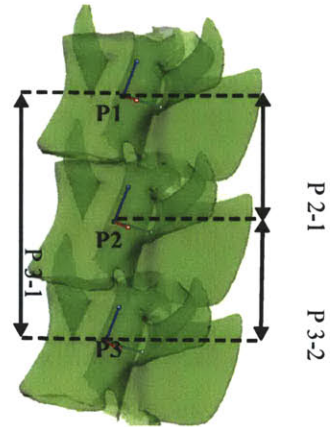
The spatial positions of the vertebral bodies during the motion on the MTS machine and the manual flexion-extension activities were reproduced in Rhinoceros software through 3D to 2D imaging matching, detailed in the last section. To evaluate the accuracy of the image matching technique in reproducing vertebral motion, three positions were chosen from the dynamic motion path of the spine that was created using the MTS machine. The exact (to four decimal places) time for each position was obtained from the fluoroscopic radiation impulse data file recorded during the experiment. The distances moved by the MTS machine between the 3 positions were calculated from these time intervals and the known MTS speed. Each of the 3 positions was reproduced 5 times independently using both the CT and MR models and the dual fluoroscopic images as illustrated in the inset Fig in **Table 2-1**. The displacements of the L2 and L3 vertebrae were calculated between the 3 positions. The translational speed of the vertebra was calculated between the different positions. The displacement and speed data obtained from the 5 model image matching processes were averaged and

expressed as mean  $\pm$  standard deviation (SD). These data were compared with those of the MTS machine (gold standard) to examine the accuracy of the image matching method in reproducing the spine translation and speed.

To evaluate the repeatability of using the image matching method to reproduce the dynamic spine motion, five positions along the manual dynamic flexion-extension path were determined 5 times using both the CT and MRI based models and the corresponding dual fluoroscopic images. The positions and orientations of the L2 with respect to L3 vertebrae were calculated at each selected flexion-extension position. The repeatability in 6DOF was evaluated from the average of the SDs of matching results of the 5 positions of the spine along the flexion-extension path.

Table 2-1: Accuracy of the image matching method in terms of vertebrae motion distance and speed

		P 2-1	P 3-2	P 3-1	
Distance (mm)	<b>MTS</b>	<b>33.32 mm</b>	<b>33.33 mm</b>	<b>66.64 mm</b>	
	<b>CT</b>	<b>L2</b>	33.52 $\pm$ 0.18	33.27 $\pm$ 0.09	66.81 $\pm$ 0.19
		<b>L3</b>	33.39 $\pm$ 0.17	33.15 $\pm$ 0.13	66.55 $\pm$ 0.14
	<b>MRI</b>	<b>L2</b>	33.72 $\pm$ 0.35	33.14 $\pm$ 0.32	66.88 $\pm$ 0.23
		<b>L3</b>	33.23 $\pm$ 0.25	33.35 $\pm$ 0.17	66.72 $\pm$ 0.19
	Speed (mm/s)	<b>MTS</b>	<b>16.67 (mm/s)</b>		
<b>CT</b>		<b>L2</b>	16.77 $\pm$ 0.09	16.64 $\pm$ 0.04	16.71 $\pm$ 0.05
		<b>L3</b>	16.71 $\pm$ 0.09	16.56 $\pm$ 0.07	16.64 $\pm$ 0.03
<b>MRI</b>		<b>L2</b>	16.87 $\pm$ 0.17	16.56 $\pm$ 0.16	16.72 $\pm$ 0.06
		<b>L3</b>	16.63 $\pm$ 0.13	16.66 $\pm$ 0.08	16.65 $\pm$ 0.05



## Results

The displacements of the spine segment between the three positions along the MTS moving path were 33.32 mm (P1-P2), 33.33 mm (P2-P3) and 66.64 mm (P1-P3), respectively, for both L2 and L3 vertebra. The model matching process showed a high accuracy in determining the positions of the spinal segments (**Table 2-1**). Both CT and MR image-based models could determine the spine traveling distances with an absolute mean accuracy below 0.2 mm. The maximal differences compared to those of the MTS machine measurements were 0.20 mm for the CT model and 0.40 mm for the MR model. Compared with the standard MTS speed of 16.67 mm/s, the CT model reproduced a speed between 16.58 and 16.77 mm/s. The MR model reproduced a speed between 16.57 and 16.87 mm/s. The absolute speed errors were within 0.2 mm/s for both CT and MR models. The accuracy validation using the MTS as a gold standard did not show a significant difference between CT and MR model matching ( $p=0.2$ ) in determination of traveling distance and speed of the spine.

The matching process of the dual orthogonal fluoroscopic system was found to be highly repeatable in determining the 6DOF positions and orientations of the vertebrae using both the CT and MR models (**Table 2-2**). From 5 positions along the flexion-extension motion path, the relative position and orientation of L2 with respect to L3 were determined with a SD less than 0.2 mm using the CT model and 0.25 mm using the MR model. The relative orientation could be determined to be  $0.4^\circ$  to  $0.6^\circ$  for CT model and  $0.6^\circ$  to  $0.9^\circ$  for MR model.

Table 2-2: 6DOF repeatability of reproducing the relative vertebral positions. x: left-right (medial lateral), y: anterior-posterior, z: proximal-distal,  $\alpha$ : flexion-extension,  $\beta$ : left-right bending,  $\gamma$ : left-right rotation

	Translation DOFs (mm)			Rotational DOFs (°)		
	x	y	z	$\alpha$	$\beta$	$\gamma$
<b>CT</b>	0.18	0.11	0.18	0.42	0.59	0.53
<b>MR</b>	0.26	0.18	0.25	0.55	0.79	0.89

## 2.2.2 Human cadaveric lumbar spine validation

### Experiment setup

Consider the potential anatomic and functional difference between the ovine and human, a validation test was designed to evaluate the accuracy of the imaging technique in the determination of human lumbar spine kinematics. A human cadaveric lumbar spine with all the surrounding soft tissues intact was selected and L3, L4 and L5 vertebrae were focused for this study (Fig 2-12). The spine was implanted with titanium beads of 4 mm diameter and MR scanned according to the protocol in the previous section. The contours of L3, L4 and L5 and the beads were digitized to reconstruct 3D mesh models. A local coordinate system was created for each spine vertebral segment model according to section 2.1.6. The specimen was manually flexed to simulate dynamic physiologic flexion-extension motion. Dynamic orthogonal images were taken simultaneously from the anteromedial and anterolateral directions aimed at the target spine.

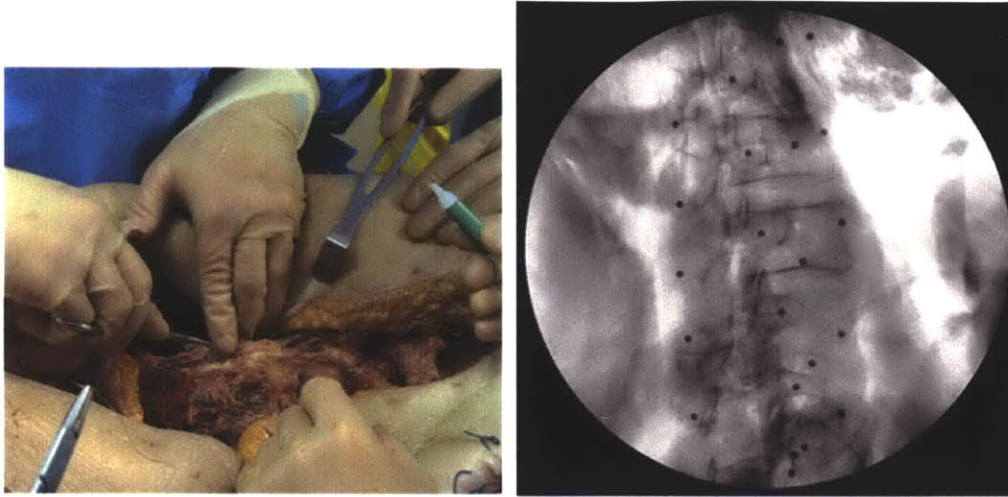


Fig 2-12. Implantation of metal beads in human cadaveric spine for RSA validation

The spatial positions of the vertebral bodies during the manual flexion-extension activities were reproduced in Rhinoceros software through 3D to 2D imaging matching (**Fig 2-13**). To evaluate the accuracy of the image matching technique in reproducing vertebral motion, five positions were chosen along the dynamic motion path of the spine: maximum flexion, sub flexion, upright, sub extension and maximum extension. At each of the position, two kinds of 3D to 2D matching were performed: manual matching and RSA matching (gold standard). Ignoring the beads, the vertebrae were individually matched to their bony outlines as which will be performed in real *in vivo* studies. In addition, ignoring the vertebrae and based on the idea of RSA [18], the set of beads were automatically calculated to match their outlines. This is achieved by using a custom Matlab code that calculates the optimized position and orientation of the beads set where the sum of the distances between the projections of the beads and their actually locations on the fluoroscopic images is minimized. The corresponding positions of the vertebrae when the beads were at the optimized calculated locations were determined and chosen as gold standard. The accuracy

of the matching technique was evaluated by comparing the vertebrae positions and orientations from manual matching to RSA matching.

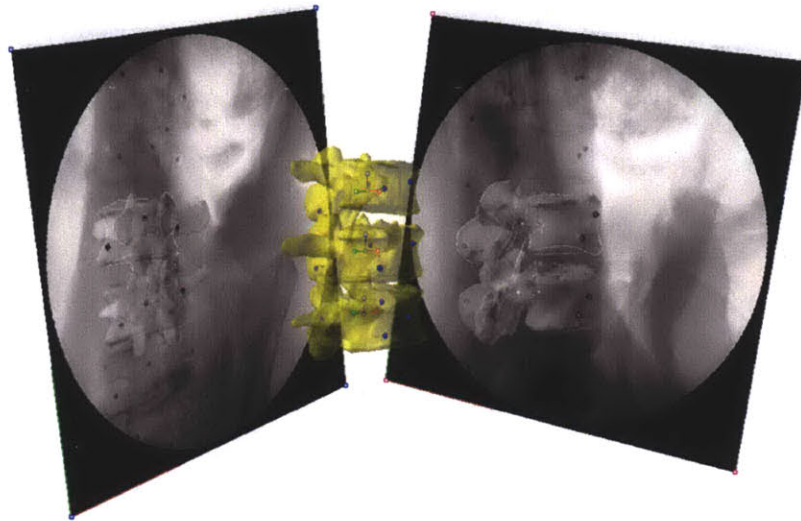


Fig 2-13. Image matching of the human cadaveric spine implanted with beads

Table 2-3. Average 6DOF accuracy in reproduce positions and orientations of lumbar vertebrae with respect to RSA as gold standard. x: left-right (medial lateral), y:anterior-posterior, z: proximal-distal,  $\alpha$ : flexion-extension,  $\beta$ : left-right bending,  $\gamma$ : left-right rotation

	Translation DOFs (mm)			Rotational DOFs ( $^{\circ}$ )		
	x	y	z	$\alpha$	$\beta$	$\gamma$
<b>L3</b>	0.22	0.09	0.23	0.55	0.52	0.63
<b>L4</b>	0.18	0.11	0.25	0.57	0.60	0.69
<b>L5</b>	0.25	0.21	0.30	0.63	0.70	0.74



## Results

The model matching process showed a high accuracy in determining the positions of the spinal segments. The average translational and rotational accuracy of L3, L4 and L5 vertebrae were within 0.3 mm and 0.7° from the 5 tested positions along the flexion-extension path. (**Table 2-3**)

### 2.2.3 *In vivo validation*

#### Experiment setup

Consider the difference between the *in vitro* and *in vivo* subject motion, the image matching method was again applied to a living subject (Female, 60 years old) to evaluate the repeatability of the model matching method. Prior to the initiation of the study, approval by the institutional review board (IRB) and written consent from the subject were obtained. The subject was evaluated for the absence of LBP and other spinal disorders. The subject underwent an MR scan of the lumbar spine using the same protocol as in 2.1.1. The 3D MR images were used to construct the 3D model of lumbar spine. A CT scan was not performed to avoid the extensive radiation on the subject. The subject was protected by specifically designed lead vests and skirts (**Fig 2-14a**) and was asked to stand in the DFIS and the lumbar spine was imaged in the following sequence of positions: standing, maximal left twist, maximal right twist, and forward flexion at approximately 45°. Using the matching method, the relative position of the L2 with respect to L3 vertebra was reproduced 5 times at each tested position (**Fig 2-14b**). The repeatability of this technique to evaluate *in vivo* lumbar kinematics was determined by the SDs of 6DOF translations and rotations (**Fig 2-15**) from 5 times of matching.

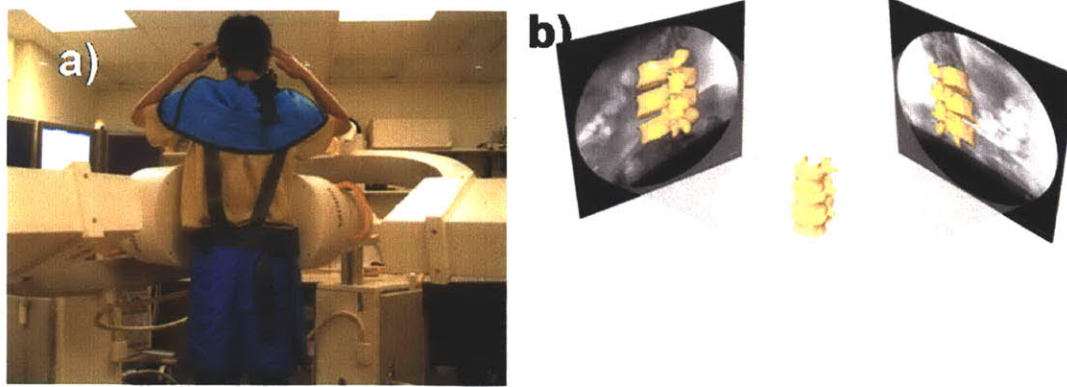


Fig 2-14. a) Experiment setup of testing living subjects in DFIS b) Reproduction of the *in vivo* vertebrae position from matching

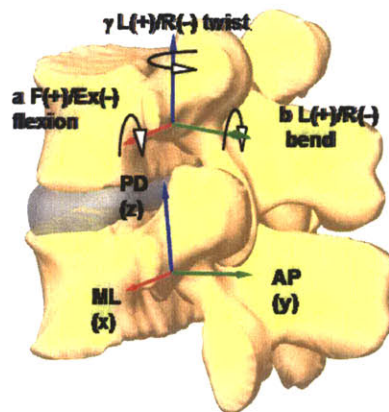


Fig 2-15. Vertebral models and local coordinates used to determine 6DOF kinematics.

L/R: left/right, ML: medial-lateral, AP: anterior-posterior, PD: proximal-distal.

## Results and discussion

The repeatability in reproducing *in vivo* human spine kinematics (the relative positions of the L2 segment with respect to the L3 segment) was shown in **Table 2-4** for various *in vivo* spine positions. For all the *in vivo* physiologic loading positions, the relative translation could be determined within a SD of 0.3 mm, while the orientation could be determined within 0.7°, which is comparable with the ovine validation studies from **2.2.3**.

Table 2-4: 6DOF repeatability of the relative positions of L2 with respect to L3 from 5 times of matching at various body positions. x: left-right, y: anterior-posterior, z: proximal-distal,  $\alpha$ : flexion-extension,  $\beta$ : left-right bending,  $\gamma$ : left-right rotation

	Translation DOFs (mm)			Rotational DOFs (°)		
	x	y	z	$\alpha$	$\beta$	$\gamma$
<b>Standing</b>	0.29	0.28	0.21	0.46	0.65	0.47
<b>Flexion</b>	0.30	0.22	0.22	0.56	0.62	0.63
<b>Left Twist</b>	0.29	0.27	0.23	0.68	0.56	0.43
<b>Right Twist</b>	0.33	0.24	0.18	0.75	0.66	0.56

### 2.2.4 Summary

We have developed an imaging matching technique using 3D vertebral models from CT/MRI and 2D spine images from DFIS to measure *in vivo* spine kinematics. Three tests were designed using DFIS to rigorously evaluate the accuracy and repeatability of this technique. In literature, a few pioneer studies have investigated spinal vertebral motion using CT imaging [5-8, 14, 20] with accuracy larger than 1 mm in translation and 1° in orientation. The MR combined DFIS technique is able to determine 6DOF vertebral translations and orientations within high accuracy of 0.3 mm and 0.7°, and repeatability of 0.3 mm and 0.6°.

## 2.3 Discussion and Conclusion

Quantitative knowledge of *in vivo* vertebral biomechanics is instrumental for understanding spinal pathology and for the improvement of the surgical treatment of spinal disorders. The MR combined DFIS image matching method showed a potential non-invasive way for studying *in vivo* spine kinematics under physiologic functional weight-bearing activities. This Chapter described the system setup and technical details as well as presented a rigorous validation of the MRI/CT combined DFIS image matching technique for the measurement of spinal motion. The accuracy of this technique was first validated using an ovine specimen for the determination of vertebral displacement and speed using those from MTS machine as gold standard. The accuracy of this technique was validated again using human cadaveric lumbar spine and RSA as gold standard. The data indicated that the method has accuracy within 0.3 mm and 0.7° in determination of vertebra translations and orientations. The repeatability of the method was also examined using both *in vitro* and *in vivo* experimental design setups. Both the CT and MR image-based model showed similar accuracy and repeatability in the *in vitro* tests. The *in vivo* human spine experiment using MR model demonstrated a high repeatability of the method in determination of vertebra within 0.3 mm and 0.7° for vertebral translations and orientations.

The MR models resulted in similar and sufficient accuracy and repeatability for the purpose of this study compare to CT models. CT images may facilitate automatic segmentation with commercially available software. In contrast, automatic segmentation for MR models is currently time consuming. However, the radiation dosage to which the subjects are exposed when using CT may present a safety and ethical concern for the safety of the individuals being tested. Alternatively, MR model provide us with greater visualization of the ligamentous

components surrounding the lumbar vertebra as well as their relation to relevant neurologic structures in this area. Therefore, MRI is preferred and used in most cases in the following Chapters unless the subject is a patient and CT is part of the clinical routine check.

It should be pointed out that despite the highly accurate and reliable results obtained during the validation trials, there is certainly a learning process during the development of this technique. This applies not only to our ability to perform this technique but also to obtain images that are most suitable for the study. It is also significantly more difficult to image *in vivo* subjects as motion artifact becomes a concern. We anticipate that there will be a progressive improvement in our ability to obtain fluoroscopic and MR images that were not available at the time of this study. The MR sequences are continuously undergoing adjustment during our ongoing studies in order to improve the resolution of the anatomic features. We therefore anticipate that with further refinement of our technique, coupled with technological advancements in fluoroscopic and MR imaging modalities, the accuracy and reliability of the technique will be improved.

In conclusion, this Chapter presented the system setup of a novel combined CT/MR and DFIS imaging technique. The validation tests indicated that this technique is accurate in determination of vertebral position in space. Therefore, the technique can be a useful tool to investigate *in vivo* spine biomechanics in a non-invasive manner. In the following Chapters, the method will be applied for the investigation of vertebral motion of both healthy subjects and patients under various *in vivo* functional activities. The data will enhance our understanding of spinal pathology and help to improve the current surgical treatment methods for spinal diseases that aiming at restoring normal spine biomechanics.

## 2.4 References

1. Wang, S., et al., *Measurement of Vertebral Kinematics Using Non-invasive Image Matching Method - Validation and Application*. Spine, 2008.
2. Disler, D.G., et al., *Fat-suppressed spoiled GRASS imaging of knee hyaline cartilage: technique optimization and comparison with conventional MR imaging*. AJR Am J Roentgenol, 1994. **163**(4): p. 887-92.
3. Li, G., et al., *In vivo articular cartilage contact kinematics of the knee: an investigation using dual-orthogonal fluoroscopy and magnetic resonance image-based computer models*. Am J Sports Med, 2005. **33**(1): p. 102-7.
4. Canny, J., *A computational approach to edge detection*. IEEE Transactions on Pattern Analysis and Machine Intelligence, 1986. **8**(6): p. 679-698.
5. Siddiqui, M., et al., *Effects of X-STOP device on sagittal lumbar spine kinematics in spinal stenosis*. J Spinal Disord Tech, 2006. **19**(5): p. 328-33.
6. Si-Hoe, K.M., S.H. Teoh, and J. Teo, *Radio-translucent 3-axis mechanical testing rig for the spine in micro-CT*. J Biomech Eng, 2006. **128**(6): p. 957-64.
7. Simon, S., et al., *CT imaging techniques for describing motions of the cervicothoracic junction and cervical spine during flexion, extension, and cervical traction*. Spine, 2006. **31**(1): p. 44-50.
8. Gocen, S., H. Havitcioglu, and E. Alici, *A new method to measure vertebral rotation fROM CT scans*. Eur Spine J, 1999. **8**(4): p. 261-5.
9. Martin, H., et al., *Noninvasive assessment of stiffness and failure load of human vertebrae fROM CT-data*. Biomed Tech (Berl), 1998. **43**(4): p. 82-8.
10. Rho, J.Y., M.C. Hobatho, and R.B. Ashman, *Relations of mechanical properties to density and CT numbers in human bone*. Med Eng Phys, 1995. **17**(5): p. 347-55.
11. Moga, P.J., et al., *Torso muscle moment arms at intervertebral levels T10 through L5 fROM CT scans on eleven male and eight female subjects*. Spine, 1993. **18**(15): p. 2305-9.
12. Lindsey, D.P., et al., *The effects of an interspinous implant on the kinematics of the instrumented and adjacent levels in the lumbar spine*. Spine, 2003. **28**(19): p. 2192-7.
13. Breau, C., A. Shirazi-Adl, and J. de Guise, *Reconstruction of a human ligamentous lumbar spine using CT images—a three-dimensional finite element mesh generation*. Ann Biomed Eng, 1991. **19**(3): p. 291-302.
14. Ochia, R.S., et al., *Three-dimensional in vivo measurement of lumbar spine segmental motion*. Spine, 2006. **31**(18): p. 2073-8.

15. Ge, Y., C. Maurer, and J. Fitzpatrick, *Surface-based 3-D image registration using the iterative closest point algorithm with a closest point transform*. Medical Imaging: Image processing, 1996. **2710**: p. 358-67.
16. Gronenschild, E., *The accuracy and reproducibility of a global method to correct for geometric image distortion in the x-ray imaging chain*. Med Phys, 1997. **24**(12): p. 1875-88.
17. Hanson, G.R., et al., *Investigation of in vivo 6DOF total knee arthroplasty kinematics using a dual orthogonal fluoroscopic system*. J Orthop Res, 2006. **24**(5): p. 974-81.
18. Park, S.A., et al., *Comparison of Cobb technique, quantitative motion analysis, and radiostereometric analysis in measurement of segmental range of motions after lumbar total disc arthroplasty*. J Spinal Disord Tech, 2009. **22**(8): p. 602-9.
19. Wilke, H.J., et al., *Anatomy of the sheep spine and its comparison to the human spine*. Anat Rec, 1997. **247**(4): p. 542-55.
20. Ishii, T., et al., *Kinematics of the upper cervical spine in rotation: in vivo three-dimensional analysis*. Spine, 2004. **29**(7): p. E139-44.





# Chapter 3

## Segmental vertebral motion of normal healthy subjects *in vivo*

### 3.1 Introduction

Accurate knowledge of the physiological motion of the lumbar spine vertebrae is important to the understanding of the etiology of spinal diseases such as discogenic low back pain. This knowledge is also necessary for the improvement of surgical treatments of spinal diseases that involve either segmental arthrodesis (fusion) or artificial disc arthroplasty (replacement) which may alter the vertebral motion patterns. However, the limitations of current technology and the complicated anatomy of the lumbar spine have made it difficult to measure the 6DOF vertebral motion under functional activities. Numerous *in vitro* experiments have reported on cadaveric spine kinematics [1-4] when a spine specimen was subjected to simulated loading conditions. *In vivo* spinal research to date has mainly concentrated on the measurement of range of motion (ROM) and the evaluation for instability using methods such as bilateral radiographs, magnetic resonance imaging (MRI) [5-9], computerized topography (CT) [10], electrogoniometer [11-14], and videofluoroscopy [15, 16]. For example, early research used planar radiographs to examine the spinal motion of living subjects during flexion-extension positions [17, 18]. However, the out-of-

plane motion information cannot be obtained and the measurement accuracy may be affected by the projection plane of the radiographs. Subsequently, MR imaging technique [19-21] and CT-based methodology [22, 23] have been used to measure 3D spinal segmental positions in human subjects. However, the physical constructions of the MR and CT machines limited the positions of the subject to only supine or prone. Even with the recent emergence of open MRI, which takes images of the subjects at standing postures, the long acquisition time makes it very difficult to keep the subject at still and study functional activities. To date there has been no accurate information published concerning *in vivo* lumbar vertebral motion during functional activities.

In the previous Chapter, the combined MR/CT and DFIS imaging matching method has been validate to determine lumbar spine kinematics [24]. The system was shown to be appropriate for the investigation of lumbar spine motion during weight-bearing functional activities. In this Chapter, this technique was used to determine the 6DOF vertebral motion of the lumbar spine of living asymptomatic human subjects in flexion-extension, left-right side bending, and left-right twisting [25]. The purpose of this Chapter was to determine segmental *in vivo* vertebral motion during functional human lumbar spine activities. It was hypothesized that the lumbar vertebrae at different levels demonstrated distinct motion characters during active *in vivo* spine motion.

## **3.2 Material and Methods**

Details of the general experiment setup and testing procedures of the combined MR and DFIS were included in the **Chapter 2**. Specific steps used in this study were listed below.

Eleven asymptomatic subjects with an age ranging from 50-60 years (5

males and 6 females) were recruited for this study (mean age, 54.4 years; mean height, 164.7 cm; mean weight, 63.5 kg). Approval of the experimental design by the authors' institutional review board (IRB) was obtained prior to the initiation of the study. A signed consent form was obtained from each subject before any testing was performed. The subjects were evaluated for the absence of low back pain and other spinal disorders. The presence of any of the following were used as indications for exclusion from the study based on the evaluation by an attending spine surgeon prior to participation: current or prior back pain, history of spinal surgery, a diagnosis of disease or anatomical anomaly in the spine, prior radiation within a year, and pregnancy.

The lumbar segments of each subject underwent an MRI scan to build 3D lumbar spine models of L2, L3 and L4 (**Fig 3-1**). The MR images of each subject were carefully examined. Two subjects were found to have presence of early disc degeneration in the absence of clinical symptoms as determined by the radiologist. Additionally, one subject was found to have slight scoliosis ( $>10^\circ$ ) without symptoms. These three subjects were excluded from further investigation.

Following MR scanning, the lumbar spines of the subjects were imaged using DFIS. The target spinal segments were then exposed to fluoroscopic scanning. The subject was asked to stand and position their lumbar spines within the view of both fluoroscopes and actively move to different postures in a predetermined sequence: standing position;  $45^\circ$  flexion of the trunk relative to the vertical; maximal extension; maximal left-right bending; maximal left-right twisting. The subjects were asked to position themselves in the various postures to the maximum extent that they were able to so as to replicate their normal physiological limitations. The exception to this was forward flexion which was limited to  $45^\circ$  (using a protractor) in order to keep the subject within view of the

fluoroscopes. Care was taken to ensure that no constraint was applied to the hips of the subjects while performing the active motions in order to replicate normal activity. During testing, the subject was exposed to approximately 7 pairs of fluoroscopic projections. The entire experiment took about 10 minutes.

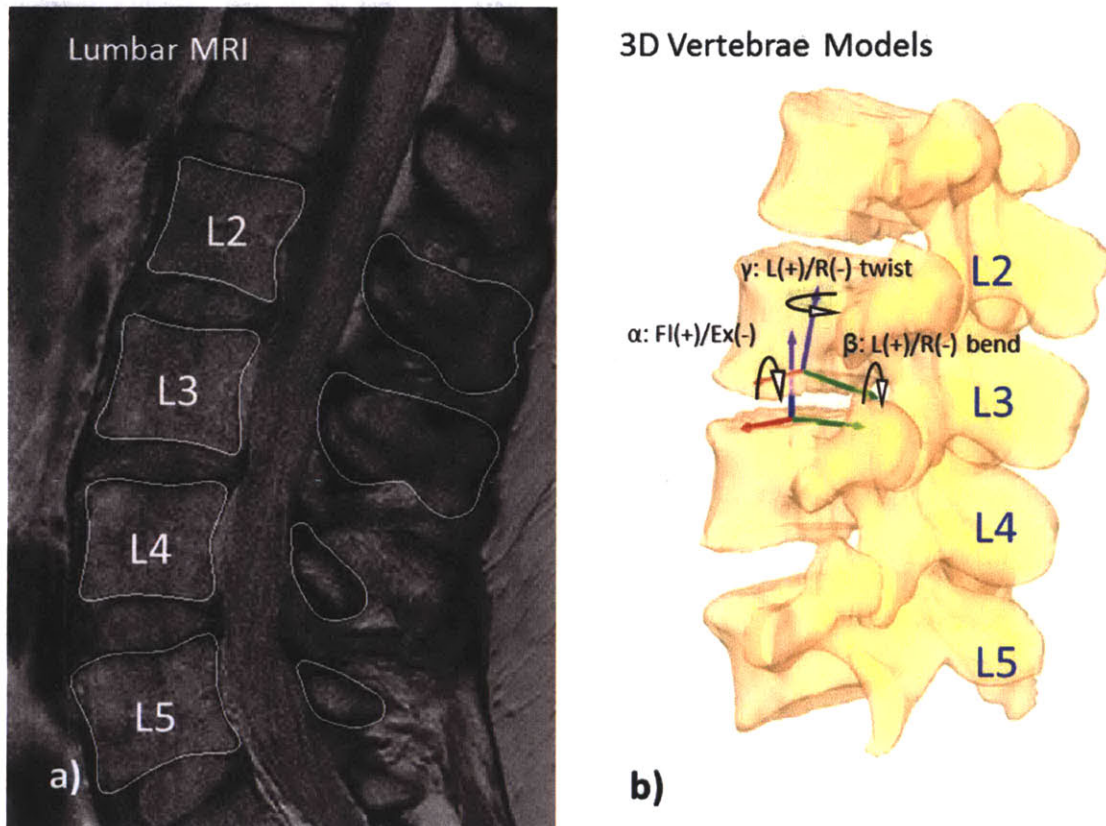


Fig 3-1. a) Vertebral segmentation on MRI. b) 3D reconstructed vertebrae models from MRI and local coordinate system.

The *in vivo* positions of the vertebrae at various weight-bearing body positions were reproduced in the Rhinoceros® solid modeling software by matching the 3D models of the vertebrae and the orthogonal fluoroscopic images [24] (**Fig 3-2**). Vertebral positions during *in vivo* weight-bearing activities were reproduced, representing the 6DOF kinematics of the vertebrae at each *in vivo* posture (**Fig 3-3**).

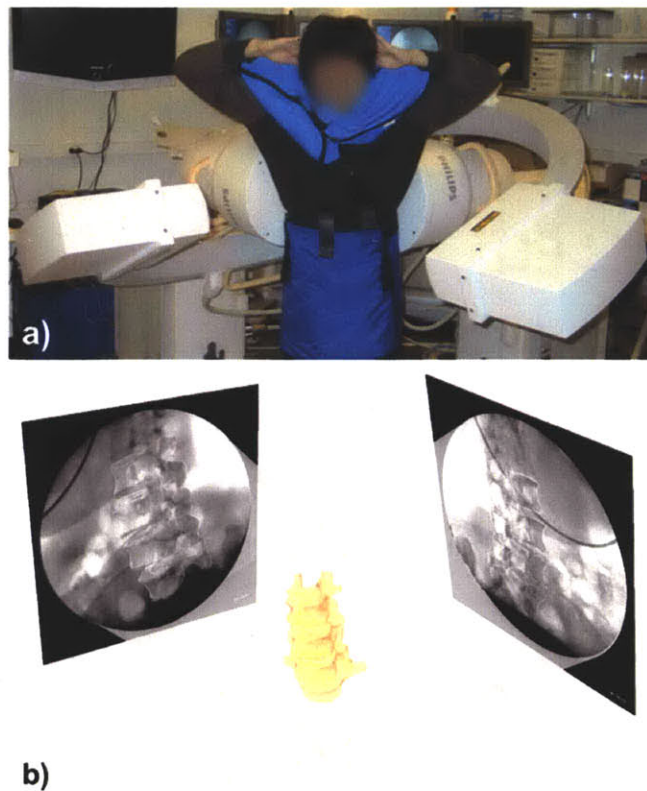


Fig 3-2. a) DFIS setup. b) Reproduction of *in vivo* position of L2-L5.

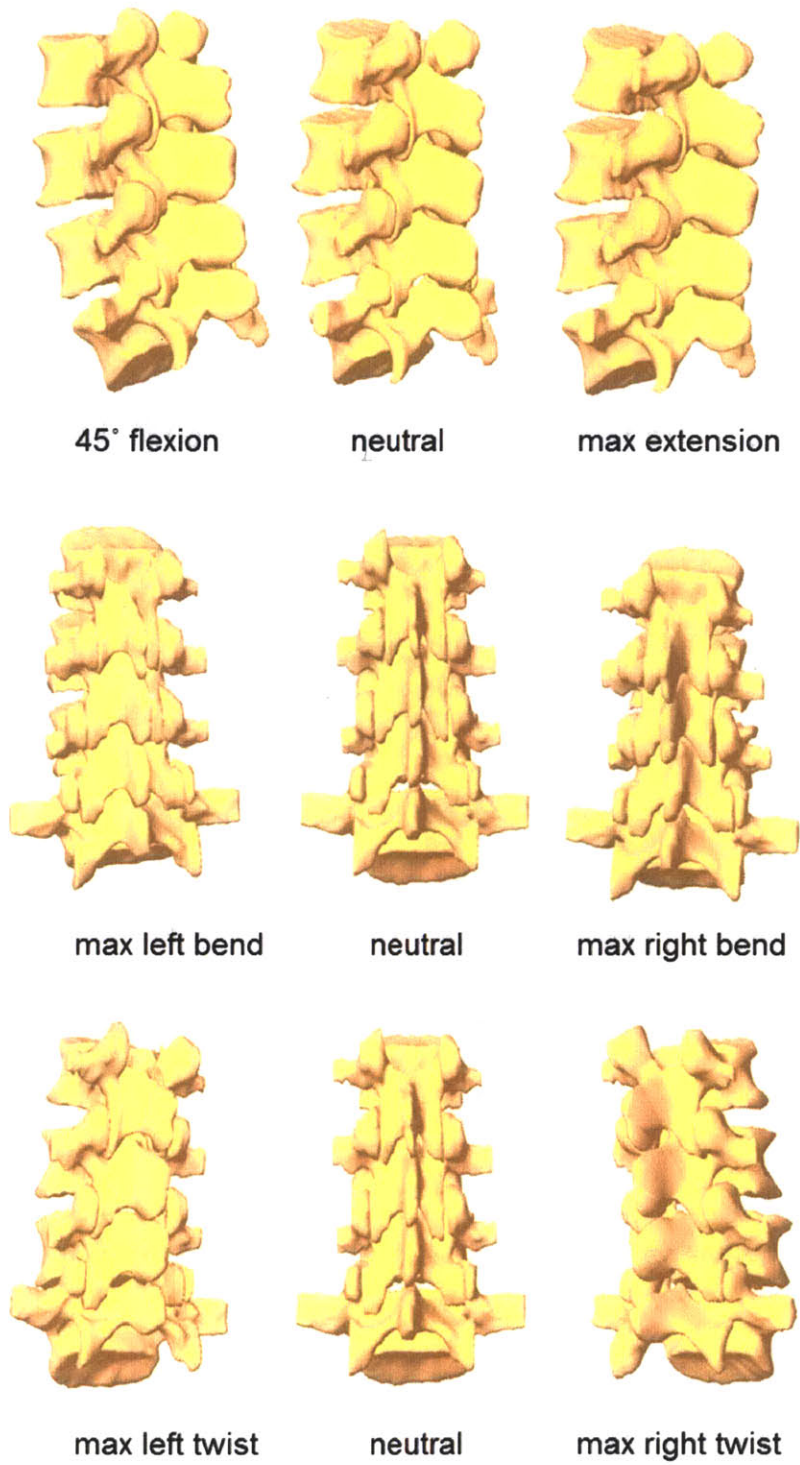


Fig 3-3. *In vivo* positions of the lumbar spine under various functional activities

After reproducing the *in vivo* vertebral positions using the 3D anatomic vertebral models, the relative motions of the vertebrae were analyzed using right hand Cartesian coordinate systems constructed at the endplates of each vertebra (**Fig 3-1b**). The geometric center of the endplate was chosen as the origin of the coordinate system. The X-axis was in frontal plane and pointed to the left direction; the Y-axis was in the sagittal plane and pointed to the posterior direction; and the Z-axis was vertical to the X-Y plane and pointed proximally. The relative motions of the proximal vertebrae with respect to the distal vertebrae were calculated at 3 vertebral levels: L2-3, L3-4 and L4-5. Three translations were defined as the motions of the proximal vertebral coordinate system origin in the distal coordinate system: anterior-posterior, left-right and distal-proximal translations. Three rotations were defined as the orientations of the proximal vertebral coordinate system in the distal vertebral coordinate system using Euler angles (in X-Y-Z sequence): flexion-extension, left-right bending and left-right twisting rotations (**Fig 3-1b**).

From the local coordinate systems, the ROM between adjacent vertebrae were determined between flexion-extension, left-right bending and left-right twisting. The ROM data included both the primary rotations and coupled translations and rotations in all 6 DOFs. A repeated measure ANOVA was used to compare the ROM at L2-3, L3-4 and L4-5 vertebral levels at each of the three functional activities. Statistical significance was set at  $p < 0.05$ . When a statistically significant difference was detected a Newman-Keuls post-hoc test was performed. The statistical analysis was done using Statistica (Statsoft, Tulsa, OK).

### 3.3 Results

#### 3.3.1 Primary rotations

During flexion-extension motion, the cranial level generally had larger range of flexion-extension than the caudal level (**Fig 3-4a**). The L2-3 and L3-4 had flexion-extension ranges of  $5.4\pm 3.8^\circ$  and  $4.3\pm 3.4^\circ$ , respectively; but neither of these were statistically different ( $p=0.06$ ). The L4-5 had a range of flexion-extension of  $1.9\pm 1.1^\circ$ , which was statistically larger smaller that at L2-3 level.

During left-right bending motion, the cranial level generally had smaller range of lateral bending than the caudal level (**Fig 3-4b**). The L2-3 and L3-4 had left-right bending rotation ranges of  $2.9\pm 2.4^\circ$  and  $3.4\pm 2.1^\circ$ , respectively; but neither of these was statistically different. The L4-5 had a range of lateral bending of  $4.7\pm 2.4^\circ$ , which was statistically larger than that at L2-3 level.

During left-right twisting, the 3 vertebral levels showed no significant difference in the range of twist rotations (**Fig 3-4c**). The twist rotation ranges were  $2.5\pm 2.3^\circ$  for L2-3,  $2.4\pm 2.6^\circ$  for L3-4 and  $2.9\pm 2.1^\circ$  for L4-5.

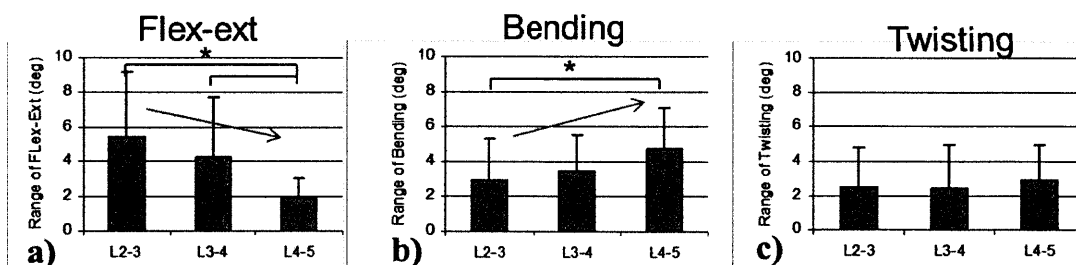


Fig 3-4. Range of primary rotations during: a) flexion-extension. b) left-right lateral bending. and c) left-right twisting.



### **3.3.2 Coupled translations and rotations**

During the active flexion-extension motion, there were coupled translations in all three directions (**Table 3-1**). The coupled motions in left-right and anterior-posterior directions were not significantly different and were, on average, between 0.7 and 1.5 mm. The coupled translation in proximal-distal direction is significantly lower at L2-3 ( $0.2\pm 0.2$  mm) than at L3-4 ( $0.6\pm 0.4$  mm) and L4-5 ( $0.7\pm 0.6$  mm) ( $P<0.05$ ). The coupled rotations in left-right bending and twisting were not significantly different and were, on average, between  $1.7^\circ$  and  $2.9^\circ$ . They are significantly lower than primary rotations at L2-3 and L3-4 levels.

During the active left-right bending motion, the coupled translations in left-right and anterior-posterior directions were not significantly different in all the vertebral levels and on average, ranged between 0.8 and 1.1 mm (**Table 3-1**). The coupled translation in proximal-distal direction (between 0.4 and 0.6 mm) was lower compared to those at the other directions ( $p<0.05$ ). The coupled flexion rotation range was between  $1.3^\circ$  and  $2.1^\circ$  at the L2-3, L3-4 and L4-5 levels, which was lower than their corresponding primary bending rotations ( $p<0.05$ ). However, the coupled twist rotations were at similar magnitudes as the primary bending rotation; ranged between  $2.2^\circ$  and  $3.8^\circ$ .

During the active left-right twisting motion, on average, the translation in anterior-posterior direction was between 1.1 and 1.2 mm, while in left-right direction was between 0.5 and 1.0 mm and in proximal-distal direction was between 0.3 and 0.6 mm (**Table 3-1**). The anterior-posterior translation is significant larger at L2-3 and L4-5 levels than that in the other two directions. Both left-right and anterior-posterior showed significantly larger translation than proximal-distal translation at L3-4. The coupled flexion range was between  $0.9^\circ$  and  $2.3^\circ$  and the coupled bending rotation was between  $2.0^\circ$  and  $3.0^\circ$ . The only

statistical difference was found at L4-5 flexion range compare to those of bend and twist.

Table 3-1: 6DOF ROM of lumbar vertebrae at different levels during various functional activities. Primary rotations were *italicized*. Coupled ranges of translations were labeled as LR (left-right), AP (anterior-posterior) and PD (proximal-distal). Ranges of rotations were labeled as FE (flexion-extension), Bend (left-right bending) and Twist (left-right twisting).  $p < 0.05$ , \*: statistically different compare to other levels. # statistically different compare to other DOFs.

	Translation (mm)			Rotation (°)		
	LR	AP	PD	FE	Bend	Twist
<b>Flexion and extension</b>						
L2-3						
Mean	1.5	1.0	0.2**	5.4	2.3	1.9#
SD	0.9	0.8	0.2	3.8	2.6	2.1
L3-4						
Mean	1.1	0.7	0.6	4.3	2.0	1.7#
SD	0.7	0.6	0.4	3.4	1.6	1.5
L4-5						
Mean	1.0	1.4	0.7	1.9	2.1	2.9
SD	0.7	1.1	0.6	1.1	1.8	2.9
<b>Bending left and right</b>						
L2-3						
Mean	0.9	0.8	0.4#	2.1	2.9	2.2
SD	0.4	0.6	0.4	1.2	2.4	2.2
L3-4						
Mean	0.8	0.8	0.3#	1.3#	3.4	3.8
SD	0.9	0.7	0.2	0.8	2.1	2.3
L4-5						
Mean	1.0	1.1	0.6#	1.9#	4.7	2.8
SD	0.6	1.2	0.4	2.1	2.4	2.6
<b>Twisting left and right</b>						
L2-3						
Mean	0.7	1.1	0.6	1.7	2.6	2.5
SD	0.4	0.7	0.5	2.9	1.2	2.3
L3-4						
Mean	1.0	1.2	0.4#	2.3	2.0	2.4
SD	0.9	1.1	0.3	2.9	2.0	2.6
L4-5						
Mean	0.5	1.1	0.3#	0.9**	3.0	2.9
SD	0.6	0.6	0.2	0.8	1.6	2.1

### 3.4 Discussion

Quantitative data on *in vivo* vertebral motion is critical to enhance our understanding of spinal pathology and to improve the current surgical treatment methods for spinal diseases. In this Chapter, the ranges of lumbar vertebral motion at L2-3, L3-4 and L4-5 were investigated in asymptomatic living subjects when they performed unrestricted functional weight-bearing activities. The data demonstrated that the cranial vertebrae had larger ranges of flexion-extension than the caudal vertebrae during functional flexion-extension of the body. The caudal vertebrae had larger ranges of bending than the cranial vertebrae during functional left-right bending of the body. No statistical difference was observed in left-right twist among the 3 studied vertebral levels. This could be related to the different anatomic orientation of the facet joints at different levels as the L2-3 facet is oriented more vertically than L4-5 [26] which facilitates flexion-extension. In addition to the primary rotations, coupled motions and rotations were determined in all other DOFs. The coupled translation in the left-right and anterior-posterior directions, on average, reached above 1 mm, while below 1mm in the proximal-distal direction. Coupled bending and twisting motions were in general than coupled flexion-extension.

This data provides necessary preliminary information on the normal ROM of the lumbar vertebrae. Overall, in this group of healthy asymptomatic subjects segmental ROM measured was small with a mean of  $< 2\text{mm}$  and  $< 6^\circ$ . For clinical purposes, several radiographic diagnostic criteria in the sagittal plane during flexion-extension have been proposed for lumbar spinal instability: vertebral translation  $>3\text{-}5\text{mm}$  or relative endplate orientation  $>10\text{-}20^\circ$  in the sagittal plane. However, at present, there is no consensus [27]. In the future, increase the number of subjects will increase the statistical power in order to help establish a standard,

and to include translational and rotational limits in the coronal plane for this new standard.

Numerous studies have been carried out using *in vitro* experimental setups to investigate the biomechanics of the lumbar spine. For example, Kettler et al. [3] indicated that the finite helical axes of motion are useful tools to describe the 3D *in vitro* kinematics of the intact and stabilized spine. Fujiwara et al. [15] conducted an *in vitro* anatomic and biomechanical study using human cadaveric lumbar spines. They evaluated the changes in the intervertebral foramen during flexion and extension, lateral bending, and axial rotation of the lumbar spine. The authors correlated these changes with the flexibility of the spinal motion segments by imaging the spine before and after the application of rotational and loading movements. All these studies used invasive techniques to measure spine motion which are not possible to be carried to *in vivo* setup, and are thus difficult to compare with *in vivo* studies and to interpret in the clinical setting for living patients.

To our knowledge, no previous study has reported data regarding *in vivo* vertebral motion during unrestricted functional activities in humans. Pearcy et al.[18] investigated lumbar vertebral motion during maximal flexion-extension using a biplanar radiography technique, where the pelvis and hips were limited in motion by using a frame. They reported similar ranges of motion for all vertebrae. However, our study found the cranial levels had a larger range of flexion than the caudal levels. This differing trend in flexion range may be due to two factors. First, in our testing the subject was allowed free weight-bearing motion of the body. No restriction was applied to the pelvis or hips. Therefore, pelvic rotation could conceivably affect the rotation of the lumbar vertebrae. A second factor may be that maximal flexion was only allowed at approximately 45° for the upper

body which is not the maximal flexion angle of the body. While overall their coupled range of translation was found to be similar in magnitude to our data, the coupled rotation data was lower in magnitude than ours. The differences between the two studies emphasize the importance of weight-bearing conditions and motion patterns when investigating the vertebral kinematics.

Pearcy et al. [17] also investigated left-right bending rotation motion (also referred to as lateral bending rotation) of asymptomatic living subjects using their biplanar radiography technique. Overall, they found larger ranges of lateral bending rotation than those in this study. They also reported larger bending ranges in the cranial segments compared to the caudal levels of the vertebrae. In our data, however, we found that the caudal level L4-5 had a larger range of bending rotation than the cranial two levels. Similarly to the flexion-extension motion, the lateral bending motion was also affected by the motion of the pelvis and hips. In our study, an unrestricted lateral bending was performed by all subjects. It might be difficult to directly compare the results between different studies given that the weight-bearing conditions were different.

There are several studies that have investigated left and right twisting (also referred to as left and right torsion or axial rotation in literature) of lumbar spine in living subjects under various conditions [17, 18, 20, 22]. For example, Pearcy and Tilbrewal [17] studied a similar twisting movement at standing and showed a range of axial rotation of approximately  $2^\circ$  at each vertebral level, which is similar to our findings. Breen et al. described a novel technique (Objective Spinal Motion Imaging Assessment system – OSMIA) based on low-dose fluoroscopy and image processing to study *in vivo* lumbar spine motion. Although their technique has the benefit of minimizing radiation exposure, the major limitation of the technique was the exclusion of translations and axial rotations, making the possibility of

combining the data to measure coupled and 3D motion impossible. In addition, it requires skillful radiography to achieve optimal positioning and dose limitation. Haughton et al. [20] investigated lumbar twisting using MRI with the subjects lying supine and showed an average range of axial rotation between 1 to 2° in the 3 vertebral levels. Their measurement was carried by rotation of the lower body  $\pm 8^\circ$  to examine the rotation range of the vertebrae. More recently, Ochia et al. [22] determined that the cranial lumbar motion segments had greater amounts of axial rotation range compared to the caudal segments when the upper body was passively rotated to  $\pm 50^\circ$  in the supine position while undergoing CT scanning. Their range of rotation was almost twice that found in the above mentioned studies.

These large discrepancies in vertebral rotation data could be explained by the various loading conditions used in these studies that were caused by different experimental setups. Percy and Tibrewal studied similar active weight-bearing axial rotations compared with our study. However, both Haughton et al.[20] and Ochia et al. [22] studied passive axial rotation of the body in the supine position. Haughton et al. rotated the subject's hip  $\pm 8^\circ$  to investigate the lumbar spine rotation while Ochia et al. rotated the upper body  $\pm 50^\circ$ . In both of these two studies, however, the spine was not under weight-bearing conditions. A quantitative comparison between these studies might be difficult and a comparison of lumbar vertebral motions has to consider the different loading conditions that were present among these studies.

Few studies have gone further to investigate coupled vertebral motions with the primary rotations [18, 22]. Percy et al. found that coupled translation in left-right and anterior-posterior directions were around the range of 1 mm during primary flexion-extension motion, which are similar to our findings. However, the

accuracy of their system was around 1 mm [17]. Their coupled motion in left-right bending and axial rotation was also similar to ours. During primary axial rotation, Ochia et al. [23] found that the coupled range of translation in the left-right direction was over 8 mm at L2-3, over 4 mm at L3-4 and over 1 mm at L4-5 levels. These values are larger than those measured from our study during standing weight-bearing axial rotation. Their coupled translations in the anterior-posterior and proximal-distal directions were lower than those reported in our study. These comparisons indicated again that the coupled vertebral motions are also dependent upon weight-bearing condition.

There are several limitations to the current study. Our small sample size limited our ability to detect differences in movement patterns. This may also explain why some of the differences that were found were not statistically significant as well as the relatively large SDs that were seen. Even though no restriction was applied to body motion, the flexion was not studied at the maximal flexion position of the subject. In order to keep the targeted lumbar spine within the field view of the two fluoroscopes, the subject was instructed to limit flexion to approximately 45° from a standing position. Also, only the ranges of motion of the L2-3, L3-4 and L4-5 segments were examined during the 3 functional body motions. The *in vivo* instantaneous positions of the vertebrae were not examined during dynamic motion of the body. Finally, the subjects were within the age distribution of 50 to 60 years. In future, living subjects in various age ranges should be investigated to examine the age effect on vertebral kinematics. Nevertheless, the data obtained from this study will hopefully contribute to our knowledge on physiological motion of the human lumbar vertebrae.

In conclusion, this Chapter used DFIS to investigate functional lumbar spine motion in healthy asymptomatic human subjects under weight-bearing

conditions. The advantage of this system for spinal research is its flexibility to accommodate various functional activities. This Chapter reported data on lumbar vertebral motion ranges during 3 unrestricted body motions commonly used during clinical examinations of the spine. Vertebral motion at different levels responded to external loads differently. These data may provide new insight into the *in vivo* function of human spines. In the following Chapter, IVD deformation was examined using the 6DOF vertebral kinematics determined in this study. Later in **Chapter 8**, a similar approach was taken to study the *in vivo* vertebral kinematics of patients to analyze how degenerative disc diseases will affect the spinal biomechanics.



### 3.5 References

1. White, A.A. and M.M. Panjabi, *Clinical biomechanics of the spine*. 2nd ed. 1990, Philadelphia: Lippincott. xxiii, 722 p.
2. Auerbach, J.D., et al., *Evaluation of spinal kinematics following lumbar total disc replacement and circumferential fusion using in vivo fluoroscopy*. Spine (Phila Pa 1976), 2007. **32**(5): p. 527-36.
3. Kettler, A., et al., *Finite helical axes of motion are a useful tool to describe the three-dimensional in vitro kinematics of the intact, injured and stabilised spine*. Eur Spine J, 2004. **13**(6): p. 553-9.
4. Lindsey, D.P., et al., *The effects of an interspinous implant on the kinematics of the instrumented and adjacent levels in the lumbar spine*. Spine (Phila Pa 1976), 2003. **28**(19): p. 2192-7.
5. Kulig, K., et al., *Segmental lumbar mobility in individuals with low back pain: in vivo assessment during manual and self-imposed motion using dynamic MRI*. BMC Musculoskelet Disord, 2007. **8**: p. 8.
6. Karadimas, E.J., et al., *Positional MRI changes in supine versus sitting postures in patients with degenerative lumbar spine*. J Spinal Disord Tech, 2006. **19**(7): p. 495-500.
7. Fazey, P.J., et al., *An MRI investigation of intervertebral disc deformation in response to torsion*. Clin Biomech (Bristol, Avon), 2006. **21**(5): p. 538-42.
8. Perie, D., et al., *Assessment of compressive modulus, hydraulic permeability and matrix content of trypsin-treated nucleus pulposus using quantitative MRI*. J Biomech, 2006. **39**(8): p. 1392-400.
9. Jinkins, J.R., J.S. Dworkin, and R.V. Damadian, *Upright, weight-bearing, dynamic-kinetic MRI of the spine: initial results*. Eur Radiol, 2005. **15**(9): p. 1815-25.
10. Simon, S., et al., *CT imaging techniques for describing motions of the cervicothoracic junction and cervical spine during flexion, extension, and cervical traction*. Spine, 2006. **31**(1): p. 44-50.
11. McGregor, A.H., Z.S. Patankar, and A.M. Bull, *Spinal kinematics in elite oarswomen during a routine physiological 'step test'*. Med Sci Sports Exerc, 2005. **37**(6): p. 1014-20.
12. Burnett, A.F., et al., *Spinal kinematics and trunk muscle activity in cyclists: a comparison between healthy controls and non-specific chronic low back pain subjects-a pilot investigation*. Man Ther, 2004. **9**(4): p. 211-9.
13. Holt, P.J., et al., *Kinematics of spinal motion during prolonged rowing*. Int J Sports Med, 2003. **24**(8): p. 597-602.
14. Steffen, T., et al., *A new technique for measuring lumbar segmental motion*

- in vivo. Method, accuracy, and preliminary results.* Spine, 1997. **22**(2): p. 156-66.
15. Fujiwara, A., et al., *The effect of disc degeneration and facet joint osteoarthritis on the segmental flexibility of the lumbar spine.* Spine, 2000. **25**(23): p. 3036-44.
  16. Lee, S.W., et al., *Development and validation of a new technique for assessing lumbar spine motion.* Spine, 2002. **27**(8): p. E215-20.
  17. Percy, M.J. and S.B. Tibrewal, *Axial rotation and lateral bending in the normal lumbar spine measured by three-dimensional radiography.* Spine, 1984. **9**(6): p. 582-7.
  18. Percy, M.J., *Stereo radiography of lumbar spine motion.* Acta Orthop Scand Suppl, 1985. **212**: p. 1-45.
  19. Fujii, R., et al., *Kinematics of the lumbar spine in trunk rotation: in vivo three-dimensional analysis using magnetic resonance imaging.* Eur Spine J, 2007.
  20. Haughton, V.M., et al., *Measuring the axial rotation of lumbar vertebrae in vivo with MR imaging.* AJNR Am J Neuroradiol, 2002. **23**(7): p. 1110-6.
  21. Blankenbaker, D.G., et al., *Axial rotation of the lumbar spinal motion segments correlated with concordant pain on discography: a preliminary study.* AJR Am J Roentgenol, 2006. **186**(3): p. 795-9.
  22. Ochia, R.S., et al., *Three-dimensional in vivo measurement of lumbar spine segmental motion.* Spine, 2006. **31**(18): p. 2073-8.
  23. Ochia, R.S., et al., *In vivo measurements of lumbar segmental motion during axial rotation in asymptomatic and chronic low back pain male subjects.* Spine, 2007. **32**(13): p. 1394-9.
  24. Wang, S., et al., *Measurement of Vertebral Kinematics Using Non-invasive Image Matching Method - Validation and Application.* Spine, 2008.
  25. Li, G., et al., *Segmental in vivo vertebral motion during functional human lumbar spine activities.* Eur Spine J, 2009. **18**(7): p. 1013-21.
  26. Masharawi, Y., et al., *Facet orientation in the thoracolumbar spine: three-dimensional anatomic and biomechanical analysis.* Spine, 2004. **29**(16): p. 1755-63.
  27. Kasai, Y., et al., *A new evaluation method for lumbar spinal instability: passive lumbar extension test.* Phys Ther, 2006. **86**(12): p. 1661-7.

# Chapter 4

## Overall geometric deformation of lumbar discs under *in vivo* weight-bearing standing

### 4.1 Introduction:

Degeneration of the intervertebral disc (IVD) is thought to be responsible for most cases of back pain, resulting in several pathologic conditions such as spinal stenosis, instability, disc herniation, etc. Knowledge of IVD deformation under physiological loading conditions is instrumental for understanding the mechanisms of IVD related spinal pathology and for helping to improve surgical treatments of spinal diseases. Numerous *in vitro* studies have thus been conducted to investigate the biomechanical behavior of human lumbar discs [1-16]. Cadaveric experiments have been simulated physiological loads on the disc to study deformation [1-3, 9-11] of the IVD under various loading conditions. Data on and disc behavior such as its material properties, shear, creep, intradiscal pressure and disc bulging have also been widely reported [1-3, 9-11]. In addition, finite element (FE) models have been developed to simulate the relationships between applied loads and IVD deformation [5-8, 16]. However, it is difficult to accurately mimic *in vivo* disc deformation using *in vitro* experimental setups since the effects of fluid exchange, muscle activities and ligamentous tension are difficult to quantify.

Due to the complicated spinal anatomy and physiological loading conditions of the spine, it has been a challenge in the past to determine the *in vivo* deformation of the IVD [17]. To our knowledge, there has been no data reported on *in vivo* deformation of the human IVD under physiological weight-bearing conditions. An *in vitro* MRI study by O’Connell had utilized MRI technique to study IVD strain and had the potential to use on living human subjects [4]. However, limitations such as limited study postures due to long acquisition time and confined space of the MR scanner make it difficult to investigate real time IVD deformation under weight-bearing conditions.

In this Chapter, the combined MRI and DFIS imaging technique was used to non-invasively quantify 3D lumbar IVD geometric deformation in healthy subjects under physiological weight-bearing standing [18]. We hypothesize that the IVD deformations would be unique at different vertebral levels. Later in **Chapter 9** of the thesis, the IVD deformation were also examined in various functional activities, such as flexion-extension, lateral bending and twisting in both healthy subjects and patients with DDD.

## **4.2 Material and Methods**

Details of the general experiment setup and testing procedures of the combined MR and DFIS were included in **Chapter 2**. The lumbar vertebral kinematics from the same subject group in **Chapter 3** was used in line with the geometry of the IVD endplates to calculate overall disc geometric deformation. Specific steps used in this study were listed below.

The volume between the adjacent vertebral bodies was occupied by the intervertebral disc. Thus, overall IVD deformation can be reasonably calculated from the volume change between the inferior endplate of the proximal vertebra

and the superior endplate of the distal vertebra. First, the disc shape was approximated by the 3D volume between adjacent vertebral endplates (**Fig 4-1a**). For each disc, right-handed Cartesian coordinate systems were placed at the geometric center of the inferior endplate of the proximal vertebrae and at the superior endplate of the adjacent distal vertebrae (i.e. the upper and lower surfaces of a disc) (**Fig 4-1a**). In the plane parallel to the disc surfaces, the x axis was set pointing left and the y axis was set pointing posterior. The z axis was set perpendicular to x-y plane and pointing proximally.

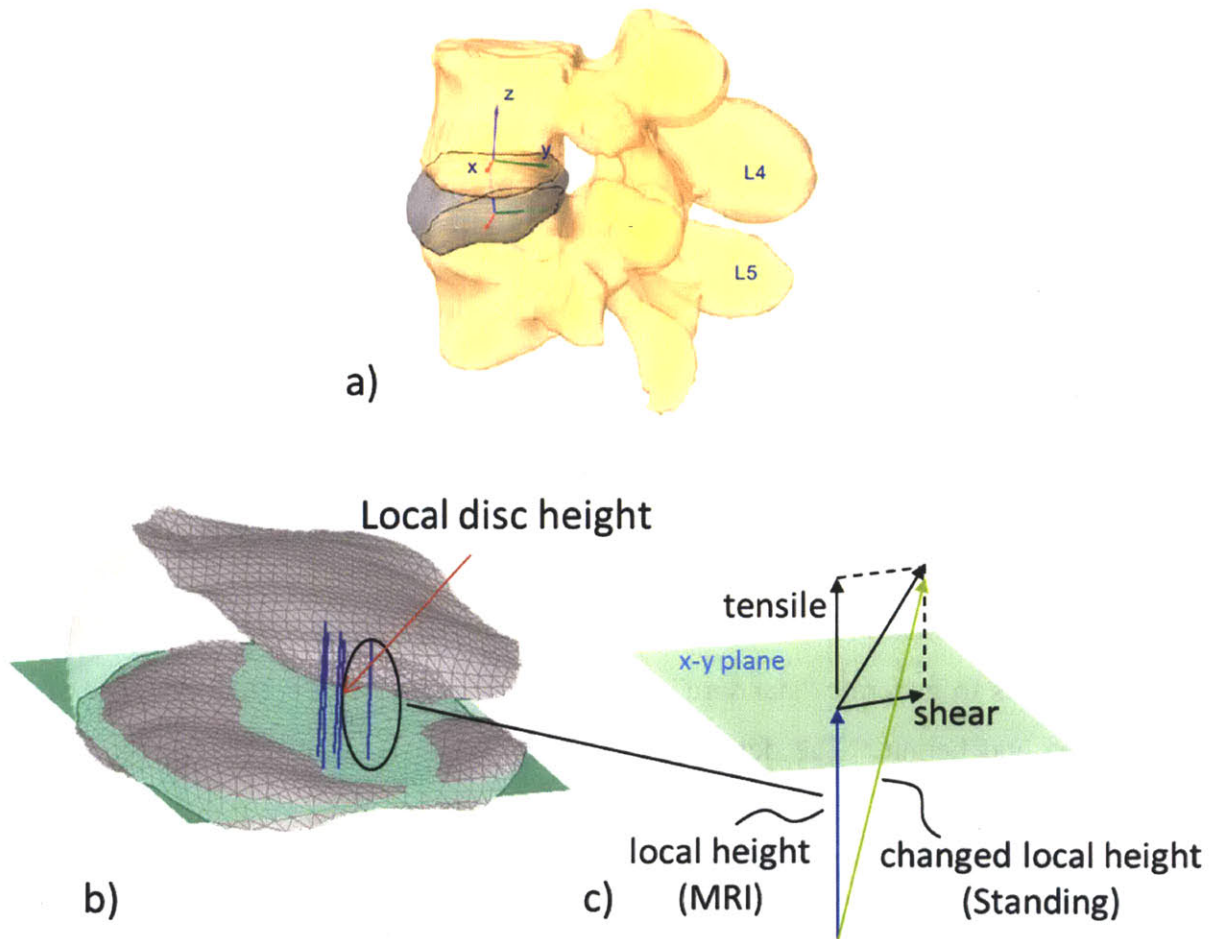


Fig 4-1. a) Coordinate systems to characterize the kinematics of the disc endplates. b) Definition of local disc heights. c) Calculation of overall tensile and shear deformation

6DOF kinematics of the endplates of the vertebral segments L2-3, L3-4 and L4-5 at standing position (weight-bearing) was determined from DFIS and compared with those during MRI supine position (non-weight-bearing) as a reference. Deformation of the disc was calculated using evenly distributed mesh vertices on the upper and lower disc surfaces (approximately 800 points per surface). Local disc heights were defined to be the pairs of the vertex points of minimum distance using the iterative closest point method [19] (**Fig 4-1b**). The change of local disc heights from non-weight-bearing (MRI supine) to weight-bearing (standing) represented the overall deformation at different locations of an IVD throughout the disc thickness. In addition, with respect to the lower disc surface, overall tensile deformation (elongation/disc height) was measured in the proximal distal direction (z axis direction) in the reference coordinate system and plotted on a color map plot. Overall shear deformation (displacement/disc height) was obtained using the projection of the elongation in the x-y plane of the reference coordinate system and plotted on a gradient (quiver) plot showing both magnitude and direction (**Fig 4-1c**).

Disc deformation patterns of tensile and shear deformation were obtained from the average of the eight subjects in the following steps. First, the average disc sizes of L2-3, L3-4 and L4-5 were calculated from the 3D mesh models of all subjects to generate “standard” discs at these levels with normalized disc surface area and height. The deformations of each subject were then mapped onto the standard discs to investigate deformation patterns of the discs at different vertebral levels under weight-bearing condition. Quantitatively, the magnitude of tensile and shear deformations were also determined at nine representative locations on the surfaces of the discs: anterior, right-anterior, right, right-posterior, posterior, left-posterior, left, left-anterior, and center points of each disc (**Fig 4-2**). A two-way repeated measure ANOVA using disc level and location on the disc as the two

factors were used to compare the overall deformation of the disc between the different vertebral levels: L2-3, L3-4 and L4-5. Post-hoc Newman-Keuls analysis was performed and statistical significance was achieved when  $p < 0.05$ .

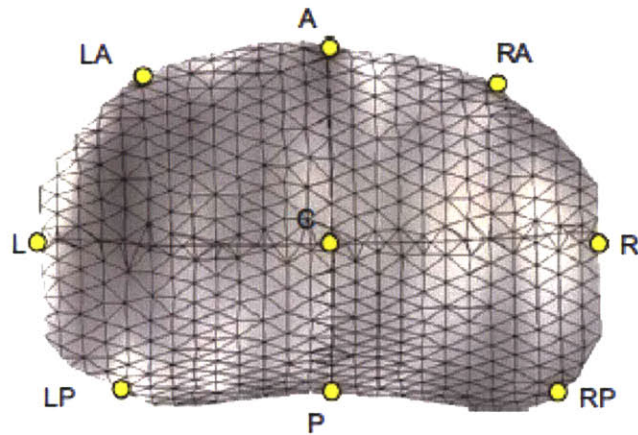


Fig 4-2. Representative locations: A-Anterior, P-Posterior, L-Left, R-Right, C-Center

## 4.3 Results:

### 4.3.1 *Disc deformation patterns*

Going from the MRI supine (non-weight-bearing) to the standing (weight-bearing) positions, the anterior one third of the L2-3 disc was in tension (+) while the posterior one third was in compression (-) (**Fig 4-3a**). The magnitude changed along the anterior-posterior direction from +24% to -21%. The L3-4 disc had a similar conversion; however, the change in magnitude occurred from left anterior (+19%) to right posterior (-16%). For the L4-5 disc, the right portion was under tension (+9%) which gradually changed to compression at the left portion (-14%).

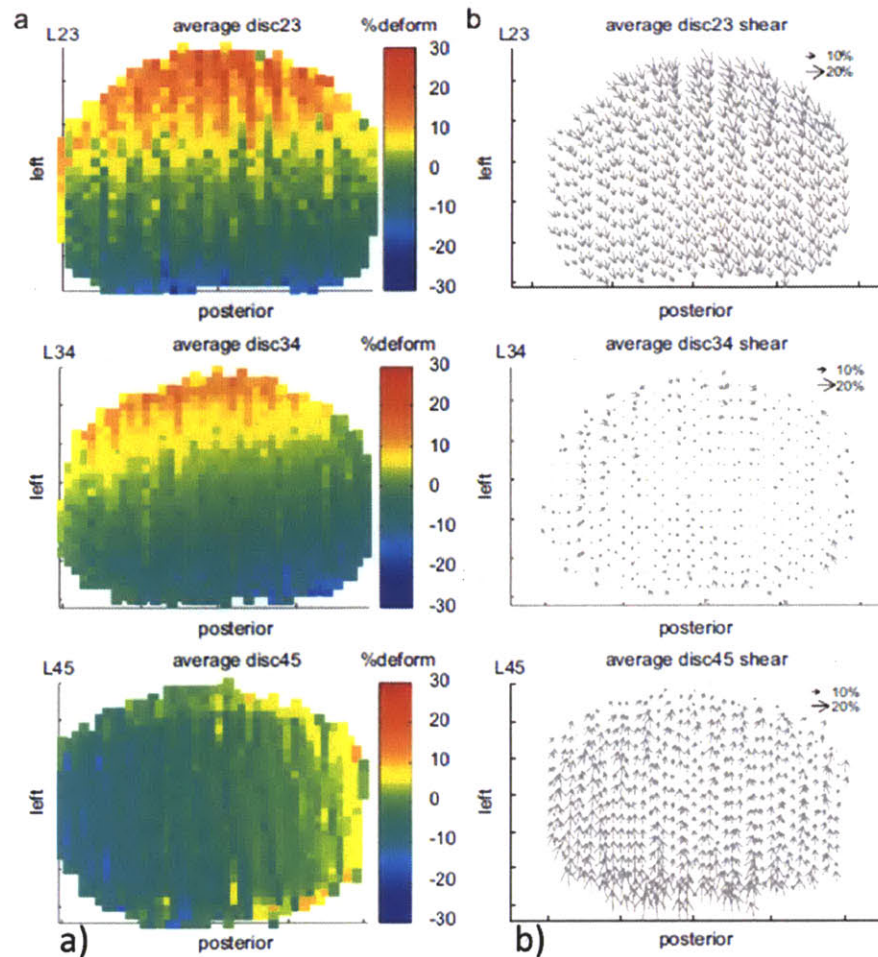


Fig 4-3. a) Overall tensile deformation. b) Overall shear deformation. Averaged from 8 subjects and mapped on “standard discs” at different vertebral levels.

The L2-3 disc experienced overall shear deformation from anterior to posterior with a magnitude of 5% to 21%, and the maximum deformation was at the anterior portion of the disc (**Fig 4-3b**). The L3-4 disc experienced minimal shear deformation (<8%) in the diagonal direction. The L4-5 disc experienced shear deformation from posterior to anterior with a magnitude of 4% to 26%, and the maximum deformation was at the posterior portion of the disc.



### **4.3.2 Quantitative measurements at representative locations**

Tensile and shear deformations were quantitatively described at the nine representative locations and plotted (**Fig 4-4**). Tensile deformations at the L2-3 and L3-4 discs had similar trends but at different locations on the disc surfaces. At the anterior location, tensile deformations were 20% and 13% ( $p=0.26$ ) at the L2-3 and L3-4 discs, respectively. The deformations decreased along the disc edge towards the posterior direction. The deformations were close to zero at the right, left, and center locations and changed to compressive deformation at the posterior locations, where the compressive deformation was  $-9%$  ( $p=0.84$ ) for both the L2-3 and L3-4 discs. The L4-5 disc showed minimal deformation at the anterior, posterior and center locations. It had peak tensile deformation of 8% at the right location and peak compressive deformation of  $-11%$  at the left-posterior location. At anterior, right-posterior, and left-anterior locations, the deformations of the L4-5 discs were significantly different than those of both the L2-3 and L3-4 discs.

The magnitudes of shear deformation of the nine locations on the L3-4 disc were rather constant (**Fig 4-5**), and on average, were statistically smaller than the L2-3 and L4-5 discs at the anterior portion of the disc. Shear deformations of the L4-5 discs were significantly larger than the L2-3 and L3-4 discs at the posterior portion of the disc (**Fig 4-5**). For instance, at the right-posterior location the L4-5 disc had shear deformation of 23% while both the L2-3 and L3-4 discs had 11% shear deformation ( $P=0.001$  for both).

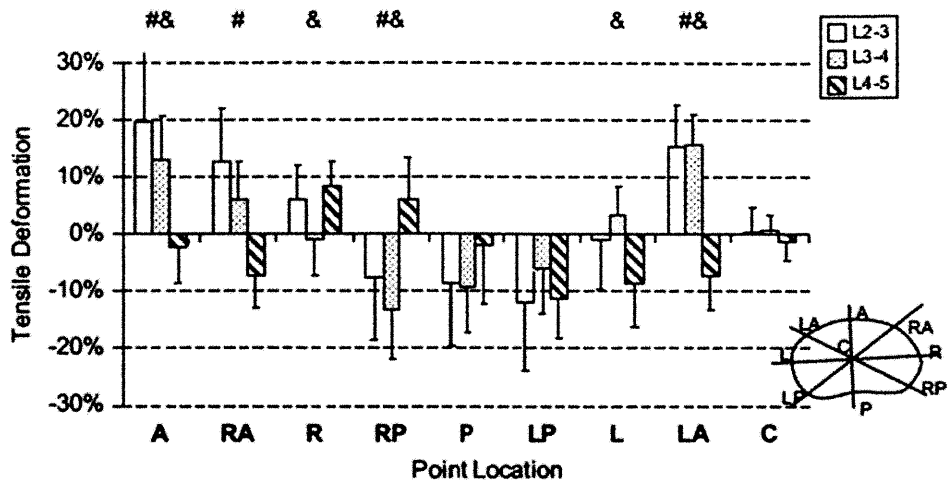


Fig 4-4. Tensile deformation at the 9 representative locations on disc surfaces. A- Anterior, P-Posterior, L-Left, R-Right, C-Center. Error bars shows the standard deviation from 8 subjects. \*: L2-3 different from L3-4, #: L2-3 different from L4-5, &: L3-4 different from L4-5,  $p < 0.05$ .

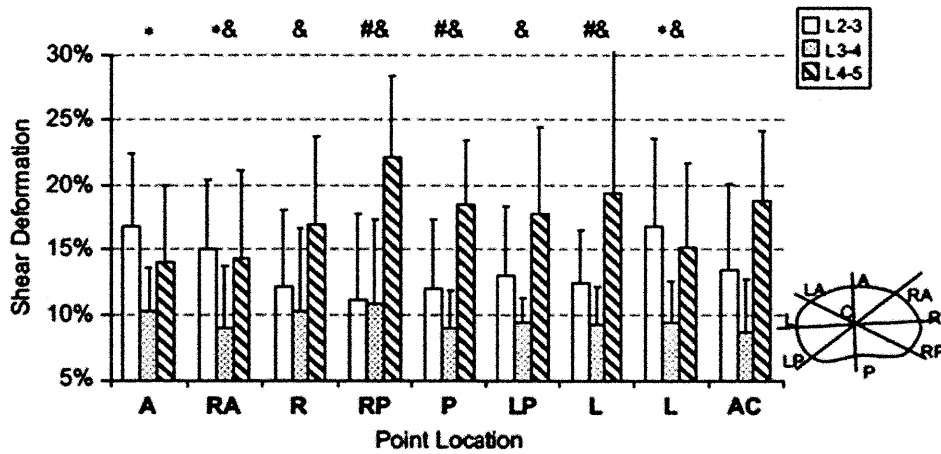


Fig 4-5. Shear deformation at the 9 representative locations on disc surfaces. A- Anterior, P-Posterior, L-Left, R-Right, C-Center. Error bars shows the standard deviation from 8 subjects. \*: L2-3 different from L3-4, #: L2-3 different from L4-5, &: L3-4 different from L4-5,  $p < 0.05$ .

## **4.4 Discussion:**

In this Chapter, the lumbar vertebral disc deformation of living human subjects were investigated under weight-bearing standing with respect to non-weight bearing MRI supine positions, utilizing the non-invasive imaging method described in the previous Chapters [20]. The kinematics of the endplates of adjacent vertebrae was determined and used to calculate the overall disc deformation throughout the disc height. Compared to the non-weight-bearing supine position, the weight-bearing standing condition caused an average tensile deformation between -21% to 24% and shear deformation within 26% for all target lumbar discs L2-3, L3-4 and L4-5. The center portion of the discs in general experienced minimum deformation. Discs at different vertebral levels showed different deformation patterns.

These different patterns can be explained by the physiological structure and function of the lumbar spine. To sustain body weight during standing, lumbar lordosis increases (more concavity towards the back) which causes the anterior portion of discs L2-3 and L3-4 to be under tension and the posterior portion under compression. Anatomically the facet joints of L4-5 are oriented more in “left-right” direction compared to those of L2-3 and L3-4, thus limiting the “anterior-posterior tensile pattern” while facilitating the “left-right tensile pattern”. Although the deformation of the discs were not found to be individually left-right symmetric at each level, the disc deformation pattern of L4-5 (left portion compression, right portion tension) may balance that of L3-4 (left anterior tension, right-posterior tension) to achieve an overall left-right symmetry, and thus stability of the lumbar column. We also found that L2-3 and L4-5 experienced shear from opposing directions and L3-4 had minimum shear, which can also be attributed to lordosis. The spine maintains stability by balancing shear in different directions

while the anatomic inflection point of the lordotic curvature is roughly located at the L3-4 disc.

Although most of the subjects showed similar disc deformation patterns, inter-subject variation was expected and observed, despite our efforts to standardize the experiment. Variation within the data may result from differences in individual standing habits and anatomic structures. The data from a typical subject as well as an extreme subject are presented in **4.5 Appendix** to further demonstrate this inter-subject variation.

In the literature, there are many *in vitro* disc deformation studies that have used axial compressive loads with or without moments to simulate physiological weight-bearing loads [1-4]. Costi et al. [1] used radiographic markers and inserted metal grid frames at the mid transverse plane of the IVD to study shear under compression using a displacement control robot. In five human lumbar discs (T12-L5), they investigated maximum shear of 9% under 1mm robot input and estimated shear under physiological weight-bearing to be 13% by assuming linear extrapolation. Tsantrizos et al. [2] also used metal beads and wires to study IVD deformation of ten L2-3 and L4-5 discs after resecting all soft tissues, posterior elements and endplates. Under 1000N axial compression load, they reported average maximum circumferential strain of 5% and radial strain of -4% to 6%.

To avoid interfering with the disc structure, Heuer et al. [3] used a novel laser scanner to measure the surface strain of the disc, where the outer surface map of the annulus fibrosus of IVD was obtained before and after applying a compression load (500N). From six intact L2-3 motion segment units, the average maximum disc surface strain in the proximal-distal axial direction (tensile) was reported as -5% in compression and 3% in tension. Using the same protocol, Heuer et al. applied coupled compression (500N) and flexion-extension moments

(7.5Nm) and measured a strain of 12% in the annulus fiber direction. O'Connell et al. [4] calculated 2D disc deformation from mid sagittal MR images of the lumbar spine using pixel correlation analysis under a 1000N axial compression load in the L1-2 or L2-3 discs. They found average maximum compressions of -11.3% at the anterior, -7.8% at the center and -6.1% at the posterior of the discs and an average maximum shear of 8.1% pointing posterior.

Finite element models have been used to quantify the deformation at different regions of the IVD [5-7]. Goel et al. [5] determined a 0.17mm to 1.51mm axial compression displacement (with a disc height of 11mm) of an intact L3-4 disc with a load ranging from 200N to 2000N. They further assumed the load experienced by a subject standing upright to be 413 N and found the axial displacement to be 0.32mm. Shirazi-Adl et al. [6] reported a 1.3mm displacement in the L2-3 disc (with a disc height of 11mm) under a 1500N compression load. Schmidt et al. [7] studied the IVD deformation used a FE model of a lumbar L4-5 spinal segment that had been validated with *in vitro* loading experiments. They simulated the application of a combined axial compression load of 500N and a moment of 7.5Nm in various anatomic planes and found a maximum shear strain of 42% with a flexion moment and 39% with an extension moment at the posterior portion of the disc.

*In vitro* studies have the advantage of investigating disc deformation under controlled loading conditions. However, the results vary largely due to different experimental setups and different loading conditions applied. For example, various segments from T12 to L5 have been included [1, 3, 5-7]. Motion segment units with or without the posterior elements present as well as isolated IVDs have been tested [1-3]. Loads applied during testing have ranged from 500N to 1500N with or without flexion or extension moments present [6, 7, 12]. These factors

make it difficult to directly compare our *in vivo* disc deformation data with those measured using *in vitro* techniques. Going from the supine to the physiological weight-bearing posture, increased lordosis may cause a complicated combination of compressive and shear loading and rotational moments. On the other hand, active muscle forces and fluid exchange of the disc may play important roles in regulating *in vivo* disc deformation, which were implicitly accounted for in our study design since we measured the actual position of the subject. It is suggested that we have to have a clear understanding of the experimental conditions when we cite specific disc deformation data from literature.

It should be noted that it might be possible to investigate disc deformation using supine MR images and MR images obtained from a stand-up MRI scanner. However, the long image acquisition time and confined space of the MRI coil limits the possibility to further study disc deformation in real time during weight-bearing functional activities. Our combined DFIS and MR imaging technique has the advantage of capturing the instantaneous configuration of the disc so that error in data collection secondary to creep deformation of the soft tissues can be avoided.

It should also be noted that our study calculated the lumbar IVD geometric deformation from the relative 6DOF translation and orientation of the two adjacent endplates. The combined DFIS and MR imaging technique used to determine the endplate kinematics has been shown to have an accuracy of 0.3mm in translation and 0.7° in orientation between two adjacent vertebrae [20]. Using the accuracy data on vertebral kinematics, the maximum error on the disc deformation data was estimated to be approximately 4%. In addition, the endplates were assumed to be rigid in our studies. Hulme et al. [21] reported that the endplate could deform up to 0.1mm at a 2000N compressive load. Therefore, we did not think that endplate

deformation would cause dramatic alternations in the deformation calculated in our study. Another limitation of our study is that the method can only provide data on overall disc deformation on the outer surfaces of the disc and cannot directly quantify the deformation of the inner portion of the disc. This overall deformation value should be lower than the peak deformation experienced inside the disc. A FE model that uses the deformation data determined in this study as boundary conditions would be necessary to quantify the missing information such as strain and stress distribution inside the disc. This proposed procedure was carefully validated and pilot study was performed in Chapter 13 and 14.

In conclusion, the Chapter used the combined MR and DFIS technique to non-invasively determine lumbar disc deformation in living human subjects. Disc deformation under physiological weight-bearing condition, i.e. standing was determined using the supine, non-weight-bearing condition as a reference. The data indicated that the discs of L2-3, L3-4 and L4-5 had different deformation behaviors. This method can be used to investigate the effect of various loading configurations such as flexion-extension, lateral bending and twisting of the trunk and the effect of pathology such as DDD on lumbar disc deformation, which is detailed in **Chapter 9** of the thesis.

## 4.5 Appendix:

In this study, lumbar spine disc deformation of levels L2-3, L3-4 and L4-5 under physiological weight-bearing were studied in 8 healthy living subjects. Average tensile and shear deformation of the discs were presented in **Fig 4-3**. Inter-subject variability were also expected and observed. The data from a typical subject and an extreme one were listed here next to each other (**Fig 4-6** and **Fig 4-7**).

For the typical subject under weight-bearing, the anterior one third of the L2-3 disc was in tension (+) while the posterior one third was in compression (-) (**Fig 4-6a**). The magnitude changed along the anterior-posterior direction from +27% to -26%. The L3-4 disc had a similar conversion; however, the change in magnitude occurred from left anterior (+21%) to right posterior (-26%). For the L4-5 disc, the right portion was under tension (+8%) which gradually changed to compression at the left portion (-16%). The overall shear deformation was determined throughout the height of the discs (**Fig 4-7a**). The L2-3 disc experienced shear deformation from anterior to posterior with a magnitude of 4% to 18%, and maximum deformation was at the anterior portion of the disc. The L3-4 disc experienced minimal shear deformation (<12%) from left posterior to right anterior. The L4-5 disc experienced shear deformation from right posterior to left anterior with a magnitude of 5% to 25%, and maximum deformation was at the left posterior left portion of the disc. All the deformation pattern and magnitude were very close to the average data we obtained.

For the extreme subject, the magnitude of L2-3 disc deformation changed along the anterior-posterior direction from +30% to -32%, which is notably larger than typical subjects (**Fig 4-6b**). The L3-4 disc had a change in magnitude along anterior-posterior direction compare to those of typical ones from left anterior to



right posterior. The change in magnitude was similar to typical ones to be from +21% to -25%. For the L4-5 disc, both the pattern and magnitude were different. The right anterior portion was under tension (+16%) which gradually changed to compression at the left posterior portion (-20%). On the other hand, the L2-3 disc experienced shear deformation from right anterior to left posterior with a relative large magnitude of 17% to 24% (**Fig 4-7b**). The L3-4 disc experienced a relative large shear deformation (13% to 19%) from left to right. The L4-5 disc experienced shear deformation from right posterior to left anterior with a magnitude of 3% to 23%, with maximum deformation at the left posterior portion of the disc.

Either the deformation pattern or magnitude (or both) of this extreme subject were not very similar to the average data we obtained. However, all subjects showed varied deformation behaviors at different disc levels. In general, the higher level discs have higher deformation magnitudes.

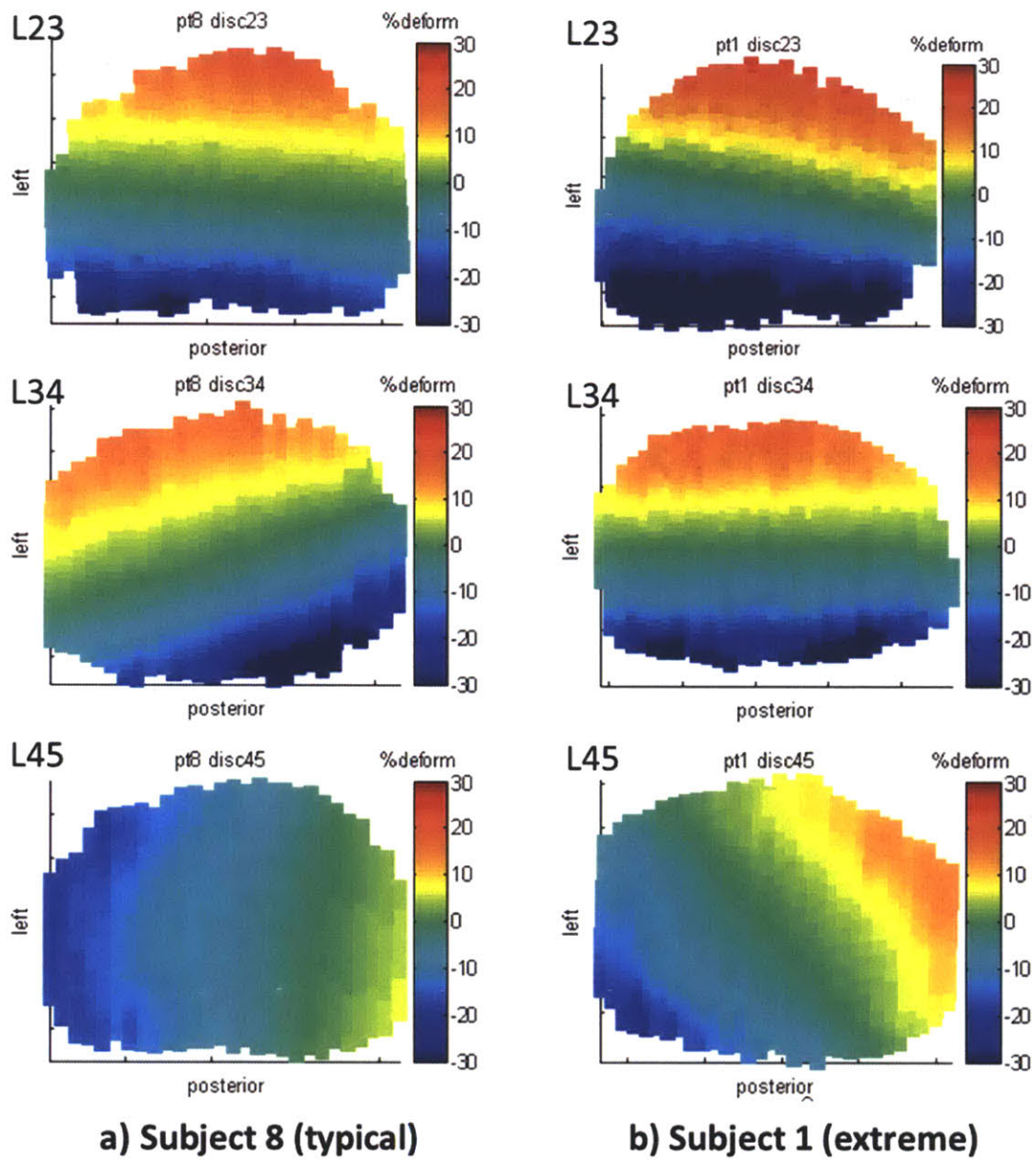


Fig 4-6. Tensile deformation of a) a typical case and; b) an extreme case

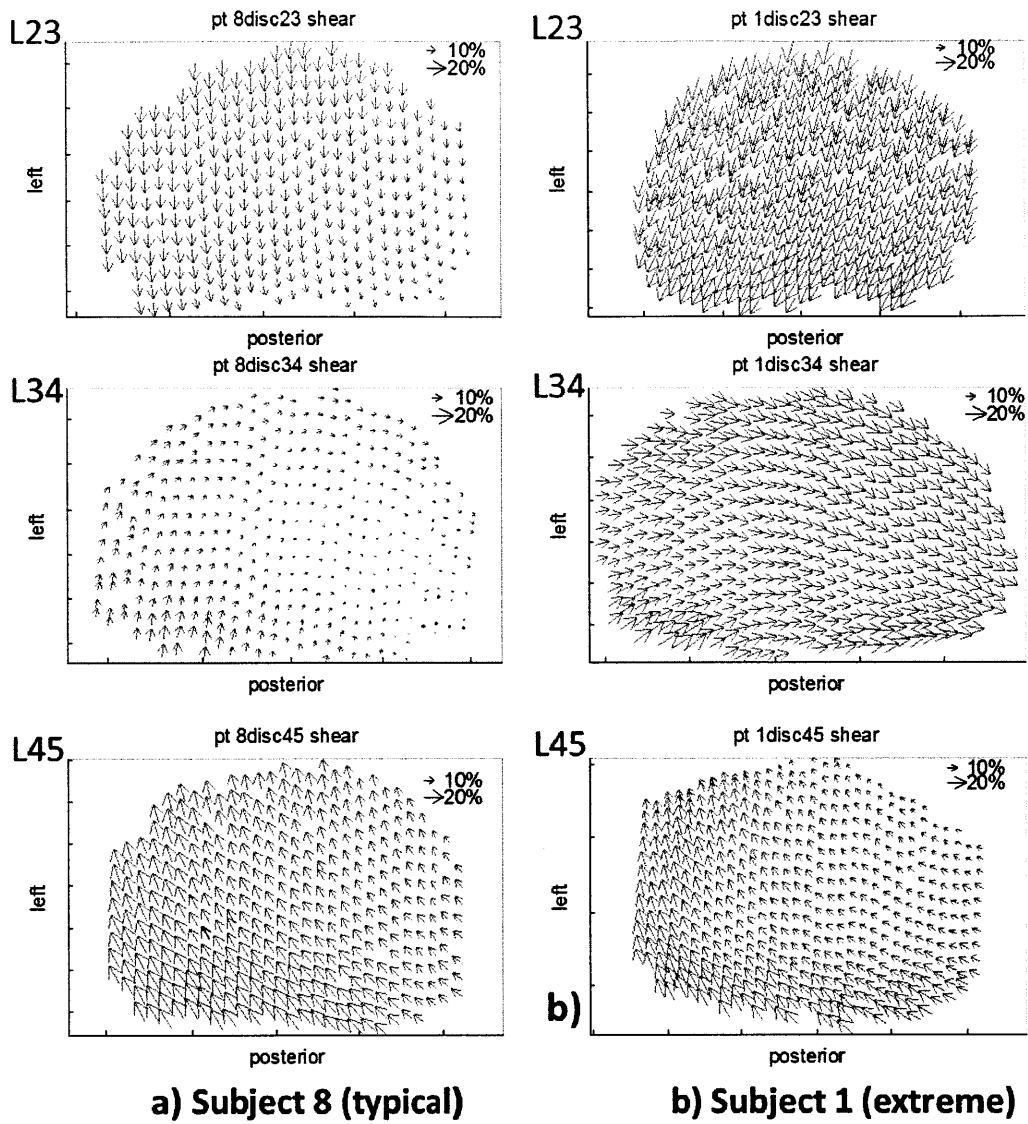


Fig 4-7. Shear deformation of a) a typical case and; b) an extreme case

## 4.6 References

1. Costi, J.J., et al., *Direct measurement of intervertebral disc maximum shear strain in six degrees of freedom: motions that place disc tissue at risk of injury*. J Biomech, 2007. **40**(11): p. 2457-66.
2. Tsantrizos, A., et al., *Internal strains in healthy and degenerated lumbar intervertebral discs*. Spine, 2005. **30**(19): p. 2129-37.
3. Heuer, F., H. Schmidt, and H.J. Wilke, *The relation between intervertebral disc bulging and annular fiber associated strains for simple and complex loading*. J Biomech, 2008. **41**(5): p. 1086-94.
4. O'Connell, G.D., et al., *Human internal disc strains in axial compression measured noninvasively using magnetic resonance imaging*. Spine, 2007. **32**(25): p. 2860-8.
5. Goel, V.K., et al., *Interlaminar shear stresses and laminae separation in a disc. Finite element analysis of the L3-L4 motion segment subjected to axial compressive loads*. Spine, 1995. **20**(6): p. 689-98.
6. Shirazi-Adl, A., *Analysis of large compression loads on lumbar spine in flexion and in torsion using a novel wrapping element*. J Biomech, 2006. **39**(2): p. 267-75.
7. Schmidt, H., et al., *Intradiscal pressure, shear strain, and fiber strain in the intervertebral disc under combined loading*. Spine, 2007. **32**(7): p. 748-55.
8. Natarajan, R.N., J.R. Williams, and G.B. Andersson, *Modeling changes in intervertebral disc mechanics with degeneration*. J Bone Joint Surg Am, 2006. **88 Suppl 2**: p. 36-40.
9. Iatridis, J.C., J.J. McClean, and D.A. Ryan, *Mechanical damage to the intervertebral disc annulus fibrosus subjected to tensile loading*. J Biomech, 2005. **38**(3): p. 557-65.
10. Adams, M.A., et al., *Mechanical initiation of intervertebral disc degeneration*. Spine, 2000. **25**(13): p. 1625-36.
11. Stokes, I.A., *Bulging of lumbar intervertebral discs: non-contacting measurements of anatomical specimens*. J Spinal Disord, 1988. **1**(3): p. 189-93.
12. Shah, J.S., W.G. Hampson, and M.I. Jayson, *The distribution of surface strain in the cadaveric lumbar spine*. J Bone Joint Surg Br, 1978. **60-B**(2): p. 246-51.
13. Kim, Y., *Prediction of peripheral tears in the annulus of the intervertebral disc*. Spine, 2000. **25**(14): p. 1771-4.
14. Lu, Y.M., W.C. Hutton, and V.M. Gharpuray, *Do bending, twisting, and diurnal fluid changes in the disc affect the propensity to prolapse? A*

- viscoelastic finite element model*. Spine, 1996. **21**(22): p. 2570-9.
15. Argoubi, M. and A. Shirazi-Adl, *Poroelastic creep response analysis of a lumbar motion segment in compression*. J Biomech, 1996. **29**(10): p. 1331-9.
  16. Silva, P., et al., *An experimental and finite element poroelastic creep response analysis of an intervertebral hydrogel disc model in axial compression*. J Mater Sci Mater Med, 2005. **16**(7): p. 663-9.
  17. Natarajan, R.N., J.R. Williams, and G.B. Andersson, *Recent advances in analytical modeling of lumbar disc degeneration*. Spine, 2004. **29**(23): p. 2733-41.
  18. Wang, S., et al., *Measurement of geometric deformation of lumbar intervertebral discs under in vivo weight-bearing condition*. J Biomech, 2009. **42**(6): p. 705-11.
  19. Ge, Y., C. Maurer, and J. Fitzpatrick, *Surface-based 3-D image registration using the iterative closest point algorithm with a closest point transform*. Medical Imaging: Image processing, 1996. **2710**: p. 358?67.
  20. Wang, S., et al., *Measurement of vertebral kinematics using noninvasive image matching method-validation and application*. Spine, 2008. **33**(11): p. E355-61.
  21. Hulme, P.A., S.J. Ferguson, and S.K. Boyd, *Determination of vertebral endplate deformation under load using micro-computed tomography*. J Biomech, 2008. **41**(1): p. 78-85.



## **Chapter 5**

# **Range of Motion and Orientation of the Lumbar Facet Joints *In vivo***

### **5.1 Introduction**

The zygoapophyseal (facet) joints play a major role in stabilizing the segmental spine unit. With the onset of degeneration in the lumbar spine, increased stress is experienced posteriorly resulting in alterations in the mechanical properties of the facet joints.[1-3] This has known clinical implications, as it is thought that facet joint arthropathy can be the primary etiology in many patients experiencing chronic low back pain.[4]

A review of the literature reveals that little data has been reported on the motion patterns of the lumbar facet joints. Adams and Hutton[5] applied various loads to cadaveric lumbar spines in order to determine the mechanical function of the facet joints. Shariz-Adl[6] constructed a non-linear 3D finite element model in order to study intersegmental biomechanics of the lumbar spine under sagittal moments in order to determine the role of the facets joints. Lastly, Wood et al.[7] studied *in vivo* facet motion in a canine model using an instrumented spatial linkage method. However, adequate information on the native (*in vivo*) kinematics of the lumbar facet joints, which can be used as a baseline from which to measure the changes that occur in dynamic non-fusion systems including disc preserving posterior element replacement systems,[8, 9] has yet to be reported. It is also

important for the evaluation of traumatic and degenerative changes that occur in the facet joints as well as the remaining elements of the segmental spine unit and for improving the surgical treatment of spinal diseases using dynamic stabilization; such as the use of disc preserving posterior element replacement systems for the treatment of facet joint arthropathy.[8, 9]

The purpose of this Chapter was to quantify the motion of the lumbar facet joints in asymptomatic volunteers during unrestricted functional body movements with physiologic weight-bearing. We used the validated combined MRI and DFIS technique to measure the facet joint motion from the L2 to L5 vertebrae in the lumbar spine.[10, 11] We hypothesized that facet joint motion would be dependent on loading conditions and vertebral level. In **Chapter 10**, the same technique was applied on a group of patients with pathology, and clinical relevance was drawn from the results.

## **5.2 Material and Methods**

Details of the general experiment setup and testing procedures of the combined MR and DFIS were included in **Chapter 2**. The motion of the facet joints were calculated from the same subject group used in **Chapter 3** and **4**. Specific steps used in this study were listed below.

### **5.2.1 Lumbar facet joint motion**

Each subject was asked to stand and position the lumbar area within the view of both fluoroscopes and actively move to different positions in a predetermined sequence: standing position, trunk flexion, extension, maximal left-right bending, and maximal left-right twisting. The *in vivo* positions of the vertebrae at various weight-bearing body positions were reproduced using the DFIS.



Right-hand Cartesian coordinate systems were created at the center of each facet joint (**Fig 5-1**) at the MRI (supine) position. The center was designated to be located at the volumetric center of the facet capsule. Based on the geometry of the facet, the x-axis was set perpendicular to the sagittal plane in order to represent the medial-lateral direction and pointed in the left direction. The y-axis was set in the sagittal plane in order to represent anterior-posterior direction of the facet joint motion and pointed in the posterior direction; and the z-axis was set in the sagittal plane perpendicular to the y axis, and along the long axis of facet joint in order to represent cranial-caudal direction and pointed cranial. The same coordinate systems were adopted for both the inferior facet of cranial vertebra and the superior facet of caudal vertebra at the supine position during MR scanning. This enabled the coordinate systems to be set for both the left and right facet joint at the MRI position. After reproducing the *in vivo* vertebral positions using the 3D anatomic vertebral models, the inferior facet motion of the cranial vertebra was determined with respect to the superior facet of the caudal vertebra. Standing position (weight-bearing) was compared to the supine MRI (non-weight-bearing) position and the ROM from the end-points of flexion-extension, left-right bending and left-right torsion of the trunk were also determined.

### **5.2.2 Facet orientation**

The longitudinal and transverse facet angles were measured in relation to the midsagittal plane of the vertebral body (**Fig 5-2, 5-3**). This was done in a fashion consistent with other reported measurements of facet orientation in the literature.[12, 13]

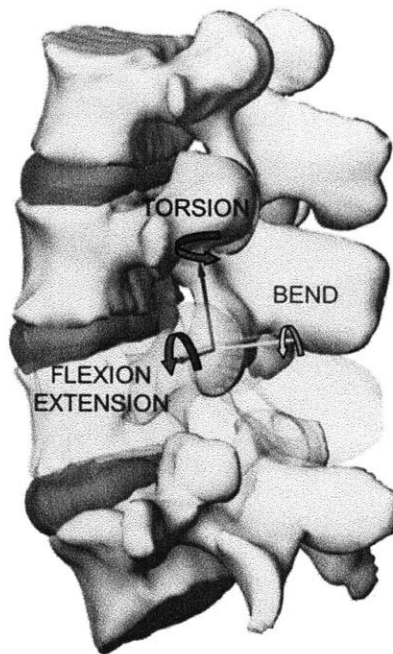


Fig 5-1. Anatomical coordinate system to measure facet motion

### **5.2.3 Statistical analysis**

A three-way repeated measures ANOVA was used to compare the facet range of motion at the L2-L3, L3-L4, and L4-L5 vertebral levels. The kinematics was the dependent variable and the vertebral level, laterality and activity were the independent variables. Level of statistical significance was set at  $p < 0.05$ . A two-way repeated measures ANOVA was employed to compare the facet orientation with the angle being the dependent variable and the level and side being the independent variables. When a statistically significant difference was detected, a post-hoc Newman-Keuls test was performed, and the level of significance was again chosen at  $p < 0.05$ . The statistical analysis was done using software (Statistica<sup>®</sup> v. 8.0, Statsoft, Tulsa, OK).

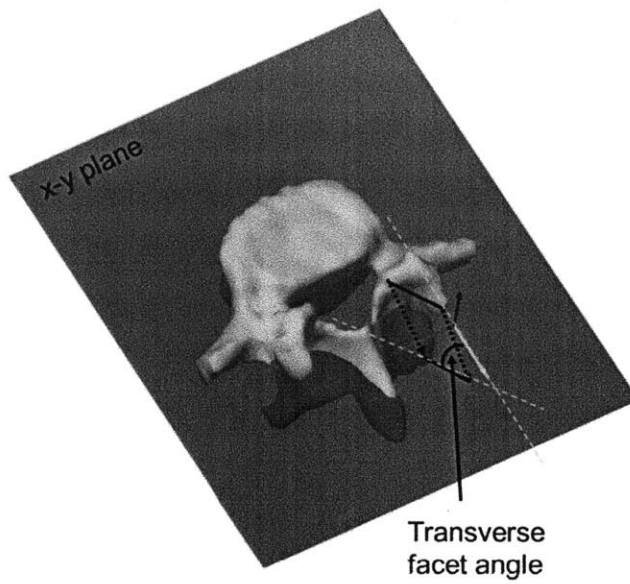


Fig 5-2. Measurement of transverse facet angle: the angle between the line of the facet width projected onto the transverse plane and the anterior-posterior axis of the vertebra.

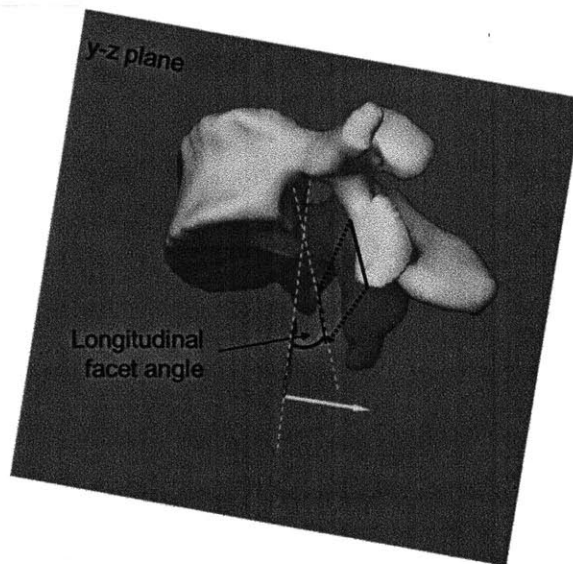


Fig 5-3. Measurement of longitudinal facet angle: the angle between the line of the facet length projected onto the sagittal plane and the cranial-caudal axis of the vertebra.

## 5.3 Results

### 5.3.1 Facet motion fROM supine position to standing

When going from the supine (MRI) to the standing (weight-bearing) position, rotation of the facet joints occurred mainly around the mediolateral axis, (mean  $<6^\circ$  **Fig 5-4a**), while translation occurred mainly in the cranial-caudal direction (mean  $<3$  mm, **Fig 5-5a**). The range of flexion-extension rotation was greatest at the most cranial L2-L3 segment ( $4.3\pm 1.4^\circ$ ) and significantly decreased caudally towards L4-L5 ( $1.4\pm 0.7^\circ$ ,  $p<0.04$ ). Likewise, the cranial-caudal translation was greatest at the L2-L3 facet joints ( $2.4\pm 1.7$  mm and  $2.5\pm 2.0$  mm for the left and right joint, respectively; **Fig 5-5a**) and smallest at the L4-L5 facets ( $1.6\pm 0.8$  mm and  $0.5\pm 0.3$  mm for the left and right joint, respectively;  $p<0.05$ ). While the range of translation in the craniocaudal direction decreased from cephalad to caudad vertebral segments, the range of anteroposterior translation was not significantly different between the levels ( $p=0.3$ ). Additionally, slight asymmetry was observed in the range of anteroposterior translation between the left and right facet of the L2-L3 ( $p=0.04$ ) and craniocaudal translation at the L3-L4 and L4-L5 levels ( $p=0.04$  and  $p=0.034$ , respectively).

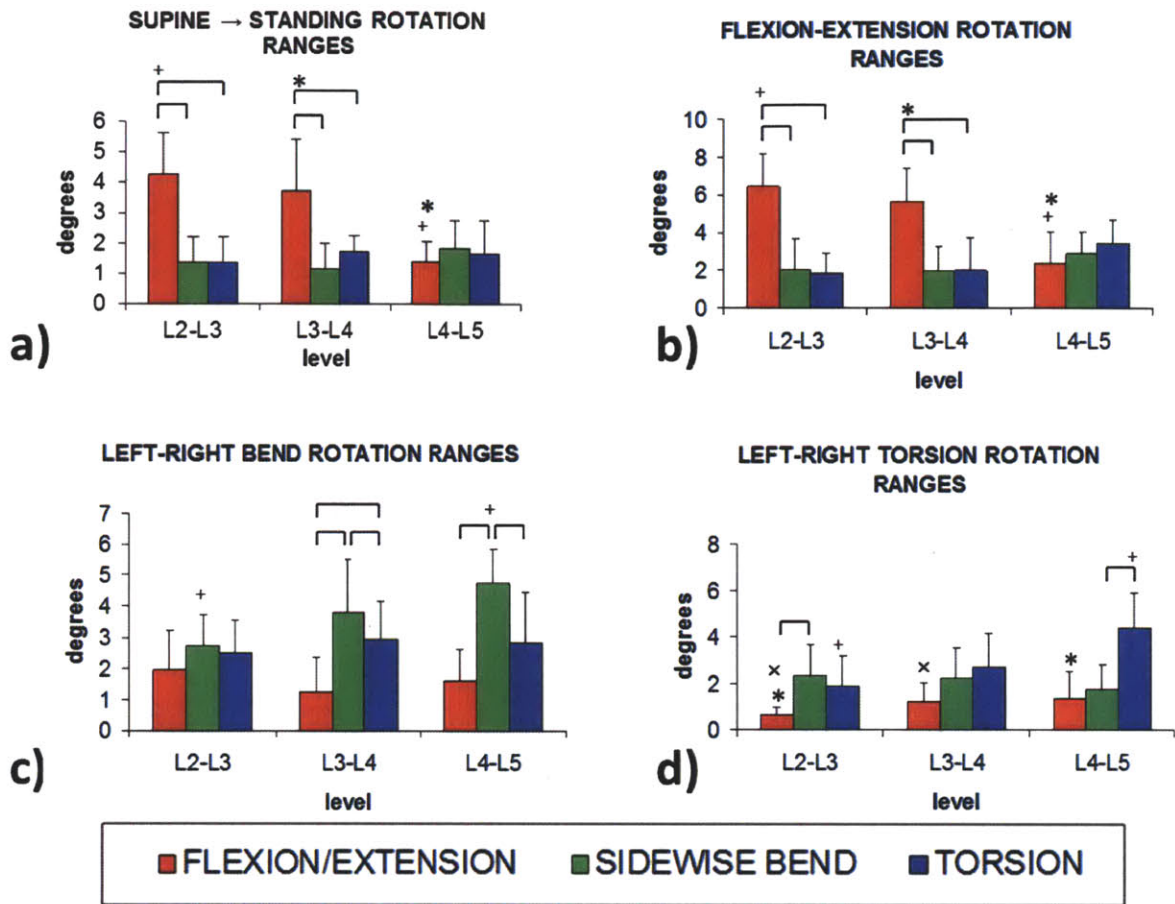


Fig 5-4. Ranges of facet joint rotations in 6DOF. The bars represent statistical significance upon within-level comparison while the symbols (\*,+,x) represent statistical significance upon between-level comparison.  $p < 0.05$ .

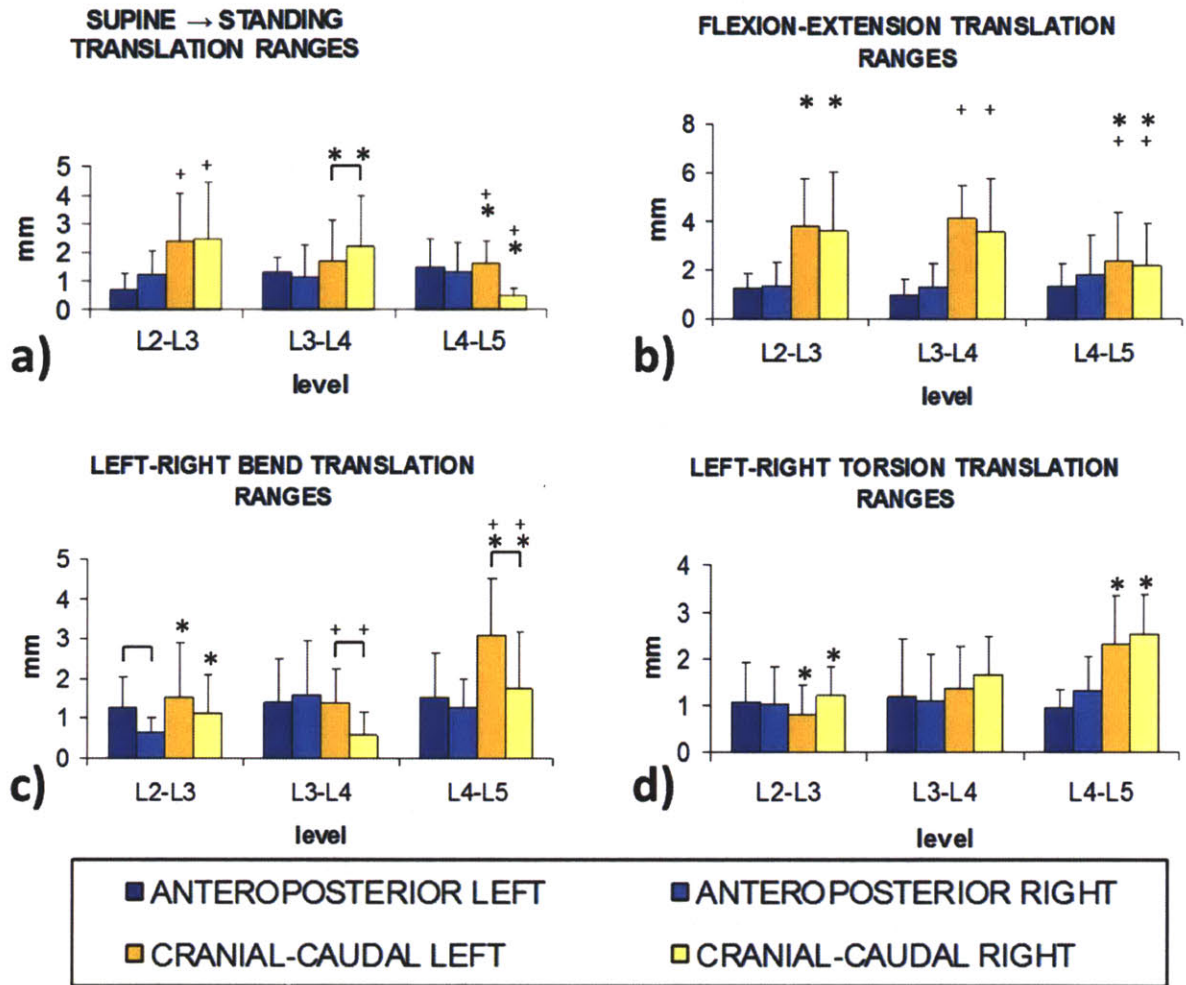


Fig 5-5. Ranges of facet joint translations in 6DOF. The bars represent statistical significance upon within-level comparison while the symbols (\*,+,x) represent statistical significance upon between-level comparison.  $p < 0.05$

### **5.3.2 Facet motion during flexion to extension of the trunk**

During flexion-extension movements of the trunk, the predominant motions of the lumbar facet joints were rotation along the medial-lateral axis (mean  $<6.5^\circ$ ) and cranial-caudal translation (mean  $<4$  mm) (**Fig 5-4b**). The range of flexion-extension rotation was greatest at the cranial L2-L3 segment ( $6.4\pm 1.7^\circ$ ) and smallest at the caudal L4-L5 ( $2.4\pm 1.7^\circ$ ,  $p<0.01$ ). Ranges of lateral bend and torsion had similar magnitudes at the studied vertebral segments ( $p>0.77$ ). The translation occurred mainly in the craniocaudal direction and its magnitude was also greatest at the cranial levels of L2-L3 ( $3.8\pm 2.1$  mm and  $3.6\pm 2.4$  mm for the left and right joints, respectively; **Fig 5-5b**) and L3-L4 ( $4.1\pm 1.4$  mm and  $3.6\pm 2.2$  mm for the left and right joints, respectively) and smallest at the caudal L4-L5 level ( $2.4\pm 1.4$  mm and  $2.6\pm 1.2$  mm for the left and right joints, respectively;  $p<0.02$ ). The translations in the anteroposterior direction were not significantly different between the studied lumbar vertebral levels ( $p=0.311$ ). In addition, the translations ranges in the anteroposterior and craniocaudal directions were not significantly different between the left and right facet joint of the same level ( $p=0.566$  and  $p=0.593$ , respectively).

### **5.3.3 Facet motion during side to side bending of the trunk**

During side to side bending of the trunk, the motion of the facet joints was found to be a coupling of rotations and translations in different directions (**Fig 5-4c**). The primary rotation during this motion was about the antero-posterior axis and its magnitude was greatest in the caudal L4-L5 segments ( $4.7\pm 1.1^\circ$ ) and smallest in the cranial L2-L3 segments ( $2.7\pm 1.0^\circ$ ,  $p=0.04$ ). The differences between the primary and coupled rotations (axial and flexion-extension) were significant only at the two caudal levels and only between bending and flexion-extension rotations ( $p<0.02$ ). With respect to translations, the range of craniocaudal translation was shown to be significantly greater in the caudal L4-L5

level than in the more cranial L2-L3 and L3-L4 levels ( $p<0.04$ , **Fig 5-5c**). Translations in the anteroposterior direction were not significantly different across the studied levels ( $p=0.22$ ). Furthermore, we noted asymmetry in the range of anteroposterior translation between the left and right facet joint that was significant at the L2-3 level ( $p=0.036$ ).

#### **5.3.4 Facet motion during left to right torsion of the trunk**

Torsion of the trunk was also achieved by coupled rotations in different directions (**Fig 5-4d**). The primary rotation during this motion was about the craniocaudal axis and its magnitude was greatest in the caudal L4-L5 segments ( $4.4\pm 1.5^\circ$ ) and smallest in the cranial L2-L3 segments ( $1.9\pm 1.4^\circ$ ,  $p=0.004$ ). The range of lateral flexion-extension rotation was also greatest at the most caudal L4-L5 segment (mean  $2.3\pm 1.4^\circ$ ) and decreased cranially to L2-L3 (mean  $1.7\pm 1.1^\circ$ ,  $p<0.01$ ). The bending rotation remained fairly constant across the studied levels ( $p=0.89$ ). With respect to translations, the range of craniocaudal translation was shown to be significantly greater in the caudal L4-L5 level than in the more cranial L2-L3 and L3-L4 levels ( $p<0.02$ , **Fig 5-5d**). Translations in the anteroposterior direction were not significantly different between the studied levels ( $p=0.63$ ).

#### **5.3.5 Facet orientation**

The transverse facet angle of both the superior and inferior facets increased from cephalad to caudad ( $p<0.05$ , **Table 5-1**). The longitudinal orientation of the superior articular facets was not found significantly different across the studied levels ( $p>0.5$ , **Table 5-2**). On the other hand, the inferior facets were found to be more vertically oriented in the caudad to cephalad direction ( $p<0.02$ ).



Table 5-1: Transverse Orientation of Lumbar Facets in Degrees°

Transverse Facet Orientation				
	Superior		Inferior	
	Left	Right	Left	Right
L2			22 ± 13	21 ± 11
L3	18 ± 6	21 ± 8	29 ± 16	30 ± 12
L4	27 ± 10	29 ± 7	40 ± 16	39 ± 13
L5	38 ± 16	41 ± 12		

\*The values represent average and standard deviation, respectively.

Table 5-2: Longitudinal Orientation of Lumbar Facets in Degrees°

Longitudinal Facet Orientation				
	Superior		Inferior	
	Left	Right	Left	Right
L2			170 ± 6	170 ± 5
L3	167 ± 7	168 ± 5	166 ± 4	166 ± 5
L4	167 ± 7	167 ± 8	163 ± 6	163 ± 6
L5	168 ± 5	168 ± 5		

\*The values represent average and standard deviation, respectively.

## 5.4 DISCUSSION

This Chapter measured the motions of the lumbar facet joints in 6DOF that occurred in response to different weight-bearing positions in asymptomatic volunteers. Overall, these results indicate that the facet joint motion was dependent upon body position and vertebral level. The data revealed that the lumbar joints have a range of motion that is of considerable magnitude. For example, during flexion-extension of the trunk the average range of translation was 3.5 mm and the average range of rotation was 6.5°. The facet joints of the cranial lumbar levels are more mobile during flexion-extension and the caudal levels during bending and torsion of the spine. The orientation of the facets was also different at different levels. In the more cranial levels the facets were oriented more sagittally and vertically and in the caudal lumbar vertebrae the orientation was more coronal and horizontal. During flexion-extension movements of the trunk, the facet joints rotated primarily along the medial-lateral axis and were translated in the cranial-caudal direction. However, during lateral bending and twisting, the facet joints did not rotate or translate in one dominant direction. Instead, the resulting motion represented a coupling of rotation and translation in different directions. Additionally, we observed that the translation was not symmetrical between the left and right sides at the same level.

There have only been a few studies published regarding facet joint kinematics in cadaveric human specimens.[5, 6, 14] Adams and Hutton[5] determined that the primary role of the lumbar facets were to resist intervertebral shear forces and secondarily to assist in resisting intervertebral compressive force in lordotic postures in order to prevent excessive motion.[5] Based on the CT scan of a cadaveric specimen of a 65-year-old man, Shariz-Adl[6] performed an analysis using a non-linear three-dimensional finite element model showing that intersegmental results were nonlinear and varied from one level to the next.

Overall, larger facet forces were computed in extension whereas flexion caused negligible contact forces. Currently there are no reports in the scientific literature on the 6DOF kinematics of the human lumbar facet joints *in vivo* during physiological weight-bearing motion.

There have been several prior attempts to study the kinematics of the native lumbar facet joints *in vivo* in animal models. Wood et al.[7] developed a canine model and measured the facet excursions at the L2-L3 motion segment during various functional activities using instrumented spatial linkage. They noted that during walking the average excursions between opposing facets were  $3.4 \pm 1.3$  mm as the facet surfaces glided on a ventral to dorsal slope, representing approximately 35% of the canine facet surface. Using a similar canine model, Schendel et al.[15] measured lumbar spine intervertebral and facet motion in the L2-L3 segment before and after instrumentation of the caudal motion segments (L3-L7). They observed similar magnitudes of excursion to those reported by Wood et al.[7] Further, they noted that following instrumentation of L3-L7, the excursions in the L2-L3 motion segment increased about 75% in length and 100% in width. Although it is difficult to compare this data directly to measurements obtained in human studies, we found similar overall magnitudes in facet translation in our study.

The kinematic differences noted in this Chapter may be related to the different orientation of the lumbar facets. The facets of the cranial segments (L2-L3) are oriented closer to the midsagittal plane of the vertebral body, while those of the caudal lumbar segments (L4-L5) are oriented further away from that plane. Such orientation has also been documented in larger series in the literature.[12] This may result in the opposing articulating surfaces blocking each other during axial torsion, thus preventing further motion and accounting for the smaller rotational ranges that we found in the cranial lumbar segments seen during axial torsion of the trunk. Furthermore, the inferior facets were more vertically inclined

in the cranial levels which may also explain the greater craniocaudal excursions that were seen in the cranial L2-L3 segment with progressively decreasing values caudally towards L4-L5, as well as the kinematic disparities measured during side-to-side bending of the trunk. During various physiological postures (flexion-extension or supine-standing) the range of motion was different at the two more cranial levels (L2-L4) from that of L4-L5. This may be related to the natural lordosis of the lumbar spine, since L4-L5 is in most cases located at the apex of the curve or directly below it.[16] The above mentioned factors (facet orientation and lordosis) may explain why the L4-L5 level behaves differently from L2-L3 and L3-L4. We noted that while L2-L3 and L3-L4 are more mobile in the sagittal plane, the L4-L5 level is more mobile in torsion and bending.

The findings of this Chapter may have important clinical implications. It is well documented that discogenic back pain is more common in the caudal (L4-L5 and L5-S1) than in the cranial lumbar levels[17-19] and that the annulus fibrosus is most likely to fail in torsion and bending.[20] This study shows that the cranial levels (L2-L3 and L3-L4) with more sagittal and vertical orientation of facets allow for greater motion to occur in the sagittal plane i.e., during flexion-extension of the trunk but are not as permitting to bending and torsion as the caudal L4-L5 level. Therefore, in the upper levels the intervertebral disc may be better protected from excessive torsion. Artificial designs should reproduce the level-specific motion range. Implants significantly limiting motion at the instrumented segments might put the adjacent segments at risk of developing degenerative changes[21-24] and conversely, excessive motion may abnormally stress the intervertebral disc.[25]

There are several limitations to this study. Firstly, in order to minimize the exposure to radiation, we chose to examine the endpoints of the studied motion arcs and did not examine the *in vivo* instantaneous positions of the vertebrae during dynamic motion of the body. Second, due to the limited field of view of

the fluoroscopes, we also had to limit our study to investigation of the L2-L5 segments during the three functional body movements. The L5-S1 segment was not included and should be a subject to further study. Another limitation is that the study focused on a narrow age range. However, it is important to note that the age range in this study closely reflects the demographics of the population that most commonly presents with facet joint generated symptoms.[4] In **Chapter 10**, the motion of facet joints of an age-matched group of patients with DDD was studied and compared with this healthy group. Despite the above limitations, our study represents the first non-invasive *in vivo* measurement of facet joint motion with various physiological loading conditions.

In conclusion, this Chapter utilized the imaging matching technique to quantitative study the motion of the lumbar facet joints during various weight-bearing positions. These findings provide baseline information to enable the study of kinematic changes that occur in pathologic conditions of the spine and to determine how these are affected following surgical intervention. For example, these findings may suggest that a segment level specific implant is necessary in order to accommodate the ROM of the lumbar facet joints under various physiological loading conditions. In the future, this information will help make improvements in posterior-element replacement designs and surgical techniques for the management of facet joint arthropathy. In **Chapter 10**, the motion of the facet joints of the healthy group was used as reference to compare with those of patients with DDD and clinical relevance was draw from the results.

## 5.5 References

1. Butler, D., et al., *Discs degenerate before facets*. Spine, 1990. **15**(2): p. 111-3.
2. Dunlop, R.B., M.A. Adams, and W.C. Hutton, *Disc space narrowing and the lumbar facet joints*. J Bone Joint Surg Br, 1984. **66**(5): p. 706-10.
3. Fujiwara, A., et al., *The relationship between disc degeneration, facet joint osteoarthritis, and stability of the degenerative lumbar spine*. J Spinal Disord, 2000. **13**(5): p. 444-50.
4. Cohen SP, R.S., *Pathogenesis, diagnosis, and treatment of lumbar zygapophysial (facet) joint pain*. Anesthesiology, 2007. **106**(3): p. 591-614.
5. Adams MA, a.H.W., *The mechanical function of the lumbar apophyseal joints*. Spine, 1983. **8**(3): p. 327-330.
6. Shirazi-Adl, A., *Biomechanics of the lumbar spine in sagittal/lateral moments*. Spine, 1994. **19**(21): p. 2407-14.
7. Wood KB, S.M., Pashman RS, Buttermann GR, Lewis JL, Ogilvie JW, Bradford DS, *In vivo analysis of canine intervertebral and facet motion*. Spine, 1992. **17**(10): p. 1180-1186.
8. Zhu Q, L.C., Sjøvold SG, Rosler DM, Keynan O, Wilson DR, Crompton PA, Oxland TR, *Biomechanical evaluation of the Total Facet Arthroplasty System*. Spine, 2007. **32**(1): p. 55-62.
9. Wilke HJ, S.H., Schmolz W, Drumm J., *Biomechanical evaluation of a new total posterior-element replacement system*. Spine, 2006. **31**(24): p. 2790-2796.
10. Wang S, P.P., Li G, Li G, Wood KB., *Measurement of vertebral kinematics using noninvasive image matching method-validation and application*. Spine, 2008. **33**: p. E355-E361.
11. Kozanek, M., et al., *Range of motion and orientation of the lumbar facet joints in vivo*. Spine (Phila Pa 1976), 2009. **34**(19): p. E689-96.
12. Masharawi, Y., et al., *Facet orientation in the thoracolumbar spine: three-dimensional anatomic and biomechanical analysis*. Spine, 2004. **29**(16): p. 1755-63.
13. Panjabi, M.M., et al., *Human lumbar vertebrae. Quantitative three-dimensional anatomy*. Spine, 1992. **17**(3): p. 299-306.
14. Miao, J., et al., *[Instant and fatigue stability analysis of anterior lumbar interbody fusion with stand-alone cage]*. Zhonghua Yi Xue Za Zhi, 2008. **88**(7): p. 457-60.
15. Schendel MJ, D.M., Ogilvie JW, Olsewski JM, Wallace LJ., *Kinematics of the canine lumbar intervertebral joints: An in vivo study before and after*

- adjacent instrumentation*. Spine, 1995. **20**(23): p. 2555-2564.
16. Rousouly, P., et al., *Classification of the normal variation in the sagittal alignment of the human lumbar spine and pelvis in the standing position*. Spine, 2005. **30**(3): p. 346-53.
  17. Dammers, R. and P.J. Koehler, *Lumbar disc herniation: level increases with age*. Surg Neurol, 2002. **58**(3-4): p. 209-12; discussion 212-3.
  18. Hsu, K., et al., *High lumbar disc degeneration. Incidence and etiology*. Spine, 1990. **15**(7): p. 679-82.
  19. Spangfort, E.V., *The lumbar disc herniation. A computer-aided analysis of 2,504 operations*. Acta Orthop Scand Suppl, 1972. **142**: p. 1-95.
  20. Hickey, D.S. and D.W. Hukins, *Relation between the structure of the annulus fibrosus and the function and failure of the intervertebral disc*. Spine, 1980. **5**(2): p. 106-16.
  21. Quinell, R.C. and H.R. Stockdale, *Some experimental observations of the influence of a single lumbar floating fusion on the remaining lumbar spine*. Spine, 1981. **6**(3): p. 263-7.
  22. Yang, S.W., N.A. Langrana, and C.K. Lee, *Biomechanics of lumbosacral spinal fusion in combined compression-torsion loads*. Spine, 1986. **11**(9): p. 937-41.
  23. Lee, C.K. and N.A. Langrana, *Lumbosacral spinal fusion. A biomechanical study*. Spine, 1984. **9**(6): p. 574-81.
  24. Xia, Q., et al., *Diagnosis and treatment of discogenic low back pain*. Zhonghua Guke Zazhi - Chinese Journal of Orthopaedics, 2007. **27**(3): p. 162-166.
  25. Zander, T., et al., *Influence of graded facetectomy and laminectomy on spinal biomechanics*. Eur Spine J, 2003. **12**(4): p. 427-34.





# Chapter 6

## ***In vivo* range of motion of the spinous process**

### **6.1 Introduction:**

Previous kinematic studies of the spine have primarily focused on the anterior elements of the spine, such as the vertebral bodies[1-5]and intervertebral discs [1]. The majority of these studies have measured the relative translation and rotation of adjacent vertebrae in the sagittal plane under various loading conditions. More recent studies have also tried to determine 6DOF intervertebral kinematics [2, 3, 6]. In contrast, limited data has been reported on the motion patterns of the posterior elements of the spine, such as basic kinematic data on the facet joints and interspinous processes (ISPs). In the last Chapter, the *in vivo* motion of the facet joints has been investigated. This Chapter has extended the focus to the motion of the spinous process. The information is necessary for the evaluation of traumatic injuries and degenerative changes in the posterior elements, as well as for improving the surgical treatment of spinal diseases using posterior procedures; such as the use of interspinous process devices (ISPD) for the treatment of spinal stenosis [7].

A review of the current literature reveals that a paucity of data has been reported on the motion patterns of the spinous processes. Neumann et al.[8] described a simple method using plain anterior-posterior (AP) radiographs in

asymptomatic subjects for the measurement of ISP distances between adjacent lumbar spine levels in order to detect ruptures of the posterior ligamentous structures. In another study, Fisher et al.[9] measured ISP distance in normal subjects in the sitting position, with and without hip flexion, using a medial-lateral fluoroscopic imaging technique. Positional MRI has been used by Siddiqui et al. [1, 10] to study spinal canal dimensions as well as sagittal kinematics of the vertebrae and intervertebral discs both prior to and following ISPD implantation. Lastly, Lindsey et al. [11] also performed cadaveric testing to measure spinous process motion. However, adequate information on the native kinematics of the lumbar spinous processes, which can be used as a baseline from which to measure the changes that occur post-implantation of ISPDs, has yet to be reported.

The purpose of this Chapter was to quantify the kinematics of the lumbar spinous processes in asymptomatic patients during un-restricted functional body movements with physiologic weight-bearing, using the combined MRI and DFIS technique[12]. We hypothesized that motion of spinous processes would be dependent on loading conditions and vertebral level.

## **6.2 Materials and Methods:**

Details of the general experiment setup and testing procedures of the combined MR and DFIS were included in **Chapter 2**. The motion of the spinous was calculated from the same subject group used in **Chapter 3**. Specific steps used in this study were listed below.

3D models of the lumbar vertebrae L2-L5 of eight normal subjects were obtained from supine MRI. Using the DFIS, kinematics of the lumbar spine of during standing, flexion-extension and left-right twisting were determined. The relationship between the spinous processes at different positions was directly

measured from the reproduced vertebrae models. First, the shortest distances between the spinous processes were measured in the modeling software at supine, standing, flexion and extension positions (**Fig 6-1a**). The ISP distances at approximated ISPD locations were also measured (details provided in **6.5 Appendix**). In addition, right handed Cartesian coordinate systems were also established at the tips of the spinous processes (**Fig 6-1b**). For the purposes of this study, rotation about the z (proximal-distal) axis and displacement in the x (medial-lateral) axis were used to determine the interspinous rotation and displacement in the transverse plane, respectively, during left-right twisting body motion.

A repeated measure ANOVA was used to compare the ISP relationship at the L2-3, L3-4, and L4-5 vertebral levels in the same posture as well as the same level during different the weight-bearing positions. Statistical significance was set at  $p < 0.05$ . When a statistically significant difference was detected a Newman-Keuls post-hoc test was performed. The statistical analysis was done using a software program (Statistica, Statsoft, Tulsa, OK).

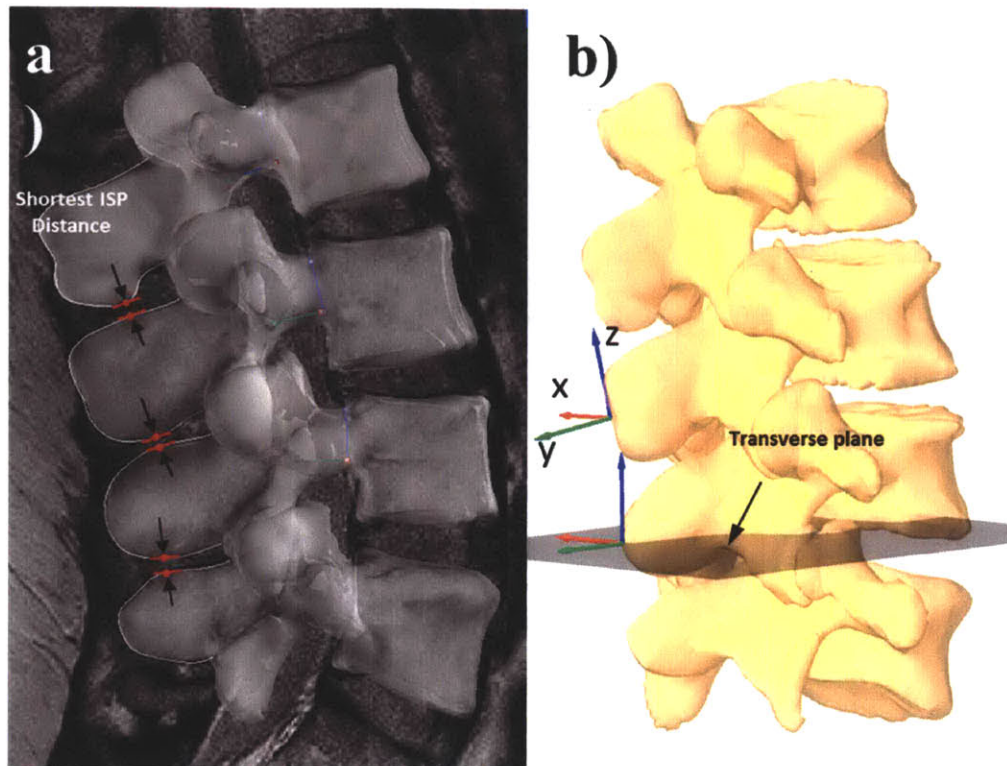


Fig 6-1. a) shortest distance was measured between adjacent processes; b) Local coordinate systems were established at the tip of the process to measure rotational angle and displacement in the transverse plane

### 6.3 Results:

The shortest ISP distances were determined at the L2-L3, L3-L4, and L4-L5 motion segments in the supine, standing, extension and flexion positions (**Table 6-1**). The shortest ISP distances decreased from the supine position at MRI scan to the weight-bearing standing position. Statistical significance was found for the L2-L3 ( $P = 0.036$ ) and L3-L4 ( $P = 0.025$ ) motion segments but not for L4-L5 ( $P = 0.309$ ). They also slightly decreased when going from standing to maximal extension but no statistical difference was determined ( $P > 0.05$ ). Predictably, they increased significantly when going from standing to maximal flexion for L2-L3 ( $P = 0.028$ ) and L3-L4 ( $P = 0.018$ ) but no significant difference was found for L4-L5 ( $p = 0.288$ ). They also increased significantly when going from maximal extension to flexion for L2-3 ( $P = 0.004$ ) and L3-4 ( $P = 0.005$ ), but not for L4-5 ( $P = 0.191$ ). (**Fig 6-2**)

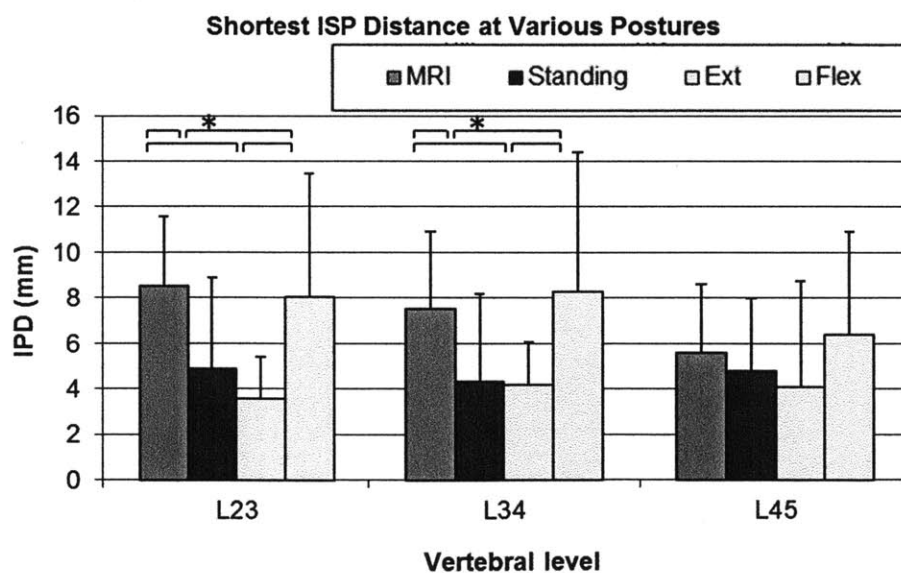


Fig 6-2. Shortest distance between processes at various postures and different levels (\*  
 $p < 0.05$ )

Table 6-1: Shortest distance between processes (\* p<0.05 when compared with MRI; # p<0.05 when compared with Flexion)

	L2-3 (mm)	L3-4 (mm)	L4-5 (mm)
<b>MRI</b>	8.5 ± 3.1	7.5 ± 3.0	5.6 ± 3.0
<b>Standing</b>	4.9 ± 4.0* <sup>#</sup>	4.3 ± 3.9* <sup>#</sup>	4.8 ± 3.2
<b>Extension</b>	3.5 ± 1.8* <sup>#</sup>	4.2 ± 1.9* <sup>#</sup>	4.1 ± 4.7
<b>Flexion</b>	8.1 ± 5.4	8.3 ± 6.1	6.4 ± 4.5

ISP distances were also compared between different vertebral levels. The only significant difference was noticed in the MRI (supine) position. At this position, the L4-L5 distance was found to be significantly smaller than those of L2-L3 (P = 0.003) and L3-4 (P = 0.018). The distance changes that occurred while going from the flexion to the extension positions were also determined and were as follows: L2-L3 = 4.5 ± 4.8 mm, L3-L4 = 4.1 ± 5.0 mm and L4-L5 = 2.0 ± 2.3mm. **(Fig 6-3)** No significance was seen between the different levels during this positional change.

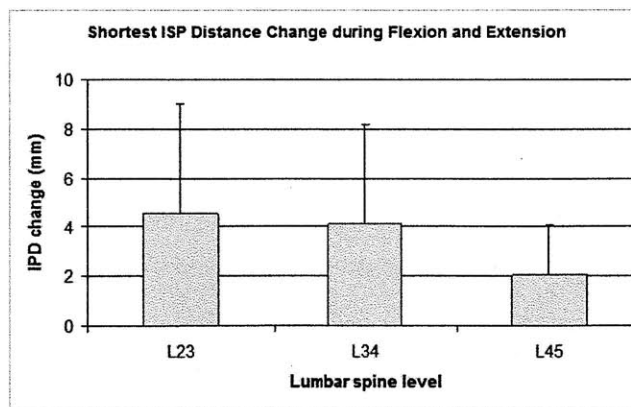


Fig 6-3. Distance change between processes during flexion and extension

During left and right twisting movements, the range of rotational angles for the spinous processes was determined for each subject to be the following: L2-L3 =  $2.1 \pm 1.2^\circ$ , L3-L4 =  $2.7 \pm 2.5^\circ$  and L4-L5 =  $3.0 \pm 2.1^\circ$  (**Table 6-2**). The mean displacement in the transverse plane ranged from 1.5 to 2.3 mm when measured from the tip of the spinous process. No statistical significance was found for either rotational angle or displacement at the different levels, despite mean rotation increasing from the L2-L3 to L4-L5 segments.

Table 6-2: ISP rotation and displacement in the transverse plane

	<b>Rotational Angle (deg)</b>	<b>Displacement (mm)</b>
<b>L2-3</b>	$2.1 \pm 1.2$	$1.5 \pm 0.9$
<b>L3-4</b>	$2.7 \pm 2.5$	$2.3 \pm 1.6$
<b>L4-5</b>	$3.0 \pm 2.1$	$1.8 \pm 1.8$

## 6.4 Discussion:

This Chapter measured the changes of the ISP distances as well as the rotation of ISP in response to different weight-bearing postures in asymptomatic living subjects. The data revealed that the ISP distance decreased from L2-L3 to L4-L5 when measured in the supine, relaxed position (during MRI scanning); with significantly higher values found at the L2-L3 and L3-L4 motion segments when compared to that of L4-L5. However, under weight-bearing conditions while in the standing position, the ISP distance ranged between 4 and 5 mm at all levels. During maximal extension the ISP distances at the L2-L3 and L3-4 motion segments were found to be significantly reduced by approximately 4.0 mm compared to flexion, but no significant changes were detected at the L4-L5 segment. During flexion, the ISP distances were not found to be significantly

different than those measured in the MRI position at all levels tested. Going from the left to right twist positions the lower motion segments had higher amounts of ISP rotation. The range of translation in the transverse plane during left and right twist was approximately 2.0 mm at all segments. Overall, these results indicate that the ISP distance changes were dependent upon body posture and vertebral level.

There have been several prior attempts to study the kinematics of the native lumbar spinous processes. Neumann et al.[8] measured lumbar ISP distance changes between adjacent levels in the standing position to detect ruptures of the posterior structures of the lumbar spine. They concluded that a difference in ISP distance between adjacent levels exceeding 7 mm was consistent with incompetence of the posterior structures and potential instability. However, it is important to note that their technique of measuring the ISP distance used the distance between the posterior ends of the spinous processes on the plain AP radiograph, which makes a direct comparison with our data difficult. In another study, Fisher et al.[9], reported mean lumbar ISP distances at the L2-L3, L3-L4, and L4-L5 motion segments of 10.9 mm, 9.9 mm and 10.1 mm, respectively. When measured with the hips flexed, these values were found to increase by 7%, 11% and 21%, respectively. Their findings also showed larger ISP distances than ours at each segmental level. This may be due to the flexed position of their subjects while sitting, in contrast to our subjects who had no physical restrictions placed on the hips during flexion and extension of the trunk.

The study of ISP distance during functional activities has direct clinical relevance. Recently, several interspinous process devices (ISPD) have been approved in the United States for the treatment of spinal stenosis [7]. These devices are implanted between the spinous processes in order to produce flexion at



the motion segment and enlarge the spinal canal and neural foramina; thereby attempting to improve the symptoms of neurogenic claudication and other conditions. Theoretically, such devices would allow for a normal ISP motion pattern at the implanted level while at the same time not affecting the kinematics of adjacent segments. However, few studies have examined the rotational and translational movement patterns of the ISP in normal lumbar spines. Most of the data that has been published concerning spinous process kinematics has been post ISPD implantation and has focused on the resultant changes that occur in the dimensions of the spinal canal, neural foramina[1, 13], and the intervertebral disc[1]. There is limited data available concerning the effects of ISPD on spinous process motion, with the available data being mainly obtained from *in vitro* studies under various loading conditions [11]. For example, a cadaveric study performed by Lindsey et al. [11] on seven lumbar spines (L2-L5) specimens demonstrated marked restriction in flexion-extension motion in the sagittal plane at the level of insertion, but not at the adjacent levels. No changes in axial rotation or lateral bending were appreciated at any level tested; including the level of insertion. Our data on normal ISP motion, that is loading and segment level dependent, can be used as a normal reference when evaluating the effect of ISPD on ISP motions.

Knowledge of *in vivo* spinous process kinematic data before and after ISPD implantation is extremely limited in the current literature. In their multicenter, prospective, randomized trial, Zucherman et al. [7] performed a radiographic analysis at each follow-up interval that included measurement of ISP distances. When compared to a control group, the treated group demonstrated no significant differences in the mean values of ISP distance or any other radiographic measurements made at either the 1-year or 2-year follow-up visits. [7] These authors used the method described by Neumann et al.[8], which includes the

height of the spinous process instead of simply measuring the ISP gap. In our study we used a method similar to that proposed by Fisher et al.[9] to measure the shortest ISP distance. The method has been shown to be more accurate for the measurement of distances between spinous processes and can also replicate ISPD location.[9, 14] Therefore, the method could be invaluable for evaluation of *in vivo* spinous process kinematics before and after ISPD implantation in patients.

There are several limitations to our study. Our sample size represented a relatively small number of subjects and the study focused on a narrow age range. However, it is important to note that the age range in this study closely reflects the demographics of the population most commonly treated for symptomatic spinal stenosis [15]. Despite the above limitations, our study represents the first *in vivo* measurement of ISP distance under various physiological loading conditions.

In conclusion, the study of this Chapter has provided us with quantitative data on the motion of the spinous processes during various weight-bearing postures. The findings may suggest that a segment level specific ISPD would be necessary in order to accommodate the ROM of ISPs under various physiological loading conditions. In the future, the information will help make improvements in ISPD design and surgical techniques for the management of spinal stenosis.

## 6.5 Appendix:

In addition to the shortest ISP distances, we also measured and compared the ISP distances at the approximated ISPD locations[3]. Using a geometric technique, smooth tangential curves were drawn through the outermost tips of the spinous processes of L2-L5 from the sagittal MRI images. The curve was offset 10 mm towards the vertebral body to replicate the location of ISPDs[3]. The ISP distance between “a” and “b” was measured at each level (Fig 6-4). When measuring this distance we anticipated that we would find similar trends and statistical differences with larger numerical values when compared to our initial technique of measuring the shortest distances.

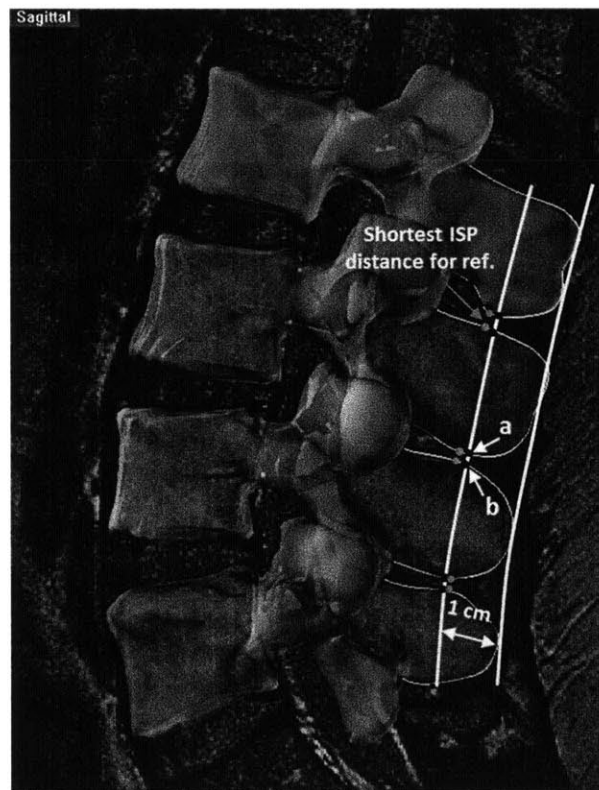


Fig 6-4. ISP distance at approximated ISPD positions (between a and b). Shortest ISP distances were also shown for reference.

The ISP distances between “a” and “b” were determined at the L2-L3, L3-L4, and L4-L5 segments for the MRI, standing, extension and flexion positions (**Table 6-3**). During movement activities, the distances between the motion segments decreased from the supine position at the time of the MRI scan to the standing position during the fluoroscopic imaging. Statistical significance was found for the L2-L3 ( $P = 0.017$ ) and L3-L4 ( $P = 0.021$ ) motion segments but not for L4-L5 ( $P = 0.742$ ). They also slightly decreased when going from standing to maximal extension but no statistical difference was determined ( $P > 0.05$ ). Predictably, they increased significantly when going from standing to maximal flexion for L2-L3 ( $P = 0.016$ ) and L3-L4 ( $P = 0.002$ ) but not significantly for L4-L5 ( $p = 0.216$ ). They also increased when going from the extension to the flexion position but no significance was found for any of the three segments that were tested ( $P > 0.05$ ) (**Fig 6-5**).

Table 6-3: Distance between processes measured between approximated ISPD location at various postures and different levels (\*  $p < 0.05$  compare with MRI; #  $p < 0.05$  compare with Flexion)

	L2-3 (mm)	L3-4 (mm)	L4-5 (mm)
<b>MRI</b>	9.3 ± 2.9	8.1 ± 3.1	6.1 ± 2.7
<b>Standing</b>	5.5 ± 4.5* <sup>#</sup>	5.2 ± 4.0* <sup>#</sup>	5.8 ± 3.4
<b>Extension</b>	4.4 ± 2.0* <sup>#</sup>	4.7 ± 2.0* <sup>#</sup>	5.1 ± 4.9
<b>Flexion</b>	8.8 ± 5.8	9.8 ± 5.4	7.6 ± 4.9

Using this technique, the ISP distances were also compared between different vertebral levels. The only significant difference was noticed in the MRI

(supine) position. The L4-L5 distance was found to be significantly smaller than the L2-L3 ( $P = 0.002$ ) and L3-4 ( $P = 0.016$ ) distances. The distance changes that occurred while going from the flexion to the extension positions were also determined and were as follows: L2-L3 =  $4.4 \pm 4.5$  mm, L3-L4 =  $5.1 \pm 4.5$  mm and L4-L5 =  $2.5 \pm 2.7$ mm. No significance was seen between the different levels during this positional change (**Fig 6-6**). Overall, the values were on average 0.5-1.5mm larger than those obtained when measuring the shortest ISP distances. However, similar trends and statistical differences were noticed as was anticipated. It is therefore conceivable that either set of values can be used as a reference for future studies.

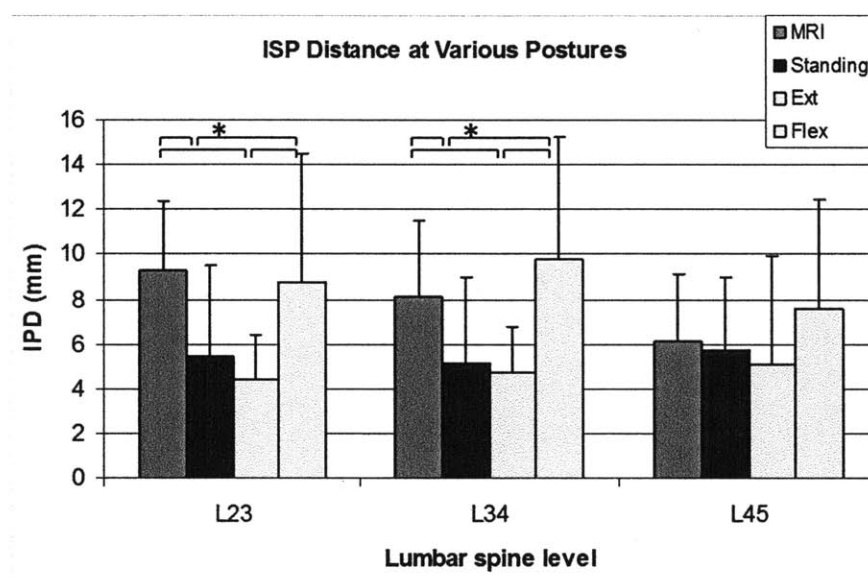


Fig 6-5. Distance between processes measured at approximated ISPD locations at various postures and different levels (\*  $p < 0.05$ )

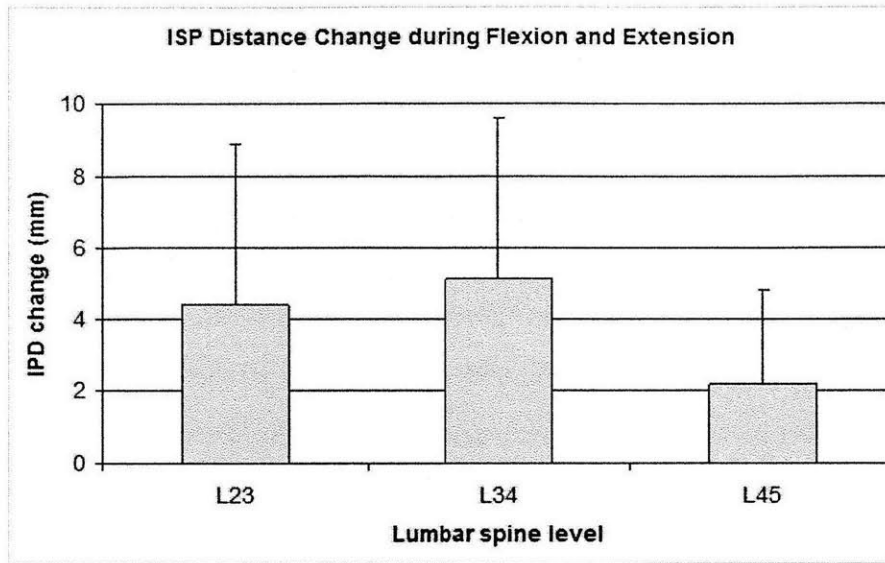


Fig 6-6. Distance change between processes during flexion and extension at different levels, measured at approximated ISPD locations

## 6.6 References

1. Siddiqui, M., et al., *Effects of X-STOP device on sagittal lumbar spine kinematics in spinal stenosis*. J Spinal Disord Tech, 2006. 19(5): p. 328-33.
2. Ochia, R.S., et al., *Three-dimensional in vivo measurement of lumbar spine segmental motion*. Spine, 2006. 31(18): p. 2073-8.
3. Wang, S., et al., *Measurement of vertebral kinematics using noninvasive image matching method-validation and application*. Spine, 2008. 33(11): p. E355-61.
4. Fujiwara, A., et al., *The effect of disc degeneration and facet joint osteoarthritis on the segmental flexibility of the lumbar spine*. Spine, 2000. 25(23): p. 3036-44.
5. Lee, S.W., et al., *Development and validation of a new technique for assessing lumbar spine motion*. Spine, 2002. 27(8): p. E215-20.
6. Steffen, T., et al., *A new technique for measuring lumbar segmental motion in vivo. Method, accuracy, and preliminary results*. Spine, 1997. 22(2): p. 156-66.
7. Zucherman, J.F., et al., *A multicenter, prospective, randomized trial evaluating the X STOP interspinous process decompression system for the treatment of neurogenic intermittent claudication: two-year follow-up results*. Spine, 2005. 30(12): p. 1351-8.
8. Neumann, P., et al., *Determination of inter-spinous process distance in the lumbar spine. Evaluation of reference population to facilitate detection of severe trauma*. Eur Spine J, 1999. 8(4): p. 272-8.
9. Fisher, A., et al., *Hip flexion and lumbar puncture: a radiological study*. Anaesthesia, 2001. 56(3): p. 262-6.
10. Siddiqui, M., et al., *Influence of X Stop on neural foramina and spinal canal area in spinal stenosis*. Spine, 2006. 31(25): p. 2958-62.
11. Lindsey, D.P., et al., *The effects of an interspinous implant on the kinematics of the instrumented and adjacent levels in the lumbar spine*. Spine, 2003. 28(19): p. 2192-7.
12. Xia, Q., et al., *In vivo range of motion of the lumbar spinous processes*. Eur Spine J, 2009. 18(9): p. 1355-62.
13. Richards, J.C., et al., *The treatment mechanism of an interspinous process implant for lumbar neurogenic intermittent claudication*. Spine, 2005. 30(7): p. 744-9.
14. Bono, C.M. and A.R. Vaccaro, *Interspinous process devices in the lumbar spine*. J Spinal Disord Tech, 2007. 20(3): p. 255-61.
15. Kim, D.H. and T.J. Albert, *Interspinous process spacers*. J Am Acad

Orthop Surg, 2007. 15(4): p. 200-7.



# Chapter 7

## ***In vivo* Motion Characteristics of Lumbar Vertebrae in the Sagittal and Transverse Planes**

### **7.1 Introduction**

Knowledge of motion patterns of lumbar vertebrae is important for motion preserving treatment of intervertebral disc diseases such as dynamic fusion or total disc replacement. Numerous studies have reported on the vertebral rotation under various simulated loading conditions [1-4]. Furthermore, many *in vitro* investigations have measured intervertebral center of rotation (COR) using cadaveric spine specimens [5-9] or finite element (FE) analysis [10-12] under applied torques to simulate flexion-extension or left-right twisting. For example, flexion-extension COR in the sagittal plane has been determined using cadaveric specimens by Gertzbein et al. [7], Haer et al. [6] and White and Panjabi [8]. Shirazi-Adl et al. [11] and Schmidt et al. [12] used FE models to analyze the center of rotation under various applied moments during flexion-extension and left-right twisting.

*In vivo* studies have mostly employed X-ray images to determine the vertebral COR in the sagittal planes [13-17]. Recently, CT, MRI and dual plane fluoroscopic imaging techniques have been used to investigate 3D motions of the vertebral body [18-21]. While these studies have reported 6DOF vertebral body motion in terms of translation and rotation, no data has been reported on the CORs

of the vertebrae in living human subjects under functional weight-bearing conditions. This knowledge is especially important since prosthesis design and surgical implantation with different CORs can alter the motion characteristics, whereby directly affecting clinical outcomes [22, 23].

From the combined MR and DFIS technique, 6DOF motion of the anatomic structures of the lumbar vertebrae has been investigated during various functional weight-bearing activities in the previous **Chapters 3 to 6** [24-26]. In this Chapter, further investigation of the CORs in the 2D sagittal and transverse planes in normal human subjects was performed from the motion characteristics of different portions of the vertebrae [27].

## **7.2 Materials and Methods**

Details of the general experiment setup and testing procedures of the combined MR and DFIS were included in **Chapter 2**. The study was performed on the same subject group in **Chapter 3**. In addition, 2 more healthy subjects were involved, resulting a total of 10 subjects. Specific steps used in this study were listed below.

### ***7.2.1 Coordinate system of the vertebral body:***

For each vertebra, the cylindrical volume of the vertebral body was obtained from the mesh model. The origin of the coordinate system was at the volumetric center calculated using the Rhinoceros software (**Fig 7-1**). The x-y plane was parallel to a plane that fitted through the mesh vertices of the endplate. The y-axis was set along the spinous process, pointing in the posterior direction. The x-axis was set perpendicular to the y axis, pointing in the left direction. The z-axis was set perpendicular to the x-y plane. The transverse plane was chosen to

be the x-y plane of the proximal vertebra of the two vertebrae to study the relative motions of the vertebrae (e.g, L2 for L23, L3 for L34) (**Fig 7-2**). The sagittal plane was chosen to be the y-z plane of the vertebra.

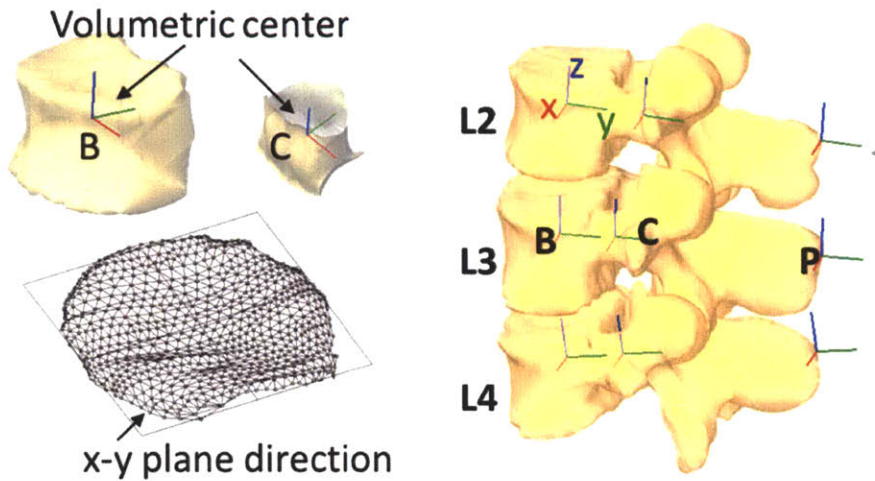


Fig 7-1. Coordinate systems at the volumetric center of the vertebral body (B), the center of spinal canal (C), and the tip of spinous process (P) based on anatomic features.

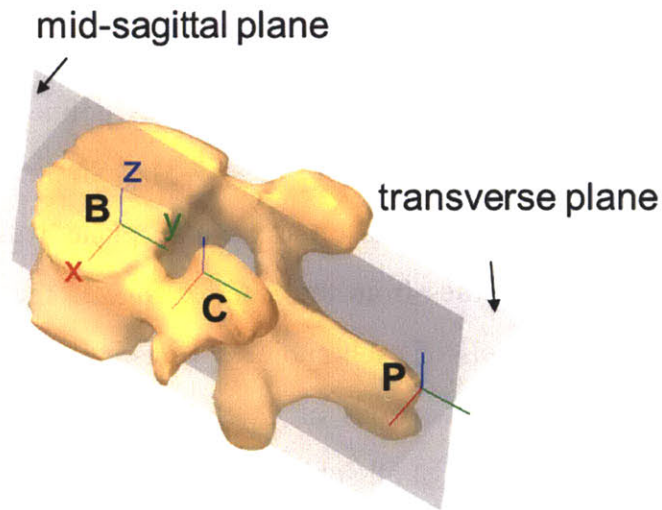


Fig 7-2. Mid-sagittal and transverse planes were determined for calculating ROMs and CORs

### **7.2.2 Coordinate system of the spinal canal:**

The volumetric center of the cylindrical volume of the canal was defined as the origin of the spine canal (Fig 7-1). The directions of the three axes were consistent with those of the vertebral body.

### **7.2.3 Coordinate system of the spinous process:**

The origin of the coordinate system of a spinous process was chosen as the intersection point of the transverse plane of the vertebral body, and the tip of the spinous process (Fig 7-1). The directions of the three axes were consistent with those of the vertebral body.

### **7.2.4 Data analysis**

Using the coordinate systems of the different portions of the vertebra, ROMs of L2 with respect to L3 (L23) and L3 with respect to L4 (L34) during the flexion-extension and left-right twisting activities were determined in the primary sagittal and transverse planes (Fig 7-2). For each subject, the ROMs at the three anatomic locations were fitted using linear least squares to calculate the point of zero displacement in the sagittal plane, which was defined as the COR during flexion-extension in the sagittal plane (Fig 7-3). Similarly, the COR of the vertebra during left-right twisting on transverse plane was determined. The lengths of the vertebral bodies from the anterior edge to the posterior edge were measured at the three levels of each subject. Considering the differences in the sizes of the vertebrae, the locations of CORs were normalized by the average length of the vertebral bodies of all subjects. In this way, the average locations of the CORs of all subjects were determined under *in vivo* weight-bearing flexion-extension and left-right twisting activities.

A repeated measures ANOVA was used to compare the differences of

ROMs at the center of the vertebral body, the center of the spinal canal and the tips of the spinous processes, and those between L23 and L34. Statistical significance was set at  $p < 0.05$ . When a statistically significant difference was detected, a Newman-Keuls post-hoc test was performed. The statistical analysis was performed using the Statistica® (Statsoft, Tulsa, OK) software.

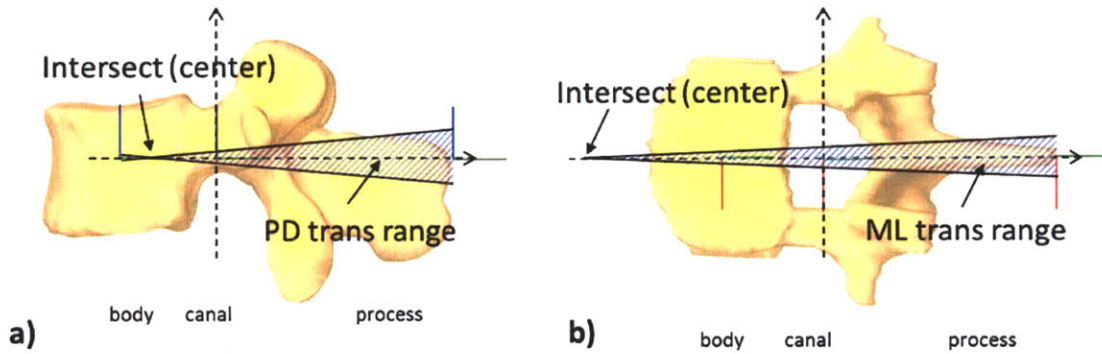


Fig 7-3. Schematic of COR's location calculated from points of zero displacement points: a) in the sagittal plane; and b) in the transverse plane

### 7.3 Result

The average morphological parameters of the vertebrae were measured in all subject (**Table 7-1**) and there is no significant difference among L2, L3 and L4.

Table 7-1: Anatomic measurement (average  $\pm$  SD) of distances: from the center of vertebral body to that of the canal (B-C), from the center of the canal to the tip of the spinous process (C-P), and from the anterior to posterior edge of the vertebral body (B)

	Anatomic Measurement (mm)		
	B	B - C	C - P
L2	29.5 $\pm$ 4.1	22.1 $\pm$ 1.1	43.1 $\pm$ 4.9
L3	29.6 $\pm$ 3.4	22.3 $\pm$ 0.9	45.2 $\pm$ 4.8
L4	30.3 $\pm$ 3.6	22.9 $\pm$ 0.9	46.9 $\pm$ 4.3

ROMs of L23 (L2 with respect to L3) and L34 (L3 with respect to L4) were determined at the center of each vertebral body, at the center of the spinal canal, and at the tip of the spinous process (**Table 7-2**). The translation of L23 and L34 segments increased proportionally ( $p < 0.05$ ) from anterior to posterior locations. No statistically significant difference was found in the ROMs between L23 and L34. During flexion-extension, the ranges of rotations of L23 and L34 in the sagittal plane were calculated to be  $6.8 \pm 2.9^\circ$  (mean  $\pm$  standard deviation) and  $6.7 \pm 2.3^\circ$ , respectively. During the left-right twisting, the ranges of rotations of L23 and L34 in the transverse plane were calculated to be  $3.2 \pm 1.9^\circ$  and for  $2.8 \pm 1.7^\circ$ , respectively.

Table 7-2: ROM (average  $\pm$  SD) measured at different anatomical locations on the lumbar vertebral segments. Centers of vertebral body (B), centers of the canal (C), tips of the spinous process (P)

<b>Translation during Flexion/Extension (mm)</b>			
	<b>B</b>	<b>C</b>	<b>P</b>
<b>L23</b>	-0.3 $\pm$ 0.3	2.5 $\pm$ 1.7	7.5 $\pm$ 3.2
<b>L34</b>	-0.6 $\pm$ 0.3	2.3 $\pm$ 1.1	7.3 $\pm$ 3.6
<b>Translation during Left-Right Twisting (mm)</b>			
	<b>B</b>	<b>C</b>	<b>P</b>
<b>L23</b>	0.7 $\pm$ 0.4	1.1 $\pm$ 1.0	1.6 $\pm$ 0.9
<b>L34</b>	1.0 $\pm$ 0.9	1.4 $\pm$ 1.3	2.3 $\pm$ 1.6

After determining the ROMs at the three anatomic locations, linear least squares fits were used to calculate the point of zero displacement in the sagittal and transverse planes. The  $R^2$  were larger than 0.99 with  $p < 0.03$  for each subject at different levels. The averaged slopes of the fitting lines were listed in **Table 7-**

3. Normalized by the average size of the vertebrae (**Table 7-1**), the CORs of flexion-extension in the sagittal plane for L23 and L34 were located at about 5.0 mm posterior to the central axis of the vertebral body (a distance about one-third the length of the vertebral body, from the posterior edge) (see **Fig 7-3a**, **Table 7-3**). The CORs of left-right twisting, in the transverse plane, were about 30 mm anterior to the front edge of the vertebral body (see **Fig 7-3b**, **Table 7-3**).

Table 7-3: Average slope of the linear fitting lines and calculated COR locations. (+) indicating a distance anterior to the anterior edge of the vertebral body and (-) indicating a distance posterior to that.

	Flexion/Extension Slope (deg)	Twisting Slope (deg)	Flexion/Extension COR (mm)	Twisting COR (mm)
<b>L23</b>	6.8 ± 2.9	3.2 ± 1.9	-19.0 ± 3.2	+35.1 ± 6.7
<b>L34</b>	6.7 ± 2.3	2.8 ± 1.7	-20.5 ± 2.9	+32.2 ± 6.1

## 7.4 Discussion

Motion of the lumbar vertebrae is difficult to describe because of the complicated geometric structures involved. This Chapter investigated the ROMs of different portions of the vertebrae and CORs of vertebral segments in the sagittal plane during flexion-extension and the transverse plane during left-right twisting of the body. The results showed that the anterior portion of the vertebrae had smaller ROM than the posterior portion. Concurrently, we observed that the vertebrae rotated with the CORs located at approximately the posterior one-third of the vertebral body in the sagittal plane. However, in the transverse plane the vertebrae rotated with respect to points which were approximately 30 mm in front of the vertebrae. The results demonstrated that the vertebrae have different CORs under different primary body rotations.

The majority of the previous *in vivo* kinematic studies has focused on measurements of the rotational ROM of the vertebral body and the translation of the proximal vertebrae with respect to the distal vertebrae[18-21, 28]. Pearcy[28] used a biplanar X-ray technique and found that coupled vertebral translations measured from the center of the vertebral body were less than 1.0 mm during flexion-extension and left-right twisting movements. Our study found similar translational ROM for the center of the vertebral body.

There are several reports in the literature on the lumbar vertebral CORs in the sagittal plane during flexion-extension of the lumbar spine [5-10, 12-17]. Yoshioka et al.[15] studied 61 healthy cases of L1-L5 lumbar segment using 2D X-ray measurements and concluded that the flexion-extension center of rotation was 2.6 to 5.9 mm posterior to the central axis of the vertebral body. Gertzbein et al.[7] studied the flexion-extension CORs of 10 cadaveric specimens and reported an average location of the COR of 11.6 mm from the posterior edge of the



vertebral body. Similar results have also been reported in separate cadaveric series by White and Panjabi [8] and Rousseau et al. [5]. In general, our data are in agreement with the data reported in the literature. We found that the COR in the sagittal plane was located posterior to the centers of the vertebral bodies for the L23 and L34 segments.

In contrast, relatively few studies have reported on the CORs of the lumbar vertebrae in the transverse plane[6, 12]. Shirazi-Adl et al.[11] analyzed motion of the L23 segment under an axial torque alone and combined a compression load using a finite element (FE) model. They found that with the application of a small torque (1 Nm), the COR in the transverse plane was located roughly at the center of the vertebral body. When a larger torque was applied, however, the COR shifted posteriorly and with hypertorsion (60Nm) it was posterior to the vertebral body. Similarly, Schmidt et al.[12] using a FE model and found that when a larger torque (7.5 Nm) was applied, the COR was closer to the facet joints. Haher et al.[6] applied rotational angle of 10° on each side of 10 cadaveric lumbar segments from T1 to S1 and found the COR at the vicinity of facet joints. More recently, Wachowski et al.[29] performed a cadaveric study of 2 L3/L4segments and reported instant helical axis migrated from one facet joint to the other along either ventrally or dorsally curved centrodes under combined compressive loads and axial torques. The CORs determined in our study during twisting were in front of the vertebral body and close to the center of the trunk in the transverse plane, which were different from the above literatures. The above literatures suggested that facet joints come into contact and the CORs of vertebrae shift towards the facet under large axial motion. In our study, the *in vivo* facet joints (Kozanek, et al., 2009) and the vertebrae[25] translated in a range within 2mm and therefore facet joints might not provide the major constrains to vertebral motion under *in vivo* loading conditions. There were contributions from all surrounding tissues.

Furthermore, under *in vivo* loading conditions the torques might be a combination of various moments that were different from those applied in FE and cadaver studies. In *in vitro* tests, the axis measured may be the rotating axis imposed by the testing machines rather than the true rotational axis. Thus, a direct comparison of our *in vivo* study data to the results reported in the literature is difficult, if not impossible.

The CORs obtained in this study may have important clinical implications for treatment of lumbar disc disease. Several short and mid-range follow-up studies have reported satisfactory clinical results using various total disc replacement designs [30-32]. Other reports argued that long-term follow-up studies of the currently available total disc replacement designs do not show better results than spinal fusion surgeries[33]. There are studies showing that the location of the artificial disc during implantation can significantly affect the clinical outcome[22]. In general clinical practice, the artificial disc was positioned in a relatively posterior position during surgery. McAfee et al.[22] described that the ideal location for placement of the Charité prosthesis is 2 mm posterior to the midpoint of the vertebral body in the sagittal plane. This is consistent with the fact that the COR in the sagittal plane is at the posterior portion of the vertebra. However, no study to date has investigated the effect of the COR of an artificial disc in the transverse plane. From a biomechanical standpoint, changes in the location of the COR in the transverse plane may introduce additional constraints to the rotational motion of the lumbar spine. Future studies are necessary to delineate the effect of the CORs of the disc replacement devices in the transverse plane on biomechanics of the vertebral segments and on clinical outcomes.

There are certain limitations that should be noted in the current study. We only investigated the maximal lumbar motions with minimal pelvic motion, and

the coupled motion of lumbar-pelvic rhythm was not considered. In fact, previous studies [34, 35] have shown that pelvic tilt could affect the posture and motion of the lumbar spine. In addition, we only investigated the end positions of the maximal trunk movements and only used a 2D linear fit method to calculate CORs in the sagittal and transverse planes. In the future 3D dynamic motion of the entire spine should be studied to explore the *in vivo* 3D helical axis of vertebral motions as well as to investigate the relationship between CORs and the range of spine motion.

In conclusion, the combined dual fluoroscopic and MR imaging technique was applied to investigate the motion characteristics of different portions of the vertebrae and CORs of lumbar vertebrae in 2D sagittal and transverse planes in normal human subjects. Of all studied portions of the vertebral segments, the vertebral body was found to have the smallest ROMs. In addition, the vertebral CORs were different under different physiological loading conditions. During flexion-extension of the torso, the COR was found at the posterior one third of the vertebral body in the sagittal plane and during left-right twisting, the COR was found at about 30 mm anterior to the vertebral body. These data may have important implication for future total disc replacement design and surgical treatment.

## 7.5 References

1. Kettler, A., et al., *Finite helical axes of motion are a useful tool to describe the three-dimensional in vitro kinematics of the intact, injured and stabilised spine*. Eur Spine J, 2004. **13**(6): p. 553-9.
2. SariAli el, H., et al., *In vivo study of the kinematics in axial rotation of the lumbar spine after total intervertebral disc replacement: long-term results: a 10-14 years follow up evaluation*. Eur Spine J, 2006. **15**(10): p. 1501-10.
3. Wong, K.W., et al., *Continuous dynamic spinal motion analysis*. Spine, 2006. **31**(4): p. 414-9.
4. Wilke, H.J., et al., *Is it possible to simulate physiologic loading conditions by applying pure moments? A comparison of in vivo and in vitro load components in an internal fixator*. Spine, 2001. **26**(6): p. 636-42.
5. Rousseau, M.A., et al., *The instant axis of rotation influences facet forces at L5/S1 during flexion/extension and lateral bending*. Eur Spine J, 2006. **15**(3): p. 299-307.
6. Haher, T.R., et al., *Instantaneous axis of rotation as a function of the three columns of the spine*. Spine, 1992. **17**(6 Suppl): p. S149-54.
7. Gertzbein, S.D., et al., *Determination of a locus of instantaneous centers of rotation of the lumbar disc by moire fringes. A new technique*. Spine, 1984. **9**(4): p. 409-13.
8. White, A.A. and M.M. Panjabi, *Clinical Biomechanics of the Spine*. 1990, Philadelphia: Lippincott Williams & Wilkins.
9. Mansour, M., et al., *Evidence for IHA migration during axial rotation of a lumbar spine segment by using a novel high-resolution 6D kinematic tracking system*. J Biomech, 2004. **37**(4): p. 583-92.
10. Shirazi-Adl, A., A.M. Ahmed, and S.C. Shrivastava, *A finite element study of a lumbar motion segment subjected to pure sagittal plane moments*. J Biomech, 1986. **19**(4): p. 331-50.
11. Shirazi-Adl, A., A.M. Ahmed, and S.C. Shrivastava, *Mechanical response of a lumbar motion segment in axial torque alone and combined with compression*. Spine, 1986. **11**(9): p. 914-27.
12. Schmidt, H., et al., *The relation between the instantaneous center of rotation and facet joint forces - A finite element analysis*. Clin Biomech (Bristol, Avon), 2008. **23**(3): p. 270-8.
13. Cunningham, B.W., et al., *Biomechanical evaluation of total disc replacement arthroplasty: an in vitro human cadaveric model*. Spine, 2003. **28**(20): p. S110-7.
14. Ogston, N.G., et al., *Centrode patterns in the lumbar spine*. Baseline

- studies in normal subjects.* Spine, 1986. 11(6): p. 591-5.
15. Yoshioka, T., et al., *Motion characteristic of the normal lumbar spine in young adults: instantaneous axis of rotation and vertebral center motion analyses.* J Spinal Disord, 1990. 3(2): p. 103-13.
  16. Percy, M.J. and N. Bogduk, *Instantaneous axes of rotation of the lumbar intervertebral joints.* Spine, 1988. 13(9): p. 1033-41.
  17. Sakamaki, T., S. Katoh, and K. Sairyo, *Normal and spondylolytic pediatric spine movements with reference to instantaneous axis of rotation.* Spine, 2002. 27(2): p. 141-5.
  18. Ochia, R.S., et al., *Three-dimensional in vivo measurement of lumbar spine segmental motion.* Spine, 2006. 31(18): p. 2073-8.
  19. Fujii, R., et al., *Kinematics of the lumbar spine in trunk rotation: in vivo three-dimensional analysis using magnetic resonance imaging.* Eur Spine J, 2007. 16(11): p. 1867-74.
  20. Haughton, V.M., et al., *Measuring the axial rotation of lumbar vertebrae in vivo with MR imaging.* AJNR Am J Neuroradiol, 2002. 23(7): p. 1110-6.
  21. Lee, S.W., et al., *Development and validation of a new technique for assessing lumbar spine motion.* Spine, 2002. 27(8): p. E215-20.
  22. McAfee, P.C., et al., *A prospective, randomized, multicenter Food and Drug Administration investigational device exemption study of lumbar total disc replacement with the CHARITE artificial disc versus lumbar fusion: part II: evaluation of radiographic outcomes and correlation of surgical technique accuracy with clinical outcomes.* Spine, 2005. 30(14): p. 1576-83; discussion E388-90.
  23. Rousseau, M.A., et al., *Disc arthroplasty design influences intervertebral kinematics and facet forces.* Spine J, 2006. 6(3): p. 258-66.
  24. Wang, S., et al., *Measurement of vertebral kinematics using noninvasive image matching method-validation and application.* Spine, 2008. 33(11): p. E355-61.
  25. Li, G., et al., *Segmental in vivo vertebral motion during functional human lumbar spine activities.* Eur Spine J, 2009.
  26. Wang, S., et al., *Measurement of geometric deformation of lumbar intervertebral discs under in vivo weight-bearing condition.* J Biomech, 2009. 42(6): p. 705-11.
  27. Xia, Q., et al., *In vivo motion characteristics of lumbar vertebrae in sagittal and transverse planes.* J Biomech, 2010. 43(10): p. 1905-9.
  28. Percy, M.J. and S.B. Tibrewal, *Axial rotation and lateral bending in the normal lumbar spine measured by three-dimensional radiography.* Spine, 1984. 9(6): p. 582-7.
  29. Wachowski, M.M., et al., *How do spinal segments move?* J Biomech, 2009.

- 42(14): p. 2286-93.
30. Blumenthal, S., et al., *A prospective, randomized, multicenter Food and Drug Administration investigational device exemptions study of lumbar total disc replacement with the CHARITE artificial disc versus lumbar fusion: part I: evaluation of clinical outcomes*. Spine, 2005. **30**(14): p. 1565-75; discussion E387-91.
  31. Zigler, J., et al., *Results of the prospective, randomized, multicenter Food and Drug Administration investigational device exemption study of the ProDisc-L total disc replacement versus circumferential fusion for the treatment of 1-level degenerative disc disease*. Spine, 2007. **32**(11): p. 1155-62; discussion 1163.
  32. Le Huec, J.C., et al., *Clinical results of Maverick lumbar total disc replacement: two-year prospective follow-up*. Orthop Clin North Am, 2005. **36**(3): p. 315-22.
  33. Putzier, M., et al., *Charite total disc replacement--clinical and radiographical results after an average follow-up of 17 years*. Eur Spine J, 2006. **15**(2): p. 183-95.
  34. Shirazi-Adl, A., et al., *Spinal muscle forces, internal loads and stability in standing under various postures and loads--application of kinematics-based algorithm*. Eur Spine J, 2005. **14**(4): p. 381-92.
  35. Arjmand, N. and A. Shirazi-Adl, *Biomechanics of changes in lumbar posture in static lifting*. Spine (Phila Pa 1976), 2005. **30**(23): p. 2637-48.

## Chapter 8

# Segmental Lumbar Motion in Patients with Discogenic Low Back Pain during Functional Weight-bearing Activities

### 8.1 Introduction:

Intervertebral discs at a vertebral level adjacent to a degenerated level have a high prevalence of degeneration[1, 2], particularly following surgical arthrodesis for treatment of the diseased level[3, 4]. While some have advocated that this degeneration might be due to the natural development of the discs[5, 6], many have assumed that altered mechanical loading and motion patterns are the causative factors of adjacent disc degeneration[7, 8]. Few quantitative data have been reported on how the degenerated level affects the biomechanical environment of the involved and adjacent discs [9].

There have been several prior attempts to study the kinematics of the lumbar spine in individuals with low back pain (LBP) using a variety of techniques. *In vitro* studies have used cadaveric lumbar specimens to determine the motion characteristics of lumbar segments with various degenerative grades[10-12]. Dynamic sagittal plane Radiographs have been used to detect the sagittal plane rotations in normal and symptomatic subjects[13]. Recently, advanced computed

tomography (CT) and magnetic resonance (MR) image techniques have also been used to measure axial rotation of normal and symptomatic subjects[14-19]. Many of these studies have focused on the study of motion in select planes, under non-physiological loading conditions, and have focused on patients with nonspecific LBP. The effect of degenerative diseases on rotations and translations in 3-dimensional (3D) space of the vertebral segments under weight-bearing physiological loading conditions is yet to be determined to our knowledge.

Using the combined MRI/CT and DFIS, *in vivo* lumbar spine kinematics in healthy asymptomatic human subjects were investigated in **Chapter 3 to 7**. In this Chapter, a cohort of patients with discogenic LBP immediately prior to undergoing spinal arthrodesis procedures were studied and compared the results to those in **Chapter 3** [20]. We hypothesized that the lumbar vertebrae at the levels immediately adjacent to those that were symptomatic would demonstrate different ranges of motion (ROMs) and distinct motion patterns during active *in vivo* spine motion prior to undergoing surgical arthrodesis.

## **8.2 Materials and Methods:**

### **8.2.1 Patient Recruitment:**

Approval of the experimental design by the authors' institutional review board was obtained prior to initiation of this study. An approved consent form was signed by each patient before any testing was performed.

Ten symptomatic LBP subjects with an age ranging from 50 to 60 years were recruited (7 men and 3 women, mean age, 51.8 years; mean height, 169.7 cm; mean weight, 65.7 kg). The patients were screened for exclusion using clinical history, physical examination, and radiographic findings. The presence of any of



the following were used as indications for exclusion from the study: previous spinal surgery, spinal abnormality at segments other than L4-S1, facet joint arthritis, ligamentum flavum hypertrophy, gross segmental instability, scoliosis, spondylolisthesis, central or foraminal spinal stenosis, presence of paralysis, lower extremity weakness, myelopathy, radicular symptoms, history of mental illness, prior radiation within a year, and pregnancy.

All patients were diagnosed as having discogenic LBP originated from L4-S1 segment. They had discogram performed by an interventional radiologist that revealed concordant symptoms at the involved levels together with discordant findings at the adjacent. Radiographic confirmation of discogenic LBP was also confirmed by the treating surgeon and a neuroradiologist. The degree of degeneration was graded using Modic[21-23] and Pfirrmann[24] scales. The Modic classification describes degenerative end-plate and vertebral body changes seen on the MRI. Type I are thought to reflect acute inflammation. Type II represents chronic changes including end-plate disruption and fatty degeneration. Type III changes correlate with end-plate sclerosis and loss of vertebral cancellous bone. The Pfirrmann grading describes the morphology of the disc as seen on axial T2-weighted MRI. Grade I represents a homogenous bright white disc with clear distinction of annulus and nucleus. Grade V then represents inhomogeneous black disc with lost distinction of annulus and nucleus. All patients were graded a minimum of Pfirrmann grade four at the L4-5 and L5-S1 discs. The mean Pfirrmann grade was  $4.2 \pm 0.8$  at L4-5 and  $4.5 \pm 0.5$  at L5-S1. L3-4 was the adjacent level with a mean Pfirrmann grade of  $1.6 \pm 0.8$ . (**Table 8-1**) An attempt at non-operative management was made for all patients for a minimum of 6 months. Following confirmation of their diagnosis, all patients were consented and scheduled to undergo surgical arthrodesis within the next two weeks in order to be considered for inclusion in this study.

Table 8-1: Disc degeneration graded using Pfirrmann grading for both normal and DDD subjects at the studied levels. Data reported as average  $\pm$  SD.

	Normal	DDD
<b>L2-3</b>	1.1 $\pm$ 0.4	1.8 $\pm$ 0.5
<b>L3-4</b>	1.6 $\pm$ 0.5	1.6 $\pm$ 0.8
<b>L4-5</b>	1.9 $\pm$ 0.6	4.2 $\pm$ 0.6
<b>L5-S1</b>	2.1 $\pm$ 0.4	4.5 $\pm$ 0.5

Eight asymptomatic subjects with an age ranging from 50 to 60 years (5 men and 3 women) were recruited as described in our previously published study[25] (mean age, 54.4 years; mean height, 164.7 cm; mean weight, 63.5 kg). The subjects were evaluated for the absence of LBP (past or present), as well as the lack of evidence of DDD and other spinal disorders. The data of this group of normal subjects served as a control. Pfirrmann scores were evaluated from MRI scans and shown in **Table 8-1**.

### **8.2.2 Combined imaging technique:**

Each subject underwent a lumbar MRI scan to build 3D vertebrae models using the protocols in **Chapter 2 and 3 (Fig 8--1)**. The lumbar spine kinematics of L2-S1 was captured during 3 physiological body motions using the DFIS in a predetermined sequence: 45° flexion of the trunk relative to the vertical and maximal extension; maximal left to right bending; maximal left to right twisting. *In vivo* positions of the vertebrae at *in vivo* weight-bearing positions were then reproduced in the modeling software using 3D models of the vertebrae and 2D orthogonal fluoroscopic images through the 3D to 2D matching protocol based on anatomic features of the vertebrae described in **Chapter 2 and 3 (Fig 8--2)**.

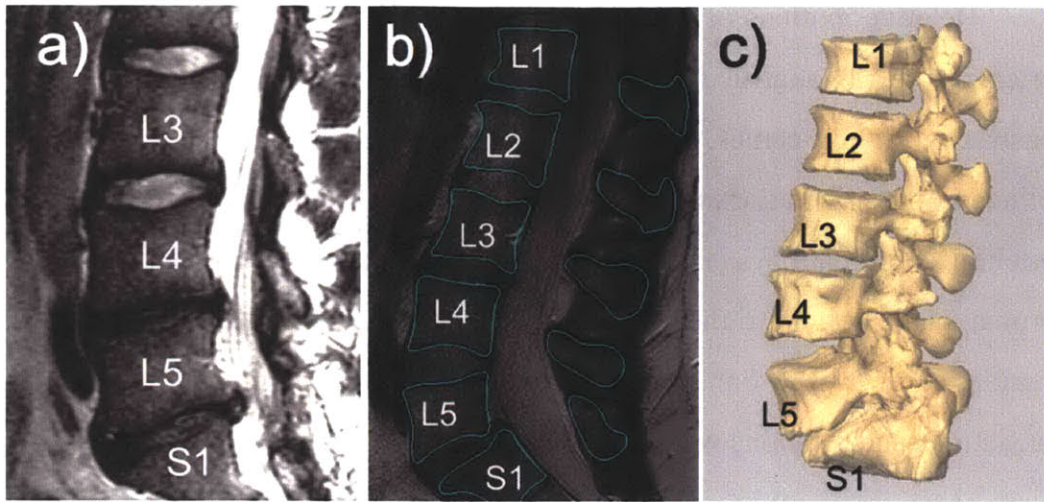


Fig 8-1. a) T2 MR image of LBP patient showing DDD at L4-5 and L5-S1. b) Digitized contours of vertebrae in the sagittal plane. c) 3D anatomic vertebral models from MRI

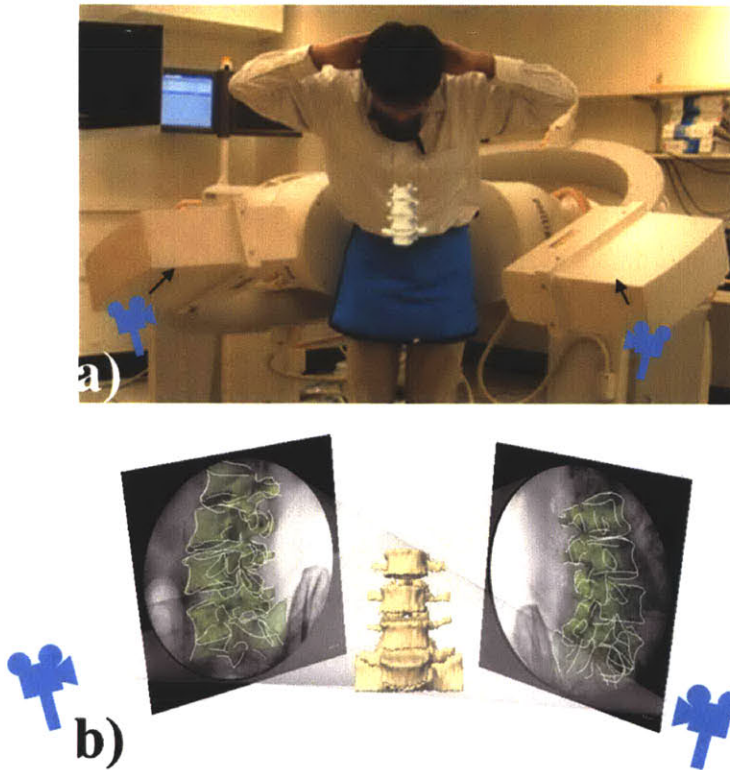


Fig 8-2. a) DFIS experiment setup. b) Reproduction of the *in vivo* vertebrae positions.

Relative motions of the proximal vertebrae with respect to the distal vertebrae were analyzed using right hand Cartesian coordinate systems constructed at the center of endplates of each vertebra. Three rotations were defined as the orientations of the proximal vertebral coordinate system in the distal vertebral coordinate system using Euler angles: sagittal plane flexion-extension, coronal plane left to right bending and transverse plane left to right twisting rotations (**Fig 8--3**). For each rotational activity, primary rotation and coupled translations and rotations were analyzed.

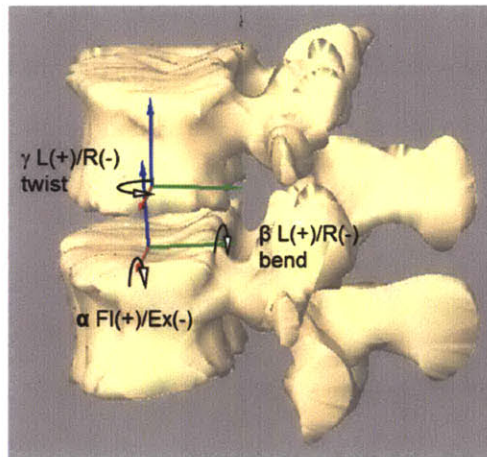


Fig 8-3. Local coordinate systems to calculate the 6DOF kinematics of the cephalad vertebra with respect to the caudad vertebra.  $\alpha$  (flexion-extension),  $\beta$  (left-right bending), and  $\gamma$  (left-right twisting).

### 8.2.3 Data analysis:

After the determination of vertebral positions at each posture, we determined the ROM of each vertebral level between flexion and extension, left and right bending and left and right axial rotation. The ROM data included both the primary rotations and coupled translations and rotations during each activity. A repeated measure ANOVA was used to compare the ROM at L2-3, L3-4, L4-5, and L5-S1 vertebral levels at each of the three functional activities. Statistical

significance was set at  $p < 0.05$ . When a statistically significant difference was detected a Newman-Keuls post-hoc test was performed. The statistical analysis was performed using software (Statistica, Statsoft, Tulsa, OK).

## **8.3 Results:**

### ***8.3.1 Primary rotations In Patients with Degenerative Disc Disease:***

We observed the following primary ROMs during movement activities. The mean flexion and extension ranges during the flexion and extension movements were  $3.7 \pm 3.3^\circ$ ,  $5.6 \pm 2.7^\circ$ ,  $4.4 \pm 2.8^\circ$  and  $2.5 \pm 2.6^\circ$  for L2-3, L3-4, L4-5, L5-S1 levels, respectively. Mean left to right bend ranges during lateral bending movements were  $3.3 \pm 2.4^\circ$ ,  $5.1 \pm 2.8^\circ$ ,  $3.2 \pm 2.6^\circ$  and  $2.1 \pm 1.7^\circ$ , and lastly, the mean left to right twist ranges during twisting movements were  $3.0 \pm 1.5^\circ$ ,  $4.2 \pm 2.5^\circ$ ,  $2.8 \pm 2.1^\circ$  and  $2.4 \pm 1.5^\circ$ , during the twisting movements, respectively. (**Table 8-2**)

During flexion-extension, the greatest ROM was observed at the L3-4 level, which was the superior adjacent level of the DDD levels. The lowest ROM was observed at L5-S1, which was statistically less than L3-4 ( $p = 0.021$ ). During LR bend, the greatest ROM was observed at the L3-4 level and the lowest ROM was observed at L5-S1. L5-S1 had statistically less ROM than L3-4 ( $p = 0.008$ ). L3-4 had a significantly larger ROM than L2-3 ( $P = 0.035$ ). During left to right twist, again, the greatest ROM was observed at the L3-4 level and the lowest ROM was observed at L5-S1. L5-S1 had statistically less ROM than L3-4 ( $p = 0.017$ ). L3-4 had a significantly larger ROM than L2-3 ( $P = 0.041$ ).

Overall, the greatest ranges were observed at the L3-4 level during all 3 movements, which was the superior adjacent level in all patients. Interestingly, the lowest range of flexion occurred at the L5-S1 level for all 3 movements. In

addition, during all three movements, L5-S1 demonstrated significantly less motion than L3-4 (P=0.21, 0.008, and 0.17 for flex/ex, LR bend, LR twist, respectively). Thus the pattern of peak motion at L3-4 and most diminished motion at L5-S1 was observed during all three activities. We did not detect any trends in movement patterns based on the available anthropometry or age of the subjects.

Table 8-2: 6DOF translational and rotational ROMs in DDD group during various body positions. Shaded cells represent the primary rotations. Data are average  $\pm$  SD.

	<u>Translation (mm)</u>			<u>Rotation (deg)</u>		
	AP	LR	PD	flex	Bend	Twist
<b>Flexion and extension</b>						
<b>L2-3</b>	1.1 $\pm$ 1.3	2.6 $\pm$ 1.8	1.3 $\pm$ 1.0	3.7 $\pm$ 3.7	3.1 $\pm$ 2.5	3.0 $\pm$ 1.4
<b>L3-4</b>	1.4 $\pm$ 1.0	2.4 $\pm$ 1.5	1.8 $\pm$ 1.9	5.6 $\pm$ 2.7	2.3 $\pm$ 2.5	4.3 $\pm$ 3.0
<b>L4-5</b>	1.8 $\pm$ 1.8	1.1 $\pm$ 0.5	1.7 $\pm$ 1.3	4.4 $\pm$ 2.8	3.0 $\pm$ 2.0	3.6 $\pm$ 2.4
<b>L5-1</b>	1.1 $\pm$ 0.8	3.1 $\pm$ 1.6	1.0 $\pm$ 1.3	2.5 $\pm$ 2.6	2.9 $\pm$ 1.9	2.5 $\pm$ 2.1
<b>Left and right bend</b>						
<b>L2-3</b>	0.9 $\pm$ 1.0	1.0 $\pm$ 0.6	0.9 $\pm$ 0.6	2.8 $\pm$ 1.9	3.3 $\pm$ 2.4	4.3 $\pm$ 1.8
<b>L3-4</b>	1.8 $\pm$ 1.4	2.1 $\pm$ 1.3	0.9 $\pm$ 0.8	2.4 $\pm$ 1.5	5.1 $\pm$ 2.8	3.2 $\pm$ 3.0
<b>L4-5</b>	1.5 $\pm$ 1.1	1.7 $\pm$ 1.2	1.1 $\pm$ 0.9	4.1 $\pm$ 2.1	3.2 $\pm$ 2.6	3.4 $\pm$ 2.5
<b>L5-1</b>	1.9 $\pm$ 1.4	2.1 $\pm$ 1.2	1.0 $\pm$ 1.8	3.1 $\pm$ 2.7	2.1 $\pm$ 1.7	4.6 $\pm$ 3.9
<b>Left and right twist</b>						
<b>L2-3</b>	2.1 $\pm$ 1.4	1.5 $\pm$ 1.2	1.1 $\pm$ 0.9	3.1 $\pm$ 2.5	3.4 $\pm$ 1.6	3.0 $\pm$ 1.5
<b>L3-4</b>	1.0 $\pm$ 0.9	1.1 $\pm$ 0.9	0.9 $\pm$ 0.7	1.8 $\pm$ 1.2	1.2 $\pm$ 1.1	4.2 $\pm$ 2.5
<b>L4-5</b>	2.6 $\pm$ 1.7	2.2 $\pm$ 2.2	0.7 $\pm$ 0.4	3.0 $\pm$ 4.5	3.2 $\pm$ 2.2	2.8 $\pm$ 2.1
<b>L5-1</b>	2.1 $\pm$ 2.2	2.7 $\pm$ 0.9	1.1 $\pm$ 0.8	3.3 $\pm$ 2.9	2.9 $\pm$ 1.3	2.4 $\pm$ 1.5

### **8.3.2 Coupled translations and rotations**

During the flexion-extension motion, there were coupled translations in all three directions (**Table 8-2**). The coupled motions in anterior-posterior and proximal-distal directions were similar. On average, the translation range was between 1.2 and 2.1 mm. The coupled translation in the left-right direction was significantly lower at L4-5 ( $1.3 \pm 0.6$  mm) than other levels. The coupled rotations in left-right bending and twisting also did not show any significantly different and were, on average, between  $2.3^\circ$  and  $4.3^\circ$ .

During the left to right bending motion, the coupled translations at all the vertebral levels were not significantly different in the three directions and on average, ranged between 1.1 and 2.4 mm (**Table 8-2**). The coupled flexion rotation range was between  $2.4^\circ$  and  $4.1^\circ$ . The coupled twist rotation range was between  $3.2^\circ$  and  $4.6^\circ$ . No statistical difference was noticed either between the levels, or between the flexion and twist rotations.

During the left to right twisting motion, the translations were in general significantly smaller at L3-4 in anterior to posterior (1.2 compare to 2.5 to 3.1 mm) and in left to right directions (1.3 compare to 1.8 to 3.2 mm). The translation in the proximal to distal direction was between 0.9 and 1.4 mm, which in general was lower than the coupled motion in the other two directions. The coupled flexion range was smaller at L3-4 ( $1.8^\circ$  compare to  $3.0^\circ$  to  $3.3^\circ$ ). The coupled bending rotation was also smaller at L3-4 ( $1.2^\circ$  compare to  $2.9^\circ$  to  $3.4^\circ$ ).

### **8.3.3 Comparison with Normal Subjects:**

Compare the motion in patients with DDD to that of the normal subjects in Chapter 4, several significant differences were noticed in primary motions [25]. The ROM during left to right bend at L3-4 was significantly larger ( $p = 0.038$ ) in the DDD group than the normal group ( $5.1 \pm 2.8^\circ$  compared to  $3.4 \pm 2.1^\circ$ ), as was the

ROM during left to right twist at L3-4 ( $p = 0.043$ ,  $4.2 \pm 2.5^\circ$  compared to  $2.4 \pm 2.6^\circ$ ). However, there was no significance during flexion ( $p = 0.29$ ) even though the mean flexion/extension ROM is still higher in the DDD patients ( $5.6 \pm 2.7^\circ$  vs.  $4.3 \pm 3.4^\circ$ ). In DDD subjects, the ROM at L4-5 was significantly larger ( $p = 0.005$ ) during flexion ( $4.4 \pm 2.8^\circ$  compared to  $1.9 \pm 1.1^\circ$  of normal subjects), and similar during LR bend ( $3.2 \pm 2.6^\circ$  vs.  $4.7 \pm 2.4^\circ$   $p = 0.32$ ) and LR twist ( $2.8 \pm 2.1^\circ$  vs.  $2.9 \pm 2.1^\circ$ ,  $p = 0.93$ ) (**Fig 8--4**). In Chapter 4, an increasing ROM were observed among normal subjects pattern in flexion, a decreasing ROM pattern in left to right bend and a flat pattern in left to right bend. However, the DDD patients in this study seemed to have a pattern of peak motion at L3-4 and diminished motion at L5-S1 independent of the activity.



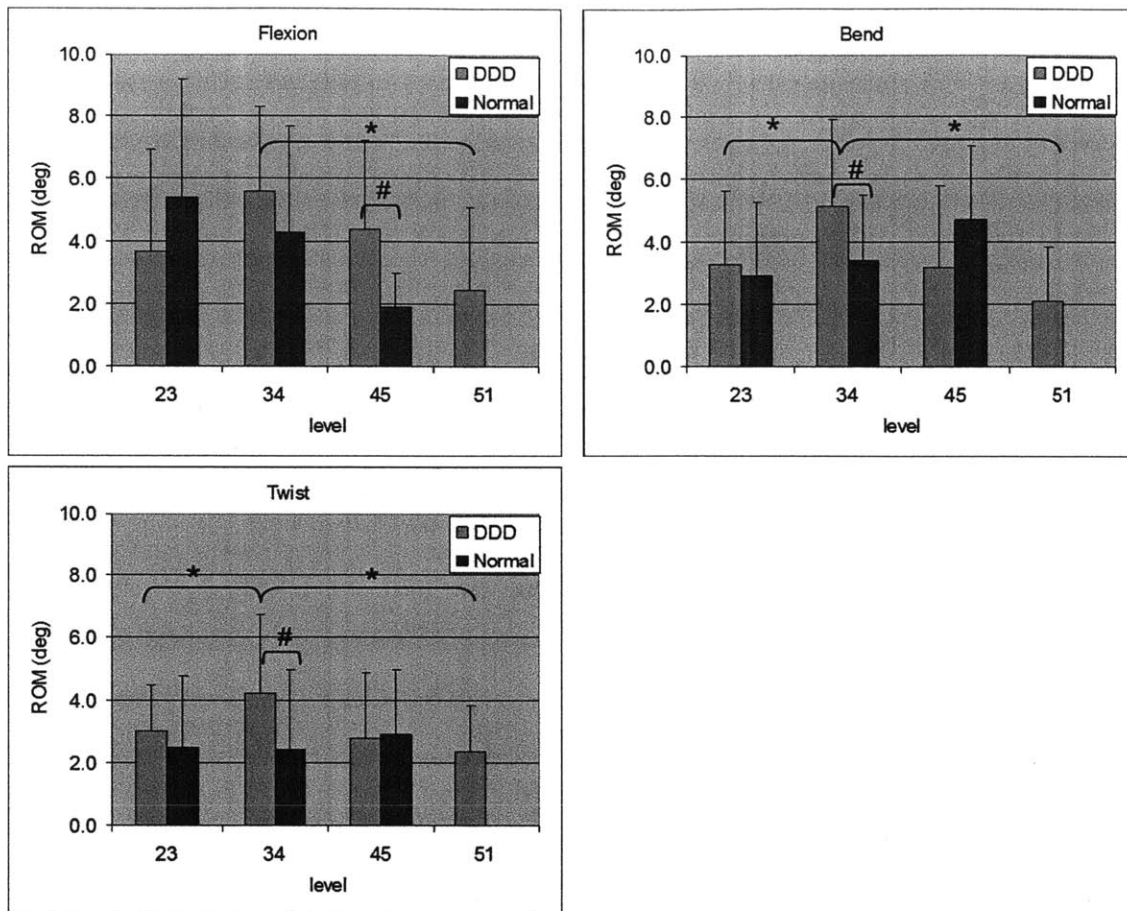


Fig 8-4. Primary rotation (and SD) of patients with DDD and normal subjects at different levels during physiological activities. The numbers on the x axis indicate the vertebral level; for example, “23” indicates L2-L3, \*: statistically significant difference within DDD group, #: statistically significant difference of DDD group compared to normal.

## 8.4 Discussion:

Although there are many contributions to DDD related LBP, mechanical dysfunction is integral to its occurrence[7]. Application of a continuous spinal load has been independently associated with LBP[26]. Bakker *et al.*[26] found that certain work-related tasks, including repetitive bending, lifting, twisting, were also associated. Stokes *et al.*[8] reviewed the literature on factors accelerating disc degeneration concluding that abnormal loading conditions can produce adaptive changes resulting in DDD[8]. The current Chapter characterizes mechanical dysfunction present among clinically confirmed discogenic LBP patients, relative to that of asymptomatic controls without evidence of DDD, by quantifying abnormal motion in 6DOF.

The data revealed interesting findings at the levels responsible for discogenic LBP. During all movements L5-S1 had the least flexion, and significantly less motion than L3-4. Given that this was the level which all patients had confirmed DDD, this leads us to believe that with severe DDD requiring surgical intervention, segmental hypomobility ensues. DDD present at L4-L5 resulted in increased ROM in flexion/extension compared to normal subjects, demonstrating that hypermobility in the sagittal plane develops at this level when adjacent to an affected L5-S1 level, despite similar grades of DDD. It should be noted that considerable inter-subject variance in ROM exists, even in healthy spines, despite consistent trends in motion across lumbar levels. For example, cephalic levels have greater ROM in the sagittal plane whereas caudad levels are more mobile in axial and coronal planes[25]. This has been attributed to different orientation of the facets at lumbar levels[27-29].

There have been several *in vitro* attempts to quantify mechanical dysfunction

in patients with non-specific LBP at affected levels; many of which have documented decreased ROM[18, 30-32]. In an imaging study on human cadaveric lumbar spines, Fujiwara et al[10] noted segmental motion initially increased with degeneration, but then decreased at extremes of disc degeneration[10]. In another study by Wilke et al,[12] segmental stability continuously increased in flexion/extension and lateral bending but decreased in axial rotational stability with increasing DDD grades. In our study, DDD increased the flexion/extension ROM, but with similar rotation in left-right bending and twisting. Comparison among these studies is difficult given different testing conditions.

Prior *in vivo* attempts to study DDD kinematics are scarce, with the majority performed in individuals with nonspecific LBP[13, 14, 33-35]. Studies that correlated DDD with abnormal movement generally focused on motion in limited planes, under non-physiological conditions, and included patients based on radiographic findings without clinical correlation. Several imaging techniques have been utilized. Digital fluoroscopic video was commonly utilized because of its ability to capture dynamic motion, despite low resolution, slow frame rates, and inaccuracy[16, 36-42]. Teyhen *et al.*[13] validated a technique with higher resolution and distortion compensated roentgen analysis to study sagittal segmental angular and linear displacement in individuals with LBP and healthy controls during flexion/extension[13]. Although linear displacement hypomobility was witnessed, it is difficult to compare these findings with ours given differences in subject populations. Teyhen *et al.*[13] included patients with a history of LBP, representing a diverse population with various etiologies. Our findings are specific to patients with discogenic LBP awaiting treatment with arthrodesis. Karadimas *et al.*[33] used upright positional magnetic resonance imaging to study changes in segmental motion while going from supine to standing positions.

Subjects were included based on the presence of LBP. They documented that in DDD, anterior and middle disc heights changed significantly between the supine and sitting position, similar to our observation of increased flexion/extension in DDD segments[33]. The major limitation of their study was inclusion of patients based on LBP and then retrospectively studying normal versus abnormal appearing discs without correlating symptoms. Only data in several degrees of freedom were determined, excluding complex movements such as bending, and actual vertebral movements, were not quantified. Furthermore, the majority of healthy discs studied were located at cephalad lumbar levels, in contrast to the degenerative levels which were located caudally.

Degenerative changes in the lumbar spine have been shown to be clinically related to future changes at adjacent levels.[1] In a long-term follow-up study, Waris *et al.*[2] demonstrated early lumbar DDD in patients with LBP predicted further development of symptomatic lumbar DDD. Biomechanical changes have also been noted at adjacent levels. Ruberte *et al.*[9] modified a 3-dimensional finite element model to simulate degeneration at the L4–L5 disc and found that the superior adjacent level (L3–L4) had increased rotation in lateral bending, axial rotation and flexion/extension.[9] We also observed that the greatest ranges were observed at the superior adjacent level (L3-4) during all three movements. The ROM during left to right bend at L3-4 was also relatively smaller in the normal group, and DDD significantly increased motion in the adjacent segment in active axial rotation. These findings lead us to believe that superior adjacent levels develop segmental hypermobility prior to undergoing surgical arthrodesis. Patients included in our study had very minimal, if any, evidence of DDD at the L3-4 level. This is important because the presence of mild DDD has been associated with increased lumbar segmental motion[10, 11]. While changes in

mechanical loading have been assumed in the progression of adjacent level DDD, our study indicates that the adjacent L3-L4 level to L4-S1 had increased ROM. It is unclear how this hypermobility is related to long term degeneration. Adjacent segment degeneration has also been widely reported in patients following arthrodesis[3, 4]. The current study found that kinematic changes already occurred at the adjacent level prior to arthrodesis. Increased rotation range could theoretically lead to increased deformation and overloading of the intervertebral discs. This demonstrates that the DDD itself can affect adjacent levels mechanically. Future studies should use finite element models to calculate stress distributions in the adjacent discs and compare them to asymptomatic spines to evaluate the effect of DDD on the adjacent loading environment. This will be instrumental for understanding the mechanisms of adjacent segment degeneration to improve surgical techniques and prevent adjacent degeneration.

In Conclusion, this Chapter used the validated *in vivo* technique to quantify abnormal motion characteristics in patients with clinically confirmed discogenic LBP prior to arthrodesis. A limitation of the present study was that the images were obtained at the end points of motion, which did not allow us to characterize midrange abnormalities[43, 44]. Although no restriction was applied to subjects, they were instructed to limit flexion in order to keep the spine within the field of view of the fluoroscopes. Comparative control data were not available at L5-S1. Because of the sample size, we were unable to investigate the effects of different degenerative disc disease grades. Despite these limitations, the present study represents the best information to date on aberrant vertebral motion in this population. Although DDD affects the involved segments in a complicated way, ROM in the cephalic adjacent level was increased. The findings represent the first reported data specific to this population which can be used to study the effects of

spinal arthrodesis on motion characteristics, and further define the mechanical component of adjacent segment degeneration.

## 8.5 References:

1. Elfering A, S.N., Birkhofer D, Zanetti M, Hodler J, Boos N, *Young investigator award 2001 winner: risk factors for lumbar disc degeneration. A 5-year prospective MRI study in asymptomatic individuals.* Spine, 2002. **27**(2): p. 125-134.
2. Waris E, E.M., Hermunen H, Kiviluto O, Paajanen H., *Disc degeneration in low back pain: A 17-year follow-up study using magnetic resonance imaging.* Spine, 2007. **32**(6): p. 681-684.
3. Kumar M, Jacquot F, and H. H., *Long-term follow-up of functional outcomes and radiographic changes at adjacent levels following lumbar spine fusion for degenerative disc disease.* Eur Spine J, 2001. **10**: p. 309-313.
4. Lee, C.K., *Accelerated degeneration of the segment adjacent to a lumbar fusion.* Spine (Phila Pa 1976), 1988. **13**(3): p. 375-7.
5. Harrop JS, Y.J., Maltenfort M, Vorwald P, Jabbour P, Bono CM, Goldfarb N, Vaccaro AR, Hilibrand AS, *Lumbar adjacent segment degeneration and disease after arthrodesis and total disc arthroplasty.* Spine, 2008. **33**: p. 1701-1707.
6. Bartolomei JC, Theodore N, and S. VK, *Adjacent level degeneration after anterior cervical fusion: a clinical review.* Neurosurg Clin N Am, 2005. **16**: p. 575-587.
7. Adams MA, et al., *Mechanical initiation of intervertebral disc degeneration.* Spine, 2000. **25**: p. 1625-36.
8. Stokes IAF and I. J, *Mechanical conditions that accelerate intervertebral disc degeneration: overload versus immobilization.* Spine, 2004. **29**(23): p. 2724-2732.
9. Ruberte LM, Natarajan RN, and A. GBJ, *Influence of single-level lumbar degenerative disc disease on the behavior of the adjacent segments-A finite element model study.* Journal of Biomechanics, 2009. **42**: p. 341-348.
10. Fujiwara A, L.T.-H., An HS, Tanaka N, Jeon CH, Andersson GBJ, Haughton VM, *The effect of disc degeneration and facet joint osteoarthritis on the segmental flexibility of the lumbar spine.* Spine, 2000. **25**(23): p. 3036-3044.
11. Tanaka N, et al., *The relationship between disc degeneration and flexibility of the lumbar spine.* Spine J, 2001. **1**(1): p. 47-56.

12. Wilke HJ, et al., *Early stages of intervertebral disc degeneration do not necessarily cause instability*. In Spine Week, Geneva, Switzerland, 2008.
13. Teyhen DS, F.T., Childs JD, Kuklo TR, Rosner MK, Polly DW, Abraham LD, *Fluoroscopic video to identify aberrant lumbar motion*. Spine, 2007. **32**: p. E220-229.
14. Ochia RS, I.N., Takatori R, Andersson GB, An HS, *In vivo measurements of lumbar segmental motion during axial rotation in asymptomatic and chronic low back pain male subjects*. Spine, 2007. **32**: p. 1304-1399.
15. Rousseau MA, B.D., Hadi TM, Pedersen KL, Lotz JC, *The instant axis of rotation influences facet forces at L5/S1 during flexion/extension and lateral bending*. Eur Spine J, 2006. **15**: p. 299-307.
16. Lee SW, W.K., Chan MK, Yeung HM, Chiu JL, Leong JC, *Development and validation of a new technique for assessing lumbar spine motion*. Spine, 2002. **27**: p. 215-220.
17. Anderst, W.J., R. Vaidya, and S. Tashman, *A technique to measure three-dimensional in vivo rotation of fused and adjacent lumbar vertebrae*. Spine J, 2008. **8**(6): p. 991-7.
18. Percy M, P.I., Shepard J, *The effect of low-back pain on lumbar spinal movements measured by three-dimensional x-ray analysis*. Spine, 1985. **10**: p. 150-153.
19. Fujii R, S.H., Mukai Y, Ishii T, Iwasaki M, Yoshikawa H, Sugamoto K, *Kinematics of the lumbar spine in trunk rotation: in vivo three dimensional analysis using magnetic imaging*. Eur Spine J, 2007. **16**: p. 1867-1874.
20. Passias, P.G., et al., *Segmental lumbar rotation in patients with discogenic low back pain during functional weight-bearing activities*. J Bone Joint Surg Am, 2011. **93**(1): p. 29-37.
21. Modic, M., *Degenerative disc disease: genotyping, MR imaging and phenotyping*. Skeletal Radiol, 2007. **36**: p. 91-93.
22. Kuisma P, K.J., Haapea M, Lammentausta E, Niinimaki J, *Modic changes in vertebral endplates: a comparison of MR imaging and multislice CT*. Skeletal Radiol, 2009. **38**: p. 141-147.
23. Kjaer P, K.L., Bendix T, Sorensen J, Leboeuf-Yde C, *Modic changes and their associations with clinical findings*. Eur Spine J, 2006. **15**: p. 1312-1319.
24. Pfirrmann C, M.A., Zanetti M, Hodler J, Boos N, *Magnetic resonance classification of lumbar intervertebral disc degeneration*. Spine, 2001. **26**: p. 1873-1878.
25. Li G, W.S., Passias PG, Xia Q, Li G, Wood KB, *Segmental in vivo vertebral motion during functional human lumbar spine activities*. Eur Spine J, 2009. **18**: p. 1013-21.

26. Bakker EWP, V.A., Lucas C, Koning JCMF, Haan de RJ, Koes BW, *Daily spinal mechanical loading as a risk factor for acute non-specific low back pain*. Eur Spine J, 2006. **16**: p. 107-113.
27. Kozanek, M., et al., *Range of motion and orientation of the lumbar facet joints in vivo*. Spine (Phila Pa 1976), 2009. **34**(19): p. E689-96.
28. Masharawi YM, A.-N.D., Steinberg N, Dar G, Peleg S, Rothschild B, Salame K, Hershkovitz I., *Lumbar facet orientation in spondylolysis: A skeletal study*. Spine, 2007. **32**(6): p. E176-E180.
29. Masharawi, Y., et al., *Facet orientation in the thoracolumbar spine: three-dimensional anatomic and biomechanical analysis*. Spine (Phila Pa 1976), 2004. **29**(16): p. 1755-63.
30. Dvorak J, P.M., Novotny J, Chang DG, Grob D, *Clinical validation of functional flexion-extension reontgenograms of the lumbar spine*. Spine, 1991. **16**: p. 943-950.
31. Kaigle AM, W.P., Hansson TH, *Muscular and kinematic behavior of the lumbar spine during flexion-extension*. J Spinal Disord, 1998. **11**: p. 163-174.
32. Vitzhum H-E, K.A., Seifert V, *Dynamic examination of the lumbar spine by using vertical, open magnetic resonance imaging*. J Neurosurg, 2000. **93**: p. 58-64.
33. Karadimas EJ, S.M., Smith FW, Wardlaw D., *Positional MRI changes in supine versus sitting postures in patients with degenerative lumbar spine*. J Spinal Disord Tech, 2006. **19**: p. 495-500.
34. Kong MH, H.H., Song KY, Chin DK, Cho YE, Yoondo H, Wang JC, *Kinetic magnetic resonance imaging analysis of abnormal segmental motion of the functional spine unit*. J Neurosurg Spine, 2009. **10**: p. 357-365.
35. Kulig K, P.C., Landel RF, Chen H, Fredericson M, Guillet M, Butts K, *Segmental lumbar mobility in individuals with low back pain: in vivo assessment during manual and self-imposed motion using dynamic MRI*. BMC Musculoskelet Disord, 2007. **8**: p. 8.
36. Okawa A, S.K., Komori H, Muneta T, Arai Y, Nakai O, *Dynamic motion study of the whole lumbar spine by videofluoroscopy*. Spine, 1998. **23**: p. 1743-1749.
37. Kanayama M, A.K., Kaneda K, Tadano S, Ukai T, *Phase lag of the intersegmental motion in flexion-extension of the lumbar and lumbosacral spine. An in vivo study*. Spine, 1996. **21**: p. 1416-1422.
38. Kanayama M, T.S., Kaneda K, Ukai T, Abumi K, Ito M, *A cineradiographic study on the lumbar disc deformation during flexion and extension of the trunk*. Clin Biomech (Bristol, Avon), 1995. **10**: p. 193-199.



39. Harada M, A.K., Ito M, Kaneda K, *Cineradiographic motion analysis of normal lumbar spine during forward and backward flexion*. Spine, 2000. **25**: p. 1932-1937.
40. Takayanagi K, T.K., Yamagata M, Moriya H, Kitahara H, Tamaki T, *Using cineradiography for continuous dynamic-motion analysis of the lumbar spine*. Spine, 2001. **26**: p. 1858-1865.
41. Vander Kooi D, A.G., Basford JR, et al., *Using cineradiography for continuous dynamic-motion analysis of the lumbar spine*. Spine, 2001. **29**: p. 100-104.
42. Otani K, O.A., Shinomiya K, Nakai O, *Spondylolisthesis with postural slip reduction shows different motion patterns with video fluoroscopic analysis*. J Orthop Sci, 2005. **10**: p. 152-159.
43. Panjabi, M., *The stabilizing system of the spine. Part I. Function, dysfunction, adaptation, and enhancement*. J Spinal Disord, 1992. **5**: p. 383-389.
44. Panjabi, M., *The stabilizing system of the spine. Part II. Neutral zone and instability hypothesis*. J Spinal Disord, 1992. **5**: p. 390-396.



# Chapter 9

## Lumbar Disc Deformation in Patients with Degenerative Disc Disease at the Cephalic Adjacent Levels

### 9.1 Introduction:

Low back pain (LBP) secondary to lumbar degenerative disc disease (DDD) is one of the most common causes of disability in working population[1, 2]. It has been reported that in patients with DDD, the intervertebral discs (IVD) adjacent to the diseased levels have a greater tendency to degenerate[3-5], especially after surgical fusion treatment of the diseased segments[6-9]. Numerous studies have suggested that altered biomechanics, such as abnormal loading and/or motion patterns[10-12], are the causative factors of adjacent segment degeneration (ASD). However, it remains unclear whether these changes are due to the natural development triggered by the DDD[13-16] or to the consequence of spinal surgeries[6, 17, 18]. Therefore, a quantitative knowledge of the disc deformation at the adjacent segments under physiological weight-bearing conditions is instrumental to delineate the biomechanical factors associated with ASD.

Many studies have examined the biomechanics of the adjacent segments

after lumbar fusion or disc arthroplasty *in vivo* and *in vitro*. For example, segmental mobility[19-23] and change in disc height[9, 18, 19, 24, 25] have been measured using sagittal plane X-rays in patients after surgical treatments of the diseased discs. *In vitro* cadaveric tests and computational simulations have been used to investigate the effect of surgical treatments on loadings of the facet joints[26-30], intradiscal pressure[31-34], disc bulging[35], and stress-strain distribution[36-38]. Few studies have investigated the effect of DDD on the biomechanics of the adjacent segments before surgical treatments. In finite element studies[35, 39], disc degeneration was simulated by changing the disc height and its material properties, and adjacent segmental motions and disc stress-strain distributions were calculated under combined axial compressive forces and moments[35, 39]. However, the disc deformation at the segments adjacent to the DDD levels in living patients before surgical treatments remains unclear.

In **Chapter 4**, a combined MRI and dual fluoroscopic imaging system (DFIS) technique was used to quantify the disc geometric deformation *in vivo* in healthy asymptomatic subjects[40]. The purpose of this Chapter was to quantitatively evaluate the effect of lumbar DDD on the disc deformation at the adjacent level and the level one above the adjacent level during *in vivo* end ranges of lumbar spine motions, which corresponded to the extreme motions experienced during daily activities [41]. In 10 DDD patients with degenerated discs between L4 and S1, disc L3-4 and L2-3 were studied and compared to those of the 8 asymptomatic healthy subjects in **Chapter 4**. We hypothesized that DDD can cause the healthy cephalic L3-4 and L2-3 segments to undergo larger deformation compared to normal subjects.

## 9.2 Material and Methods:

### 9.2.1 Subject recruitment:

Ten patients with DDD (the same group in **Chapter 8**) who were diagnosed with discogenic LBP originated from L4-S1 were included consecutively in this study. A group of eight age, height and weight-matched healthy subjects were used as a reference comparison. The L3-4 (the adjacent level to the degenerated discs) and L2-3 (the level one above the adjacent level) lumbar discs of each subject were investigated, resulting in a total of 36 discs studied. The degrees of degeneration of the lumbar spine discs L2-S1 were graded from MR images using the 5-level Pfirrmann's scales[42], by both a radiology specialist and an experienced spine surgeon blinded to the group membership (**Table 9-1**). Both the patients and normal subjects had non-statistically different Pfirrmann's scores of less than *III* at the L2-3 and L3-4 discs, where grade *I* and *II* represent minimal degeneration and grade *V* represent severe degeneration as a collapsed disc[42].

Table 9-1: Numbers of subjects fall into each disc degeneration grade of Pfirrmann's classification. The grading was performed by both a radiologist and a spine surgeon.

	<i>Graded by radiologist</i>					<i>Graded by surgeon</i>				
	<i>I</i>	<i>II</i>	<i>III</i>	<i>IV</i>	<i>V</i>	<i>I</i>	<i>II</i>	<i>III</i>	<i>IV</i>	<i>V</i>
	<b>DDD (n=10)</b>					<b>DDD (n=10)</b>				
<b>L2-3</b>	6	4				6	4			
<b>L3-4</b>	5	5				5	4	1		
<b>L4-5</b>			3	3	4			1	5	4
<b>L5-1</b>				5	5				5	5
	<b>Normal (n=8)</b>					<b>Normal (n=8)</b>				
<b>L2-3</b>	7	1				6	2			
<b>L3-4</b>	4	4				4	4			
<b>L4-5</b>	2	6				2	4	2		
<b>L5-1</b>	1	7					6	2		

The subject was then scanned using DFIS[43] in standing position and at 6 end-ranges of motion: maximal left-right torsion, side-to-side bending and flexion-extension of the torso, which corresponded to the motions experienced during daily activities. In each posture, the *in vivo* positions of the vertebrae L2, L3 and L4 were reproduced in a solid modeling software (Rhinoceros®, Robert McNeel & Associates, Seattle, WA) by matching the projections of the 3D MR image-based vertebral models at supine to their 2D osseous contours in the fluoroscopic images at various end ranges of lumbar motion (**Fig 9-1**).

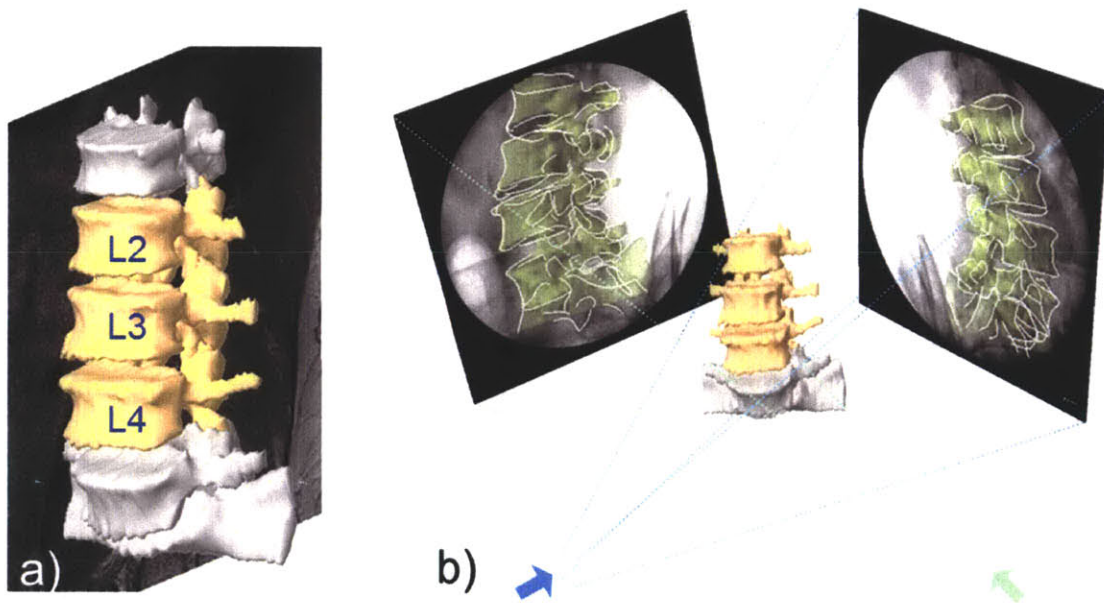


Fig 9-1: a): 3D vertebrae models were constructed from sagittal MR images. b): reproduction of *in vivo* vertebrae positions by matching 3D model projections to 2D osseous contours

### 9.2.2 Calculation of IVD deformation:

The overall IVD deformation was calculated based on the positions and orientations of the disc endplates (L2-3, L3-4) from the reproduced kinematics of the vertebrae in each posture. As shown in **Fig 9-2**, local disc heights were determined by calculating the shortest distances between mesh vertices of the upper and lower endplates (about 1000 points per endplate) using a custom Matlab® code (MathWorks, Natick, MA). The local disc height of each vertex in standing position was used as a reference to calculate the disc deformations at various end ranges of motion of the torso. To do this, a reference plane was created for each disc by automatically fitting a transverse plane through the lower disc endplate using Rhinoceros® (**Fig 9-2**). Tensile deformation at each vertex was defined as the component of the local height change that perpendicular to the transverse plane. It was calculated in Matlab® and plotted on a color-coded map plot showing magnitudes with respect to the reference disc height at standing (**Fig 9-3**). Similarly, shear deformation at each vertex was defined as the component parallel to the transverse plane and plotted on a gradient (quiver) plot showing both magnitudes and directions.

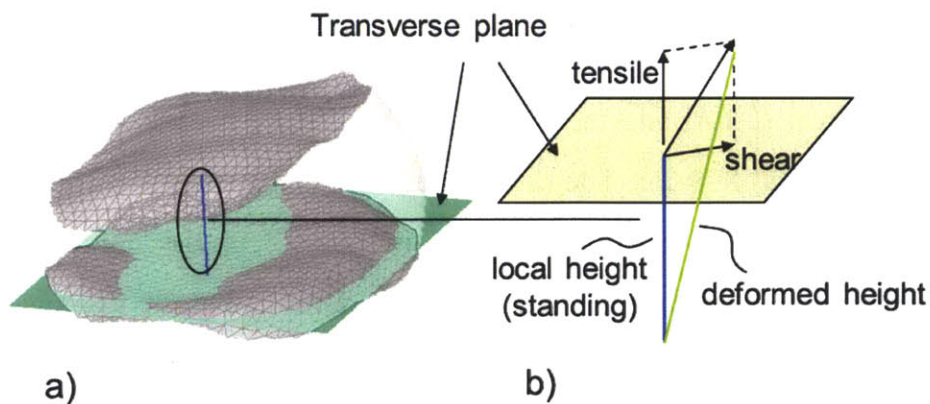


Fig 9-2. a): Local heights and disc transverse plane were determined. b): Calculation of the tensile and shear deformations, with respect to local heights in standing as references.

The characteristics of the disc deformation of the patients with DDD were quantitatively compared to those of the normal subjects under various end ranges of motion of the torso. These included: areas of minimal deformation (defined as <5% deformation), deformations at the center of the discs, and maximum tensile (tension and compression) and shear deformations. The areas of minimal deformation (defined as <5% deformation) were calculated in a custom Matlab code. The 5% criterion was empirically picked based on the magnitude of deformation near the center of a disc, which was observed to be the minimum among different portions of a disc in general. Two-way mixed model ANOVA were used to compare the data of the two groups of subjects at the two disc levels, where disc levels was considered as a within-factor. A statistical significance was defined as  $p < 0.05$ . When a statistically significant difference was detected, a Newman-Keuls post-hoc test was performed. The statistical analysis was performed in Statistica (Statsoft, Tulsa, OK).

## **9.3 Results:**

### ***9.3.1 Deformation patterns:***

In the patients with DDD, the areas of minimal IVD deformation (<5%) at the adjacent level (L3-4) and the level one above (L2-3) were smaller than the normal subjects (**Table 9-2**). The differences were statistically significant except for L3-4 and L2-3 under left torsion. On average, in the normal subjects, approximately 45% of the discs were minimally deformed at the two disc levels. While in the patients with DDD, the areas of minimal deformation was only about 18% of the disc area at the two disc levels (**Fig 9-3**). Although not quantitatively evaluated, the areas of minimal deformation were observed to locate near the centers of the discs in the healthy group while shifted off the central axis in the



DDD group. Furthermore, at the center of the discs, both the patients with DDD and the normal subjects had similar tensile deformations with average magnitudes less than 6% (**Table 9-3**). No statistically significant difference was observed between the two groups, except for L3-4 disc during extension, where the average tensile deformation was  $-6\pm 6\%$  (compression) for the patients with DDD and  $1\pm 4\%$  for the normal subjects. At the center of the discs, shear deformations were generally larger in the patients with DDD compared to the healthy subjects for all postures (**Table 9-3**). And significant differences were observed at the L3-4 level during left bending ( $26\%$  DDD versus  $9\%$  healthy) and at the L2-3 level during right torsion ( $21\%$  DDD versus  $9\%$  healthy), during left bending ( $25\%$  DDD versus  $9\%$  healthy), and during right bending ( $28\%$  DDD versus  $10\%$  healthy)

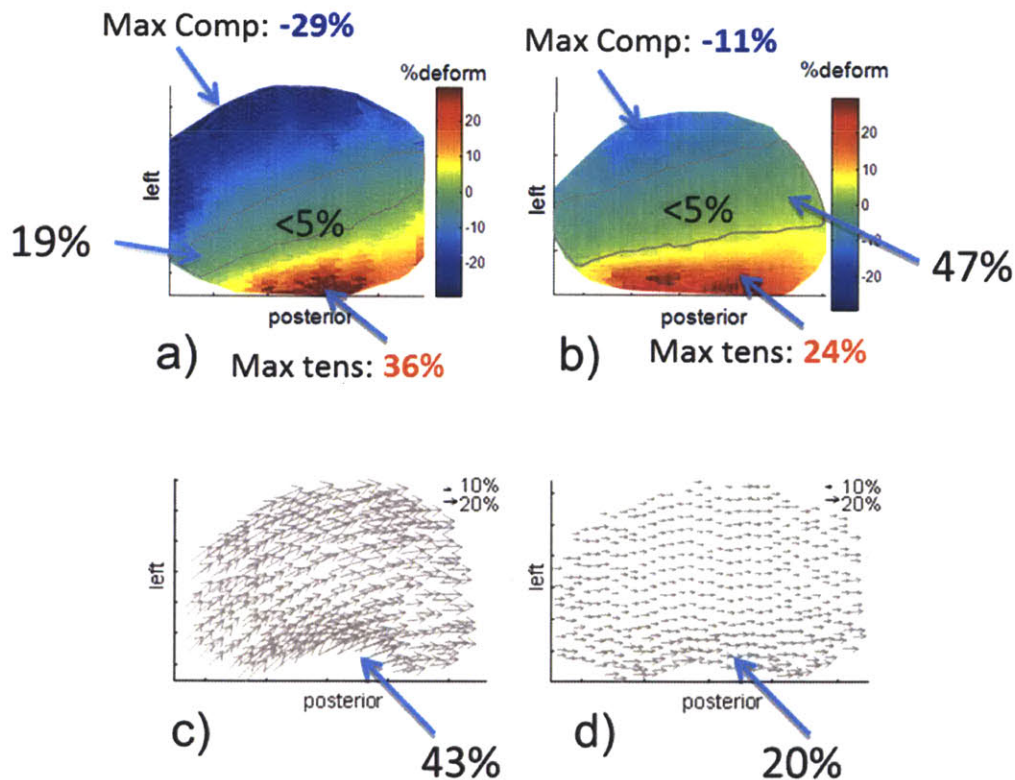


Fig 9-3. Typical disc tensile deformation of a): patient with DDD and b): healthy subject.

Typical disc shear deformation of c): patient with DDD and d): healthy subject.

Table 9-2: Area (average  $\pm$  SD) of the discs under minimal deformation (<5%) during end ranges of torso motion. \*:  $p < 0.05$  between DDD and normal subjects

	Left Torsion	Right Torsion	Left Bend	Right Bend	Extension	Flexion
<b>L2-3</b>						
<b>DDD</b>	23 $\pm$ 29%	14 $\pm$ 14%*	15 $\pm$ 11%*	19 $\pm$ 16%*	20 $\pm$ 12%*	18 $\pm$ 8%*
<b>Normal</b>	37 $\pm$ 15%	57 $\pm$ 22%*	41 $\pm$ 24%*	43 $\pm$ 19%*	54 $\pm$ 24%*	34 $\pm$ 12%*
<b>L3-4</b>						
<b>DDD</b>	28 $\pm$ 25%	12 $\pm$ 15%*	15 $\pm$ 8%*	18 $\pm$ 8%*	19 $\pm$ 19%*	14 $\pm$ 7%*
<b>Normal</b>	48 $\pm$ 27%	61 $\pm$ 15%*	50 $\pm$ 14%*	48 $\pm$ 21%*	44 $\pm$ 15%*	44 $\pm$ 19%*

Table 9-3: Tensile and shear deformations (average  $\pm$  SD) at the center of the discs in the patients with DDD and in the normal subjects during end ranges of motion of the torso.

\*: significant differences between DDD and normal subjects,  $p < 0.05$

		Left Torsion	Right Torsion	Left Bend	Right Bend	Extension	Flexion
<b>L2-3</b>							
<b>tensile</b>	<b>DDD</b>	3 $\pm$ 19%	4 $\pm$ 16%	1 $\pm$ 16%	-4 $\pm$ 21%	3 $\pm$ 13%	4 $\pm$ 12%
	<b>Normal</b>	-1 $\pm$ 6%	0 $\pm$ 4%	-1 $\pm$ 7%	1 $\pm$ 3%	0 $\pm$ 6%	-1 $\pm$ 5%
<b>shear</b>	<b>DDD</b>	26 $\pm$ 14%	21 $\pm$ 13%*	25 $\pm$ 14%*	28 $\pm$ 16%*	26 $\pm$ 18%	27 $\pm$ 17%
	<b>Normal</b>	16 $\pm$ 10%	9 $\pm$ 6%*	9 $\pm$ 5%*	10 $\pm$ 4%*	15 $\pm$ 8%	14 $\pm$ 7%
<b>L3-4</b>							
<b>tensile</b>	<b>DDD</b>	3 $\pm$ 7%	-1 $\pm$ 10%	-4 $\pm$ 8%	2 $\pm$ 10%	-6 $\pm$ 6%*	-2 $\pm$ 10%
	<b>Normal</b>	1 $\pm$ 5%	-2 $\pm$ 4%	1 $\pm$ 3%	0 $\pm$ 6%	1 $\pm$ 4%*	-1 $\pm$ 3%
<b>shear</b>	<b>DDD</b>	19 $\pm$ 12%	20 $\pm$ 21%	26 $\pm$ 13%*	32 $\pm$ 24%	20 $\pm$ 19%	32 $\pm$ 31%
	<b>Normal</b>	9 $\pm$ 7%	12 $\pm$ 6%	9 $\pm$ 5%*	15 $\pm$ 12%	14 $\pm$ 4%	17 $\pm$ 9%

### **9.3.2 Maximum tensile and shear deformations:**

At the adjacent level (L3-4), in all postures, maximum tension deformations were larger in the patients with DDD (ranging from 18% to 45%, on average) compared to the healthy subjects (ranging from 10% to 26%) in all postures (**Table 9-4**). Significant differences were observed during right torsion (26% DDD versus 10% healthy), during right bending (35% DDD versus 12% healthy), and during flexion (47% DDD versus 22% healthy). Maximum compressive deformations were also larger in the patients with DDD (ranging from -7% to -41%) compared to the healthy subjects (ranging from -9% to -17%), except for left torsion. Significant differences were only observed during left bending (-31% DDD versus -13% healthy). Maximum shear were larger in the patients with DDD (ranging from 53% to 66%) compared to the healthy subjects (ranging from 15% to 34%) in all postures. Significant differences between the patients with DDD and the healthy subjects were observed in most postures, except during right torsion and during flexion.

At the level one above (L2-3) the adjacent, maximum tension deformations were larger in the patients with DDD (ranging from 23% to 47%, on average) compared to the healthy subjects (ranging from 10% to 22%) in all postures (**Table 9-4**). Significant differences were observed in most postures, except during left bending and right bending. Maximum compressive deformations were also larger in the patients with DDD (ranging from -11% to -31%) compared to the healthy subjects (ranging from -10% to -15%), except for left torsion. Significant difference was only observed during left bending (-41% DDD versus -13% healthy). Maximum shear deformations were larger in the patients with DDD (ranging from 50% to 64%) compared to the healthy subjects (ranging from 21% to 29%) in all postures. Significant differences between the patients with DDD

and the healthy subjects were observed in most postures, except during left torsion and during extension.

Table 9-4: Maximum tensile (tension and compression) and shear deformation (average  $\pm$  SD) of the discs in the patients with DDD and in the normal subjects during end ranges of motion of the torso. \*:  $p < 0.05$  between DDD and normal subjects,

		Left Torsion	Right Torsion	Left Bend	Right Bend	Extension	Flexion
<b>L2-3</b>							
<b>tension</b>	<b>DDD</b>	29 $\pm$ 20%*	38 $\pm$ 33%*	25 $\pm$ 22%	18 $\pm$ 19%	32 $\pm$ 21%*	45 $\pm$ 11%*
	<b>Normal</b>	10 $\pm$ 8%*	11 $\pm$ 9%*	12 $\pm$ 9%	18 $\pm$ 6%	12 $\pm$ 11%*	26 $\pm$ 9%*
<b>compr.</b>	<b>DDD</b>	-7 $\pm$ 24%	-14 $\pm$ 20%	-41 $\pm$ 32%*	-22 $\pm$ 22%	-20 $\pm$ 13%	-18 $\pm$ 13%
	<b>Normal</b>	-12 $\pm$ 11%	-9 $\pm$ 6%	-13 $\pm$ 16%*	-14 $\pm$ 10%	-13 $\pm$ 14%	-17 $\pm$ 8%
<b>shear</b>	<b>DDD</b>	53 $\pm$ 27%	53 $\pm$ 24%*	65 $\pm$ 32%*	56 $\pm$ 23%*	55 $\pm$ 34%	66 $\pm$ 30%*
	<b>Normal</b>	34 $\pm$ 17%	20 $\pm$ 12%*	15 $\pm$ 8%*	23 $\pm$ 11%*	31 $\pm$ 19%	18 $\pm$ 16%*
<b>L3-4</b>							
<b>tension</b>	<b>DDD</b>	26 $\pm$ 26%	26 $\pm$ 19%*	24 $\pm$ 24%	35 $\pm$ 25%*	23 $\pm$ 20%	47 $\pm$ 25%*
	<b>Normal</b>	18 $\pm$ 16%	10 $\pm$ 8%*	15 $\pm$ 9%	12 $\pm$ 10%*	16 $\pm$ 13%	22 $\pm$ 13%*
<b>compr.</b>	<b>DDD</b>	-11 $\pm$ 10%	-17 $\pm$ 21%	-31 $\pm$ 17%*	-24 $\pm$ 20%	-24 $\pm$ 20%	-28 $\pm$ 21%
	<b>Normal</b>	-13 $\pm$ 9%	-10 $\pm$ 7%	-13 $\pm$ 10%*	-12 $\pm$ 7%	-14 $\pm$ 9%	-15 $\pm$ 10%
<b>shear</b>	<b>DDD</b>	62 $\pm$ 23%*	50 $\pm$ 31%	63 $\pm$ 26%*	64 $\pm$ 27%*	62 $\pm$ 28%*	54 $\pm$ 32%
	<b>Normal</b>	26 $\pm$ 17%*	29 $\pm$ 21%	21 $\pm$ 14%*	28 $\pm$ 18%*	26 $\pm$ 10%*	29 $\pm$ 17%

### 9.3.3 Difference between L3-4 and L2-3 discs:

No statistically significant difference ( $p > 0.05$ ) was found between L3-4 and L2-3 in any of the studied postures, in either groups, in terms of the areas of minimal deformation, tensile and shear deformations at the center of the discs, or maximum tensile and shear deformations.

## 9.4 Discussion:

This Chapter investigated and compared the lumbar IVD deformation of the adjacent level (L3-4) and the level one above (L2-3) the adjacent level between the patients with DDD at L4 to S1 and the healthy subjects in end ranges of motion of the torso, using the non-invasive imaging technique described in the previous Chapters. The results showed that in the patients with DDD, IVDs of both L3-4 and L2-3 underwent larger tensile and shear deformations in all postures compared to the normal subjects. The maximum tensile deformations were larger by up to 23% (of the local disc height in standing) and the maximum shear deformations were larger by approximately 25-40% (of the local disc height in standing) when compared to the deformation of the healthy subjects at the same levels during the same *in vivo* postures. On the other hand, the deformation patterns were also different, as the areas bearing minimal deformation (<5%) were significantly smaller in the patients with DDD by approximately 25% of the total disc areas. Although not quantitatively evaluated, in the patients with DDD these areas were observed to shift away from the disc centers. At the center of the discs, both groups experienced similar small tensile deformations of <6%. However, shear deformations in the patients with DDD were larger than those of the normal subjects by approximately 10% during all end ranges of motion. Despite these differences between the two groups, no statistically significant difference was found between L3-4 and L2-3 discs within each group.

These differences can be directly related to the increased motion/loading at the adjacent levels of the DDD discs as observed by others [35, 39]. Kim et al.[35] developed a two motion segment (L3-4 and L4-5) finite element model and investigated the effects of disc degeneration (simulated at the L4-5 level) on the adjacent intact L3-4 level. They found increased maximum stress-strain,

intradiscal pressure and disc bulging at the L3-4 disc under axial compressive load. They concluded that these changes may trigger the degenerative process at the L3-4 disc over time. More recently, Ruberte et al.[39] modified a finite element model of lumbar spine (L1-S1) to simulate degeneration at the L4-5 disc. Under compressive preload and moments in three principal planes, they found that the motion at the cephalic adjacent level (L3-4) increased by 26% (of the normal motion) under axial torsion, 21% under lateral bending and 28% under flexion/extension. They also reported increases in stress range from 30% to ten-fold and suggested that degeneration can increase the risk for injury at the adjacent levels. Although there are substantial differences between the experimental setups of our *in vivo* patient measurements and these finite element studies, our study and the finite element models showed similar trends of the effects of DDD on the deformation of the discs at the adjacent segments.

The disc deformations in two cephalic levels were different in the patients with DDD than the healthy subjects. There was no statistically significant difference between the two cephalic levels. The results showed that DDD can affect the levels other than the immediately adjacent levels. Ruberte et al.[39] used a finite element model of lumbar spine L1-S1 to simulate degeneration at the L4-5 disc and had only reported the findings on the degenerated level and the immediately adjacent level. To the best of our knowledge, our study is the first showing multilevel biomechanics above the degenerated discs in living human subjects.

Most previous studies have investigated ASD in patients after surgical treatments and some have suggested a correlation between fusion and the development of radiographic and symptomatic ASD[9, 17, 45]. In a literature review by Park et al.[12], the incidence of lumbar ASD after arthrodesis has been

reported to range from 5.2% to 100%, whereas the incidence of symptomatic ASD range from 5.2% to 18.5%. Although the early result of total disc replacement are satisfactory, the basic premise that motion preservation will diminish ASD is yet to be proven[36, 46]. A recent review by Harrop et al.[17] noted that the incidence of ASD is approximately 9% after arthroplasty, whereas the incidence of symptomatic ASD is approximately 1%. Abnormal biomechanical changes at the adjacent segments after surgical treatments of the DDD have been reported in both arthrodesis and arthroplasty patients, in terms of mobility[19-23], change in disc height[18, 19, 24, 25], loading on the facet joints[26-30], intradiscal pressure[31-34], disc bulging[35], and stress-strain[36-38]. All of these suggest surgical treatments can have an adverse effect on ASD[10-12]. However, no studies have reported on the quantitative effect of the spine surgeries on the disc deformation at the adjacent segments in living patients and under physiological motions of the spine. Fusion or other surgical treatments may further change the adjacent discs deformation in a way that maybe related to the mechanism of high occurrence of ASD. Our study indicated that the disc deformation characteristics at the adjacent level and at the level one above in the patients with DDD were different from the healthy subjects even before the surgeries. Our results warrant a further investigation on the correlation between the deformation of the adjacent discs and the development of ASD in this group of patients after surgical treatments, which may provide invaluable information for prosthesis designs and surgical plans to include their effects on the entire lumbar spine, rather than focus merely on the DDD levels.

Controversially, several studies have suggested that ASDs are subsequent to the natural development instead of the surgical intervention, based on comparing radiographic changes between age and gender matched surgical and control groups[13-15, 47]. In a recent biomechanical study, Axelsson et al.[16] observed

hypermobility of the segments adjacent to fusions in 9 patients both before and 5 years after surgery. The hypermobility was found not to significantly change over time. They therefore concluded that the abnormal biomechanics at the adjacent level may not associate with progressive degeneration due to fusion. In our study, we found in the patients with DDD, both the adjacent level and the level one above had different disc deformation patterns and larger maximum deformations before surgery compared to the healthy subjects. We therefore postulate that the adjacent discs might have gradually adapted to the changing environment during the DDD development in the L4-L5-S1 levels, although they were rather healthy based on MRI findings in this group of patients. Whether this may or may not further trigger radiographic or clinical ASD over time even without surgical intervention is unclear. It would be of clinical interests to perform a long term follow up study of these patients to longitudinally examine how disc deformation may change at the adjacent levels and correlate to the development of ASD, or even LBP, if eventually surgical treatments were not performed.

There are certain limitations of this study. The sample sizes in the two groups were relatively small, which might limit our ability to detect differences. This may also explain why some of the differences were not statistically significant as well as the relatively large SDs that were observed. Even though we have tried to standardize the motion of the torso, patients may be more or less likely to perform combined movements. However we would expect little effect of the combined movements on the deformation results reported, since the differences were generally observed between the two groups, not among different postures. As reported in **Chapter 2 and 4**[40, 44], the maximum error in calculation of the geometric deformation was 4% when considering both the accuracy of the imaging technique and the deformation of the endplates. Simplifications in calculation of the deformation were made as we only



determined the overall geometric deformation throughout the thickness of the disc. The results were only overall strains of the discs. In **Chapter 11 and 12**, a preliminary finite element study using the kinematic results from the normal subjects as boundary conditions was presented to further investigate the *in vivo* stress-strain distributions inside the discs. In the future, more subjects could be involved and modification of the modeling approach to simulate discs with DDD can be considered. In addition, it will be of great value to follow up this patient group, whether or not they will have surgical treatments, to further study the adjacent discs longitudinally and to investigate the biomechanical mechanism of ASD.

In conclusion, disc deformations were studied using the combined MRI and DFIS imaging technique in a group of patients and a group of normal subjects. In patients with lumbar DDD, the discs at the adjacent level and at the level one above experienced higher deformations during various end ranges of motion of the torso when compared to those of the normal subjects. Both tensile and shear deformations were larger at the adjacent segment and the segment one above the adjacent level. Disc areas bearing minimal deformation were significantly smaller. These differences in disc deformations were otherwise not detectable using conventional MRI techniques that classify the degeneration of the discs. Future studies should quantify how surgical treatments, such as fusion and total disc replacement, would further alter the disc deformation at the adjacent segments.

## 9.5 References

1. Adams, M.A., *Biomechanics of back pain*. Acupunct Med, 2004. **22**(4): p. 178-88.
2. Luoma, K., et al., *Low back pain in relation to lumbar disc degeneration*. Spine (Phila Pa 1976), 2000. **25**(4): p. 487-92.
3. Elfering, A., et al., *Risk factors for lumbar disc degeneration: a 5-year prospective MRI study in asymptomatic individuals*. Spine (Phila Pa 1976), 2002. **27**(2): p. 125-34.
4. Waris, E., et al., *Disc degeneration in low back pain: a 17-year follow-up study using magnetic resonance imaging*. Spine (Phila Pa 1976), 2007. **32**(6): p. 681-4.
5. Ghiselli, G., et al., *Adjacent segment degeneration in the lumbar spine*. J Bone Joint Surg Am, 2004. **86-A**(7): p. 1497-503.
6. Lee, C.K., *Accelerated degeneration of the segment adjacent to a lumbar fusion*. Spine (Phila Pa 1976), 1988. **13**(3): p. 375-7.
7. Goel, V.K., J.N. Weinstein, and editors, *Biomechanics of the Spine - Clinical and Surgical Perspective*. 1990, Boca Raton, FL: CRC press.
8. Kumar, M.N., F. Jacquot, and H. Hall, *Long-term follow-up of functional outcomes and radiographic changes at adjacent levels following lumbar spine fusion for degenerative disc disease*. Eur Spine J, 2001. **10**(4): p. 309-13.
9. Phillips, F.M., J. Reuben, and F.T. Wetzel, *Intervertebral disc degeneration adjacent to a lumbar fusion. An experimental rabbit model*. J Bone Joint Surg Br, 2002. **84**(2): p. 289-94.
10. Adams, M.A., et al., *Mechanical initiation of intervertebral disc degeneration*. Spine (Phila Pa 1976), 2000. **25**(13): p. 1625-36.
11. Stokes, I.A. and J.C. Iatridis, *Mechanical conditions that accelerate intervertebral disc degeneration: overload versus immobilization*. Spine (Phila Pa 1976), 2004. **29**(23): p. 2724-32.
12. Park, P., et al., *Adjacent segment disease after lumbar or lumbosacral fusion: review of the literature*. Spine (Phila Pa 1976), 2004. **29**(17): p. 1938-44.
13. Seitsalo, S., et al., *Disc degeneration in young patients with isthmic spondylolisthesis treated operatively or conservatively: a long-term follow-up*. Eur Spine J, 1997. **6**(6): p. 393-7.
14. Van Horn, J.R. and L.M. Bohnen, *The development of discopathy in lumbar discs adjacent to a lumbar anterior interbody spondylodesis. A retrospective matched-pair study with a postoperative follow-up of 16 years*. Acta Orthop Belg, 1992. **58**(3): p. 280-6.

15. Hambly, M.F., et al., *The transition zone above a lumbosacral fusion*. Spine (Phila Pa 1976), 1998. **23**(16): p. 1785-92.
16. Axelsson, P., R. Johnsson, and B. Stromqvist, *Adjacent segment hypermobility after lumbar spine fusion: no association with progressive degeneration of the segment 5 years after surgery*. Acta Orthop, 2007. **78**(6): p. 834-9.
17. Harrop, J.S., et al., *Lumbar adjacent segment degeneration and disease after arthrodesis and total disc arthroplasty*. Spine (Phila Pa 1976), 2008. **33**(15): p. 1701-7.
18. Ekman, P., et al., *A prospective randomised study on the long-term effect of lumbar fusion on adjacent disc degeneration*. Eur Spine J, 2009. **18**(8): p. 1175-86.
19. Frymoyer, J.W., et al., *A comparison of radiographic findings in fusion and nonfusion patients ten or more years following lumbar disc surgery*. Spine (Phila Pa 1976), 1979. **4**(5): p. 435-40.
20. Stokes, I.A., et al., *1980 Volvo award in clinical sciences. Assessment of patients with low-back pain by biplanar radiographic measurement of intervertebral motion*. Spine (Phila Pa 1976), 1981. **6**(3): p. 233-40.
21. Axelsson, P., R. Johnsson, and B. Stromqvist, *The spondylolytic vertebra and its adjacent segment. Mobility measured before and after posterolateral fusion*. Spine (Phila Pa 1976), 1997. **22**(4): p. 414-7.
22. Panjabi, M., et al., *Hybrid testing of lumbar CHARITE discs versus fusions*. Spine (Phila Pa 1976), 2007. **32**(9): p. 959-66; discussion 967.
23. Auerbach, J.D., et al., *Segmental contribution toward total lumbar range of motion in disc replacement and fusions: a comparison of operative and adjacent levels*. Spine (Phila Pa 1976), 2009. **34**(23): p. 2510-7.
24. Guigui, P., et al., *[Long-term influence of associated arthrodesis on adjacent segments in the treatment of lumbar stenosis: a series of 127 cases with 9-year follow-up]*. Rev Chir Orthop Reparatrice Appar Mot, 2000. **86**(6): p. 546-57.
25. Schulte, T.L., et al., *Disc height reduction in adjacent segments and clinical outcome 10 years after lumbar 360 degrees fusion*. Eur Spine J, 2007. **16**(12): p. 2152-8.
26. Lee, C.K. and N.A. Langrana, *Lumbosacral spinal fusion. A biomechanical study*. Spine (Phila Pa 1976), 1984. **9**(6): p. 574-81.
27. Bastian, L., et al., *Evaluation of the mobility of adjacent segments after posterior thoracolumbar fixation: a biomechanical study*. Eur Spine J, 2001. **10**(4): p. 295-300.
28. Denoziere, G. and D.N. Ku, *Biomechanical comparison between fusion of two vertebrae and implantation of an artificial intervertebral disc*. J

- Biomech, 2006. **39**(4): p. 766-75.
29. Rohlmann, A., et al., *Comparison of the effects of bilateral posterior dynamic and rigid fixation devices on the loads in the lumbar spine: a finite element analysis*. Eur Spine J, 2007. **16**(8): p. 1223-31.
  30. Park, C.K., K.S. Ryu, and W.H. Jee, *Degenerative changes of discs and facet joints in lumbar total disc replacement using ProDisc II: minimum two-year follow-up*. Spine (Phila Pa 1976), 2008. **33**(16): p. 1755-61.
  31. Chow, D.H., et al., *Effects of short anterior lumbar interbody fusion on biomechanics of neighboring unfused segments*. Spine (Phila Pa 1976), 1996. **21**(5): p. 549-55.
  32. Chen, C.S., C.K. Cheng, and C.L. Liu, *A biomechanical comparison of posterolateral fusion and posterior fusion in the lumbar spine*. J Spinal Disord Tech, 2002. **15**(1): p. 53-63.
  33. Weinhoffer, S.L., et al., *Intradiscal pressure measurements above an instrumented fusion. A cadaveric study*. Spine (Phila Pa 1976), 1995. **20**(5): p. 526-31.
  34. Cunningham, B.W., et al., *The effect of spinal destabilization and instrumentation on lumbar intradiscal pressure: an in vitro biomechanical analysis*. Spine (Phila Pa 1976), 1997. **22**(22): p. 2655-63.
  35. Kim, Y.E., et al., *Effect of disc degeneration at one level on the adjacent level in axial mode*. Spine (Phila Pa 1976), 1991. **16**(3): p. 331-5.
  36. Chen, S.H., et al., *Biomechanical comparison between lumbar disc arthroplasty and fusion*. Med Eng Phys, 2009. **31**(2): p. 244-53.
  37. Chiang, M.F., et al., *Biomechanical comparison of instrumented posterior lumbar interbody fusion with one or two cages by finite element analysis*. Spine (Phila Pa 1976), 2006. **31**(19): p. E682-9.
  38. Kumar, N., et al., *Analysis of stress distribution in lumbar interbody fusion*. Spine (Phila Pa 1976), 2005. **30**(15): p. 1731-5.
  39. Ruberte, L.M., R.N. Natarajan, and G.B. Andersson, *Influence of single-level lumbar degenerative disc disease on the behavior of the adjacent segments--a finite element model study*. J Biomech, 2009. **42**(3): p. 341-8.
  40. Wang, S., et al., *Measurement of geometric deformation of lumbar intervertebral discs under in vivo weight-bearing condition*. J Biomech, 2009. **42**(6): p. 705-11.
  41. Wang, S., et al., *How does lumbar degenerative disc disease affect the disc deformation at the cephalic levels in vivo?* Spine (Phila Pa 1976), 2011. **36**(9): p. E574-81.
  42. Pfirrmann, C.W., et al., *Magnetic resonance classification of lumbar intervertebral disc degeneration*. Spine (Phila Pa 1976), 2001. **26**(17): p. 1873-8.

43. Li, G., et al., *Segmental in vivo vertebral motion during functional human lumbar spine activities*. Eur Spine J, 2009. **18**(7): p. 1013-21.
44. Wang, S., et al., *Measurement of vertebral kinematics using noninvasive image matching method-validation and application*. Spine (Phila Pa 1976), 2008. **33**(11): p. E355-61.
45. Yang, J.Y., J.K. Lee, and H.S. Song, *The impact of adjacent segment degeneration on the clinical outcome after lumbar spinal fusion*. Spine (Phila Pa 1976), 2008. **33**(5): p. 503-7.
46. Anderson, P.A. and J.P. Rouleau, *Intervertebral disc arthroplasty*. Spine (Phila Pa 1976), 2004. **29**(23): p. 2779-86.
47. Penta, M., A. Sandhu, and R.D. Fraser, *Magnetic resonance imaging assessment of disc degeneration 10 years after anterior lumbar interbody fusion*. Spine (Phila Pa 1976), 1995. **20**(6): p. 743-7.



# Chapter 10

## Lumbar Facet Joint Motion in Patients with Degenerative Disc Disease

### 10.1 Introduction:

The facet joints are one of the main structures that stabilize the lumbar spine. Facet joints are also believed to be the pain generator of approximately 15% to 37% of patients with low back pain (LBP).[1, 2] Previous studies showed that disc degeneration may precede facet joint osteoarthritis.[3, 4] Furthermore, with the onset of lumbar disc degeneration disease (DDD), it has been theorized that the increased loads on the facet joints due to decreasing disc height and altered mechanical properties in DDD affected levels result in alterations in facet degeneration and LBP.[5, 6] In addition, lumbar DDD has also been assumed to affect the biomechanical behavior of the facet joints of the adjacent segments [7].

Numerous surgical techniques have been used to treat lumbar degenerative diseases with variable outcomes. These include: fusion[8], disc arthroplasty[9], facet joints arthroplasty[10] and interspinous process devices (ISPD)[11]. An objective evaluation of the biomechanical functions of the facet joints of Patients with DDD is important for improving the surgical treatment efficiency. Therefore, it is necessary to determine the facet joints kinematics during functional activities. Few studies have used cadaveric specimens or animal models to examine the

motion characteristics of the facet joints.[12, 13] Facet kinematics were also measured in living human subjects using computerized topography (CT)[14] and kinematic MRI[15, 16]. However, a literature review reveals deficiency in the knowledge of lumbar facet joint motion in Patients with DDD. It is unclear how the lumbar DDD affects the mechanical properties of the facet joints in the diseased segments and in the segments adjacent to the degenerative levels.

In **Chapter 5**, the combined MRI and DFIS technique was used to investigate the 6 DOF motion of the lumbar vertebrae and the facet joints of living asymptomatic human subjects.[17-19] The findings have provided baseline information for studying the kinematic changes that occur in pathologic lumbar spines such as with DDD. The purpose of this Chapter was to evaluate the influences of DDD on the 6DOF motions of the facet joints during functional weight-bearing activities [20]. We studied a cohort of patients with clinically confirmed discogenic LBP at L4/5 and L5/S1 and compared the results with those of the asymptomatic healthy group without degeneration at both the discs and facet joints[19]. We hypothesized that the facet joints at the DDD levels and at the immediately adjacent levels would demonstrate distinct alterations in motion characteristics during active spinal motion *in vivo* when compared to those of the healthy subjects.



## 10.2 Materials and Methods

The 6DOF facet joints motion of ten discogenic LBP patients in **Chapter 8** was studied and compared to the eight normal asymptomatic patients in **Chapter 3** degeneration of the facet joints were graded using Weishaupt scales[21] (**Table 10-1**).

The subject was asked to stand and actively move the lumbar spine to different positions: standing position, maximum trunk flexion-extension, maximal left-right bending, and maximal left-right torsion. The *in vivo* positions of the vertebrae at various weight-bearing body positions were reproduced in the modeling software using the MRI-based 3D models and the two orthogonal fluoroscopic images.[17]

Table 10-1: Weishaupt's classification of lumbar facet joint in normal subjects and in Patients with DDD. The values were presented as mean (standard deviation).

	<u>L2/3</u>		<u>L3/4</u>		<u>L4/5</u>		<u>L5/S1</u>	
	Left	Right	Left	Right	Left	Right	Left	Right
Normal (n=8)	0	0	0.1(0.4)	0	0.1(0.4)	0.1(0.4)	0.3(0.5)	0.4(0.5)
range of grade	0	0	0~1	0	0~1	0~1	0~1	0~1
DDD (n=10)	0.8(0.5)	0.8(0.5)	0.8(0.5)	0.8(0.5)	2.5(0.8)	2.4(0.7)	2.3(0.9)	2.3(0.9)
range of grade	0~1	0~1	0~1	0~1	1~3	1~3	1~3	1~3

Right-hand Cartesian coordinate systems were created to quantify the facet joints motions (Fig 10-1). The volumetric center of the facet capsule was selected as the origin of the coordinate systems at each vertebral level. The X-axis was perpendicular to the facet joint surface in order to represent the medial-lateral direction. The Z-axis was set in the plane parallel to the facet sliding surface and along the long axis of facet joint to represent cranial-caudal direction of the facet joint motion and pointed in the cranial direction; and the Y-axis was set in the sagittal plane perpendicular to the Z-X plane to represent anterior-posterior direction and pointed posteriorly. A set of two same coordinate systems were adopted for both the inferior facet of cranial vertebra and the superior facet of caudal vertebra at the standing position such that the standing position is used as a reference. After reproduction of the *in vivo* vertebral positions, the kinematics of the facet joints at different trunk positions was directly measured from the coordinate system of the inferior facet joint with respect to that of the superior facet joint. Three translations were defined as the motions of the superior facet joint in the inferior facet joint coordinate system: medial-lateral, anterior-posterior and cranial-caudal translations. Three rotations were defined as the orientations of the superior facet joint around the origin of the inferior facet joint coordinate system using Euler angles in X-Y-Z sequence (in flexion, bending, and twisting sequence). The range of motion (ROM) of the facet joints were then determined from the end-ranges of motions of flexion-extension, left-right bending and left-right torsion of the trunk.

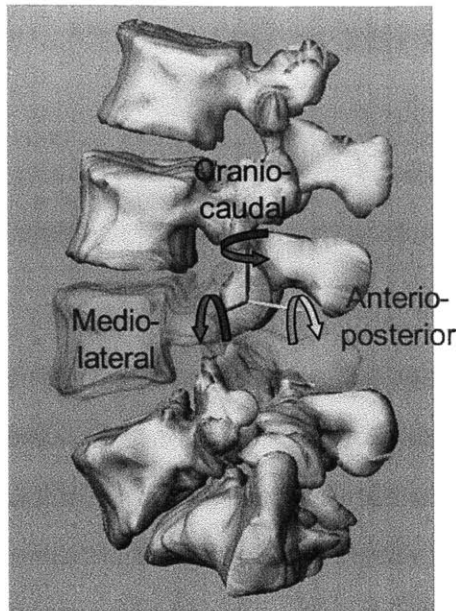


Fig 10-1. Anatomical coordinate system to measure kinematics of the facet joints.

Within each group, a two-way repeated measures ANOVA was used to compare the facet ROM at the L2-L3, L3-L4, L4-L5 and L5-S1 vertebral levels. The kinematics was the dependent variable and the vertebral level and activity were the independent variables. Level of statistical significance was set at  $P < 0.05$ . Another multi-way ANOVA was used to compare the kinematics between LBP patients and healthy subjects. The subject group was the categorical factor and the level and the activity were the independent variable. When a statistically significant difference was detected, a post-hoc Newman-Keuls test was performed, and the level of significance was again chosen at  $P < 0.05$ . The statistical analysis was done using Statistica software (Statistica<sup>®</sup> v. 8.0, Statsoft, Tulsa, OK).

## **10.3 Results**

### **10.3.1 *Ranges of motion of facet joints in Patients with DDD***

#### **Facet Motion during Left to Right Torsion of the Trunk**

During left-right torsion of the trunk, the facet joint experienced coupled rotations and translations (**Fig 10-2a, 10-3a**). At the DDD levels (L4-5 and L5-S1), the mean ranges of rotations around all three axes were from 2.6° to 3.6°. At the adjacent levels (L2-3 and L3-4), the mean ranges of rotations around all three axes were from 2.0° to 3.4°. There was no significant difference in the magnitude of rotations between different levels. The range of translations along anterior-posterior (y-) axis was significantly greater in the caudal L5-S1 level than in the more cranial levels ( $p=0.036$ ). The mean ranges of translations along all three axes were from 1.5mm to 2.7mm at the DDD levels and 1.0mm to 1.9mm at the adjacent levels. Translations along cranial-caudal (z-) axis were not significantly different between the studied levels.

#### **Facet Motion during Left to Right Bending of the Trunk**

During left-right bending of the trunk, there were also coupled rotations and translations found in all directions (**Fig 10-2b, 10-3b**). There was no predominant rotation and translation axis during this motion. At the DDD levels the mean ranges of rotations around all three axes were from 2.6° to 3.6°, while they were between 2.3° and 3.3° at the adjacent levels L2-3 and L3-4. There was no significant difference in the magnitude of rotations between different levels. The mean translations along all three axes were between 1.4mm and 2.0mm at the DDD levels, and between 1.0mm and 2.0mm at the adjacent levels. There was no significant difference between the studied levels in the ranges of translation.

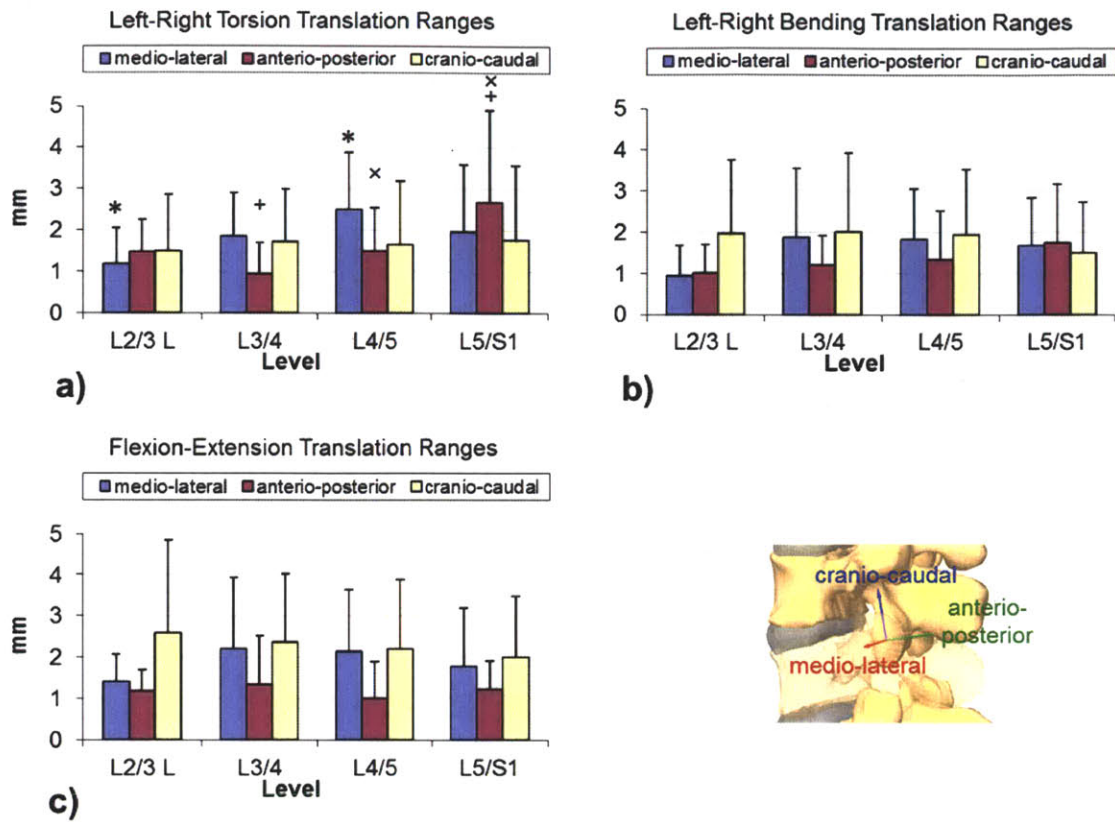


Fig 10-2. Ranges of facet joint translations of patients with DDD along three principal axes under : a) torsion, b) bending, and c) flexion of the torso. The symbols (\*, +, x) represent statistical significance upon between-level comparison ( $p < 0.05$ ).

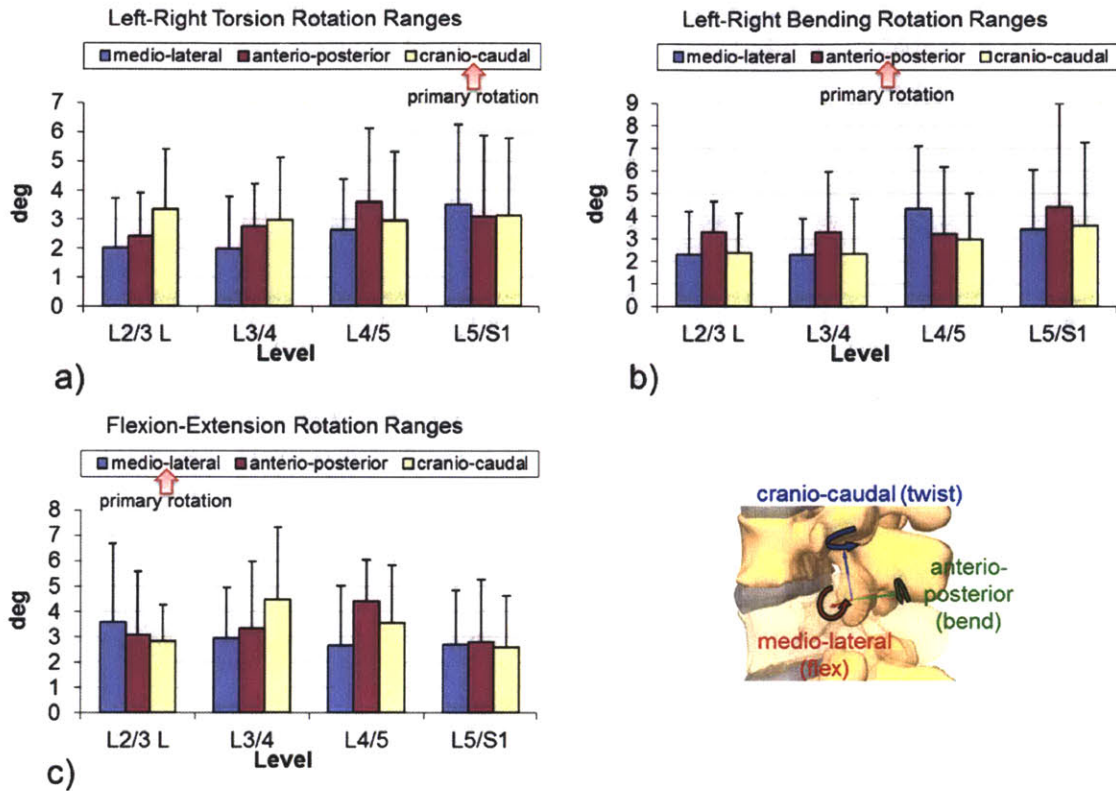


Fig 10-3. Ranges of facet joint rotations of patients with DDD around three principal axes under: **a)** torsion, **b)** bending, and **c)** flexion of the torso. There was no statistical difference between levels.

### Facet Motion during Flexion to Extension of the Trunk

During flexion-extension movements of the trunk, there was no predominant rotation and translation axis (**Fig 10-2c, 10-3c**). The mean ranges of rotations around all three axes were between 2.6° and 4.4° at the DDD levels and between 2.8° and 4.5° at the adjacent levels. There was no significant difference in the rotations between different levels. The ranges of translation along all three axes were between 1.0mm and 2.2mm at the DDD levels and between 1.2mm and 2.6mm at the adjacent levels, which were not significantly different.

### **10.3.2 Comparison with healthy subjects**

#### **Translations**

The ranges of translation at L2-3, L3-4 and L4-5 were compared between the Patients with DDD and the healthy subjects. In the Patients with DDD, the ranges of translations were between 0.8mm and 3.15mm, while in the healthy subjects, these were between 0.8mm and 4.1mm at all levels and in all activities. In general, there was no significant difference between the two groups of subjects.

#### **Rotations during Left to Right Torsion of the Trunk**

At the DDD level (L4-5), the primary rotations around cranial-caudal axis were not significantly different, although lower, than the healthy subjects (**Table 10-2**). The coupled rotations of the Patients with DDD increased in general. Around the anterior-posterior (y-) axis, the Patients with DDD had a range of rotation of  $3.6 \pm 2.5^\circ$  while the healthy subjects had  $1.7 \pm 1.1^\circ$  ( $p=0.056$ ). At the adjacent level L3-4, no significant differences were observed between healthy subjects and Patients with DDD. At the L2-3 level, the rotation around medial-lateral (x-) axis was significantly higher in the Patients with DDD (healthy  $0.6^\circ \pm 0.3^\circ$  vs. DDD  $2.0^\circ \pm 1.7^\circ$ ,  $P < 0.05$ ).

#### **Rotations during Left to Right Bending of the Trunk**

At the DDD level (L4-5), the primary rotations around anterior-posterior axis were not significantly different, although lower, than the healthy subjects (**Table 10-2**). The coupled rotations of the Patients with DDD increased in general. Around the medial-lateral (x-) axis, the Patients with DDD had a range of rotation of  $4.3 \pm 2.8^\circ$  while the healthy subjects had  $1.6 \pm 1.0^\circ$  ( $p=0.014$ ). At the adjacent level L3-4 and L2-3 level, the ranges of rotations during left-right

bending activity were similar between the two groups.

Table 10-2: Comparison of rotation ranges between normal and DDD groups. Primary axes of rotation were shaded. Values were mean (standard deviation) in degrees. Red Font: \* P<0.05, ML: medial-lateral, AP: anterior-posterior, and CC: cranial-caudal.

	L2/3			L3/4			L4/5		
	ML	AP	CC	ML	AP	CC	ML	AP	CC
<b>Left-right torsion</b>									
Normal	0.6(0.3)	3.3(1.4)	1.9(1.4)	1.3(0.8)	2.2(1.3)	2.7(1.4)	1.4(1.1)	1.7(1.1)	4.4(1.5)
DDD	2.0(1.7)*	2.4(1.5)	3.4(2.1)	2.0(1.8)	2.8(1.5)	3.0(2.2)	2.6(1.8)	3.6(2.5)	3.0(2.3)
P value	0.032	0.221	0.090	0.265	0.455	0.743	0.100	0.056	0.122
<b>Left-right bend</b>									
Normal	1.9(1.3)	2.7(1.0)	2.5(1.0)	1.3(1.1)	3.8(1.7)	2.9(1.2)	1.6(1.0)	4.7(1.1)	2.9(1.6)
DDD	2.3(1.9)	3.3(1.4)	2.4(1.8)	2.3(1.6)	3.3(2.7)	2.3(2.5)	4.3(2.8)*	3.2(3.0)	3.0(2.1)
P value	0.668	0.322	0.828	0.128	0.657	0.516	0.014	0.173	0.898
<b>Flexion-extension</b>									
Normal	6.5(1.7)	2.0(1.7)	1.9(1.0)	5.7(1.7)	1.9(1.4)	2.0(1.8)	2.4(1.7)	2.9(1.2)	3.5(1.2)
DDD	3.8(3.1)*	3.1(2.5)	2.8(1.4)	2.9(2.0)**	3.3(2.7)	4.5(2.9)*	2.7(2.3)	4.4(1.6)*	3.6(2.3)
P value	0.028	0.303	0.105	0.009	0.171	0.042	0.764	0.037	0.921

### Rotations during Flexion to Extension of the Trunk

At the DDD level (L4-5), the primary rotations around medial-lateral axis were not significantly different compare to the healthy subjects (Table 10-2). The coupled rotations of the Patients with DDD increased in general. Around the anterior-posterior (y-) axis, the Patients with DDD had a range of rotation of  $4.4^{\circ} \pm 1.6^{\circ}$  while the healthy subjects had  $2.9^{\circ} \pm 1.2^{\circ}$  ( $p=0.037$ ). At the adjacent level L3-4, the Patients with DDD showed significantly lower rotation around the primary medial-lateral (x-) axis ( $2.9^{\circ} \pm 2.0^{\circ}$  vs.  $5.7^{\circ} \pm 1.7^{\circ}$ ,  $p=0.009$ ), but had an



increased coupled rotation around the cranial-caudal(z-) axis ( $4.5^{\circ}\pm 2.9^{\circ}$  vs.  $2.0^{\circ}\pm 1.8^{\circ}$ ,  $P=0.042$ ). At the L2-3 level, the rotation around primary medial-lateral (x-) axis was significantly lower in the Patients with DDD (Healthy  $6.5^{\circ}\pm 1.7^{\circ}$  vs. DDD  $3.8^{\circ}\pm 3.1^{\circ}$ ,  $P=0.028$ ), while at the coupled rotations, the average values increased in Patients with DDD, but not significantly.

## 10.4 Discussion

This Chapter reports on the motion characteristics of the lumbar facet joints in Patients with DDD. Patients had DDD at L4-5 and L5-S1 levels and were studied in different weight-bearing positions of the trunk. The ROM of the facet joints were compared with those of the healthy control group[19] determined during the same trunk postures in **Chapter 5**. Our data indicated that disc degeneration alters the ROM of the facet joints at both the affected level and at the adjacent level. Not like normal subjects, there was no predominant direction of rotation and translation of the facet joints during each movement of the trunk in patients with DDD. The DDD level had similar range of primary rotations when compared to the healthy subjects, but significantly greater coupled rotations during all activities. In the adjacent levels, differences were mainly observed during flexion-extension of the trunk, while the primary rotations significantly decreased with DDD and the coupled rotations increased.

In the literature, capsular strain measurement of the facet joints has been conducted using cadaveric specimens. Ianuzzi et al.[22] performed a cadaveric experiment and found that the strain of the facet joints increased in magnitude with increasing displacements of vertebrae during lumbar motion. Little et al.[23] found increased strain of facet joint capsule at the levels adjacent to the fixation level during lumbar motion. Few studies have reported on the facet joint

kinematics *in vivo*. Wood et al.[13] measured the facet excursions at the L2-3 motion segment during various functional activities using a canine model. They found that during walking the average excursions between opposing facets were  $3.4\pm 1.3$ mm as the facet surfaces glided on a ventral to dorsal slope. The similar magnitudes of excursion were reported by Schendel et al[24] using a similar canine model. Although there are studies investigating vertebral motions in healthy human subjects and Patients with DDD[14], there is no study reported on the effect of disc degeneration on facet joint kinematics.

Since the role of the facet joints in pathogenesis of LBD remains unclear, these data may have valuable clinical and scientific implications. The hypermobility of the facet joints in coupled rotations of the Patients with DDD may cause increased compressive stresses between the articulating surfaces and facilitate cartilage degeneration[5, 6]. Furthermore, the lumbar facet joint capsule is innervated with nociceptors and mechanoreceptors. The strain of the facet joint capsule is thought to play an important role in LBP [25, 26]. The hypermobility of the facet joints in 6DOF, which can hardly be detected using dynamic X-rays or even dynamic MRI, might cause an increase in the strain of the facet joint capsule contributing to LBP in Patients with DDD.

There are many techniques used to treat lumbar degenerative disease.[8-11] All these techniques and instruments might influence the facet joint biomechanics. For example, Rousseau et al. [27] reported that disc arthroplasty may cause changes in the facet forces. However, few surgical technique or implant designs have considered the biomechanics of the facet joints. The data of this study demonstrated that disc degeneration alters the kinematics and ROM of the facet joints in both DDD-affected and adjacent levels. The superior adjacent levels can

also develop facet joint hypermobility in patients with DDD. Therefore, more attention should be paid to the lumbar facet joints when treating patients with DDD.

There are several limitations to the current study. It is not a generic comparison of Patients with DDD and asymptomatic subjects. The patients involved in the study were specifically selected with DDD at L4-5 and L5-S1 levels, which only represented a portion of all Patients with DDD. It is possible that in groups with different degenerative patterns (e.g., DDD at different levels), the result can be different. Future studies should include patients with DDD at other segments such as single-level DDD at L4-5 or at L5-S1. The sample sizes in the two groups were relatively small. Before the study, statistical power calculations showed that with 8 and 10 subjects in t groups, 80% power can be achieved to detect a difference of  $2.5 \pm 2^\circ$  (mean  $\pm$  SD). However, statistical power varies with different mean and SD in each studied position, which might limit our ability to detect differences. Even though we have tried to standardize the movement, Patients with DDD may move more or less differently. We did not artificially alter the motion in order to capture the true *in vivo* biomechanics. In addition, we only investigated the end-point positions of each trunk posture. Continuous and dynamic motions of the trunk should be investigated in future studies.

The study focused on the kinematics of the facet joints and the forces imposed upon the facets were not considered. It is not clear the forces generated under the DDD conditions would be sufficient to cause degeneration and pain in the facets. A technique using kinematics data to predict disc loads in finite element analysis is presented in **Chapter 11** and **12** of the thesis work. In the future, similar technique should be developed to predict forces in the facet joints.

In conclusion, this Chapter used the imaging technique to quantify abnormal motion characteristics of lumbar facet joints in patients with DDD. While DDD was shown to increase the coupled motion of the facet joints in DDD levels, it also reduced the primary rotations and increased the coupled rotations at the adjacent levels. The data can be used to evaluate the effects of surgical treatments of DDD on facet joint motion. Furthermore, knowledge of motion patterns of the lumbar facet joints is important for improving treatments of DDD and management of facet joint arthropathy, especially those aiming at restoration of normal motion, such as dynamic stabilization techniques and such as total disc arthroplasty.

## 10.5 References

1. Dreyfuss, P., et al., *Efficacy and validity of radiofrequency neurotomy for chronic lumbar zygapophysial joint pain*. Spine (Phila Pa 1976), 2000. **25**(10): p. 1270-7.
2. Schwarzer, A.C., et al., *The false-positive rate of uncontrolled diagnostic blocks of the lumbar zygapophysial joints*. Pain, 1994. **58**(2): p. 195-200.
3. Fujiwara, A., et al., *The relationship between facet joint osteoarthritis and disc degeneration of the lumbar spine: an MRI study*. Eur Spine J, 1999. **8**(5): p. 396-401.
4. Oegema, T.R., Jr. and D.S. Bradford, *The inter-relationship of facet joint osteoarthritis and degenerative disc disease*. Br J Rheumatol, 1991. **30** Suppl 1: p. 16-20.
5. Panjabi, M.M., M.H. Krag, and T.Q. Chung, *Effects of disc injury on mechanical behavior of the human spine*. Spine (Phila Pa 1976), 1984. **9**(7): p. 707-13.
6. Dunlop, R.B., M.A. Adams, and W.C. Hutton, *Disc space narrowing and the lumbar facet joints*. J Bone Joint Surg Br, 1984. **66**(5): p. 706-10.
7. Ruberte, L.M., R.N. Natarajan, and G.B. Andersson, *Influence of single-level lumbar degenerative disc disease on the behavior of the adjacent segments--a finite element model study*. J Biomech, 2009. **42**(3): p. 341-8.
8. Cheh, G., et al., *Adjacent segment disease following lumbar/thoracolumbar fusion with pedicle screw instrumentation: a minimum 5-year follow-up*. Spine (Phila Pa 1976), 2007. **32**(20): p. 2253-7.
9. Schmidt, H., et al., *The effect of different design concepts in lumbar total disc arthroplasty on the range of motion, facet joint forces and instantaneous center of rotation of a L4-5 segment*. Eur Spine J, 2009. **18**(11): p. 1695-1705.
10. Zhu, Q., et al., *Biomechanical evaluation of the Total Facet Arthroplasty System: 3-dimensional kinematics*. Spine (Phila Pa 1976), 2007. **32**(1): p. 55-62.
11. Siddiqui, M., et al., *Influence of X Stop on neural foramina and spinal canal area in spinal stenosis*. Spine (Phila Pa 1976), 2006. **31**(25): p. 2958-62.
12. Adams, M.A. and W.C. Hutton, *The mechanical function of the lumbar apophyseal joints*. Spine (Phila Pa 1976), 1983. **8**(3): p. 327-30.
13. Wood, K.B., et al., *In vivo analysis of canine intervertebral and facet motion*. Spine (Phila Pa 1976), 1992. **17**(10): p. 1180-6.
14. Ochia, R.S., et al., *In vivo measurements of lumbar segmental motion during axial rotation in asymptomatic and chronic low back pain male*

- subjects. *Spine (Phila Pa 1976)*, 2007. **32**(13): p. 1394-9.
15. Kong, M.H., et al., *Lumbar segmental mobility according to the grade of the disc, the facet joint, the muscle, and the ligament pathology by using kinetic magnetic resonance imaging*. *Spine (Phila Pa 1976)*, 2009. **34**(23): p. 2537-44.
  16. Kulig, K., et al., *Segmental lumbar mobility in individuals with low back pain: in vivo assessment during manual and self-imposed motion using dynamic MRI*. *BMC Musculoskelet Disord*, 2007. **8**: p. 8.
  17. Wang, S., et al., *Measurement of vertebral kinematics using noninvasive image matching method-validation and application*. *Spine (Phila Pa 1976)*, 2008. **33**(11): p. E355-61.
  18. Li, G., et al., *Segmental in vivo vertebral motion during functional human lumbar spine activities*. *Eur Spine J*, 2009. **18**(7): p. 1013-21.
  19. Kozanek, M., et al., *Range of motion and orientation of the lumbar facet joints in vivo*. *Spine (Phila Pa 1976)*, 2009. **34**(19): p. E689-96.
  20. Li, W., et al., *Lumbar facet joint motion in patients with degenerative disc disease at affected and adjacent levels: an in vivo biomechanical study*. *Spine (Phila Pa 1976)*, 2011. **36**(10): p. E629-37.
  21. Weishaupt, D., et al., *MR imaging of inflammatory joint diseases of the foot and ankle*. *Skeletal Radiol*, 1999. **28**(12): p. 663-9.
  22. Ianuzzi, A., et al., *Human lumbar facet joint capsule strains: I. During physiological motions*. *Spine J*, 2004. **4**(2): p. 141-52.
  23. Little, J.S., et al., *Human lumbar facet joint capsule strains: II. Alteration of strains subsequent to anterior interbody fixation*. *Spine J*, 2004. **4**(2): p. 153-62.
  24. Schendel, M.J., et al., *Kinematics of the canine lumbar intervertebral joint. An in vivo study before and after adjacent instrumentation*. *Spine (Phila Pa 1976)*, 1995. **20**(23): p. 2555-64.
  25. Cavanaugh, J.M., et al., *Lumbar facet pain: biomechanics, neuroanatomy and neurophysiology*. *J Biomech*, 1996. **29**(9): p. 1117-29.
  26. Cohen, S.P. and S.N. Raja, *Pathogenesis, diagnosis, and treatment of lumbar zygapophysial (facet) joint pain*. *Anesthesiology*, 2007. **106**(3): p. 591-614.
  27. Rousseau, M.A., et al., *Disc arthroplasty design influences intervertebral kinematics and facet forces*. *Spine J*, 2006. **6**(3): p. 258-66.

# Chapter 11

## Predict forces and moments on the lumbar intervertebral disc – a validation study

### 11.1 Introduction

The pathologies of human lumbar spine are often thought to be related to abnormal biomechanics, such as excessive forces and moments on the lumbar spine during daily activities[1, 2]. It is therefore critically important to understand the loading environment in different anatomic structures of the lumbar spine, in order to investigate the disease mechanisms and develop surgical treatment technologies[3, 4]. However, determination of the *in vivo* spinal loads remains a challenge in biomedical engineering due to the complexity of the spinal geometry, limitations in experimental technologies, as well as the accompanied risks in *in vivo* measurements[5-8].

Alternatively, numerous numerical models of the spine such as finite element analysis (FEA) have been developed and simulated the spine biomechanics, various spinal injuries and surgical treatment methods[9-16]. Using the analytical technique, numerous studies have provided invaluable information for understanding lumbar spine biomechanics and function. The mechanics and functions of different structures of the lumbar spine, such as vertebral bone, discs, facets, ligaments and muscles have been studied[17-23]. Finite element (FE)

models of the normal lumbar spine were also modified to simulate defects and/or clinical symptoms to determine their mechanical influences on the lumbar spine[24-31]. For example, existing FE studies simulated spondylolisthesis[26, 27], ligament transection[28], herniated disc[29, 30], and muscle dysfunction[31] and suggested those changed force distribution in the lumbar spine and may adversely progress the pathologies and increase the risks of injury. Especially, disc degeneration, one of the most common pathologies, have been widely investigated in FE studies by changing the geometry, mechanical properties, and permeability and porosity of discs[14, 32-39]. The results greatly enhanced the understanding of the degeneration progression of the lumbar spine and showed the impact of degeneration both on the diseased level and the healthy adjacent levels.

Furthermore, FEA has also contributed greatly to evaluate the influence of surgical treatments or spinal implantations on the biomechanical response of the lumbar spine[15, 27, 40-59]. Traditional spinal surgeries such as decompression[27, 40-42], and fixation/fusion[43-50] and newly adopted surgeries such as artificial disc[51-56], interspinous spacer[15, 57], and dynamic stabilization[58, 59] have all been simulated using modified FE models. With the advantage of quantify stress-strain distribution in the spine, the implant, and their interface, FEA enabled detailed comparisons of the spine biomechanics before and after surgeries. This provided guideline for the surgeries and helped to find and explain potential risks and complications.

In most of the numerical models, external loadings were usually applied to the spine to calculate the kinematic responses and the internal forces and moments of different spinal structures. Despite all the advantages of FEA, it is critically important but challenging to determine the appropriate forces applied to simulate *in vivo* loading conditions[60] in FEA. The validity and accuracy of the results



largely depend on the simulated external loadings, especially when studying complex functional motions[61, 62]. Currently, most studies applied compressive forces and/or pure rotational moments in the three principal planes[63]. A few investigations have reported improved FEA results by using modified external loading conditions that were calculated from the kinematic models of the lumbar spine[64-68].

The non-invasive imaging technique that combines 3D CT/MRI modeling and DFIS technique showed high accuracy in determination of subject-specific *in vivo* spine kinematics[69]. With this technique, *in vivo* kinematics of the vertebrae, the IVDs and the facet joints of both healthy subjects and patients with spinal diseases have been determined in the previous Chapters of this thesis[70-77]. Therefore, instead of using simulated external loadings, it is possible to use the *in vivo* spine kinematics as input boundary conditions in the well-established FE models of the lumbar spine to estimate the *in vivo* spinal loads.

As a first step, the current study focused on the lumbar IVD, which plays an important role in the lumbar biomechanics and is closely related to most spinal pathologies and injuries. The aim of this study is to demonstrate that it is possible to use subject specific kinematics of the IVD endplates in FE analysis to estimate the forces and moments in the IVD (**Fig 11-1**). For this purpose, *in vitro* robotic loading experiments were performed on three lumbar IVDs. The kinematics of the IVD endplates during the experiments was determined using the DFIS. FE models of the IVDs were built based on CT scans and existing literature. The forces and moments in the IVDs were calculated from FE analyses using the kinematics as input boundary conditions, and compared to the experimental measurements for validation.

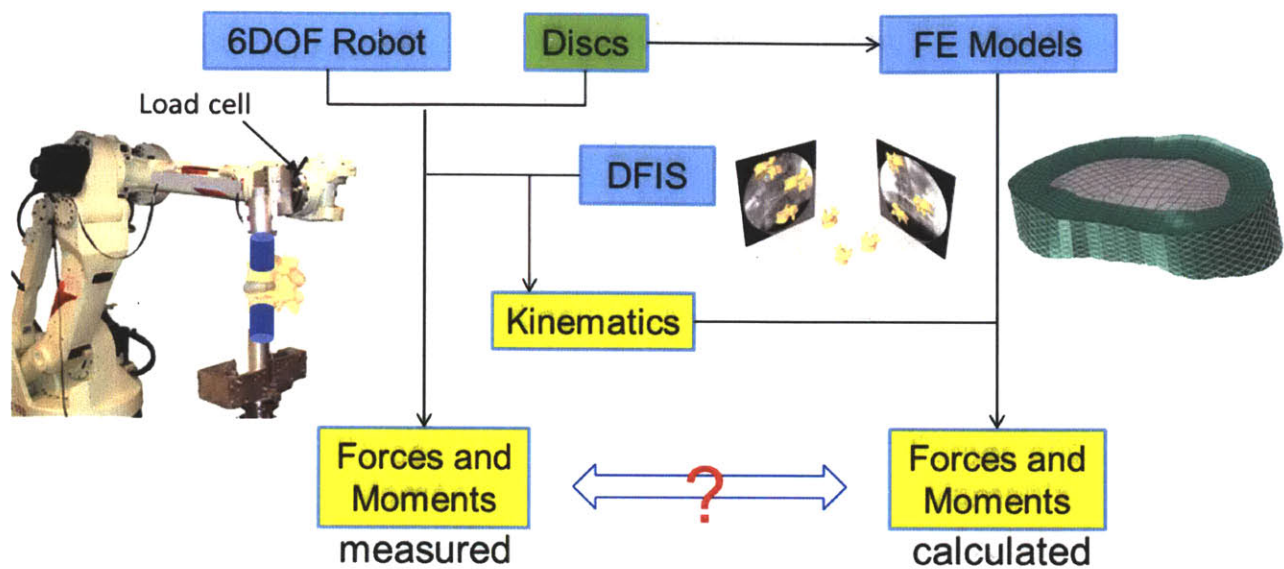


Fig 11-1. Experiment design

## 11.2 Material and Methods

### 11.2.1 Specimen preparation

Three fresh-frozen cadaveric lumbar spinal functional spinal units (FSUs) (two L2/3 and one L4/5, 23 to 44 years old) with healthy IVDs were selected from 3 donors. The FSUs were evaluated using a fluoroscope before the experiments and were dissected after the experiments to check for any abnormality in the IVDs. Each FSU was thawed and carefully dissected to remove the soft tissues and posterior elements in order to focus only on the force-displacement behavior of the IVD. The vertebral bodies were then potted in bone cement for fixation onto the testing system. In addition, 8 titanium beads were implanted on the bone cement. The specimen was then CT scanned with slice thickness of 0.6 mm (LightSpeed Pro16, GE, Waukesha, WI).

### **11.2.2 *In vitro testing protocol***

To study the force-displacement behavior of the IVDs, we used a 6 DOF robotic testing system (Kawasaki UZ150, Kawasaki Heavy Industry, Japan) (**Fig 11-2a**). Its operation has been detailed in previous studies[78]. Briefly, each IVD was tested under 7 loading cases: a 400N compression, 5Nm flexion/extension, left/right lateral bendings and left/right torsions. The center of the disc and the principal directions were determined using a 3D digitization platform (MicroScribe 3DX Digitizer, Immersion Corporation, San Jose, CA) and recorded in a coordinate system. The titanium beads implanted on the bone cement were also digitized and used as reference points so that the same coordinate system can be registered with the FE models.

During the experiments, the inferior endplate of each IVD was fixed and the superior endplate was free for movement by the robot. The robotic system determined the optimized loading path for each loading case[78], from 0 to 100% of the magnitude of the target loading (400N or 5Nm) in 10% increments. An optimized loading path is described as the positions of the specimen where the resultant force in the tested 1 DOF was within the error ( $<10$  N or  $<0.3$ Nm) of its 10% increment step, and the resultant forces and moments in all other 5 DOFs were minimal ( $<10$  N and  $<0.3$ Nm, respectively). In other words, in each loading case the specimen was loaded in only 1 DOF while the forces and moments along the other coupled 5 DOFs were minimized to zero. During each loading case, fluoroscopic images of the specimens were captured using the DFIS (**Fig 11-2b**). At the same time, forces and moments were recorded by the load cell (JR3 DSP-based force sensor receiver, JR3 Inc., Woodland, CA) attached to the robotic system and transferred to the center of the disc using a custom Matlab code (Matlab 2010a, MathWorks Inc., Natick, MA). During each loading case, the

robot moving speed was set to be similar to the normal moving speed of human lumbar spine. Between each loading case, the discs were kept still for 30 minutes at the neutral position to minimize any residue forces and moments due to the viscoelastic behavior.

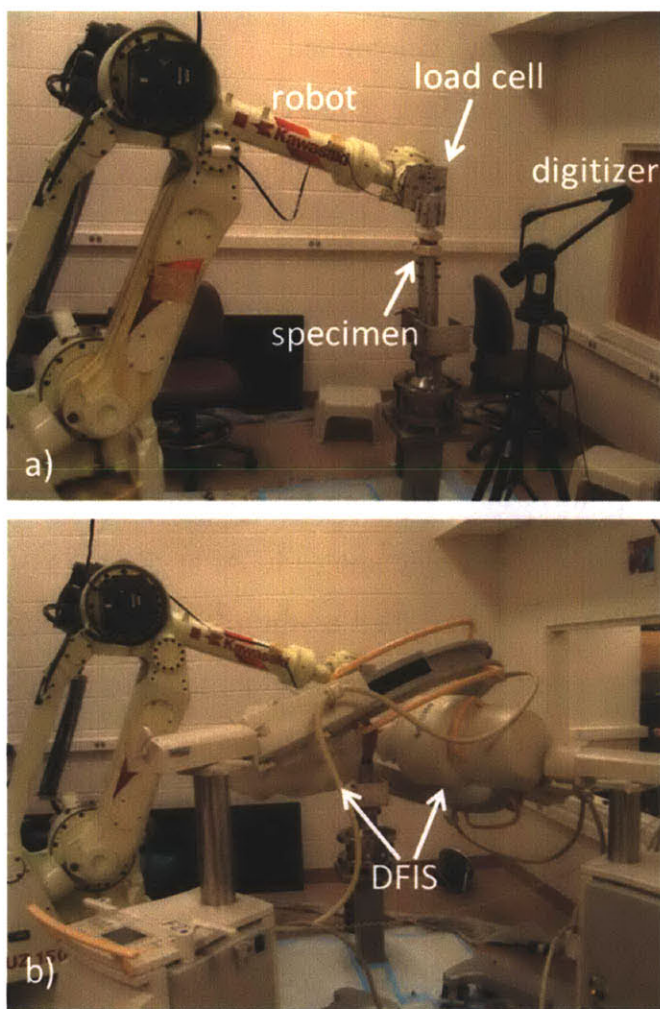


Fig 11-2. Experiment setup a) Installation of the lumbar MSU on the 6DOF robotic system. b) Capturing fluoroscopic images of the MSU using DFIS.

### **11.2.3 Determination of the kinematics of the disc endplates**

For each specimen, 3D geometric models were reconstructed from the CT images. The positions of the vertebrae during the loading history on the robot were then reproduced in a commercial solid modeling software (Rhino, Robert McNeel & Associates, Seattle, WA), where the projections of the 3D CT models were matched to their 2D osseous contours on the fluoroscopic images obtained in the robot experiments (**Fig 11-3**). This technique has been detailed in **Chapter 2** and has been validated to have accuracy within 0.3 mm in translation and 0.7° in rotation [69, 70]. Similarly, the positions of the implanted titanium beads were reproduced using the DFIS (**Fig 11-4**). Since the relationship between the locations of the titanium beads and the coordinate system were recorded during the experiment using the digitizer, the same center of the disc and principal directions can be determined and registered with the 3D model (**Fig 11-4**). The relative motion of the superior endplate with respect to the inferior endplate were determined from the vertebral kinematics, and described in the coordinate system using Euler angles in the flexion-bending-torsion order. Therefore, both the geometric details of the IVD endplates and their kinematics during each loading case were obtained for the FE modeling of the IVDs.

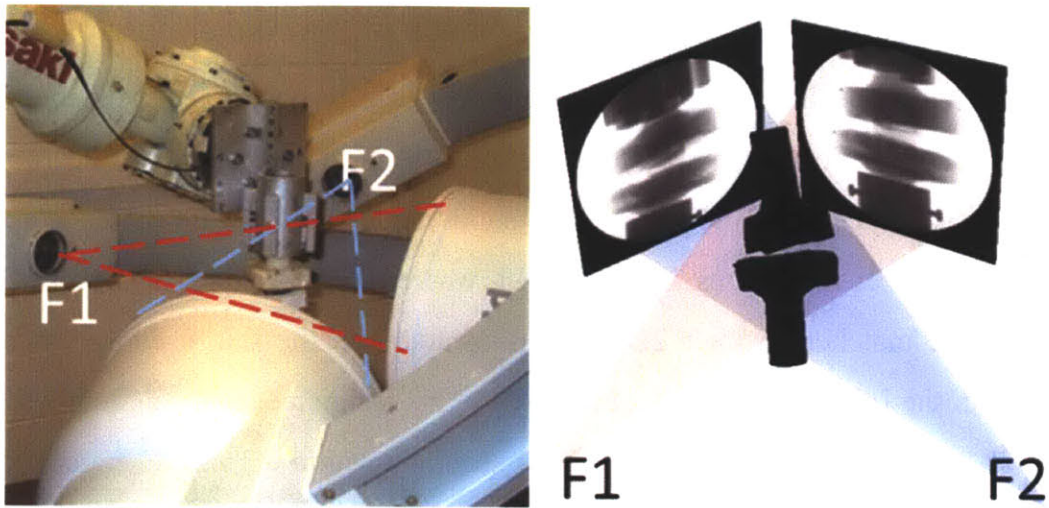


Fig 11-3. Reproduction of the positions of the vertebrae using an established image matching protocol.

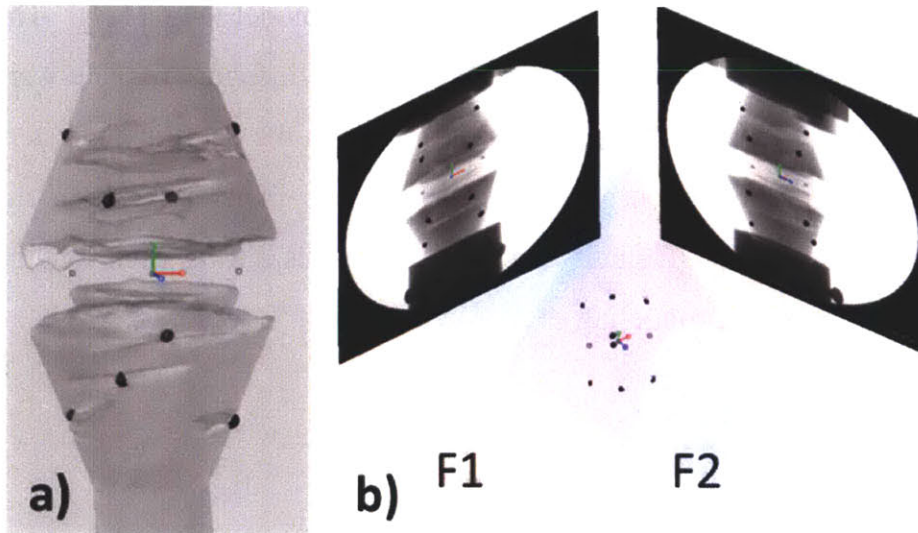


Fig 11-4. Determination of the coordinate system for the IVD center and the principal directions. a) Recording the relative position of the coordinate system and several titanium beads using a digitizer. b) Registering the coordinate system with the FEA model by matching the titanium beads.

#### **11.2.4 Finite element models of the IVDs**

A custom Matlab code was used to create subject geometric-specific FE models with hexahedral elements from the 3D CT models (**Fig 11-5**). In this study, the vertebral bodies were assumed to be rigid, thus only FE models of the IVDs were built. Anatomically, the discs are composed of the annulus fibrosus (AF) and the nucleus pulposus (NP). The AF makes up the outer part of the disc. It consists of a fibrous collagen matrix embedded within an aqueous gel of proteoglycans, water and other proteins [79] and arranged in concentric layers called lamellae (**Fig 11-5**). Within each lamella, the fibers are oriented obliquely about  $30^\circ$  to the horizontal and reversed in each adjacent layer. The NP is the gelatinous internal substance of the disc. From these anatomic features and with simplifications, a common FE modeling strategy was adopted (**Fig 11-5**): each IVD was modeled into three parts: NP, eight layers of AF, and two endplates. Material properties were taken from literature (**Table 11-1**) [9, 24, 35, 53, 80-82]. NP was estimated to occupy 40% volume of the whole disc and modeled as hydraulic fluid[35, 53, 80]. The volumetric center of the NP was chosen as a reference node of the NP fluid and the initial pressure was set as 0. The disc AF was modeled with tension only fibers to represent the matrix constituents that resist tension, namely the collagen fibers, and with AF bulk of hyper elastic bricks to represent the rest of AF. Fibers were located at the outer surface and between each two layers of AF. They were tension only truss element with gradually changing stiffness for each layer[9, 24, 81, 82]. The angles between the fibers and disc endplates were set to be  $30^\circ$  and  $150^\circ$ . Physiological cross sectional area of the fibers was calculated to take up to 16% volume of each AF layer. Inferior and superior endplates were modeled as rigid plates. There were totally about 10,000 elements and 4,000 nodes in each IVD model.

Abaqus Standard/6.10 (Simulia, Providence, RI) was used for FE calculations. For each FE IVD model, the inferior endplate was fixed in all directions and the superior endplate was moved according to the 6DOF kinematics measured by the DFIS during the experiments. Resultant forces and moments were calculated and compared with those measured in the experiment in the same coordinate system for validation.

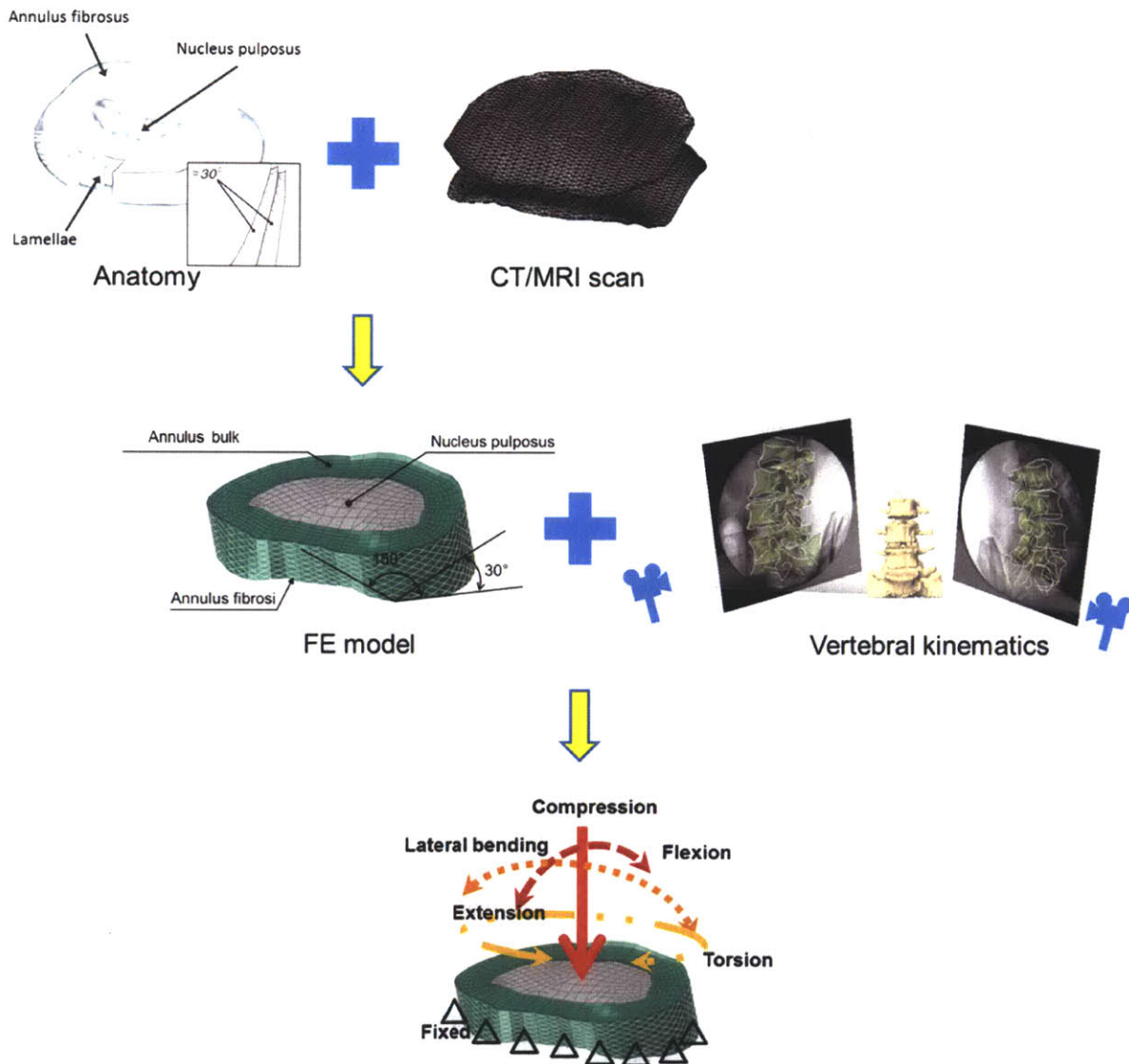


Fig 11-5. FE modeling of IVD and kinematic inputs to calculated disc loads.



Table 11-1: Material properties used in FE models.

	Type of element	Elastic modulus (MPa)	Poisson's ratio
<b>Nucleus pulposus</b> *	Hydraulic fluid element	-	-
<b>Annulus bulk</b> **	Neo-Hookean Hexahedral solid element C10=0.348, D1=0.3	-	-
<b>Annulus fibrosus</b> ***	Tension only	550	0.3
	elastic truss	495	0.3
	element	421.5	0.3
		357.5	0.3
<b>Endplates</b>	Rigid shell element	-	-

\*Rohlmann, et al. 2005, Rohlmann, et al. 2006, Rohlmann, et al. 2009b

\*\*Rohlmann, et al. 2006

\*\*\* Shirazi-Adl, et al. 1984, Goel, et al. 1995, Smit, et al. 1997, Polikeit, et al. 2003

Table 11-2: Errors in estimation of the forces and moments at the end steps of various loading cases.

	L2/3#1	L2/3#2	L4/5	Average
<b>Comp</b>	2.1%	12.4%	4.8%	6.5%
<b>Flex</b>	29.5%	14.4%	0.5%	14.8%
<b>Ext</b>	11.5%	25.9%	1.3%	12.9%
<b>BendL</b>	45.4%	18.1%	31.3%	31.6%
<b>BendR</b>	1.7%	0.8%	20.4%	7.6%
<b>TwistL</b>	38.0%	24.6%	26.8%	29.8%
<b>TWistR</b>	26.9%	12.0%	35.9%	24.9%
<b>Average</b>	22.0%	15.5%	17.3%	

## 11.3 Results

The forces and moments calculated by the subject-specific FE analysis had good agreements with those recorded in the *in vitro* experiments in the whole range. **Fig 11-6 to 8** showed the force-displacement (or moment-rotation) behaviors of the three IVDs under different loading cases. The x axes were the primary translations or rotations (the DOF corresponding to each loading case) of the superior endplates with respect to the inferior endplates, where the rotations were described using Euler angles in the flexion-bending-torsion order. The y axes were the primary forces or moments at the center of the disc. We quantitatively compared: (1) the forces or moments at the end steps of the loading cases, and (2) the overall areas under the force-displacement or moment-rotation curves (which were related to the energy of disc deformation) between FEA and *in vitro* experiment results. The overall average differences were 18% and 19%, respectively.

### 11.3.1 Accuracy in each tested DOF

Under 400N compressive loads, the FE analyses had average differences of 6.5% in estimation of the forces at the end steps, and 9.4% in estimation of the overall areas under the force-displacement curves when compared to the robot measurements (**Table 11-2, 3, Fig 11-6 to 8**). Under 5Nm flexion/extension moments, the FE analyses had average differences of 14.8% and 12.9% in estimation of the moments at the end steps; and 19.1% and 14.2% in estimation of the overall areas under the force-displacement curves for flexion and extension, respectively when compared to the robot measurements (**Table 11-2, 3, Fig 11-6 to 8**). Under 5Nm left/right lateral bending moments, the FE analysis had average differences of 31.6% and 7.6% in estimation of the moments at the end steps; and 33.5% and 15.9% in estimation of the overall areas under the force-displacement

curves for left bending and right bending, respectively when compared to the robot measurements (Table 11-2, 3, Fig 11-6 to 8). Under 5Nm left/right torsion moments, the FE analysis had average differences of 29.8% and 24.9% in estimation of the moments at the end steps; and 23.6% and 20.0% in estimation of the overall areas under the force-displacement curves for left torsion and right torsion, respectively when compared to the robot measurements (Table 11-2, 3, Fig 11-6 to 8).

**11.3.2 Accuracy in the other 5 DOF**

During the experiment, the robot measurements of the forces and moments in the 5 DOF other than the loaded DOF were almost zero due to the experiment setup. The FE analyses yielded good agreements with the experiment results. Forces and moments were consistently less than 50N and 1Nm, respectively, in the 5 DOF other than the tested DOF in each loading case.

Table 11-3. Errors in estimation of the overall area under the force-displacement curves of various loading cases.

	L2/3#1	L2/3#2	L4/5	Average
<b>Comp</b>	7.1%	12.2%	8.8%	9.4%
<b>Flex</b>	19.6%	33.7%	3.8%	19.1%
<b>Ext</b>	7.5%	29.0%	6.1%	14.2%
<b>BendL</b>	30.4%	28.8%	41.4%	33.5%
<b>BendR</b>	10.0%	17.4%	20.3%	15.9%
<b>TwistL</b>	28.7%	22.2%	19.9%	23.6%
<b>TwistR</b>	15.0%	11.2%	33.9%	20.0%
<b>Average</b>	16.7%	22.1%	19.2%	

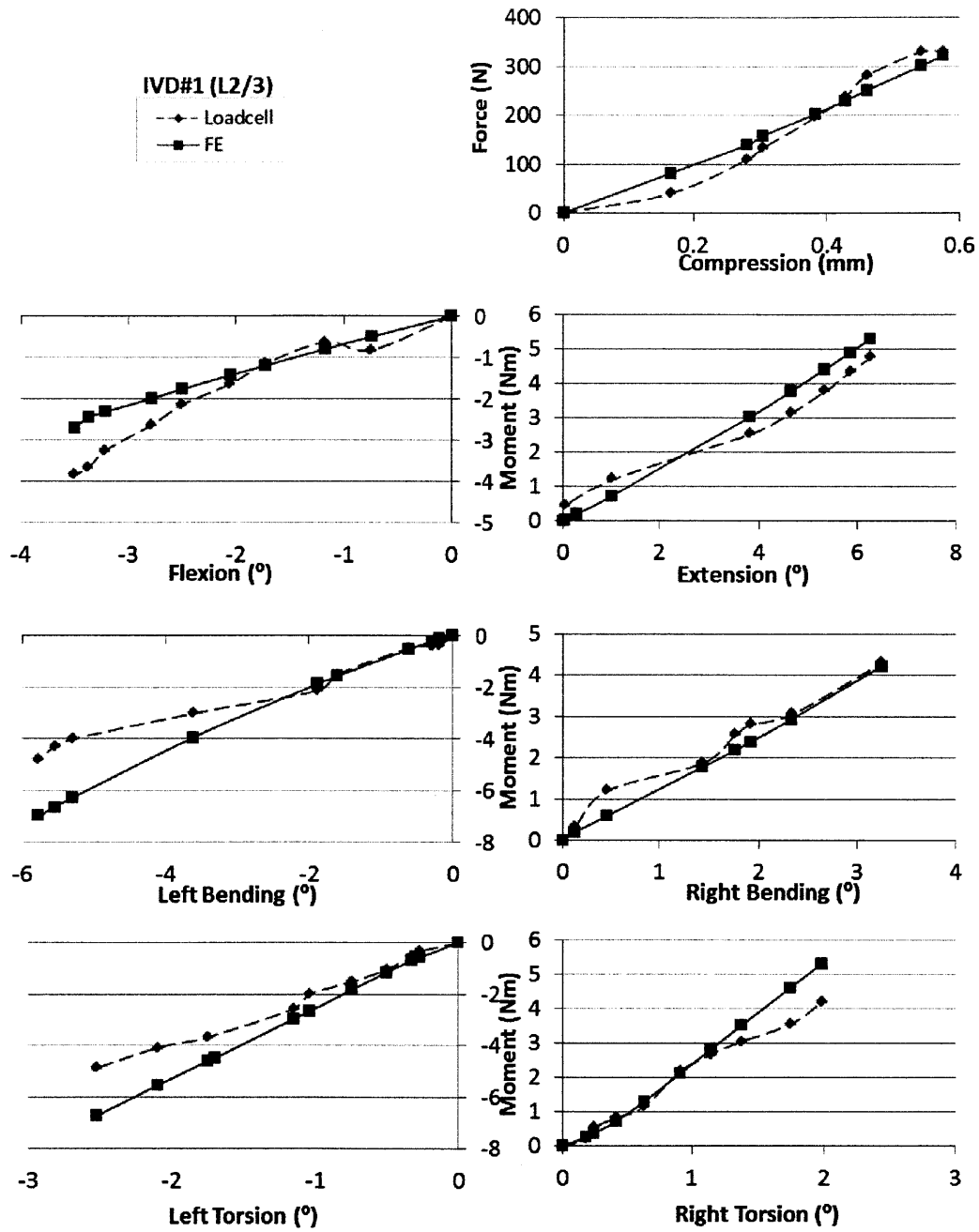


Fig 11-6. Comparison of the force-displacement curves between FEA and experiment measurements under various loading cases for IVD#1.

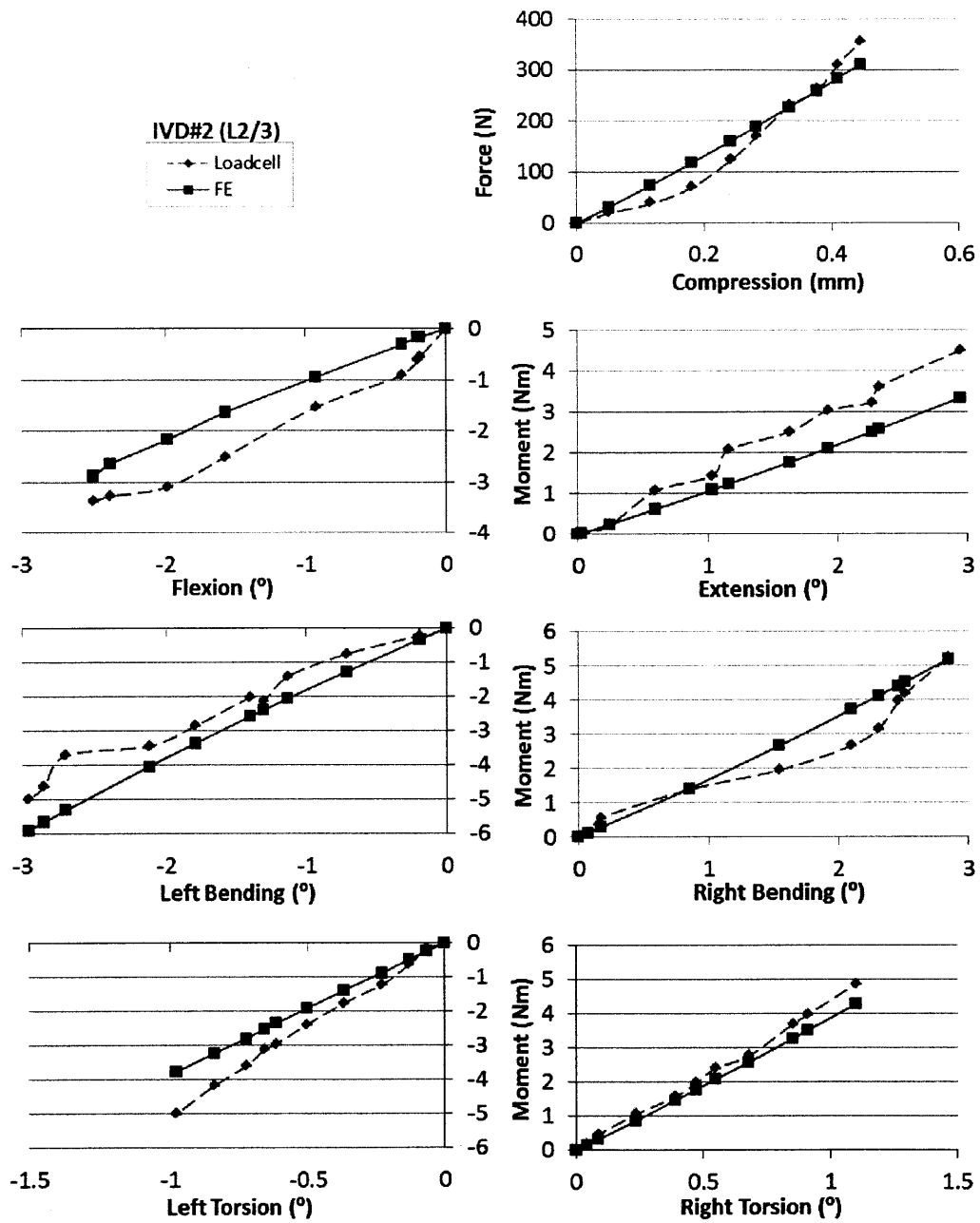


Fig 11-7. Comparison of the force-displacement curves between FEA and experiment measurements under various loading cases for IVD#2.

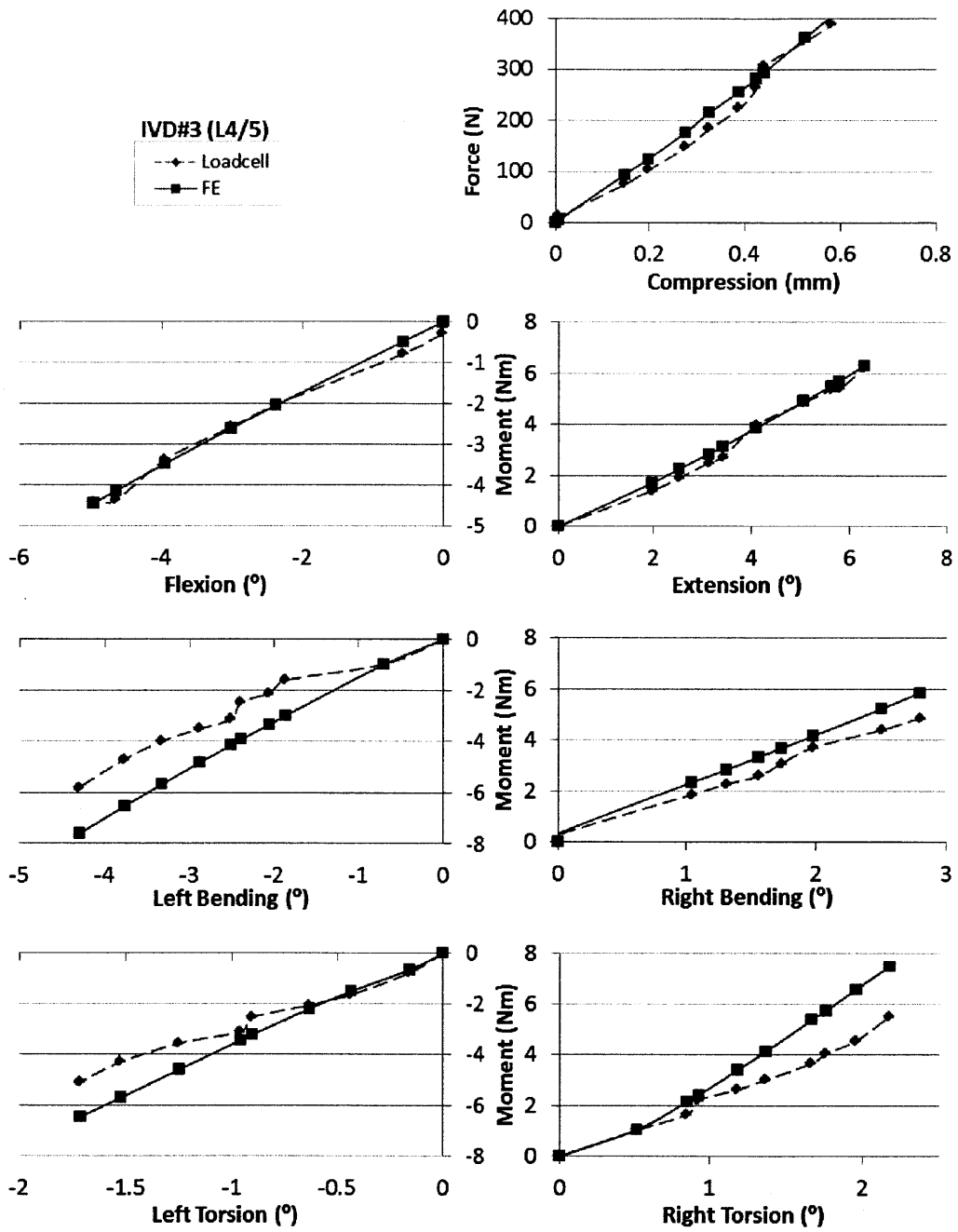


Fig 11-8. Comparison of the force-displacement curves between FEA and experiment measurements under various loading cases for IVD#3.

## 11.4 Discussion

Accurate determination of the loads on the lumbar spine presents a challenge in biomedical engineering. In this Chapter, the forces and moments of the IVDs were validated to be estimated using subject-specific 3D FE IVD models and the kinematics of the same IVD measured during functional activities. The data indicated that the forces and moments in the IVDs could be estimated within an average error of 20% of the actual loads.

In literature, most validations of the FE models were performed by comparing various kinematic responses of the lumbar spine of the FE calculation to those obtained from multiple *in vitro* experiments under controlled external loadings[9-12, 21, 64]. Because of the high variability inherent to experimentation, an FE model is commonly considered valid when its predicted result is within the standard deviation of several experiment results and quantitative results may not be reported. Shirazi-Adl et al.[9] validated an FE model by comparing the model estimations to the *in vitro* experiment results in terms of axial displacement, disc bulge, end-plate bulge and intradiscal pressure under several external loadings. Natarajan et al.[11] validated an FE model by comparing the model estimations to the *in vitro* experiment results in terms of axial displacement and segmental rotations. Goel et al.[64] validated an FE model by comparing the model estimations to the *in vitro* experiment results in terms of the axial displacement, segmental rotations, and intradiscal pressure under external loadings. Rohlmann et al.[21, 35] validated an FE model by comparing the model estimations to the *in vitro* experiment results in terms of axial displacement, segmental rotations, and intradiscal pressure. These FE models have then played important roles to investigate spine biomechanics under various simulated loading conditions[9-16, 70-77].

In this validation study, instead of validating the kinematic responses, the force responses of the FE models were validated by directly comparing those with the *in vitro* experiment results of the same IVDs using kinematics as input boundary conditions. It is not a conventional approach, since the force responses are very sensitive with respect to the kinematic inputs, which cannot be measured accurately enough previously. It is made possible by taking advantage of some recently developed imaging techniques, such as DFIS[69], where all 6DOF translations and rotations can be accurately determined to certain extent. Further technological development in imaging techniques such as better image resolution and contrast can possibly improve the accuracy of the proposed technique.

There are only few previous techniques measured the *in vivo* spinal forces[5-8], mainly because that direct measurements can be invasive and highly risky. Pressure transducers have been used to measure intradiscal pressure during sitting, standing and other daily activities to provide information for physiotherapy, rehabilitation programs and workplace recommendations[5, 6]. Rohlmann et al.[7] used a telemeterized internal spinal fixation device to measure the forces in spinal implants and investigated load sharing after fusion. The combined numerical and experimental technique validated in this paper could provide an alternative way to estimate the *in vivo* spinal forces non-invasively. Similar to this validation study, 3D subject-specific FE vertebral models can be generated from the subject-specific CT/MRI geometric models. *In vivo* vertebral kinematics can be measured using the combined CT/MRI and DFIS technique[69, 70] during experiments when subjects perform different activities. The vertebral kinematics can then be input into the corresponding 3D FE IVD models as boundary conditions to calculate the *in vivo* forces and moments on the IVD.



Although the FE results showed overall good agreement with the experiment measurements in the whole range, a couple relatively high percentage errors were observed, especially during bending left (**Table 11-2, 3**). It is partially because the FE models were stiffer during bending, giving large percentage errors when using experiment measurements as basis, but not necessary large absolute errors. Similarly, in the literature most FE validation studies could not have perfect matches under all loading conditions. Describing the IVD material behavior is a still ongoing task, which has been tried for decades. The properties of the discs underlie a larger variability in literature, as well as intra- and inter-subject variation. In the future, it should be interesting to test more IVDs and run a probabilistic design analysis to find the optimization material properties.

Since the kinematics of the disc endplates were used as input boundary conditions, only IVDs were necessary in the FE models. It greatly simplified the calculation and reduced the time and effort to determine the geometries, characterize the material properties and analyze the force interactions of the different structures of the lumbar spine. It also helps to explain why the force-displacement (or moment-rotation) curves showed less non-linearity in both the experiments and the FE analyses compared to existing literature. In our validation, the force-displacement curves only represented the response of the IVDs without taking the highly non-linear spinal ligaments into account.

As any other finite element analyses, there are a series of factors that may affect the accuracy of the estimations of *in vivo* spinal forces using our FE modeling technique. Certain assumptions and simplifications have been made in our study in the FE modeling and *in vitro* experiments. For instance, the vertebrae were considered as rigid bodies in the FE models. However, the bone compliance may play a role in spine biomechanics as indicated by Shirazi-Adl et al[17] and

Goel et al[19]. We also did not include cartilage endplate and disc bulging in the FE models. Although there was a 30 minutes resting time between any two loading cases during the experiments to minimize residue forces due to the viscoelastic behavior, viscoelastic behavior of the IVDs[14, 35] can still play a role during each loading phase but was not included in the FE modeling. There were hysteresis effects and load-deformation curves were slightly different between loading and unloading. In the current study, the ones during loading were taken for comparison with FEA. In addition, the IVD properties may be subject-specific and segment-specific in the *in vivo* physiological environment which may require further investigation. With all these limitations, the proposed technique was shown to estimate forces and moments on the lumbar IVDs within an average error of 20%.

In conclusion, a validation study of a technique that uses endplates kinematics as inputs in the FE models to estimate the forces and moments in the human lumbar IVDs were performed. The forces and moments could be estimated within an average error of 20%. Therefore, this technique can be a promising tool for non-invasive estimation of the forces and moments of the IVDs during various functional activities of living subjects, which may benefit the numerical and biomechanical community by providing the baseline data, and thus may contribute to help understand injury mechanism of the lumbar spine, prevent low back pain and develop treatment techniques and surgical implants.

## 11.5 References

1. Stokes, I.A. and J.C. Iatridis, *Mechanical conditions that accelerate intervertebral disc degeneration: overload versus immobilization*. Spine (Phila Pa 1976), 2004. **29**(23): p. 2724-32.
2. Mulholland, R.C., *The myth of lumbar instability: the importance of abnormal loading as a cause of low back pain*. Eur Spine J, 2008. **17**(5): p. 619-25.
3. Adams, M.A., et al., *Mechanical initiation of intervertebral disc degeneration*. Spine (Phila Pa 1976), 2000. **25**(13): p. 1625-36.
4. Pope, M.H., *Biomechanics of the lumbar spine*. Ann Med, 1989. **21**(5): p. 347-51.
5. Nachemson, A.L., *Disc pressure measurements*. Spine (Phila Pa 1976), 1981. **6**(1): p. 93-7.
6. Wilke, H.J., et al., *New in vivo measurements of pressures in the intervertebral disc in daily life*. Spine (Phila Pa 1976), 1999. **24**(8): p. 755-62.
7. Rohlmann, A., et al., *2000 Volvo Award winner in biomechanical studies: Monitoring in vivo implant loads with a telemeterized internal spinal fixation device*. Spine (Phila Pa 1976), 2000. **25**(23): p. 2981-6.
8. Polga, D.J., et al., *Measurement of in vivo intradiscal pressure in healthy thoracic intervertebral discs*. Spine (Phila Pa 1976), 2004. **29**(12): p. 1320-4.
9. Shirazi-Adl, S.A., S.C. Shrivastava, and A.M. Ahmed, *Stress analysis of the lumbar disc-body unit in compression. A three-dimensional nonlinear finite element study*. Spine (Phila Pa 1976), 1984. **9**(2): p. 120-34.
10. Goel, V.K. and L.G. Gilbertson, *Applications of the finite element method to thoracolumbar spinal research--past, present, and future*. Spine (Phila Pa 1976), 1995. **20**(15): p. 1719-27.
11. Natarajan, R.N. and G.B. Andersson, *The influence of lumbar disc height and cross-sectional area on the mechanical response of the disc to physiologic loading*. Spine (Phila Pa 1976), 1999. **24**(18): p. 1873-81.
12. Schmidt, H., et al., *Application of a calibration method provides more realistic results for a finite element model of a lumbar spinal segment*. Clin Biomech (Bristol, Avon), 2007. **22**(4): p. 377-84.
13. Gilbertson, L.G., et al., *Finite element methods in spine biomechanics research*. Crit Rev Biomed Eng, 1995. **23**(5-6): p. 411-73.
14. Natarajan, R.N., J.R. Williams, and G.B. Andersson, *Modeling changes in intervertebral disc mechanics with degeneration*. J Bone Joint Surg Am, 2006. **88** Suppl 2: p. 36-40.

15. Zander, T., A. Rohlmann, and G. Bergmann, *Influence of different artificial disc kinematics on spine biomechanics*. Clin Biomech (Bristol, Avon), 2009. **24**(2): p. 135-42.
16. Schmidt, H., et al., *Response analysis of the lumbar spine during regular daily activities--a finite element analysis*. J Biomech, 2010. **43**(10): p. 1849-56.
17. Shirazi-Adl, A., *Analysis of role of bone compliance on mechanics of a lumbar motion segment*. J Biomech Eng, 1994. **116**(4): p. 408-12.
18. Shirazi-Adl, A., *Nonlinear stress analysis of the whole lumbar spine in torsion--mechanics of facet articulation*. J Biomech, 1994. **27**(3): p. 289-99.
19. Goel, V.K., et al., *Cancellous bone Young's modulus variation within the vertebral body of a ligamentous lumbar spine--application of bone adaptive remodeling concepts*. J Biomech Eng, 1995. **117**(3): p. 266-71.
20. Kiefer, A., A. Shirazi-Adl, and M. Parnianpour, *Stability of the human spine in neutral postures*. Eur Spine J, 1997. **6**(1): p. 45-53.
21. Zander, T., et al., *Estimation of muscle forces in the lumbar spine during upper-body inclination*. Clin Biomech (Bristol, Avon), 2001. **16 Suppl 1**: p. S73-80.
22. Schmidt, H., F. Heuer, and H.J. Wilke, *Interaction between finite helical axes and facet joint forces under combined loading*. Spine (Phila Pa 1976), 2008. **33**(25): p. 2741-8.
23. Natarajan, R.N., et al., *Biomechanical response of a lumbar intervertebral disc to manual lifting activities: a poroelastic finite element model study*. Spine (Phila Pa 1976), 2008. **33**(18): p. 1958-65.
24. Goel, V.K., et al., *Interlaminar shear stresses and laminae separation in a disc. Finite element analysis of the L3-L4 motion segment subjected to axial compressive loads*. Spine (Phila Pa 1976), 1995. **20**(6): p. 689-98.
25. Rohlmann, A., T. Zander, and G. Bergmann, *Spinal loads after osteoporotic vertebral fractures treated by vertebroplasty or kyphoplasty*. Eur Spine J, 2006. **15**(8): p. 1255-64.
26. Natarajan, R.N., et al., *Effects of slip severity and loading directions on the stability of isthmic spondylolisthesis: a finite element model study*. Spine (Phila Pa 1976), 2003. **28**(11): p. 1103-12.
27. Sairyo, K., et al., *Biomechanical rationale of endoscopic decompression for lumbar spondylolysis as an effective minimally invasive procedure - a study based on the finite element analysis*. Minim Invasive Neurosurg, 2005. **48**(2): p. 119-22.
28. Zander, T., A. Rohlmann, and G. Bergmann, *Analysis of simulated single ligament transection on the mechanical behaviour of a lumbar functional*

- spinal unit*. Biomed Tech (Berl), 2004. **49**(1-2): p. 27-32.
29. Natarajan, R.N., et al., *Effect of annular incision type on the change in biomechanical properties in a herniated lumbar intervertebral disc*. J Biomech Eng, 2002. **124**(2): p. 229-36.
  30. Goel, V.K., Y.E. Kim, and T.H. Lim, *Possible role of stresses in inducing spinal stenosis--a long term complication following disk excision*. J Biomech Eng, 1990. **112**(4): p. 478-81.
  31. Kong, W.Z., et al., *Effects of muscle dysfunction on lumbar spine mechanics. A finite element study based on a two motion segments model*. Spine (Phila Pa 1976), 1996. **21**(19): p. 2197-206; discussion 2206-7.
  32. Kim, Y.E., et al., *Effect of disc degeneration at one level on the adjacent level in axial mode*. Spine (Phila Pa 1976), 1991. **16**(3): p. 331-5.
  33. Natarajan, R.N., J.H. Ke, and G.B. Andersson, *A model to study the disc degeneration process*. Spine (Phila Pa 1976), 1994. **19**(3): p. 259-65.
  34. Natarajan, R.N., J.R. Williams, and G.B. Andersson, *Recent advances in analytical modeling of lumbar disc degeneration*. Spine (Phila Pa 1976), 2004. **29**(23): p. 2733-41.
  35. Rohlmann, A., et al., *Analysis of the influence of disc degeneration on the mechanical behaviour of a lumbar motion segment using the finite element method*. J Biomech, 2006. **39**(13): p. 2484-90.
  36. Schmidt, H., et al., *The risk of disc prolapses with complex loading in different degrees of disc degeneration - a finite element analysis*. Clin Biomech (Bristol, Avon), 2007. **22**(9): p. 988-98.
  37. Schmidt, H., F. Heuer, and H.J. Wilke, *Dependency of disc degeneration on shear and tensile strains between annular fiber layers for complex loads*. Med Eng Phys, 2009. **31**(6): p. 642-9.
  38. Ruberte, L.M., R.N. Natarajan, and G.B. Andersson, *Influence of single-level lumbar degenerative disc disease on the behavior of the adjacent segments--a finite element model study*. J Biomech, 2009. **42**(3): p. 341-8.
  39. Galbusera, F., et al., *The mechanical response of the lumbar spine to different combinations of disc degenerative changes investigated using randomized poroelastic finite element models*. Eur Spine J, 2011. **20**(4): p. 563-71.
  40. Natarajan, R.N., et al., *Study on effect of graded facetectomy on change in lumbar motion segment torsional flexibility using three-dimensional continuum contact representation for facet joints*. J Biomech Eng, 1999. **121**(2): p. 215-21.
  41. Zander, T., et al., *Influence of graded facetectomy and laminectomy on spinal biomechanics*. Eur Spine J, 2003. **12**(4): p. 427-34.
  42. Ivanov, A.A., et al., *The effect of removing the lateral part of the pars*

- interarticularis on stress distribution at the neural arch in lumbar foraminal microdecompression at L3-L4 and L4-L5: anatomic and finite element investigations.* Spine (Phila Pa 1976), 2007. **32**(22): p. 2462-6.
43. Goel, V.K. and M.H. Pope, *Biomechanics of fusion and stabilization.* Spine (Phila Pa 1976), 1995. **20**(24 Suppl): p. 85S-99S.
  44. Lim, T.H., et al., *Biomechanics of transfixation in pedicle screw instrumentation.* Spine (Phila Pa 1976), 1996. **21**(19): p. 2224-9.
  45. Rohlmann, A., et al., *Internal spinal fixator stiffness has only a minor influence on stresses in the adjacent discs.* Spine (Phila Pa 1976), 1999. **24**(12): p. 1192-5; discussion 1195-6.
  46. Zander, T., et al., *Comparison of the mechanical behavior of the lumbar spine following mono- and bisegmental stabilization.* Clin Biomech (Bristol, Avon), 2002. **17**(6): p. 439-45.
  47. Zander, T., et al., *Effect of bone graft characteristics on the mechanical behavior of the lumbar spine.* J Biomech, 2002. **35**(4): p. 491-7.
  48. Rohlmann, A., T. Zander, and G. Bergmann, *Comparison of the biomechanical effects of posterior and anterior spine-stabilizing implants.* Eur Spine J, 2005. **14**(5): p. 445-53.
  49. Bono, C.M., et al., *Residual sagittal motion after lumbar fusion: a finite element analysis with implications on radiographic flexion-extension criteria.* Spine (Phila Pa 1976), 2007. **32**(4): p. 417-22.
  50. Rohlmann, A., et al., *A probabilistic finite element analysis of the stresses in the augmented vertebral body after vertebroplasty.* Eur Spine J, 2010. **19**(9): p. 1585-95.
  51. Dooris, A.P., et al., *Load-sharing between anterior and posterior elements in a lumbar motion segment implanted with an artificial disc.* Spine (Phila Pa 1976), 2001. **26**(6): p. E122-9.
  52. Goel, V.K., et al., *Effects of charite artificial disc on the implanted and adjacent spinal segments mechanics using a hybrid testing protocol.* Spine (Phila Pa 1976), 2005. **30**(24): p. 2755-64.
  53. Rohlmann, A., T. Zander, and G. Bergmann, *Effect of total disc replacement with ProDisc on intersegmental rotation of the lumbar spine.* Spine (Phila Pa 1976), 2005. **30**(7): p. 738-43.
  54. Rohlmann, A., et al., *Effect of an artificial disc on lumbar spine biomechanics: a probabilistic finite element study.* Eur Spine J, 2009. **18**(1): p. 89-97.
  55. Schmidt, H., et al., *The effect of different design concepts in lumbar total disc arthroplasty on the range of motion, facet joint forces and instantaneous center of rotation of a L4-5 segment.* Eur Spine J, 2009. **18**(11): p. 1695-1705.

56. Schmidt, H., et al., *Effect of multilevel lumbar disc arthroplasty on spine kinematics and facet joint loads in flexion and extension: a finite element analysis*. Eur Spine J, 2010.
57. Vadapalli, S., et al., *Biomechanical rationale for using polyetheretherketone (PEEK) spacers for lumbar interbody fusion-A finite element study*. Spine (Phila Pa 1976), 2006. **31**(26): p. E992-8.
58. Zander, T., et al., *Effect of a posterior dynamic implant adjacent to a rigid spinal fixator*. Clin Biomech (Bristol, Avon), 2006. **21**(8): p. 767-74.
59. Wilke, H.J., F. Heuer, and H. Schmidt, *Prospective design delineation and subsequent in vitro evaluation of a new posterior dynamic stabilization system*. Spine (Phila Pa 1976), 2009. **34**(3): p. 255-61.
60. Shirazi-Adl, A., et al., *Spinal muscle forces, internal loads and stability in standing under various postures and loads--application of kinematics-based algorithm*. Eur Spine J, 2005. **14**(4): p. 381-92.
61. Adams, M.A., *Mechanical testing of the spine. An appraisal of methodology, results, and conclusions*. Spine (Phila Pa 1976), 1995. **20**(19): p. 2151-6.
62. Dreischarf, M., et al., *A non-optimized follower load path may cause considerable intervertebral rotations*. J Biomech, 2010. **43**(13): p. 2625-8.
63. Wilke, H.J., et al., *Is it possible to simulate physiologic loading conditions by applying pure moments? A comparison of in vivo and in vitro load components in an internal fixator*. Spine (Phila Pa 1976), 2001. **26**(6): p. 636-42.
64. Goel, V.K., et al., *A combined finite element and optimization investigation of lumbar spine mechanics with and without muscles*. Spine (Phila Pa 1976), 1993. **18**(11): p. 1531-41.
65. Renner, S.M., et al., *Novel model to analyze the effect of a large compressive follower pre-load on range of motions in a lumbar spine*. J Biomech, 2007. **40**(6): p. 1326-32.
66. Arjmand, N., et al., *Predictive equations to estimate spinal loads in symmetric lifting tasks*. J Biomech, 2011. **44**(1): p. 84-91.
67. Rohlmann, A., et al., *Realistic loading conditions for upper body bending*. J Biomech, 2009. **42**(7): p. 884-90.
68. Rohlmann, A., et al., *Influence of a follower load on intradiscal pressure and intersegmental rotation of the lumbar spine*. Spine (Phila Pa 1976), 2001. **26**(24): p. E557-61.
69. Wang, S., et al., *Measurement of vertebral kinematics using noninvasive image matching method-validation and application*. Spine (Phila Pa 1976), 2008. **33**(11): p. E355-61.

70. Li, G., et al., *Segmental in vivo vertebral motion during functional human lumbar spine activities*. Eur Spine J, 2009. **18**(7): p. 1013-21.
71. Wang, S., et al., *Measurement of geometric deformation of lumbar intervertebral discs under in vivo weight-bearing condition*. J Biomech, 2009. **42**(6): p. 705-11.
72. Kozanek, M., et al., *Range of motion and orientation of the lumbar facet joints in vivo*. Spine (Phila Pa 1976), 2009. **34**(19): p. E689-96.
73. Xia, Q., et al., *In vivo range of motion of the lumbar spinous processes*. Eur Spine J, 2009. **18**(9): p. 1355-62.
74. Xia, Q., et al., *In vivo motion characteristics of lumbar vertebrae in sagittal and transverse planes*. J Biomech, 2010. **43**(10): p. 1905-9.
75. Passias, P.G., et al., *Segmental lumbar rotation in patients with discogenic low back pain during functional weight-bearing activities*. J Bone Joint Surg Am, 2011. **93**(1): p. 29-37.
76. Wang, S., et al., *How does lumbar degenerative disc disease affect the disc deformation at the cephalic levels in vivo?* Spine (Phila Pa 1976), 2011. **36**(9): p. E574-81.
77. Li, W., et al., *Lumbar Facet Joint Motion in Patients with Degenerative Disc Disease at Affected and Adjacent Levels: An In vivo Biomechanical Study*. Spine (Phila Pa 1976), 2011. **36**(10): p. E629-E637.
78. Li, G., et al., *Biomechanical consequences of PCL deficiency in the knee under simulated muscle loads--an in vitro experimental study*. J Orthop Res, 2002. **20**(4): p. 887-92.
79. Iatridis, J.C., et al., *Degeneration affects the anisotropic and nonlinear behaviors of human annulus fibrosus in compression*. J Biomech, 1998. **31**(6): p. 535-44.
80. Rohlmann, A., et al., *Applying a follower load delivers realistic results for simulating standing*. J Biomech, 2009. **42**(10): p. 1520-6.
81. Polikeit, A., et al., *Factors influencing stresses in the lumbar spine after the insertion of intervertebral cages: finite element analysis*. Eur Spine J, 2003. **12**(4): p. 413-20.
82. Smit, T.H., A. Odgaard, and E. Schneider, *Structure and function of vertebral trabecular bone*. Spine (Phila Pa 1976), 1997. **22**(24): p. 2823-33.



# Chapter 12

## ***In vivo* disc loads – a preliminary investigation**

### **12.1 Introduction**

The lumbar spine undergoes internal deformations when performs the daily activities and is responsible for carrying the loads of the upper body. These deformations are primarily happened at the IVDs, which also sustain the majority of the loads. As a result, IVDs form the most important and unique joint in the lumbar spine and are closely related to most spinal pathologies and injuries. The most common reason for occupational low back pain is the overload on the spine [1]. The IVD is a fibroelastic, composite structure with two important functions. First, the IVD acts as a shock absorber, taking up much of the compressive weight of the trunk and upper extremities and distributing it between the vertebral bodies. The loads on a lumbar disc are usually much greater than the total body weight, and have been estimated to exceed three times the weight of the trunk while in the sitting position [2]. Certain dynamic activities such as weight lifting can drive the loads on the disc to an even higher level than in the static sitting position. Second, the IVD acts as a pivot point in the motion segment. It functions as a contained, deformable ball bearing to allow for motion in all degrees of freedom. This means that the disc may experience complex combined forces and moments simultaneously. In addition, due to the anisotropic material properties and irregular shape of a disc, different portion of the disc may undergo totally different

loads (e.g. tension at the anterior but compression at the posterior). It is thus a challenge to understand the biomechanics of the IVDs during functional activities, especially in living human subjects.

Previously, *in vivo* disc loads have only been calculated indirectly by measuring intradiscal pressure. Pressure transducers have been inserted into the disc nucleus in living human volunteers during sitting, standing and other daily activities [3] [1]. Overall disc loads were calculated from the intradiscal pressure and the total effective area of a disc to provide information for physiotherapy, rehabilitation programs and workplace recommendations. Although invaluable information was obtained, the process is invasive and risky and caused pain.

Immediately following the validation study in **Chapter 11**, a pilot study was performed to investigate the *in vivo* disc loads using *in vivo* kinematics data during dynamic weight lifting flexion/extension. A similar kinematic driven FE modeling approach as used in **Chapter 11** was adopted. The objective is to test the applicability of such a technique, compare the results with the existing literature and discuss some findings of the *in vivo* kinematic and kinetic responses of the disc during dynamic weight lifting flexion/extension.

## **12.2 Material and Methods**

Three healthy asymptomatic male subjects ( $48.3 \pm 2.4$  yrs,  $177.0 \pm 4.3$  cm,  $70.6 \pm 7.4$  kg) years old were involved in the study under IRB and written consent. Each subject was also MRI scanned for 3D lumbar spine models. Each subject then performed weight lifting of 15 lbs. dumbbells using two hands, with 8 lbs. in the right hand 7 lbs. in the left hand (**Fig 12-1**). The starting position was approximately  $45^\circ$  flexion of the upper body with respect to the vertical and the

ending position was maximum extension. Duration of the activity is about 2 seconds. The subjects straightened both arms and maintained fixed angle between the arms and trunk with minimum pelvis motion. In other words, there was minimum arm, shoulder and pelvis motion and the activity mainly involves lumbar spine motion. During the activity, dynamic images of the lumbar spine were taken by DFIS at 30 frames per second. Five representative frames were chosen for analysis: maximum flexion (about 45° flexion in this activity), sub flexion, upright, sub extension and maximum extension.



Fig 12-1. Weight lifting flexion-extension activity using 15lb dumbbells. The kinematics of lumbar spine were obtained from image matching.

Each subject was also MRI scanned for 3D lumbar spine models. The kinematics of L1-S1 lumbar vertebral segments during weight lifting were reproduced from 3D to 2D imaging matching technique, detailed in **Chapter 2 (Fig 12-1)**. As a preliminary investigation, only L3-4 discs were studied in this Chapter. Follow the same protocol in **Chapter 11**, a custom Matlab code was used to create subject geometric-specific FE L3-4 disc models with hexahedral elements from the 3D MR scan. A common FE modeling strategy was adopted: each IVD was modeled into three parts: NP, eight layers of AF, and two endplates. The structures and material properties of the disc were detailed in Chapter 13. In addition, two thin layers of cartilaginous endplates with simplified uniform thickness of 0.25 mm and 0.29 mm [4] for the superior and inferior endplate, respectively, were added to the FE model for visualization of the stress-strain distribution at the boundary of the disc and vertebral bodies (**Table 12-1**). The inferior endplate was fixed, and the kinematic data during weight lifting measured from DFIS were applied on the superior endplate as the input boundary conditions. The forces and moments at the center of the IVDs were calculated in Abaqus 6.10/Standard (Simulia, USA) for FE analysis. Non-weight bearing MRI supine position was used as a reference, where forces and moments in the disc were assumed to be zero. The forces were also normalized using body weight (BW).

Table 12-1: Material properties used in FE disc models.

	Type of element	Elastic modulus (MPa)	Poisson's ratio
<b>Nucleus pulposus *</b>	Hydraulic fluid element	-	-
<b>Annulus bulk **</b>	Neo-Hookean Hexahedral solid element C10=0.348, D1=0.3	-	-
<b>Annulus fibrosus ***</b>	Tension only	550	0.3
	elastic truss	495	0.3
	element	421.5	0.3
		357.5	0.3
<b>Endplates**</b>	Neo-Hookean Hexahedral solid element C10=0.348, D1=0.3	-	-

\*Rohlmann, et al. 2005, Rohlmann, et al. 2006, Rohlmann, et al. 2009b

\*\*Rohlmann, et al. 2006

\*\*\* Shirazi-Adl, et al. 1984, Goel, et al. 1995, Smit, et al. 1997, Polikeit, et al.

2003

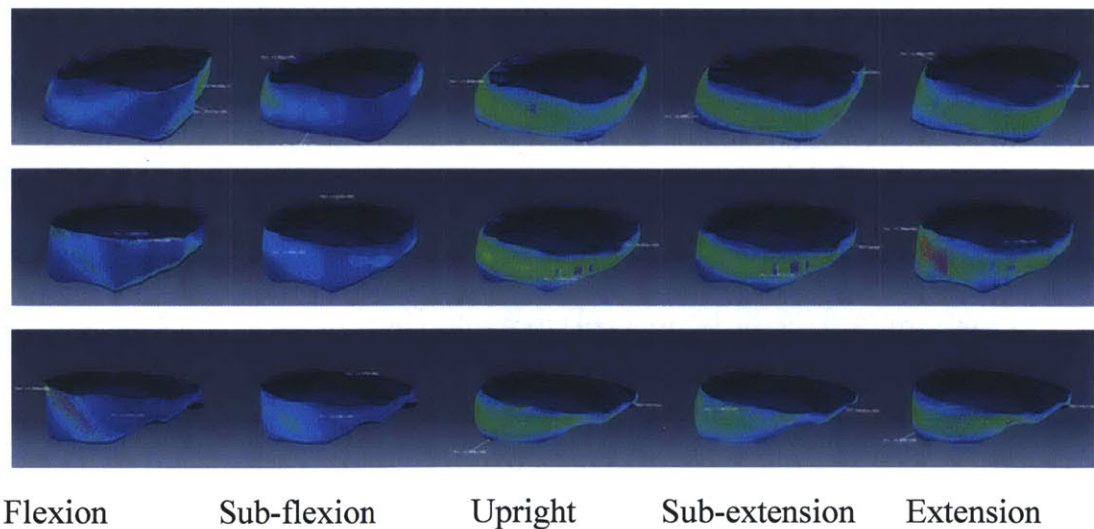


Fig 12-2. Shape of the three discs during flexion-extension.

## 12.3 Results

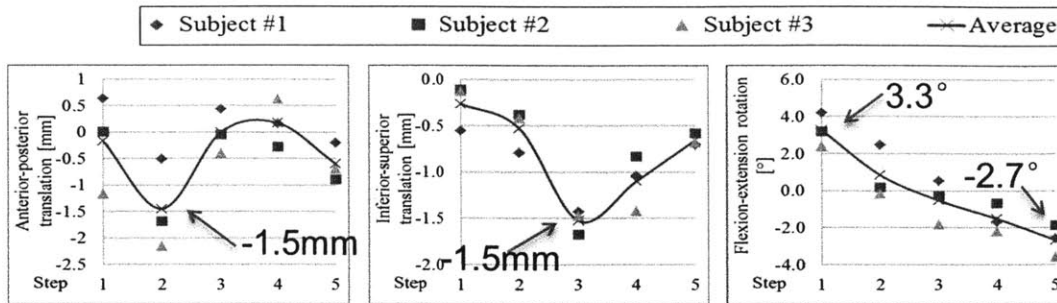
### 12.3.1 Overall disc deformation and loads

In all three subjects, the anterior part of the discs in general underwent compression at flexion to tension at extension. On the contrary, the posterior part underwent tension at flexion to compression at extension (**Fig 12-2**). This behavior agreed with the conventional thought that IVD acts as a pivot point in motion segment and functions as a ball bearing[2].

From flexion to extension, the average rotation of the disc in the sagittal plane was from  $3.3^\circ$  (2.4 to  $4.2^\circ$ ) to  $-2.7^\circ$  (-1.9 to  $-3.6^\circ$ ). Maximum compression of the L3/L4 IVDs was 1.5 (1.4 to 1.7) mm occurred at weight bearing upright position (**Fig 12-3**). Maximum average anterior-posterior shear was 1.4 (0.5 to 2.6) mm occurred at sub flexion.

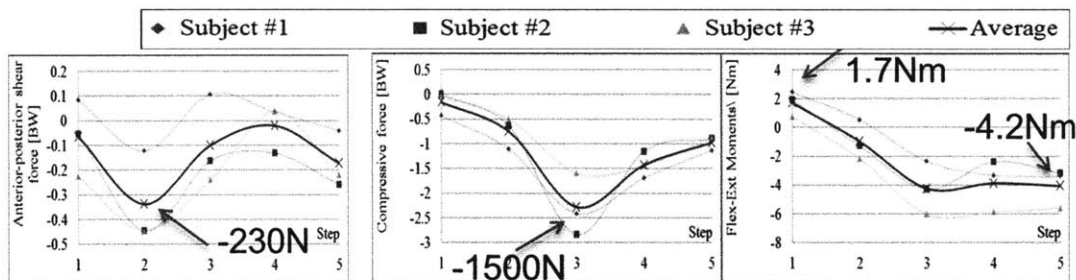
The forces and moments at the center of L3/L4 IVDs showed similar patterns with the kinematics (**Fig 12-3**). Maximum flexion moments were 1.7 (0.8 to 2.4) Nm at maximum flexion. However, extension moments were similar at maximum extension and weight bearing upright position, and were -4.1 (-3.2 to -5.6) Nm and -4.2 (-2.4 to -6.0) Nm, respectively. Maximum average compressive forces on the IVDs were 2.3 (1.6 to 2.8) BW, or -1540 (-1240 to -1700) N at weight bearing upright position. Maximum anterior-posterior shear forces were 0.34 (0.12 to 0.44) BW, or 230 (90 to 350) N at sub-maximum flexion.

### Motion:



(a) anterior(-)-posterior(+) translation, (b) inferior(-)-superior(+) translation, (c) flexion(+)-extension(-) rotation

### Loads:



(a) anterior(-)-posterior(+) force (b) inferior(-)-superior(+) force (c) flexion(+)-extension(-) moment

Fig 12-3. Overall disc deformation and loads at the center of the disc during flexion-extension. x axis from 1 to 5: from flexion to extension, respectively.

### 12.3.2 Intradiscal Pressure

The Intradiscal pressure of disc L3-4 of the three subjects followed similar trend, with average maximum pressure of 1.3 (1.1 to 1.6) MPa at standing upright and weight bearing (Fig 12-4). The average minimum pressure is 0.2 (0.1 to 0.3) MPa, at the starting position which is 45° flexion and weight bearing.

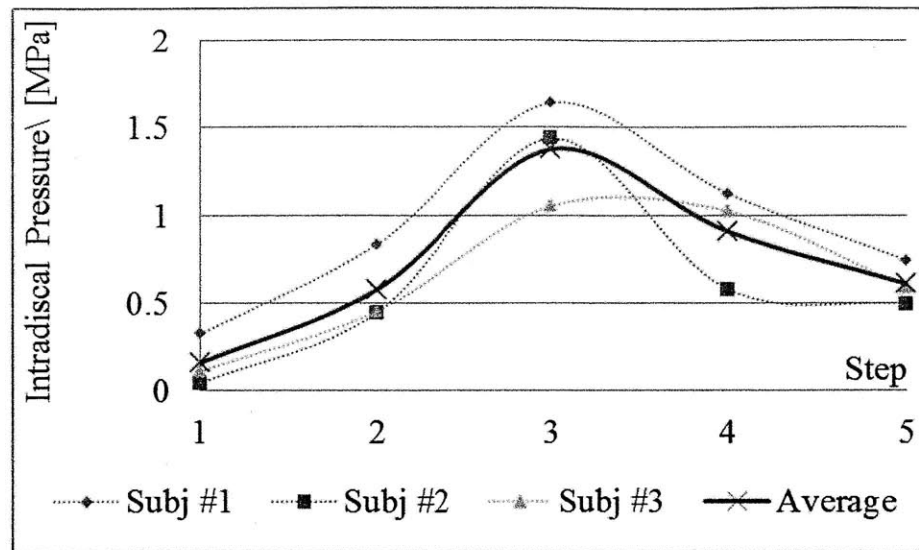


Fig 12-4. Intradiscal pressure during flexion-extension. x axis from 1 to 5: from flexion to extension, respectively.

### 12.3.3 Stress and strain in the AF fibers

The fibers of AF sustained the largest amount of stress among all structures of the disc during the activity. Maximum fiber stress always occurred in the anterolateral (n=8, 28±8 MPa) or posterolateral (n=7, 23±9 MPa) “corner” of the disc in all 3 subjects, during 5 analyzed frames for each subject (Fig 12-5). However, there is no common agreement for all subjects to predict whether maximum fiber stress should be at left /right or at anterior/posterior at a specific frame of flexion-extension. This may be due to the distinct motion pattern of each individual that including slightly left or right swing and twist during flexion extension. Corresponding to the maximum stress, the maximum fiber strain in the three subjects ranged from 2.8% to 7.9% (Table 12-2).



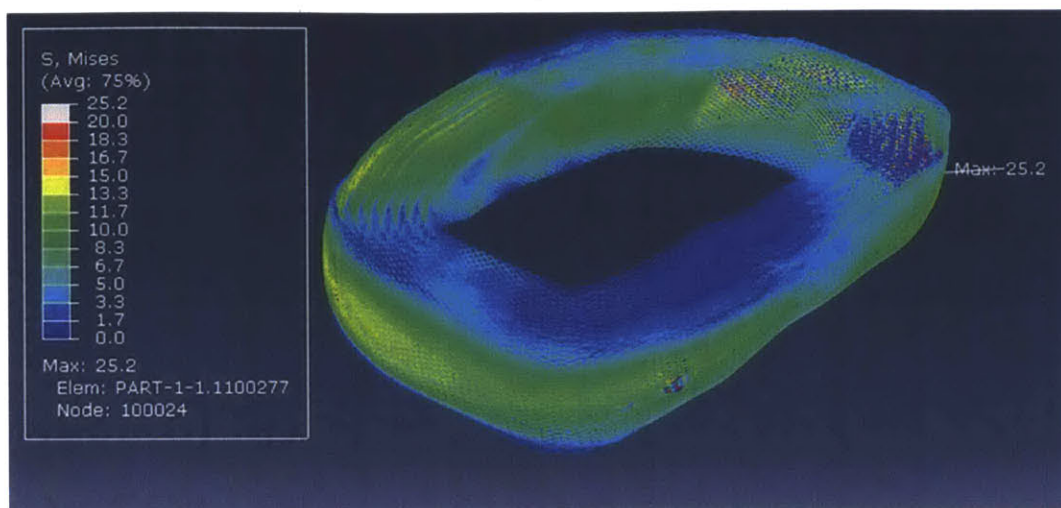


Fig 12-5. An example showing maximum fiber stress found at the posterolateral corner of the disc during upright weight-bearing.

Table 12-2: Maximum fiber strain calculated during dynamic flexion-extension, \*, compared with existing literature: Heuer [5], Schmidt [6], Tencer [7], Stokes [8] and ultimate failure strain [9].

	current study			Literature*				
	Subj 1	Subj 2	Subj 3	Heuer	Schmidt	Tencer	Stocks	Ultimate
<b>Flex</b>	3.3%	2.8%	5.5%	7.2%	7.2%	10%		
<b>sub Flex</b>	3.0%	6.6%	7.9%					
<b>Upright</b>	7.1%	6.2%	6.4%	2.7%	3.3%		3%	12.7%
<b>sub Ext</b>	4.6%	3.4%	7.1%					
<b>Ext</b>	4.0%	4.0%	4.5%	4.0%	5.9%	10%		

### 12.3.4 Stress and strain in the AF bulk

Anatomically, the AF bulk is an aqueous gel of proteoglycans, water and other proteins. It is thus less stiff and share less stress than the fibers in the AF. In two of the three subjects, the maximum stress in the annulus bulk is from 3.2 to 6.5 MPa during the flexion-extension activity. However, in the other subject, the

maximum stress was observed at 20.5 MPa at posterior at extension, which is more than 3 times the maximum value of the other subjects (**Fig 12-6**). Although these three are all healthy asymptomatic subjects, a close look on the MRI and 3D model showed narrowed disc space at posterior which cause high strain thus stress concentration at the posterior. Without considering the subject with narrowed posterior disc space, maximum strain of the annulus bulk were 34% tension at flexion, -35% compression at upright and 35% shear at flexion (**Table 12-3**).

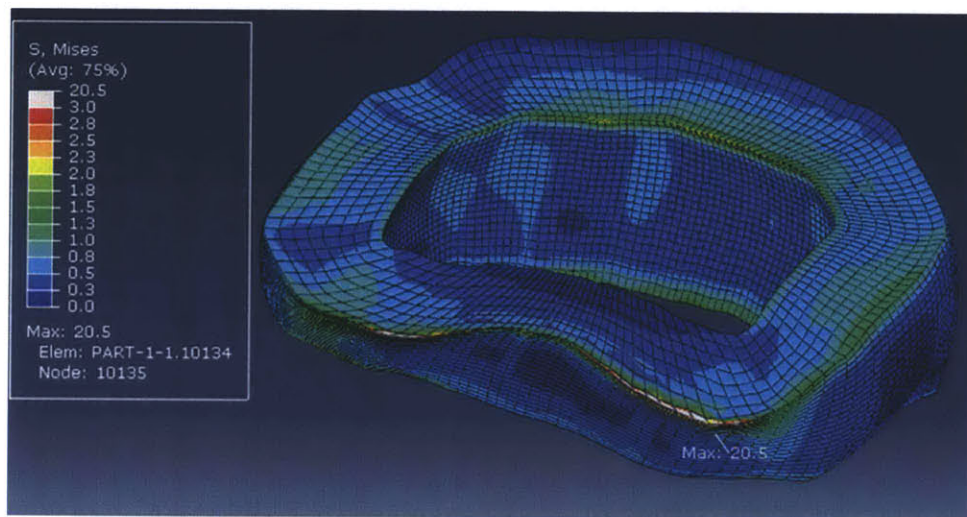


Fig 12-6. Maximum AF bulk strain in a subject with narrowed disc space at posterior.

Table 12-3: Maximum average AF bulk strain calculated during dynamic flexion-extension. \*, compare with existing *in vivo* study in **Chapter 9** [10].

	Current study			<i>In vivo</i> study*		
	Flex	Upright	Ext	Flex	Upright	Ext
<b>Tension</b>	34%	8%	11%	22±13%	19±10%	16±13%
<b>Compression</b>	-18%	-35%	-23%	-15±10%	-16±8%	-14±9%
<b>Shear</b>	35%	27%	32%	29±17%	12±10%	26±10%

## 12.4 Discussion

Most occupational low back pain is related with overload of the spine, and determination of spinal force is critical for preventing low back pain, understanding injury mechanism and developing treatment techniques and surgical implants. The pilot study showed the feasibility and applicability of the FE modeling approach to study disc loads using *in vivo* kinematics as input boundary conditions. Preliminary results of the loads on the L3/L4 IVDs of three healthy asymptomatic subjects during a dynamic weight lifting activity were obtained. There is limited literature on the *in vivo* disc deformation and loads. The preliminary results were reasonable and in range when compared to those of the existing literature. However, the results do not necessarily exactly match the existing literature due to the difference in activities and difference between different *in vivo* and *in vitro* loading conditions.

There is limited existing literature of the disc deformation and loads. In **Chapter 3** of the thesis work, the average overall *in vivo* ranges of motion of disc L3-4 of 10 healthy asymptomatic subjects during flexion-extension were studied. The new data obtained from the three subjects in the pilot study was comparable to the previous study. Regarding the kinematics, the average range of disc flexion-extension in the pilot study is 6° compared to 4.3° ± 3.4° from the previous study (**Table 12-4**). However, compression and AP shear in the current pilot study is larger than the previous study, mainly because that weight lifting activity could increase the loads thus deformation on the discs. Regarding the loads, the pilot study indicated that the IVDs experienced maximum compressive loads of about 2.3 BW (1540 N) at upright position when the moment arm of the lifted weight was the longest. This also caused larger compensatory extension moment of -4.2 Nm. Maximum shear forces were around 230N and were significantly smaller

than the compressive forces. There is no *in vivo* data available on the overall joint forces and moments of the lumbar discs. From kinematics based computational modeling, disc forces and moments were estimated at standing, flexion and extension postures with 200 N loads in hands by Shirazi-Adl, et.al [11] and Kim et.al. [12] The results from the pilot study were comparable with these obtained from kinematic based modeling (**Table 12-4**).

Table 12-4: Maximum average AF bulk strain calculated during dynamic flexion-extension. \*, compare with existing *in vivo* study in **Chapter 9** [10]. \*\*, compare with *in vitro* studies [11, 12].

	<b>current study</b>		<b>literature</b>
<b>kinematics</b>	Compression	1.5 mm	0.6+0.4 mm*
	AP shear	1.4 mm	0.7-1.5 mm*
	Flex-Ext	6°	4.3°+3.4°**
<b>loads</b>	Compressive	1540 N	702-2971 N**
	AP shear	230 N	7-277 N**
	Flex-Ext	6.5 Nm	0.7-24.7 Nm**

Intra-discal pressure has been studied both using pressure transducer *in vivo* and using finite element modeling. Using pressure transducer in 3 healthy volunteers, Wilke et.al [1] has reported intra-discal pressure of 0.1 MPa at lying supine, 0.5 MPa at relaxed standing, 1.1 MPa at standing, bent forward, 1.1 MPa at holding 20 kg, close to body and 1.8 MPa at holding 20kg 60 cm away from the chest. Rohlmann, et.al [13] has reported calculated intra-discal pressure of 0.14 to

1.2 MPa at flexion and 0.22 to 0.52 MPa at extension, using different modeling strategies in the FEA. Comparing to those results, our *in vivo* results agreed well at standing and extension, but were much smaller at flexion. One possible explanation is that the designed weight lifting flexion-extension activity is only 2 seconds. At the instance of picking up the weight, the disc did not immediately respond because of its structure and also all the ligaments, muscles and soft tissues act as springs and dampers. On the other hand, the existing literatures were designed at looking at quasi-static flexion position, with or without weight. In the future, the subject will be asked to bent forward and hold weight for a couple of seconds before start the activity to see if there's graduate increase in the disc deformation, loads and intra-discal pressure.

Although there is no literature on the AF fiber stress for comparison, several *in vitro* or FEA studies have reported maximum fiber strain. Heuer et.al [5] mounted the disc on a robotic testing apparatus and scanned the disc using a laser scanner when external loads of 500 N to simulate compression and  $\pm 7.5$  Nm to simulate flexion and extension were applied (**Table 12-2**). Schmidt et.al [6] reported fiber strain from an FE study with 500N and  $\pm 7.5$  Nm applied the disc. The ultimate AF fiber strain has been determined to be 12.7% in the literature[9]. Maximum fiber strain from the pilot study was within this limit and showed good agreement with the existing literature at extension. However, differences were observed at both flexion and standing upright. At flexion, the maximum fiber strains were 2.8% to 5.5% from the pilot study, smaller than 7.2% to 10% from the literature (**Table 14-2**). This again may due to the non-immediate response of the disc because of its own structure and the damper effect from the surrounding tissues under the *in vivo* activity. At upright standing, the maximum fiber strains were 6.2% to 7.1% from the pilot study, larger than 2.7% to 3% from the

literature. This was mainly due to the different weight bearing situation. In the pilot study, the subjects lift weight and the moment arm of the lifted weight was the longest at standing upright, causing larger disc loads and thus fiber strain.

The *in vivo* data from **Chapter 9** provided the overall deformation of the disc of 10 healthy asymptomatic subjects. Changes in local disc heights were decomposed into vectors perpendicular and parallel to the disc endplate to represent overall tensile and shear deformation. In the pilot study, the local maximum strain of the AF bulk can be determined. Without considering the subject with narrowed posterior disc space, the average local maximum strains were larger than maximum overall strains obtained from **Chapter 9 (Table 12-3)**. However, it should again be noticed that the activity is different, where the pilot study examined weight lifting flexion-extension rather than free flexion-extension. Using *in vitro* study of MRI lumbar disc images, O'Connell et.al [14] calculated disc strains under 1000 N to simulate compression and  $\pm 5^\circ$  to simulate flexion and extension. Despite some similarity in strain patterns, the pilot study found larger maximum strains up to 35% compare to up to 20% from their study (**Fig 12-7**). The difference could be explained by the difference between *in vivo* and *in vitro* experimental setup as well as different loading conditions.

For the subject with narrowed posterior disc space, some interesting findings were observed. There is no difference in the overall deformation and loads on the discs, intra-discal pressure and maximum fiber strains of this subject compare with those of the other two. However, maximum stress and strain in the rest of AF bulk were much larger, up to three times than those of the other two. In clinic, narrowing of the posterior disc space is one of the major criteria for grading disc degeneration and was suggested as a major potential risk for disc herniation. The above information may indicate that disc degeneration and/or disc herniation

could possibly initiate with the breakdown not of the AF fibers, but the rest part of the AF, and then progressively and adversely affect the whole disc. However, before drawing the conclusion, more cases of healthy asymptomatic subjects with narrowed posterior disc spaces should be studied in the future.

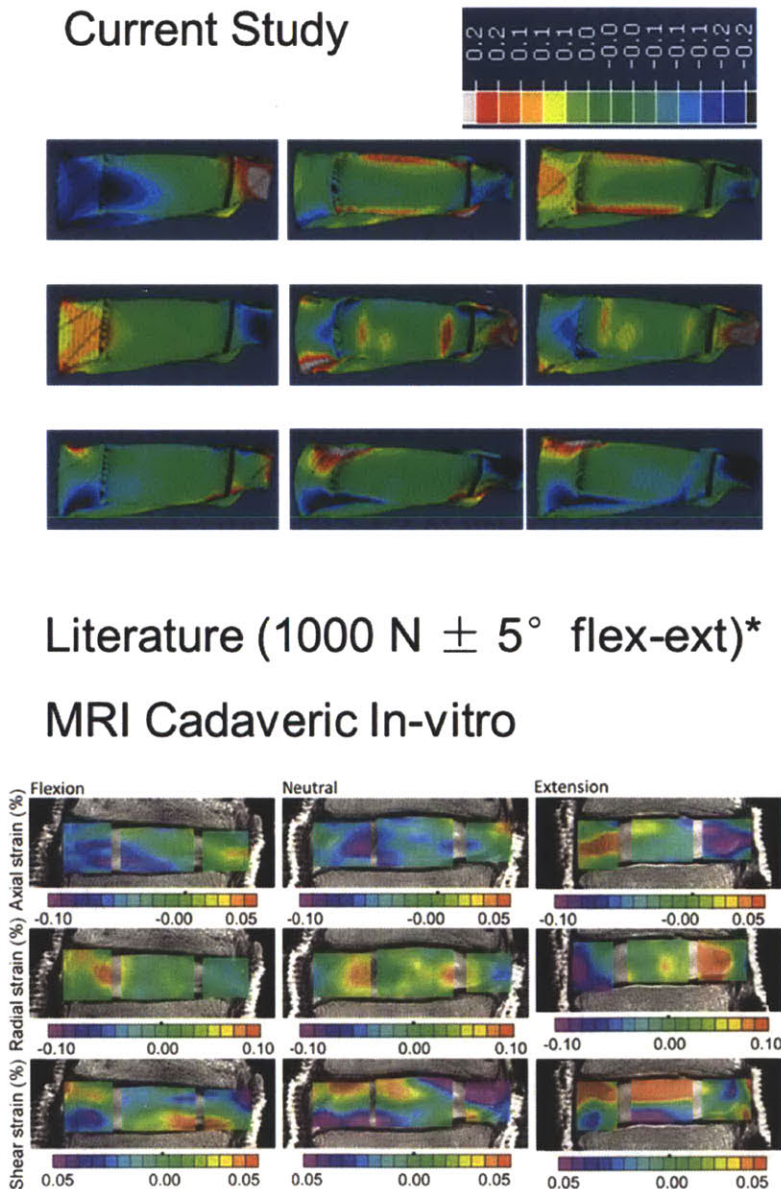


Fig 12-7. Despite some similarity in strain patterns, our study showed larger AF bulk strains than an *in vitro* MRI study from literature.

There are several limitations which can improve the FE modeling technique in the future. The bulging of the disc can be determined from subject specific MRI and included in the FE disc models. For more sophisticated and time consuming activities, viscoelastic behavior of the IVDs [15, 16] can play an important role and can be included in the FE modeling. In addition, the IVD properties may be subject-specific and segment-specific in the *in vivo* physiological environment which may require further investigation. It is also important to investigate IVDs with degenerative changes, as many studies have been performed in literature [15-23], to study the *in vivo* disc loads in patients using a similar procedure.

In conclusion, there is limited literature on the *in vivo* disc deformation and loads due to the complex lumbar spine anatomy, risk in measurements and limitation in technology. The results from the *in vivo* kinematic driven FEA were reasonable and in range when compared to those of the existing literature. However, the results does not necessary exactly match the existing literature due to the difference in activities and difference between different *in vivo* and *in vitro* loading conditions. This is expected and suggested that the disc loads are sensitive and change gradually with different loading conditions. Correspondingly, a sensitive yet reliable method is really needed to study the *in vivo* disc loads. The results from the pilot study showed that FEA using *in vivo* kinematics of the disc could be a promising tool. Upon validation, similar approach can be used to determine stress-strain in the other structures of the lumbar spine, such the facet joints. In the future, inclusion of disc bulging and viscoelastic behavior of the IVD, as well as investigation on the subject specific and pathological disc material properties can be considered.



## 12.5 References

1. Wilke, H.J., et al., *New in vivo measurements of pressures in the intervertebral disc in daily life*. Spine (Phila Pa 1976), 1999. **24**(8): p. 755-62.
2. White, A.A. and M.M. Panjabi, *Clinical biomechanics of the spine*. 2nd ed. 1990, Philadelphia: Lippincott. xxiii, 722 p.
3. Nachemson, A.L., *Disc pressure measurements*. Spine (Phila Pa 1976), 1981. **6**(1): p. 93-7.
4. Silva, M.J., et al., *Direct and computed tomography thickness measurements of the human, lumbar vertebral shell and endplate*. Bone, 1994. **15**(4): p. 409-14.
5. Heuer, F., H. Schmidt, and H.J. Wilke, *The relation between intervertebral disc bulging and annular fiber associated strains for simple and complex loading*. J Biomech, 2008. **41**(5): p. 1086-94.
6. Schmidt, H., et al., *Intradiscal pressure, shear strain, and fiber strain in the intervertebral disc under combined loading*. Spine (Phila Pa 1976), 2007. **32**(7): p. 748-55.
7. Tencer, A.F. and T.G. Mayer, *Soft tissue strain and facet face interaction in the lumbar intervertebral joint--Part II: Calculated results and comparison with experimental data*. J Biomech Eng, 1983. **105**(3): p. 210-5.
8. Stokes, I. and D.M. Greenapple, *Measurement of surface deformation of soft tissue*. J Biomech, 1985. **18**(1): p. 1-7.
9. Skaggs, D.L., et al., *Regional variation in tensile properties and biochemical composition of the human lumbar anulus fibrosus*. Spine (Phila Pa 1976), 1994. **19**(12): p. 1310-9.
10. Wang, S., et al., *How does lumbar degenerative disc disease affect the disc deformation at the cephalic levels in vivo?* Spine (Phila Pa 1976), 2011. **36**(9): p. E574-81.
11. Shirazi-Adl, A., et al., *Spinal muscle forces, internal loads and stability in standing under various postures and loads--application of kinematics-based algorithm*. Eur Spine J, 2005. **14**(4): p. 381-92.
12. Kim, K., Y.H. Kim, and S. Lee, *Investigation of optimal follower load path generated by trunk muscle coordination*. J Biomech, 2011. **44**(8): p. 1614-7.
13. Rohlmann, A., et al., *Realistic loading conditions for upper body bending*. J Biomech, 2009. **42**(7): p. 884-90.
14. O'Connell, G.D., E.J. Vresilovic, and D.M. Elliott, *Human intervertebral disc internal strain in compression: the effect of disc region, loading*

- position, and degeneration.* J Orthop Res, 2011. **29**(4): p. 547-55.
15. Rohlmann, A., et al., *Analysis of the influence of disc degeneration on the mechanical behaviour of a lumbar motion segment using the finite element method.* J Biomech, 2006. **39**(13): p. 2484-90.
  16. Natarajan, R.N., J.R. Williams, and G.B. Andersson, *Modeling changes in intervertebral disc mechanics with degeneration.* J Bone Joint Surg Am, 2006. **88 Suppl 2**: p. 36-40.
  17. Kim, Y.E., et al., *Effect of disc degeneration at one level on the adjacent level in axial mode.* Spine (Phila Pa 1976), 1991. **16**(3): p. 331-5.
  18. Natarajan, R.N., J.H. Ke, and G.B. Andersson, *A model to study the disc degeneration process.* Spine (Phila Pa 1976), 1994. **19**(3): p. 259-65.
  19. Natarajan, R.N., J.R. Williams, and G.B. Andersson, *Recent advances in analytical modeling of lumbar disc degeneration.* Spine (Phila Pa 1976), 2004. **29**(23): p. 2733-41.
  20. Schmidt, H., et al., *The risk of disc prolapses with complex loading in different degrees of disc degeneration - a finite element analysis.* Clin Biomech (Bristol, Avon), 2007. **22**(9): p. 988-98.
  21. Schmidt, H., F. Heuer, and H.J. Wilke, *Dependency of disc degeneration on shear and tensile strains between annular fiber layers for complex loads.* Med Eng Phys, 2009. **31**(6): p. 642-9.
  22. Ruberte, L.M., R.N. Natarajan, and G.B. Andersson, *Influence of single-level lumbar degenerative disc disease on the behavior of the adjacent segments--a finite element model study.* J Biomech, 2009. **42**(3): p. 341-8.
  23. Galbusera, F., et al., *The mechanical response of the lumbar spine to different combinations of disc degenerative changes investigated using randomized poroelastic finite element models.* Eur Spine J, 2011. **20**(4): p. 563-71.

# Chapter 13

## Conclusions

### 13.1 Prologue

This Chapter concludes my PhD work over the past 5 years. At the very end, I would like to begin with clearing up two common questions.

When I talked to people and mentioned I was studying lumbar spine biomechanics as my PhD work at MIT, the first thought from them is: “cool”. The following question from them would usually be: “Can paralyzed patients with spine injury stand up again now, with your research?” Unfortunately, until I finished my PhD work, the answer was still “no”. But there is hope. From centuries ago, numerous researches have been conducted on the lumbar spine, involving studies in kinematics, kinetics, biology, neurology, clinical and etc. Understandings of lumbar spine biomechanics and treatments on spinal disorders have been improved ever since from all the research inputs, step by step. I believe the dream of developing magic cures for all spine disorders and working miracles such as to make paralyzed patients stand up can eventually be achieved, with advancing science and technology.

I also mentioned my major is Mechanical Engineering and I was doing research on the lumbar spine. Most people are curious: “How is mechanical engineering related to spine research? Are you developing robotic spine?” I actually think being a Mechanical Engineering student is a best fit in the

multidisciplinary spine biomechanics research, and appreciate all the knowledge, experiences and trainings I obtained. One part of my work is to learn anatomical and clinical knowledge of the lumbar spine. The rest is essentially all Mechanical Engineering, achieved through a miscellaneous collection of understandings of mechanics, kinematics and dynamics; skills of image processing, modeling and programming; and much more.

## 13.2 Summary

Until now, quantitative understanding of kinematics and IVD deformation in the human spine under *in vivo* physiologic functional activities remains elusive. The *in vivo* measurements obtained are limited by the apparatus and methodologies. They are either not accurate enough or not able to test physiologic functional activities of everyday life. The major contribution of my work is the development and application of a novel combined MRI/CT and DFIS imaging technique to non-invasively study 6DOF lumbar biomechanics in living human subjects.

The technique exhibits several advantages compare to conventional *in vitro*, finite element or even current *in vivo* methods. First of all, the core concept of this method is image matching, which imposes minimum intervention to human body. The non-invasive characteristic is especially critical when study sensitive areas such as spine. Secondly, the technique has shown sufficient accuracy and repeatability through the studies in **Chapter 2** and **Chapter 10** on determination of *in vivo* spine kinematics and disc loads. In addition, the experiment settings are easy to access and reproduced in clinical environment. MRI, CT and fluoroscopes are commercially available and commonly used in almost every hospital. In the experimental setup, study subjects are free to move and perform physiologic

functional activities. Depending on the conditions of the testing subjects, the activities can be specified by surgeons to investigate the biomechanical data of the most relevant motion. The above advantages have made the technique a promising tool.

**Chapter 3 to 7** applied the validated technique on a group of healthy asymptomatic subjects. For the first time, 6DOF motion of different structures of the spine, such as the vertebral body, intervertebral disc, facet joint and spinous process were measured *in vivo* during functional activities. The data provided baseline information for the research on spine biomechanics, such as normal value for the development of treating method that aiming at restoring normal spine function.

**Chapter 8 to 10** applied the same technique on a group of patients with LBP secondary to DDD. 6DOF motion of the vertebral body, the intervertebral disc deformation and the facet joint motion were investigated and compare with those of the normal group. These studies have explored the relationship between abnormal *in vivo* biomechanics and the mechanisms of spinal degeneration. The knowledge obtained will help to establish guidelines for the improvement of current surgical techniques and implant design for the treatment of patients with degenerative changes.

**Chapter 11 and 12** further extended the kinematic results from the technique as boundary input conditions to calculate disc loads in FEA. Preliminary studies have shown the applicability and accuracy of this approach. Its advantages and limitations have been discussed and compared with conventional FEA approach. With further development, the approach could fulfill the missing data regarding *in vivo* forces in the lumbar spine.

### 13.3 Future Work

There are several paths of future directions and potential improvements I can see throughout my PhD work. Firstly, automatic or semi-automatic processes for the images can be possibly developed and implemented. Currently, manual segmentation of spine bony outline on MRI is time consuming and tedious. 3D to 2D matching process is time consuming and the accuracy and repeatability depend greatly on each individual. Secondly, although significant findings have been observed in both the normal group and the patient group, increasing the sample size in both groups will greatly improve the reliability and the statistical power of the results. Thirdly, it is very important to follow-up the patient group after surgery to investigate the possible effect of the surgical intervention on the lumbar spine biomechanics. Thus, a three way comparison can be obtained, i.e. between normal and patients with spinal disorders, between patients before and after surgery, and between normal and patients after surgery. Logically, this will present a more complete piece of work. Last, technological development should be focused on FEA to obtain more information regarding the forces in the lumbar spine. Improvements can be on the material properties of the disc, such as include viscoelastic behavior and modify disc with degenerative changes. In addition, upon validation, similar approach can be used to determine stress-strain in the other structures of the lumbar spine, such the facet joints.

As the long term goal, all the potential advancements mentioned above would enable a transition from research in spine biomechanics to clinical and industrial application of spinal implants. Using the techniques and procedures mentioned in this thesis, *in vivo* lumbar biomechanical data can be accumulated to clarify the design objective function based on normal lumbar spine kinematics and joint forces. The designed prototype can then be introduced into 3D computer

environment to evaluate its biomechanical behaviors. Since the native in-vivo kinematics and spinal loads has already been determined, potential impingements and stress concentration after using the prototype can be easily accessed and improved. Ultimately, in-vivo evaluation of the design can be performed before and after implantation, following the testing procedure in this thesis.

As a conclusion, the developed combined 3D and 2D imaging matching technique really opened a whole window for various in-vivo spine researches. In the future, it could serve as a promising, systematic tool for implant design and testing.